NON-CATALYTIC AND CATALYTIC CO-PYROLYSIS OF *DELONIX REGIA* AND BUTYL RUBBER TUBE WASTES: KINETIC AND THERMODYNAMIC INVESTIGATIONS

A Thesis
Submitted in Partial Fulfilment of the
Requirements for the Degree

of

DOCTOR OF PHILOSOPHY

By

DRAKSHARAPU RAMMOHAN

(Roll No.: 196107004)

DEPARTMENT OF CHEMICAL ENGINEERING
INDIAN INSTITUTE OF TECHNOLOGY GUWAHATI
GUWAHATI, ASSAM – 781039, INDIA
FEBRUARY – 2023

Dedicated

To

My Beloved Supervisors

Department of Chemical Engineering
Indian Institute of Technology Guwahati
Guwahati, Assam,
India

STATEMENT

I hereby declare that the content embodied in this thesis entitled **"Non-Catalytic and Catalytic Co-Pyrolysis of *Delonix Regia* and Butyl Rubber Tube Wastes: Kinetic and Thermodynamic Investigations"** is the result of investigations and experiments carried out by me at 210L Non-Newtonian flow laboratory, Department of Chemical Engineering, Indian Institute of Technology Guwahati, India, under the supervision of Prof. Nanda Kishore & Prof. Ramagopal V.S. Uppaluri. In keeping with the general practice of reporting scientific observations, due acknowledgements have been made wherever the work described is based on the findings of other investigators.

February 2023 Draksharapu Rammohan

Department of Chemical Engineering
Indian Institute of Technology Guwahati
Guwahati, Assam,
India

CERTIFICATE

It is certified that the work contained in this thesis entitled **"Non-Catalytic and Catalytic Co-Pyrolysis of *Delonix Regia* and Butyl Rubber Tube Wastes: Kinetic and Thermodynamic Investigations"** done by **Mr. Draksharapu Rammohan** (Roll No. 196107004) has been carried out under our supervision, and this work has not been submitted elsewhere for a degree.

February 2023

Prof. Nanda Kishore
Main Coordinating Supervisor
Department of Chemical Engineering
Indian Institute of Technology Guwahati

Prof. Ramagopal V.S. Uppaluri
Co-supervisor
Department of Chemical Engineering
Indian Institute of Technology Guwahati

CONTENTS

Chapter-I

Chapter-II

Chapter-III

Chapter-IV

Chapter-V

Chapter-VI


भारतीय प्रौद्योगिकी संस्थान गुवाहाटी
Indian Institute of Technology Guwahati

ACKNOWLEDGEMENTS

Humans are quirky; they always dislike what they have, anticipate the future, and wish for their "present" to become their "past"; nevertheless, when the future arrives, they will never let go of the past. The following members have profoundly affected my life, and I am indebted to them from the depths of my heart for their immense support and blessings:

My supervisors – Prof. Nanda Kishore & Prof. Ramagopal V.S. Uppaluri.

My doctoral committee – Prof. Tamal Banerjee, Prof. R. Prasanna Venkatesh, and Prof. Narayanasamy Selvaraju.

My faculty – Prof. Nageswara Rao Peela, Prof. Vimal Katiyar, and Prof. Kaustubha Mohanty.

My experimental facilities – Mr. Harsaraj Biswanath, Analytical Laboratory, 210L Non-Newtonian flow laboratory, Department of Chemical Engineering, Indian Institute of Technology Guwahati.

My anonymous reviewers.

My mentors – Dr. Kiran Kumar Gali, and Dr. Balendu Shekher Giri.

My colleagues – Sneha, Gaffer, and Praveen.

My mother, father, and sister – Padma, Varaha Murthy, and Aruna.

My friends – Roushni, Janaki, Aviti, Sayani, Dr. Bharath, Prasad, Nikhil, Bineeth, and Imran

ABSTRACT

The outline of this dissertation was to investigate the kinetics and thermodynamic insights for the catalytic and non-catalytic pyrolysis of *Delonix Regia* (DR) and butyl rubber tube (BRT) wastes. The specific objectives proposed in this dissertation were: 1. non-catalytic pyrolysis of DR biomass, 2. non-catalytic pyrolysis of BRT, 3. non-catalytic co-pyrolysis of DR and BRT (1:1 wt. %) wastes, 4. In – situ catalytic pyrolysis of DR biomass, and 5. In – situ catalytic co-pyrolysis of DR and BRT (1:1 wt.%) wastes. For all the stated objectives, the experimental runs were performed with a sample mass of about 6 mg at a temperature range from 25 – 1000 °C between 5 – 55 °C min^{-1} in an inert (nitrogen gas 40 mL min^{-1}) atmosphere using a thermogravimetric analyzer (TGA). Three different types of catalysts, namely zeolite (Na – Y), noble metal on activated carbon (10 wt. % Pt/C), and two–metal oxide (1:1 wt. % TiO_2 – ZnO) with loadings from 30 to 10 wt. % were utilized for the catalytic studies. For investigating the kinetic and thermodynamic, several iso-conversional techniques such as Differential Friedman (DFM), Ozawa–Flynn–Wall (OFW), Kissinger–Akahira–Sunose (KAS), Starink (STK), and Distributed Activation Energy (DAE) were applied. The reaction mechanisms were affirmed by Criado's master plot for all the objectives. Additionally, the pyrolysis performance indices (PPI) were also discussed for all the objectives.

From kinetic investigation, the average apparent activation energy (E_α, kJ mol^{-1}) and pre-exponential factor (k_o, s^{-1}) were: 202 – 206 and $4.98 \times 10^{17} - 2.04 \times 10^{20}$, 223 – 245 and $6.82 \times 10^{21} - 2.73 \times 10^{24}$, 230 – 208 and $2.55 \times 10^{30} - 5.15 \times 10^{26}$, 182 – 181 and $1.33 \times 10^{16} - 2.10 \times 10^{16}$ at DR:Na – Y (1:10 wt. %), and 200 – 179 and $3.03 \times 10^{24} - 1.39 \times 10^{19}$ at DR:BRT:Na – Y (1:1:10 wt. %) ascertained from all iso-conversional techniques for objectives 1, 2, 3, 4, and 5 respectively. From thermodynamic investigation, the average change in enthalpy (ΔH, kJ mol^{-1}) and change in Gibbs free energy (ΔG, kJ mol^{-1}) were: 197 – 201 and 183 – 206, 217 – 239 and 185 – 218, 226 – 225, and 180 – 182, 178 – 177 and 176 – 177 at

DR:Na – Y (1:10 wt. %), and 175 – 174 and 179 – 184 at DR:BRT:Na – Y (1:1:10 wt. %), determined from DFM technique between 5 – 55 °C min^{-1} for objectives 1, 2, 3, 4, and 5 respectively. Criado’s master plot confirmed the multi–step reaction mechanism for all the objectives during the pyrolysis (catalytic and non-catalytic) of DR and BRT wastes.

Keywords: *Delonix Regia*; butyl rubber tube; thermogravimetric analysis; non–catalytic pyrolysis; co – pyrolysis; catalytic pyrolysis; zeolite Na – Y; platinum on activated carbon; titanium oxide; zinc oxide; iso-conversional (model – free and model – fitting) methods; kinetic triplets; thermodynamics; Criado’s master plots; pyrolysis performance indices.

LIST OF FIGURES

LIST OF TABLES

NOMENCLATURE

Abbreviations	
BET	Brunauer-Emmet-Teller
BJH	Barrett-Joyner-Halenda
CFD	Computational fluid dynamics
CP	Catalytic pyrolysis
DAE	Distributed activation energy
DFM	Differential Friedman
DR	*Delonix regia*
DTG	Differential thermogravimetry
EPA	Environmental protection agency
HHV	Higher heating value
ICTAC	International confederation for thermal analysis and calorimetry
IPP	Indices for pyrolysis performance
KAS	Kissinger-akahira-sunose
KF	Kinetic factors
Na–Y	Sodium-Y zeolite

OFW	Ozawa-flynn-wall
Pt/C	Platinum (10 wt. %) on activated carbon
PCCP	Pyro-catalytic co-pyrolysis
Py-GC/MS	Pyrolyzer coupled with gas chromatograph/mass spectrometer
Py-FTIR	Pyrolyzer coupled with fourier transform infrared spectrometer
SA	Surface area
STK	Starink
TGA	Thermogravimetric analyzer
TiO_2	Titanium oxide
TP	Thermodynamic parameters
ZnO	Zinc oxide
Symbols	
C	Flammability index
D_b	Burnout index
D_i	Ignition index
D_v	Devolatilization index
E_α	Activation energy

$f(\alpha)$	Conversion-dependent reaction model (differential)
$g(\alpha)$	Conversion-dependent reaction model (integral)
ΔG	Change in Gibbs free energy
h	Planck’s constant
ΔH	Change in enthalpy
K_B	Boltzmann constant
k_o	Frequency factor
$k(T)$	Reaction rate constant
m_f	Mass of catalytic DR mixture at the final time
m_i	Mass of catalytic DR mixture at the initial time
m_t	Mass of catalytic DR mixture at a time
n	Reaction order
$p(x)$	Temperature approximation (integral)
R	Universal gas constant
R_p	Maximum decomposition rate
R_v	Mean decomposition rate
S	Combustion index

ΔS	Change in entropy
T	Absolute temperature
t	Time
T_b	Burnout temperature
t_b	Burnout time
T_m	Thermogram decomposition temperature
T_i	Ignition temperature
t_i	Ignition time
T_p	Maximum decomposition temperature
t_p	Maximum decomposition time
$\Delta T_{0.5}$	Temperature interval at half of R_p
$\Delta t_{0.5}$	Interval at half of the half of R_p
T_α	Temperature at α
Z_α	Reaction pathway
Greek symbols	
α	Extent of conversion
β	Heating rate

CHAPTER – I

INTRODUCTION

1. Introduction

1.1 Background

Energy scarcity and environmental pollution are the two most pressing issues confronting humanity today. This is due to the rapid industrialization, increasing population, and disposal of various solid wastes generated on regular activity. Scientists are developing advanced technologies to recover energy and valuable products from solid waste, including non-biodegradable materials, to address energy scarcity and pollution. Examples of such materials include plastics, municipal, industrial solid wastes, lignocellulosic/agricultural biomasses, and rubber wastes.

1.1.1 Lignocellulosic/Agricultural residue biomass as feedstock

All the lignocellulosic biomasses/agricultural biomasses consist of three components: cellulose, hemicellulose, and lignin. The typical compositions are cellulose (40 –50 wt. %), hemicellulose (25 – 30 wt. %), and lignin (15 – 20 wt. %) for different kinds of biomasses. **Figure 1.1** illustrates the structural information of lignocellulosic biomass *Delonix Regia* (DR.).

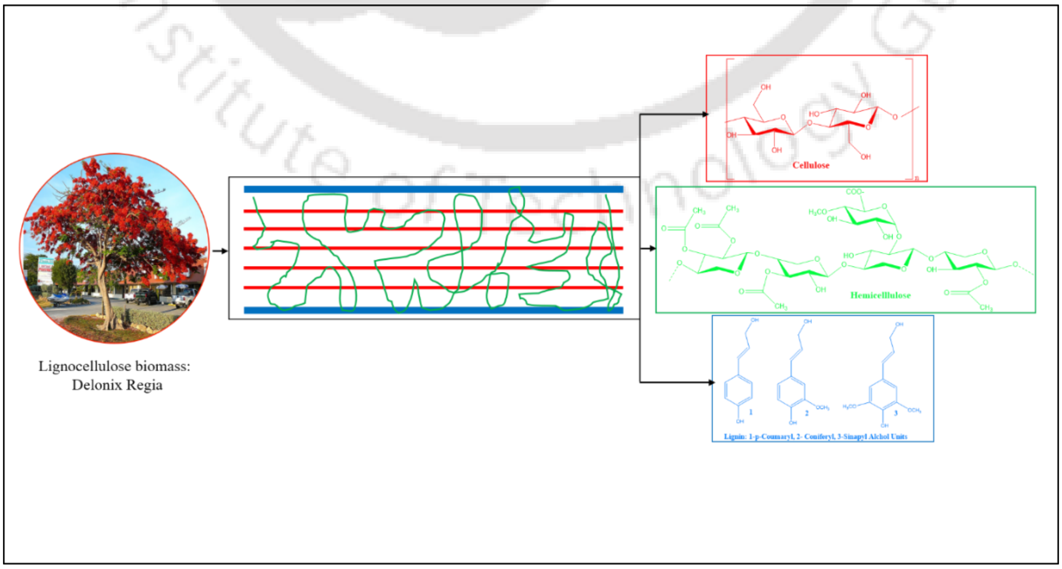

Figure 1.1 Typical structure of lignocellulosic biomass (*Delonix Regia*).

In all the lignocellulosic biomasses, the primary occurrence of cellulose is the naturally abounded material in forests, with wood as the most important source; cellulose-containing materials include woody material, grasses, and agricultural and other plant substances. There are different waste resources, and recent investigation of compositional analysis of different lignocelluloses feedstocks, including agricultural wastes and other plants parts, are:

Hardwood sources of waste include eucalyptus oak and rubberwood, which contain cellulose (40 – 45 wt. %), hemicellulose (25 – 30 wt. %), and lignin (15 – 20 wt. %) on a dry basis. Softwood sources of waste include spruce, pine, and Japanese cedar, which contains (18–38 wt. %), hemicellulose (15 – 33 wt. %), and lignin (30-60 wt. %) on a dry basis. Grasses sources of waste include bamboo, Amur silver grass, natural hay, hemp, rye, reed, sunflower, fodder, nipper, elephant, switch coastal Bermuda grass, which contains cellulose (25 – 40 wt. %), hemicellulose (25 – 50 wt. %), and lignin (10 – 30 wt. %) on a dry basis. Agricultural residual waste is the waste generated by agro-industrial activities. These include shells of walnut, groundnut, pistachio, almond, pine, hazelnut, coconut coir, cotton, and hemp stalks, acacia pruning, sugarcane bagasse, rice husk, rice, wheat, soybean, and barley straws, coffee grounds, extracted olive pomace, palm oil frond, corn Stover, corncob bamboo leaves, hazel branches, *Delonix Regia* seeds, pods, and trunks which contains cellulose (35 – 40 wt. %), hemicellulose (35 – 40 wt. %), and lignin (20 – 25 wt. %) on a dry basis [1], [2].

Delonix Regia (DR) is an abundantly available class of lignocellulosic resource and belongs to the well-known *Fabaceae* genus family. DR is a rapidly growing tree with an umbrella-shaped spreading crown (12 – 19 m), buttressed bole (up to 2 m), and significant height (10.5 – 12 m) [3], [4]. Despite sporadic flowering, DR trees can be grown at a more substantial elevation (0 – 2000 m) than advised. The tree requires sub-tropical temperature (14 – 26 °C) to flourish and grows weakly and sparsely in the shadow environment. It thrives in both locations with abundant and insufficient rainfall (700 – 1200 mm). This tree has a wide range of applications, including the production of biofuel [5], [6], timber [4], extraction of gum or resins [4], medical applications [3], and decoration of its leaves and flowers [3], [4]. The DR tree is indigenous to Madagascar, but it is now abundantly grown in tropical and subtropical areas in the world [3]. The DR is one of the most common trees in India and is recognized with several local names, such as gulmohar, shima sankesula, raktachura, boj, alasippu, and malmara. It is also known as royal poinciana, flamboyant, and flame tree on a worldwide basis. It is frequently located in North America (Mexico, Texas, Central and South Florida), South America (Paraguay, Peru, and Brazil), the Middle East and Europe (Egypt, Lebanon, Cyprus, Jordan, and Israel, and Spain, Canary Islands, Valencian coast), South and East Asia (Myanmar, Philippines, Thailand, Vietnam, Indonesia, China, Hong Kong, Taiwan), Australia (Queensland, Brisbane, Sydney, New South Wales), and many regions of Caribbean.

In the global scenario, the total consumption of lignocellulosic/agricultural residue reported by the European Biomass Association was 18.3 MT of pellets in the European nations in 2013. Global usage was predicted to rise from 22 to 50 – 80 MT by 2020 [7]. In the USA, the majority of the agricultural residues, approximately 140–350 MT, were utilized by industry. The US agricultural residues, including corn Stover and wheat straw, include 155 MT of biomass. Denmark utilizes the highest consumer of agricultural residues such as straw for energy in various purposes, namely district and domestic heating schemes (~3 – 5 and 1 – 2 MW, respectively). Also, part of it was used in industrial processes. Nevertheless, this restricts straw as a source of organic material in the soil [8]. **Figure 1.2** and **Table 1.1** show the statistical data for woody biomass.

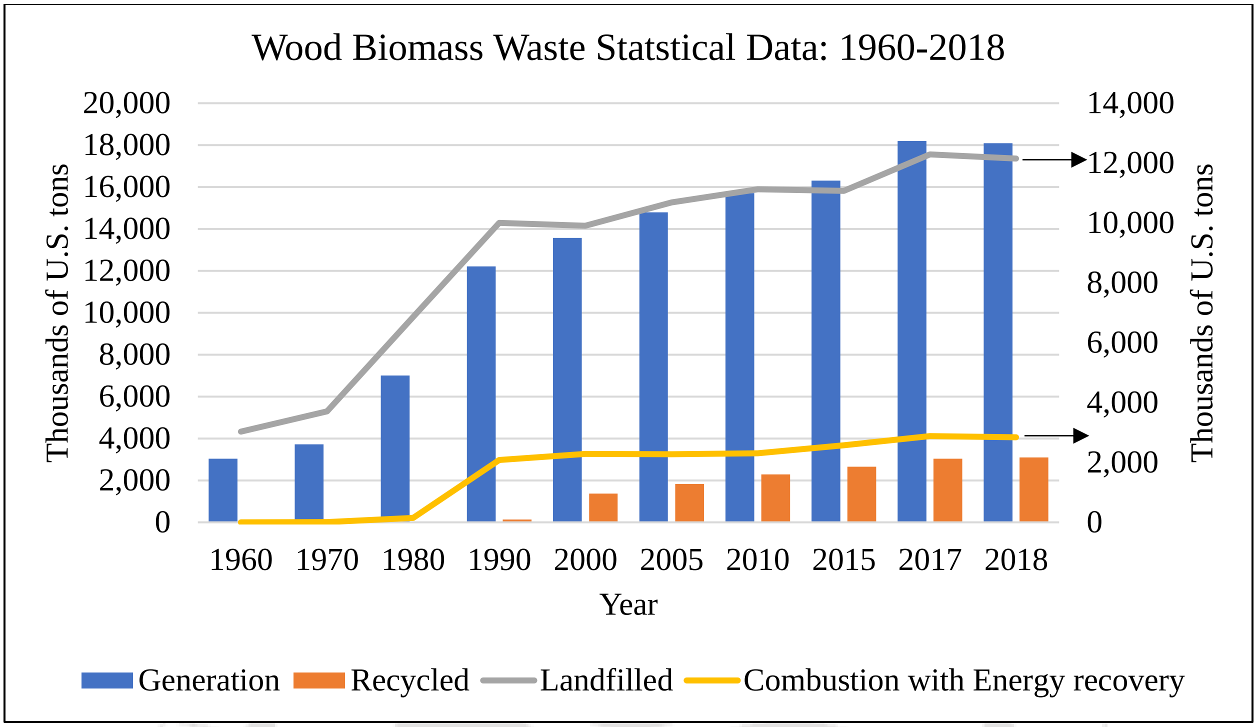

Figure 1.2 Graphical representation of statistical data of wood biomass. [9].

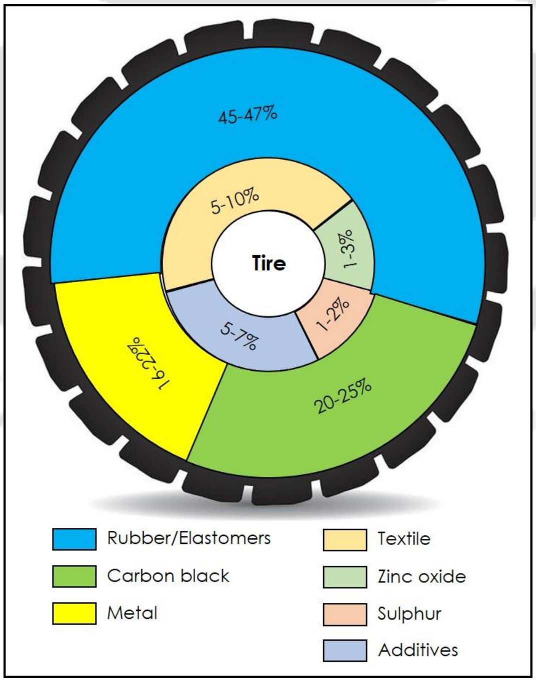

Figure 1.3 Pictorial representation of the vehicle tries composition. [10].

Table 1.1 Tabulated representation of statistical data of wood biomass [9].

Wood waste	1960	1970	1980	1990	2000	2005	2010	2015	2017	2018
Generation	3,030	3,720	7,010	12,210	13,570	14,790	15,710	16,300	18,200	18,090
Recycled	-	-	-	130	1,370	1,830	2,280	2,660	3,030	3,100
Composted	-	-	-	-	-	-	-	-	-	-
Combustion with Energy Recovery	-	10	150	2,080	2,290	2,270	2,310	2,570	2,880	2,840
Landfilled	3,030	3,710	6,860	10,000	9,910	10,690	11,120	11,070	12,290	12,150

1.1.2 Vehicle tire Waste as a feedstock

Commercial vehicle tires are manufactured from rubber (45 – 47 wt. %), carbon black (20 – 25 wt. %), metal (16 – 22 wt. %), textile (5 – 10 wt. %), additives (5 – 7 wt. %), zinc oxide (1 – 3 wt. %), and sulfur (1 – 2 wt. %) vehicle tires consist of a combination of natural (NR) and synthetic rubber (SR), namely; styrene-butadiene rubber (SBR) and butyl rubber (BR).

Figure 1.3 illustrates the general information about vehicle tires. The typical composition of vehicle tries consists of rubbers/elastomers: natural, synthetic, butyl (98% isobutylene + 2% isoprene), styrene-butadiene, carbon black, fillers silica and clay, metals, textile, additives, zinc oxide, and sulfur components. The carbon-based material is presented with high tires if rubber crumbs recycle clays from waste tires. Rubber is an elastic material classified into diene (containing C=C bonds and water) and non-diene (with C-C bonds). Diene rubbers are categorized into natural (isoprene) and synthetic (chloroprene, butadiene, styrene-butadiene, and acrylic nitrile-butadiene) rubbers. Non-diene rubbers, such as acrylic, ethylene-propylene, fluorine, urethane, silicone, and butyl, are synthetic rubbers [11]–[13]. Butyl rubber (IIR) is a copolymer of isobutylene (about 98 mass %) and isoprene (about 2 mass %), which has been used in a wide range of applications such as automobile parts, cable insulation, gas masks, pharmaceutical stoppers, protective clothing, vibration-dampers, and vehicle inner tubes [9], [14].

Waste tire and tube disposal and its management are significant environmental and economic issues in the current rapid globalization period. The following figures have exposed the causes of waste tire generation that highlight the economic and environmental issues across the globe today:

- About 7.9 billion people in the world
- About 1.9 billion vehicles (2019) are estimated to be increased to 8 billion vehicles (2035) on the road. Currently, across the globe, about 100 million new automobiles are being produced every year.
- About 1.6 billion new tires and 1 billion waste tires are generated every year

The following **Figure 1.4** shows the data of 51 countries on their waste tire generation, recovery, and management routes in 2018. According to the report of the 25.7 MT waste tire generated in 2018, for instance, tire waste is used as an additive material for enhancing concrete properties in civil engineering, and backfill accounts for 2% of generation and energy recovery, and combustion for about 67% of waste generation. The rest is about 31% of the generation as not recovered, landfill, and an unknown portion [9], [15]. This kind of utilization of high amounts of tires trend is increasing every year and making the recycling part of the waste tires challenging.

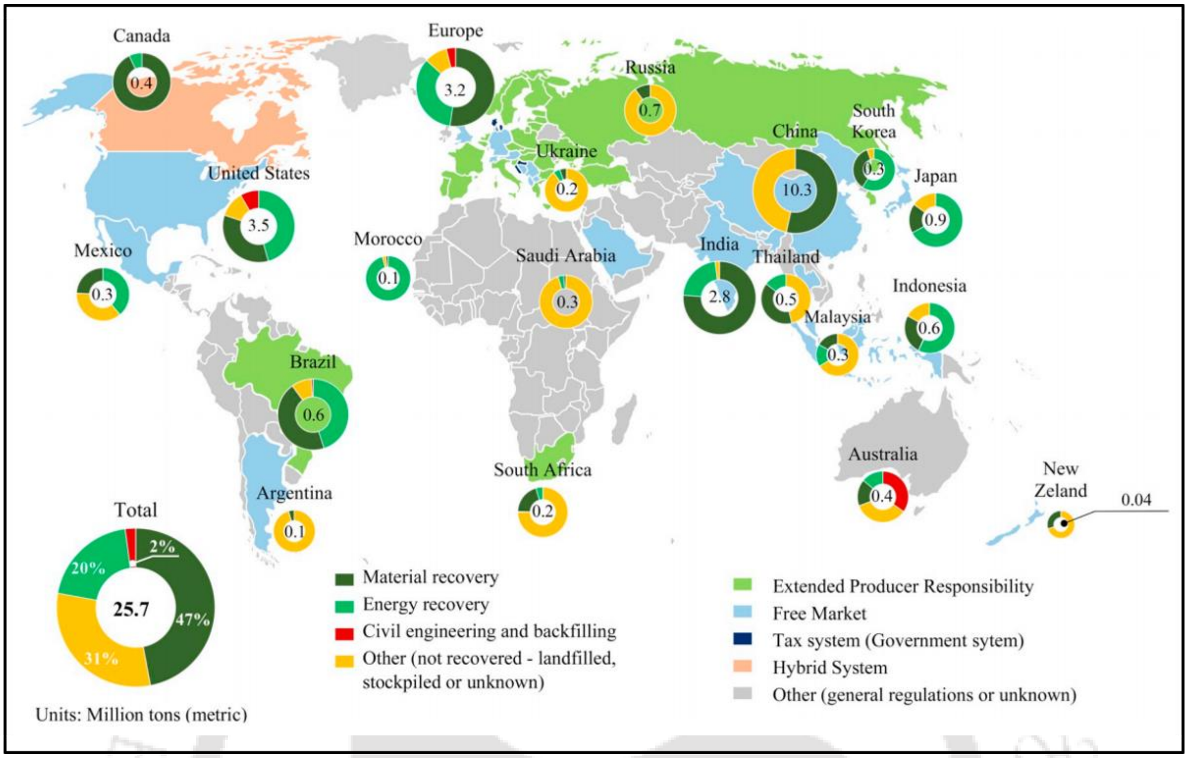

Figure 1.4 Waste tire from several countries: generation, recovery, and management. [15].

Tube and tire waste disposal and management is a significant economic and environmental challenge in the current period of growing globalization [16]–[18]. Globally, 6.5 MT of vehicle tire waste was generated in 2018, out of which 18.2 %, 27.3 %, and 54.5 %, respectively, have been assessed for energy recovery, combustion, and landfill applications [9]. **Figure 1.5** and **Table 1.2** show the statistical data for vehicle tire.

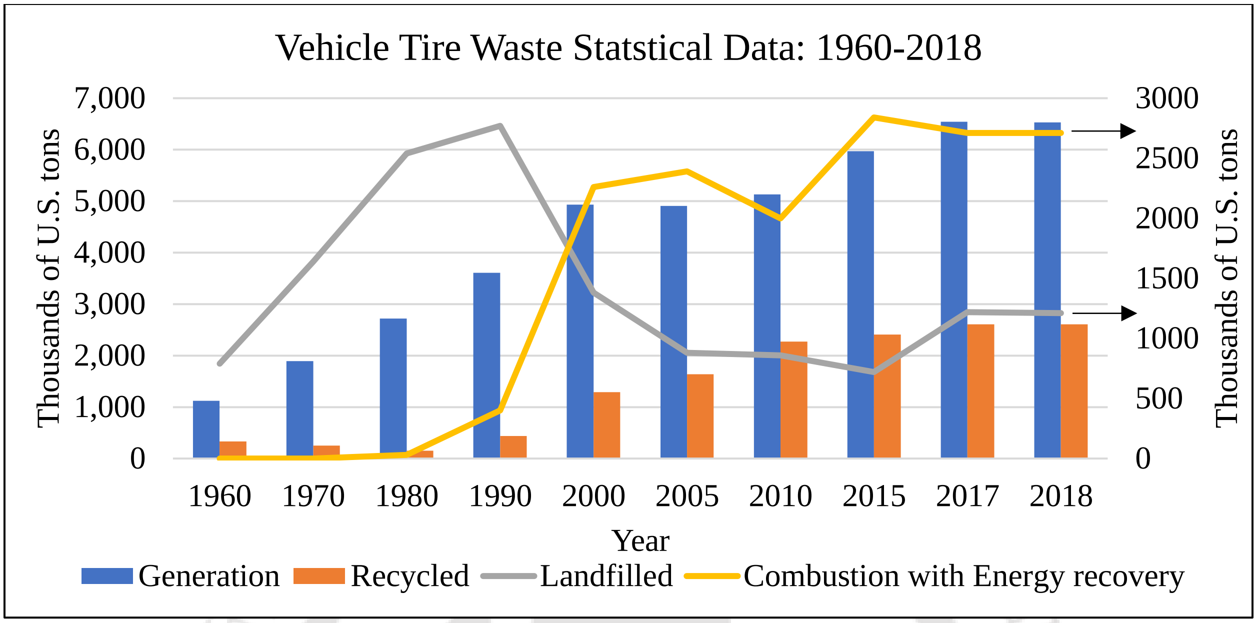

Figure 1.5 Graphical representation of vehicle tire statistical data. [9].

Table 1.2 Tabulated representation of vehicle tire statistical data. [9].

	1960	**1970**	**1980**	**1990**	**2000**	**2005**	**2010**	**2015**	**2017**	**2018**
Generation of tire	1,120	1,890	2,720	3,610	4,930	4,910	5,130	5,970	6,540	6,530
Recycled tire waste	330	250	150	440	1,290	1,640	2,270	2,410	2,610	2,610
Composted tire waste	-	-	-	-	-	-	-	-	-	-
Combustion of tire waste with Energy Recovery	-	-	30	400	2,260	2,390	2,000	2,840	2,710	2,710
Landfilled tire waste	790	1,640	2,540	2,770	1,380	880	860	720	1,220	1,210

As a result, empirical evidence on the generation of biomass, tire, and tube waste must be processed appropriately to recover the maximum amount of additional energy from its massive utility. Thus, an environmentally sustainable mechanism for DR biomass and butyl rubber tube (BRT) waste utilization is required, and pyrolysis is one of the most promising technologies.

1.1.3 Classification of biomass/tube waste conversion technologies:

The technology to convert various biomass feedstocks into bio-oil/bio-crude or bio-chemical is known as biomass conversion. The biomass/tube waste conversion technologies are mainly divided into two categories: biochemical and thermochemical conversion, shown in **Figure 1.6.**

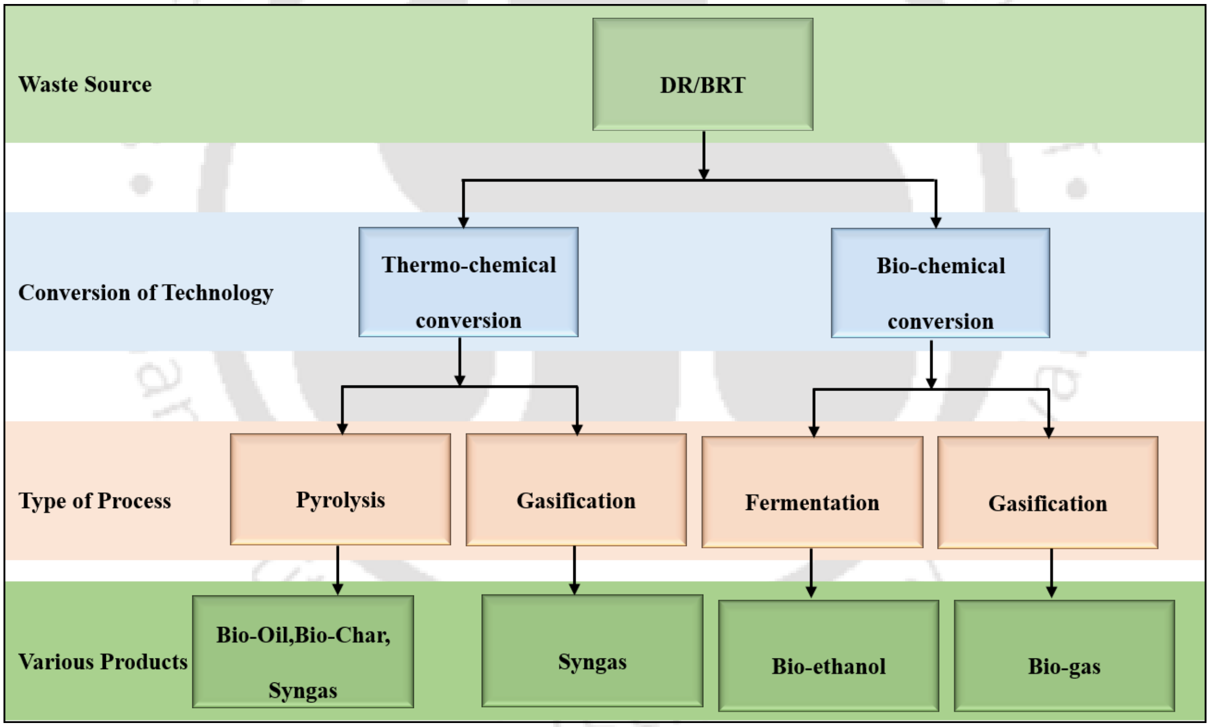

Figure 1.6 Classification of biomass/tube waste conversion technologies

The present dissertation work follows the thermochemical conversion route: and the different thermochemical conversion technologies generally employed are pyrolysis, gasification, liquefaction, and combustion. Conventional thermochemical technologies are advantageous over biochemical conversion processes such as enzymatic hydrolysis. The time taken for biomass/tube waste conversion to the final product is considered a critical advantage. It helps in the effective utilization of local biomass, which helps reduce the transportation cost of the raw material to the plant site [19]. The different types of thermochemical technologies are shown in **Figure 1.7**.

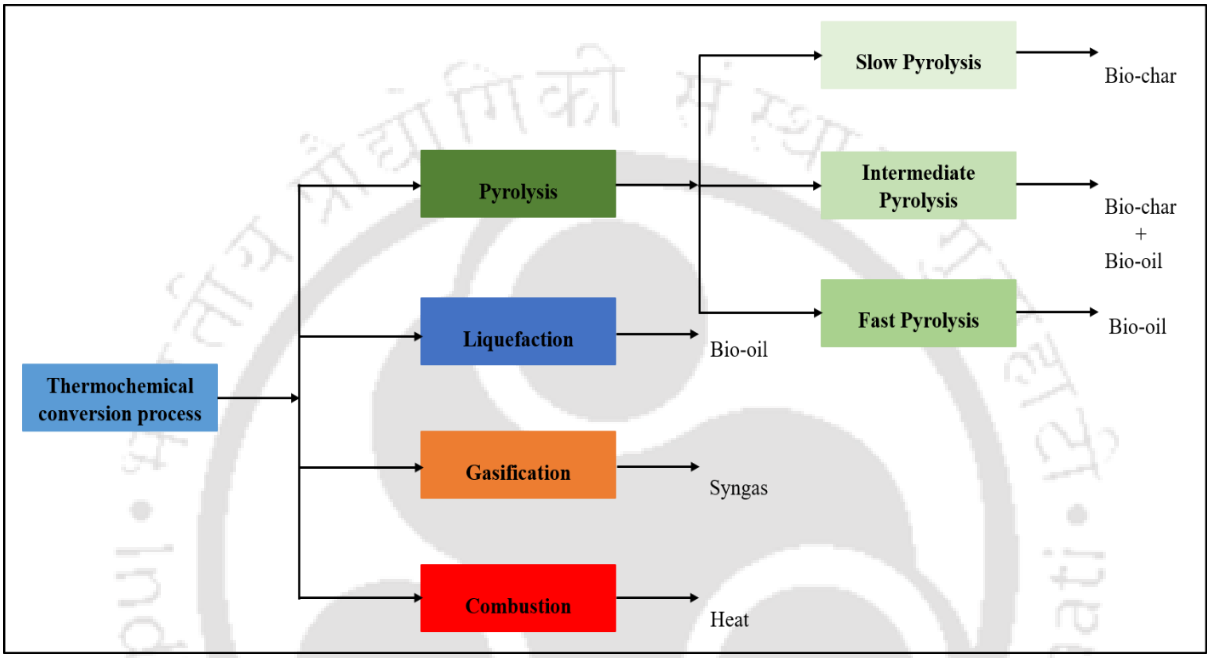

Figure 1.7 Classification of different thermochemical technologies

Pyrolysis of biomass/tube waste contemplates being one of the feasible routes to produce valuable end products [20]. It is a process in which the biomass is rapidly heated (usually a solid material) in an inert atmosphere to a temperature of 450 – 600 ºC. A dark homogeneous liquid commonly referred to as bio-oil is formed after cooling and condensing the vapor formed due to the fast heating of biomass [21]. The different process conditions and results of various pyrolysis operations are given below:

Table 1.3 Pyrolysis products result in different process conditions [22].

Pyrolysis	**Process conditions**	**Results**
Slow pyrolysis	Temperature: 300 – 700 °C	Bio-oil: ~30 wt. %
	Heating rate: 0.1 – 1 °C / s	Biochar: ~35 wt. %
	Vapor residence time: 10 – 100 min	Gases: ~35 wt. %
	Feedstock Size: 5 – 50 mm	
Fast pyrolysis	Temperature: 400 – 800 °C	Bio-oil: ~50 wt. %
	Heating rate: 10 – 200 °C / s	Biochar: ~20 wt. %
	Vapor residence time: 0.5 – 5 min	Gases: ~30 wt. %
	Feedstock Size: ~3 mm	
Flash pyrolysis	Temperature: 800 – 1000 °C	Bio-oil: ~75 wt. %
	Heating rate: ~1000 °C / s	Biochar: ~12 wt. %
	Vapor residence time: ~0.5 s	Gases: ~13 wt. %
	Feedstock Size: ~0.2 mm	

1.2 Significance of the dissertation work

This work ensures the effective and efficient utilization of agricultural waste biomass and butyl rubber tire wastes. It reduces environmental issues such as open burning and waste tire disposal (a common problem globally). Detailed studies on reaction kinetics, thermodynamic properties, and thermal analysis of the *Delonix Regia* (DR) biomass and butyl rubber tube (BRT) wastes will provide more insights into the process.

Biomass and tube waste pyrolysis through kinetic studies provides critical information associated with its decomposition. Most prominently, it delineates rudimentary information about the pertinent reaction mechanisms and the development of a numerical model to illustrate the process [23]. A critical understanding of various competent kinetic factors also aids in evaluating the economic scope of thermal pyrolysis processes [24], [25]. Kinetic studies on biomass and tube pyrolysis have been well addressed in the literature and are often conducted through two alternate handy model-fitting and model-free approaches [26], [27]. While iso-conversional methods can investigate the behavior of complex reactions, they suffer from the possibility of employing an inefficient kinetic model. This prompts the identification of inadequate kinetic factors [28].

The co-pyrolysis is one of the best-employed processes for effective and efficient utilization of more than one type of feedstock resource with the energy input that is required only for a single feedstock. In the co-pyrolysis process, the volume of waste could be significantly consumed as feedstock; this also ensures effective waste management. Additionally, the energy consumption, production cost, and processing time could be reduced considerably by co-pyrolysis. Thus, co-pyrolysis of biomass and tube waste materials serve both the purposes of biofuel generation and waste management with less impact on the environment. The co–pyrolysis of DR biomass with BRT waste is a significant and potentially promising approach. The pyro–products produced from the biomass co–pyrolysis process has lower physico–chemical properties (calorific value, density, viscosity, and moisture contents) [29].

However, the co–pyrolysis process can enhance these properties by providing hydrogen–rich radicals from rubber waste. As per the research results, the biomass and tube waste co–pyrolysis process exhibits a positive synergistic effect and increases the yields of pyrolytic products (hydrocarbons). The higher yields of pyrolytic products are ascertained by Diels–Alder reaction between the furans and hydrocarbons from biomass and rubber wastes during the co–pyrolysis [5], [30].

Pyro–catalytic co–pyrolysis (PCCP) is the preferable alternative as it utilizes an external agent to achieve an enhanced degradation reaction. The objective of PCCP is to upgrade the effectiveness of pyro–products by utilizing several catalysts. The role of several catalysts is studied in order to obtain the specific pyro–compounds. Utilization of an optimum catalyst in a process provides several advantages in the pyrolysis process, primarily enabling the two objectives. Firstly, it benefits the product by enhancing the quality and quantity of the targeted product by promoting aromatics formation in the pyrolytic products. It can be achieved by changing the lower operating conditions, including reaction time and temperature, to improve the pyrolytic decomposition, cracking, and isomerization reactions [21]. As a result, the targeted product is enhanced, and the energy consumption is reduced. Secondly, the catalyst improves the overall efficiency and energetic performance of the pyrolysis process. In addition, the catalyst exhibits a high degree of selectivity in converting aliphatic hydrocarbons to cyclic and aromatic compounds towards the production of pyrolytic products with excellent characteristics [29]. Various catalysts, including Na – Y zeolite, Pt/C, and TiO_2 – ZnO, are commonly utilized in the hydrocarbon sector to enrich the yield of the pyro–products [29], [31]–[33]. Factors such as selection (type, size, and shape) of catalyst, co–feed to catalyst ratio, operating temperature, and time have significantly affected PCCP [34]. The kinetic rates play a critical role in the transformation of co–feed material to products during PCCP. It has been established that developing an efficient co–pyrolysis process requires proper kinetic and thermodynamic modeling, which can be accomplished using thermogravimetric analyzers (TGA). [35], [36].

On a smaller scale, thermogravimetric analysis (TGA) is an accurate technique for determining the thermal degradation of solid materials. Furthermore, the kinetics and thermodynamic properties are crucial in comprehending the fundamental phenomena and mechanisms governing thermal processes and thus complement experimental analysis. In other words, the kinetics and thermodynamic findings are useful for reactor designs, process optimization, scale-up studies, industrial applications, and simulation studies using different models for biomass pyrolysis [37], [38]. Thus, this research describes the thermal degradation behavior and kinetics of DR, BRT waste and the co-pyrolysis of a 1:1 ratio of DR and BRT feedstocks via non-catalytically and catalytically at dynamic heating rates (5 – 55 °C min^{-1}); and the findings are presented. Firstly, the kinetic analysis was performed using five different iso-conversional methods to find the activation energy (E_α) and the frequency factor (k_o), and then the results were compared. The five iso-conversational models that were considered in this study are Differential Friedman (DFM), Kissinger-Akahira-Sunose (KAS), Ozawa-Flynn-Wall (OFW), Starink (STK), and Distributed Activation Energy Method (DAEM). In addition, Criado's master plot (CMP) methods are used to predict the reaction mechanism. Secondly, the thermal degradation characteristics of the co-feed materials were provided in the form of pyrolysis performance indices (PPIs). These indices include flammability, ignition, burnout, combustion, and devolatilization index values. Thirdly, the thermodynamic parameters such as a change in enthalpy (ΔH) and Gibbs free energy (ΔG) values were reported for pyrolysis of DR, BRT, DR – BRT (1 – 1 wt. %), catalytic DR, and catalytic DR – BRT mixtures. The catalysts used in this study are zeolite (Na – Y), noble metal on activated carbon (10 wt. % of Pt/C), bi-metal oxide (1 – 1 wt. % of TiO_2 – ZnO) between 30 to 10 wt. %.

1.3 Scope of the dissertation work

The aim of this dissertation is to investigate the critical findings of reaction kinetics, thermodynamic properties, and pyrolysis performance characteristics of *Delonix Regia* (DR) biomass, butyl rubber tube (BRT) wastes, and its co-feed via catalytic and non-catalytic processes.

Initially, the first objective is to elucidate the non-catalytic pyrolysis of DR biomass. The second objective is to study the non-catalytic pyrolysis of BRT waste. The third objective is to implementation of non-catalytic co-pyrolysis of DR and BRT (1:1 wt.%) wastes. The fourth objective is to examine the in – situ catalytic pyrolysis of DR biomass. Finally, the fifth objective is the evaluation of in – situ catalytic co-pyrolysis of DR and BRT (1:1 wt. %) wastes. All proposed objective findings are extensively explored in the results and discussion in chapter V of sections 5.1, 5.2, 5.3, 5.4, and 5.

1.4 Summary of the chapter I.

The following statements were obtained from the chapter I:

- Initially, the background of the research topic and statistical data of biomass and tube waste was discussed.
- The classification of different conversion technologies for biomass and tube was presented.
- A comprehensive discussion of the significance of the dissertation work has been provided.
- Finally, the scope of the dissertation work with five objectives has been proposed.

CHAPTER – II

LITERATURE REVIEW

2. Literature Review

This section rigorously discussed the literature review on several feedstocks for non-catalytic and catalytic processes, and the summary is illustrated in Table 2. Table 2 contains the different (five) subsections, namely 2.1, 2.2, 2.3, 2.4, and 2.5. The first subsection (2.1) provided a detailed summary of the non-catalytic pyrolysis of various lignocellulosic biomasses [2], [34], [39]–[43]. After an extensive literature study, it was concluded that objective 1 was not yet disclosed up to its full potential. As a result, significant research was performed, and the findings were published at the end of section 2.1. The second subsection (2.2) depicted a thorough review of the non-catalytic pyrolysis of various polymer wastes [44]–[47]. It was confirmed upon meticulous examination that any researcher did not divulge objective 2. Thus, further experiments were carried out, and the results were shown at the end of section 2.2. The third subsection (2.3) briefly discussed the non-catalytic co-pyrolysis of biomass and polymer wastes [40], [41], [47]–[51]. Following a comprehensive investigation, it was established that no literature was found on objective 3. Hence, more experimental tests were conducted, and the outcomes were published at the end of section 2.3. The fourth subsection (2.4) elucidated the critical evaluation of the in-situ catalytic pyrolysis of various biomass [34], [35], [47], [52]–[55]. No open literature was available on stated objective 4, so further investigation was undertaken, and results were described at the end of section 2.4. Finally, subsection (2.5) emphasized the in-depth assessment of the in-situ catalytic co-pyrolysis of distinct biomass and polymer wastes [40], [43], [49], [56]. Due to the paucity of data pertinent to objective 5, substantial research work was accomplished, and results were analyzed after section 2.5. In addition, the overall and specific objectives of the thesis were discussed in greater detail in the following sections, 2.6.1 and 2.6.2, and the significant findings and observations were revealed in further sections from 5.1 to 5.5 in the results and discussions (chapter V).

Table 2 Literature review summary for all the proposed objectives

2.1 Non – catalytic pyrolysis of *Delonix Regia* (DR) biomass

S.No.	Raw materials	Catalyst	TGA model	Operating conditions			Results		References
	Feed and co-feed	(wt. %)		°C	Q	β	*Kinetics	*Thermodynamics	
1	Microalgae (enteromorpha prolifera) (10 mg)	-	Netsch TG209F3	25 – 800	N_2 – 50	10, 20, 30, 40	$E_{\alpha=0.1\text{-}0.80}$: 229, 229, 229, 229, 228, by DFM, DAE, OFW, KAS,	-	[40]
2	*Delonix Regia* pods	-	Perkin Elmer STA-7	29 – 9000	N_2 – 30	5, 10, 20, 50	$E_{\alpha=0.1\text{-}0.65 \text{ and } 0.65\text{-}0.80}$: 196 and 277, 194 and 234, and 194 and 236 by DFM, OFW, STK	$E_{\alpha=0.1\text{-}0.80}$: ΔH: 214, ΔG: 143, and ΔS: 0.116	[39]
3	Moringa oleifera husk	-	Perkin Elmer STA-7	29 – 900	N_2 – 30	5, 10, 20, 50	$E_{\alpha=0.1\text{-}0.65 \text{ and } 0.65\text{-}0.80}$: 201 and 199, 200 and 364, and 292 and 296 by DFM, OFW, STK	$E_{\alpha=0.1\text{-}0.80}$: ΔH: 233, ΔG: 135, and ΔS: 0.152	[39]

4	*Delonix Regia* seeds (8 mg)	-	Perkin Elmer STA-7200	30 – 900	N_2 – 40	10, 20, 30, 40, 50	$E_{\alpha=0.1\text{-}0.80}$ and k_o: 142 and 4.29×10^{09}, 192 and 2.07×10^{19} , 152 and 1.52×10^{14}, and 148 and 4.90×10^{10} *by* KAS, OFW, DFM, DAE	$E_{\alpha=0.1\text{-}0.80}$: ΔH: 147, ΔG: 219, and ΔS: -0.114	[2]
5	Manikara zapota seeds (8 mg)	-	Perkin Elmer STA-7200	30 – 900	N_2 – 40	10, 20, 30, 40, 50	$E_{\alpha=0.1\text{-}0.80}$ and k_o: 132 and 1.56×10^{09}, 138 and 4.59×10^{18} , 143 and 3.57×10^{13}, and 177 and 1.69×10^{14} *by* KAS, OFW, DFM, DAEM	$E_{\alpha=0.1\text{-}0.80}$: ΔH: 137, ΔG: 233, and ΔS: -0.144	[2]
6	Cascabela thevetia seeds (8 mg)	-	Perkin Elmer STA-7200	30 – 900	N_2 – 40	10, 20, 30, 40, 50	$E_{\alpha=0.1\text{-}0.80}$ and k_o: 152 and 4.18×10^{09}, 162 and 2.03×10^{18} , 168 and 2.03×10^{14}, and 188 and 1.09×10^{13} *by* KAS, OFW, DFM, DAE	$E_{\alpha=0.1\text{-}0.80}$: ΔH: 163, ΔG: 235, and ΔS: -0.108	[2]

7	Corncob	-	Perkin Elmer STA-8000	25 – 900	N_2 – 50	10, 20, 30	$E_{\alpha=0.1\text{-}0.90}$: 240, 238, 241, 248, by KAS, OFW, STK, DFM	$E_{\alpha=0.1\text{-}0.80}$: ΔH: 253, ΔG: 180, and ΔS: 0.153	[41]
8	Almond shells (10 mg)	-	Exstar TG/DTA 6300	30 – 1000	N_2 – 200	10, 25, 50	$E_{\alpha=0.1\text{-}0.80}$: 153, 152, 153, by KAS, OFW, STK,	$E_{\alpha=0.1\text{-}0.80}$: ΔH: 148, ΔG: 182, and ΔS: -0.052	[42]
9	Pinewood (10 mg)	-	TA-SDT650	25 – 850	N_2 – 100	5, 10, 20	$E_{\alpha=0.1\text{-}0.90}$ 201 for KAS	-	[47]
10	Poplar sawdust (10 mg)	Fe-Ni/ZSM-5 (1:1)	Perkin Elmer STA-8000	25 – 900	N_2 – 100	5, 10, 20, 40	$E_{\alpha=0.15\text{-}0.90}$: 159, 157, 159, 157 for DFM, STK, OFW, KAS	$E_{\alpha=0.1\text{-}0.80}$: ΔH: 165, and ΔG: 164	[34]
11	*Delonix Regia* biomass: trunks/branches (6 mg)	-	Netsch TG209F1	25 – 1000	N_2 – 40	5, 10, 20, 35, 55	$E_{\alpha=0.1\text{-}0.80}$ and k_o: 202 and 4.98×10^{17}, 206 and 2.62×10^{20}, 205 and 4.98×10^{17}, 206 and 2.04×10^{20}, 206 and 1.67×10^{20} by DFM, KAS, OFW, STK, DAE	$E_{\alpha=0.1\text{-}0.80}$: ΔH: 197, ΔG: 181 and ΔS: 0.031	Objective 2.1 [57]

2.2 Non – catalytic pyrolysis of butyl rubber tube (BRT) waste									
12	Natural rubber (10 mg)	-	Mettler Toledo TGA/DSC 1	30 – 600	N_2 –100	2, 5, 10, 15, 20	$E_{\alpha=0.1-1.0}$ and k_o: 434 and 32.2 by DFM	-	[44]
13	Polyisoprene synthetic (10 mg)	-	Mettler Toledo TGA/DSC 1	30 – 600	N_2 –100	2, 5, 10, 15, 20	$E_{\alpha=0.1-1.0}$ and k_o: 372 and 27.2 by DFM	-	[44]
14	Butadiene rubber (10 mg)	-	Mettler Toledo TGA/DSC 1	30 – 600	N_2 –100	2, 5, 10, 15, 20	$E_{\alpha=0.1-1.0}$ and k_o: 244 and 15.1 by DFM	-	[44]
15	Styrene Butadiene rubber (10 mg)	-	Mettler Toledo TGA/DSC 1	30 – 600	N_2 –100	2, 5, 10, 15, 20	$E_{\alpha=0.1-1.0}$ and k_o: 235 and 14.7 by DFM	-	[44]
16	Milk packet waste (10 mg)	-	Exstar-SII 6300	35 – 800	N_2 – 100	5, 10, 20	$E_{\alpha=0.1-0.95}$ and k_o: 175 and 1.46×10^{13}, 178 and	$E_{\alpha=0.1-0.80}$: ΔH: 172, ΔG: 160, and ΔS:	[45]

							1.47×10^{13} by KAS, OFW	0.018	
17	Polyethylene	-	Perkin Elmer STA-8000	25 – 900	N_2 – 50	10, 20, 30	$E_{\alpha=0.1\text{-}0.90}$: 156, 159, 148, 171, by KAS, OFW, STK, DFM	$E_{\alpha=0.1\text{-}0.80}$: ΔH: 176, ΔG: 222, and ΔS: 0.145	[41]
18	Linear low-density polyethylene (10 mg)	-	Netsch TG209F1	30 – 800	N_2 – 20	5, 10, 20, 40	$E_{\alpha=0.1\text{-}0.80}$: 155, 157, 180, by KAS, OFW, DFM	-	[46]
	High density polyethylene (10 mg)	-	TA-SDT650	25 – 850	N_2 – 100	5, 10, 20	$E_{\alpha=0.1\text{-}0.90}$ and k_o: 246 and 6.45×10^{-13} for KAS	-	[47]
19	Butyl rubber tube waste (6 mg)	-	Netsch TG209F1	25 – 1000	N_2 – 40	5, 10, 20, 35, 55	$E_{\alpha=0.1\text{-}0.80}$ and k_o: 245 and 2.73×10^{24}, 223 and 3.01×10^{24}, 223 and 6.82×10^{21}, 223 and 2.35×10^{24}, 223 and 1.84×10^{24} by DFM, KAS, OFW, STK, DAE	$E_{\alpha=0.1\text{-}0.80}$: ΔH: 239, and ΔG: 185	Objective 2.2
2.3 Non – catalytic co – pyrolysis of DR and BRT (1:1 wt. %) wastes									

20	Rubber seed shell: HDPE (1:1)	-	Mettler Toledo TGA/DSC 1	50 – 900	N_2 – 100	10, 20, 30, 50, 100	$E_{\alpha=0.1\text{-}0.90}$ and k_o: 64 and 8.4× 10^{04} for DAE	-	[48]
21	Rural solid waste (kitchen waste (61%, plastic and rubber 16%, paper 12%, textiles 4% and leaves 3%) : microalgae (chlorella vulgaris) (1:1)	-	Mettler Toledo TGA/DSC 1	50 – 800	N_2 – 80	20, 30, 40	$E_{\alpha=0.1\text{-}0.90}$: 255 and 255 for OFW, and KAS	-	[49]
22	Microalgae (enteromorpha prolifera): High density polyethylene (1:1)	-	Netsch TG209F3	25 – 800	N_2 – 50	10, 20, 30, 40	$E_{\alpha=0.1\text{-}0.80}$: 120, 120, 119, 119, 119, by DFM, DAE, OFW, KAS,	-	[40]

23	Corncob: Polyethylene (3:1)	-	Perkin Elmer STA-8000	25 – 900	N_2 – 50	10, 20, 30	$E_{\alpha=0.1\text{-}0.90}$: 216, 216, 216, 221, by KAS, OFW, STK, DFM	$E_{\alpha=0.1\text{-}0.80}$: ΔH: 227, ΔG: 226, and ΔS: 0.015	[41]
24	Wettorrified bamboo: LLDPE (1:1)	-	Netsch TG209F1	30 – 800	N_2 – 20	5, 10, 20, 40	$E_{\alpha=0.1\text{-}0.80}$: 264, 261, 256, by KAS, OFW, DFM	-	[46]
25	Pinewood: HDPE (1:1)	-	TA-SDT650	25 – 850	N_2 – 100	5, 10, 20	$E_{\alpha=0.1\text{-}0.90}$ and k_o: 177 and 3.57×10^{17} for KAS,	$E_{\alpha=0.1\text{-}0.90}$: ΔH: 182, and ΔG: 196	[47]
26	*Delonix Regia*: Butyl rubber tube waste (1:1)	-	Netsch TG209F1	25 – 1000	N_2 – 40	5, 10, 20, 35, 55	$E_{\alpha=0.1\text{-}0.80}$ and k_o: 230 and 2.55×10^{30}, 208 and 8.31×10^{26}, 208 and 1.58×10^{24}, 208 and 6.47×10^{26}, 208 and 5.15×10^{26} by DFM, KAS, OFW, STK, DAE	$E_{\alpha=0.1\text{-}0.80}$: ΔH: 225, and ΔG: 180	Objective 2.3 [51]
2.4 In – situ catalytic pyrolysis of DR biomass									
27	Douglas fir (1 wt.%)	ZSM-5 (3 wt.%)	Mettler Toledo 188	25 – 600	N_2 – 20	10, 20, 30, 40	$E_{\alpha=0.15\text{-}0.70}$: 193 by DFM	-	[52]

			TGA/SDTA 851						
28	Beech wood (1 wt. %)	H-ZSM-5 (1 wt.%)	Q-600	25 – 900	Ar – 50	10, 20, 35, 50	$E_{\alpha=0.15\text{-}0.80}$: 116 by DFM	-	[53]
29	Beech wood (1 wt. %)	Al-MCM - 41 (1 wt.%)	Q-600	25 – 900	Ar – 50	10, 20, 35, 50	$E_{\alpha=0.15\text{-}0.80}$: 128 by DFM	-	[53]
30	Woody biomass (1 wt.%)	Na_2ZrO_3 (1 wt.%)	Q-600	30 – 600	Ar – 500	35, 40, 45	$E_{\alpha=0.15\text{-}0.80}$: 112, 117, 114 for KAS, OFW, DFM	$E_{\alpha=0.1\text{-}0.80}$: ΔH: 113, and ΔG: 157 at 35 °C min^{-1}	[54]
31	Woody biomass (1 wt.%)	$LiSiO_4$ (1 wt.%)	Q-600	30 – 600	Ar – 500	35, 40, 45	$E_{\alpha=0.15\text{-}0.80}$: 112, 117, 116 for KAS, OFW, DFM	$E_{\alpha=0.1\text{-}0.80}$: ΔH: 112, and ΔG: 157 at 35 °C min^{-1}	[54]
32	Pine needle waste (1 wt.%)	Ni/Al_2O_3 (1 wt.%)	Exstar-SII 6300	30 – 1000	N_2 – 200	10, 20, 30, 40	$E_{\alpha=0.15\text{-}0.90}$: 105, 100 for OFW, KAS	$E_{\alpha=0.1\text{-}0.80}$: ΔH: 95, and ΔG: 152	[35]
33	Sunan candlenut oilcake (1 wt.%)	FeO (5 wt.%)	Leco-701	30 – 950	N_2 – 10	10, 20, 30, 40	$E_{\alpha=0.15\text{-}0.80}$: 211, 211, 240 for OFW, KAS, DFM	-	[55]

34	Sunan candlenut oilcake (1 wt.%)	Zeolite (5 wt.%)	Leco-701	30 – 950	N_2 – 10	10, 20, 30, 40	$E_{\alpha=0.15\text{-}0.80}$: 331, 325, 418 for OFW, KAS, DFM	-	[55]
35	Sunan candlenut oilcake (1 wt.%)	ZSM-5 (5 wt.%)	Leco-701	30 – 950	N_2 – 10	10, 20, 30, 40	$E_{\alpha=0.15\text{-}0.80}$: 163, 165, 182 for OFW, KAS, DFM	-	[55]
36	Pinewood (10 mg)	HZSM – 5	TA-SDT650	25 – 850	N_2 – 100	5, 10, 20	$E_{\alpha=0.1\text{-}0.90}$: 167 for KAS	-	[47]
37	Poplar sawdust (10 mg)	Fe-Ni/ZSM-5 (1:1)	Perkin Elmer STA-8000	25 – 900	N_2 – 100	5, 10, 20, 40	$E_{\alpha=0.15\text{-}0.90}$: 156, 152, 154, 152 for DFM, STK, OFW, KAS	$E_{\alpha=0.1\text{-}0.80}$: ΔH: 163, and ΔG: 158	[34]
38	*Delonix Regia* (6 mg)	Na-Y zeolite (30, 20, 10 wt.%)	Netsch TG209F1	25 – 1000	N_2 – 40	5, 10, 20, 35, 55	$E_{\alpha=0.1\text{-}0.7}$ and k_o: 182 and 1.33×10^{16}, 181 and 2.10×10^{16}, 181 and 9.31×10^{13}, 181 and 1.69×10^{16}, 181 and 1.83×10^{17} by DFM,	$E_{\alpha=0.1\text{-}0.80}$: ΔH: 177, and ΔG: 178	Objective 2.4

							KAS, OFW, STK, DAE at 10 wt. % Na-Y		
39	*Delonix Regia* (6 mg)	Pt/C (30, 20, 10 wt.%)	Netsch TG209F1	25 – 1000	N_2 – 40	5, 10, 20, 35, 55	$E_{\alpha=0.1\text{-}0.7}$ and k_o: 200 and 9.62×10^{17}, 208 and 2.59×10^{18}, 204 and 9.56×10^{15}, 205 and 2.07×10^{18}, 205 and 2.03×10^{19} by DFM, KAS, OFW, STK, DAE at 10 wt.% Pt/C	$E_{\alpha=0.1\text{-}0.80}$: ΔH: 195, and ΔG: 178	Objective 2.4
40	*Delonix Regia* (6 mg)	TiO_2-ZnO (1:1) (30, 20, 10 wt.%)	Netsch TG209F1	25 – 1000	N_2 – 40	5, 10, 20, 35, 55	$E_{\alpha=0.1\text{-}0.7}$ and k_o: 191 and 7.34×10^{16}, 194 and 2.87×10^{17}, 194 and 1.16×10^{15}, 195 and 2.30×10^{17}, 194 and 2.30×10^{18} by DFM, KAS, OFW, STK, DAE at 20 wt.% TiO_2-ZnO	$E_{\alpha=0.1\text{-}0.80}$: ΔH: 186, and ΔG: 178	Objective 2.4
2.5 In – situ catalytic co-pyrolysis of DR and BRT (1:1 wt. %) wastes									

41	Rural solid waste (kitchen waste 61%, plastic and rubber 16%, paper 12%, textiles 4% and leaves 3%) : microalgae (chlorella vulgaris) (1:1)	CaO- (5.2%)	Mettler Toledo TGA/DSC 1	50 – 800	N_2 – 80	20, 30, 40	$E_{\alpha=0.1\text{-}0.80}$: 272 and 276 for OFW, and KAS	-	[49]
42	Rural solid waste (kitchen waste (61%, plastic and rubber 16%, paper 12%, textiles 4% and leaves 3%) : microalgae (chlorella vulgaris) (1:1)	MgO (1.57%)	Mettler Toledo TGA/DSC 1	50 – 800	N_2 – 80	20, 30, 40	$E_{\alpha=0.1\text{-}0.80}$: 221 and 223 for OFW, and KAS	-	[49]
43	Rural solid waste (kitchen waste	HZSM-5 (4.89%)	Mettler Toledo	50 – 800	N_2 – 80	20, 30, 40	$E_{\alpha=0.1\text{-}0.80}$: 225 and 223 for OFW, and KAS	-	[49]

	(61%, plastic and rubber 16%, paper 12%, textiles 4% and leaves 3%) : microalgae (chlorella vulgaris) (1:1)		TGA/DSC 1						
44	Microalgae (enteromorpha prolifera): High density polyethylene (1:1)	HZSM – 5 (2 wt.%)	Netsch TG209F3	25 – 800	N_2 – 50	10, 20, 30, 40	$E_{\alpha=0.1\text{-}0.80}$: 109, 109, 108, 107, 108, by DFM, DAE, OFW, KAS,	-	[40]
45	Wettorrified bamboo: Linear low-density polyethylene (1:1)	HZSM – 5	Netsch TG209F1	30 – 800	N_2 – 20	5, 10, 20, 40	$E_{\alpha=0.1\text{-}0.80}$: 135, 137, 135, by KAS, OFW, DFM	-	[58]
46	Pinewood: High density polyethylene (1:1)	HZSM – 5	TA-SDT650	25 – 850	N_2 – 100	5, 10, 20	$E_{\alpha=0.1\text{-}0.90}$ and k_o: 158 and 1.80×10^{-08} for KAS	$E_{\alpha=0.1\text{-}0.90}$: ΔH: 163, and ΔG: 185	[47]

47	*Delonix Regia*: Butyl rubber tube waste (1:1)	Na-Y zeolite (30, 20, 10 wt.%)	Netsch TG209F1	25 – 1000	N_2 – 40	5, 10, 20, 35, 55	$E_{\alpha=0.1\text{-}0.7}$ and k_o: 199 and 3.03×10^{24}, 179 and 1.68×10^{19}, 180 and 5.95×10^{16}, 179 and 1.34×10^{19}, 179 and 1.39×10^{19} by DFM, KAS, OFW, STK, DAE at 10 wt.% Na-Y	$E_{\alpha=0.1\text{-}0.80}$: ΔH: 175, and ΔG: 179	Objective 2.5
48	*Delonix Regia*: Butyl rubber tube waste (1:1)	Pt/C (30, 20, 10 wt.%)	Netsch TG209F1	25 – 1000	N_2 – 40	5, 10, 20, 35, 55	$E_{\alpha=0.1\text{-}0.7}$ and k_o: 220 and 9.80×10^{24}, 203 and 4.22×10^{20}, 203 and 1.31×10^{18}, 204 and 3.35×10^{20}, 203 and 3.50×10^{20} by DFM, KAS, OFW, STK, DAE	$E_{\alpha=0.1\text{-}0.80}$: ΔH: 198, and ΔG: 179	Objective 2.5
49	*Delonix Regia*: Butyl rubber tube waste (1:1)	TiO_2-ZnO (1:1) (30, 20, 10 wt.%)	Netsch TG209F1	25 – 1000	N_2 – 40	5, 10, 20, 35, 55	$E_{\alpha=0.1\text{-}0.7}$ and k_o: 195 and 2.21×10^{21}, 181 and 1.89×10^{17}, 182 and 8.11×10^{14}, 182 and 1.52×10^{17}, 181 and	$E_{\alpha=0.1\text{-}0.80}$: ΔH: 177, and ΔG: 180	Objective 2.5

							1.59×10^{17} by DFM, KAS, OFW, STK, DAE at 20 wt.% TiO_2-ZnO		

β – Heating rates (°C min^{-1})

α – Conversion

°*C* – Temperature

Q – Flowrate of carrier gas (mL min^{-1})

Iso – conversional models – Differential Friedman (DFM), Kissinger-Akahira-Sunose (KAS), Ozawa-Flynn-Wall (OFW), Starink (STK), and Distributed Activation Energy (DAE)

*Kinetics – Average values

*Thermodynamics – Average values based on DFM model at 10 °C min^{-1}

E_α – Activation energy (kJ mol^{-1})

k_o – Frequency factor (s^{-1})

ΔH – Change in enthalpy (kJ mol^{-1})

ΔG – Change in Gibbs free energy (kJ mol^{-1})

ΔS – Change in entropy (kJ mol^{-1} K^{-1})

2.6 Objectives

2.6.1 Overall Objective:

> "To investigate the kinetics and thermodynamic insights for the non-catalytic and catalytic pyrolysis of *Delonix Regia* (DR) and butyl rubber tube (BRT) wastes."

2.6.2 Specific Objectives:

2.6.2.1 Non-catalytic pyrolysis of *Delonix Regia* (DR) biomass: Reaction kinetics, and thermodynamic analysis.

2.6.2.2 Non-catalytic pyrolysis of butyl rubber tube (BRT) waste: Reaction kinetics, and thermodynamic analysis.

2.6.2.3 Non-catalytic co-pyrolysis of DR and BRT (1:1 wt. %) wastes: Reaction kinetics and thermodynamic analysis.

2.6.2.4 In – situ catalytic pyrolysis of DR biomass: Reaction kinetics, and thermodynamic analysis. Three different types of catalysts, such as zeolite (Na – Y), noble metal on activated carbon (10 wt. % Pt/C), and two–metal oxide (1:1 wt. % TiO_2 – ZnO) with loadings from 30 to 10 wt. % were explored.

2.6.2.5 In – situ catalytic co-pyrolysis of DR and BRT (1:1 wt. %) wastes: Reaction kinetics, synergism, and thermodynamic analysis. Three distinct kinds of catalysts, including zeolite (Na – Y), noble metal on activated carbon (10 wt. % Pt/C), and two–metal oxide (1:1 wt. % TiO_2 – ZnO) with dosages varying from 30 to 10 wt. % were studied.

2.7 Summary of the chapter II.

In this chapter II, a thorough literature review of the various feedstocks was performed. In addition, the specific objectives of the thesis were clearly stated.

CHAPTER – III

MATERIALS AND METHODS

3. Materials and Methods

3.1 Raw material

Delonix Regia (DR) biomass was collected as garbage (trunks and branches-fallen debris) on the campus of IIT Guwahati in Assam (India). Butyl rubber tube (BRT) waste material was gleaned from the backyards of local bicycle puncture repair shops near the IIT Guwahati campus. The collected raw materials and BRT waste materials were crushed in a woodcutter (WC1, Nutech, India) and cut with a scissor. These materials were then sieved into particles with a size < 250 µm using a standard test sieve BSS 60 mesh (Ikon™, Instruments, India). Afterward, the particles were washed with DI water, dried in the sun for four days, stored in an air-tight container, and sealed. The co-feed DR and BRT were prepared using mass ratios of 1:1 wt. % of DR and TW in a mortar and pestle and mixed well for better homogeneity. The prepared co-feed materials were used for further studies, including physio-chemical characterization and thermogravimetric analysis.

For the catalytic pyrolysis of DR and the co-pyrolysis of DR and BRT, three different catalysts were utilized. Three types of catalysts were purchased: Na – Y zeolite (SAR – 5.1:1) by Alfa Aesar, USA, zinc oxide Assay (>99.9 wt. %), and titanium oxide Assay (>99.5 wt. %) by Sisco research laboratories, India, and Pt/C (10 wt. % of platinum on activated carbon) by Sigma–Aldrich®, USA.

3.2 Physicochemical characterization

The physicochemical properties of *Delonix Regia* (DR) biomass and Butyl rubber tube (BRT) waste, including proximate analysis, ultimate analysis, and high heating value (HHV), were estimated using ASTM standards. The proximate analysis was performed according to ASTM E1756-08, ASTME872-82, and ASTM E1755-01 for moisture, volatile, and ash contents, respectively. The ultimate analysis was carried out using CHNS elemental analyzer (Euro EA

3000, Euro vector, Italy). The HHV was conducted in an oxygen bomb calorimeter (IS 1350 -1, Toshniwal, India).

The N_2 sorption analyzer (Model: Tristar–II 3020, Make: Micromeritics, USA) was used to characterize the surface area, pore size, and pore volume of each of the three catalysts. All three catalysts were degassed in a vacuum for 6 h at 180 °C to eliminate volatiles or moisture, if any, before analysis. Brunauer–Emmett–Teller (BET) and Barrett–Joyner–Halenda (BJH) models were used to determine the pore size (nm) and pore volume ($cm^3 g^{-1}$) of all three catalysts. The obtained pore size (nm) and volume ($cm^3 g^{-1}$) were: 4.91 and 0.07 for Na – Y, 5.64 and 0.07 for TiO_2 – ZnO, and 3.67 and 0.51 for Pt/C, correspondingly.

3.3 Thermogravimetric analysis

The thermal degradation profile of all raw materials (DR, BRT, co-feed (1:1 wt. %), catalytic DR, catalytic co-feed of DR and BRT) were investigated using a non-isothermal thermogravimetric analyzer unit (TG209F1, Netsch, Germany). The TGA experiments were performed at five heating rates, such as 5, 10, 20, 35, and 55 °C min^{-1}. For all the experimental runs, about 6 mg of sample was taken, 25 – 1000 °C temperature, and (40 mL min^{-1} and 20 mL min^{-1} of carrier and protective gas) of nitrogen gas was utilized to assess the kinetic triplets of the DR, BRT, co-feed (1:1 wt. %), catalytic DR, catalytic co-feed of DR and BRT.

3.4 Assessment of kinetic triplets

kinetic triplets, such as activation energy, E_α (kJ mol^{-1}), pre-exponential factor, k_o (min^{-1}), and reaction model (Z_α), were investigated in this work for all the raw materials (DR, BRT, co-feed (1:1 wt. %), catalytic DR, catalytic co-feed of DR and BRT). The activation energy and pre-exponential factor were computed in MATLAB (Version: R2021a) using five distinct iso-conversational methods and the reaction model by Criado's master plot method.

In general, the pyrolytic decomposition behavior of all the raw materials was described as follows:

$$\text{DR and BRT and DR:BRT (1:1 wt. \%)} \xrightarrow[\substack{\text{Catalysts (30 - 10 wt.\%)} \\ \text{= Na-Y, 10 wt. \% Pt/C, and TiO}_2\text{-ZnO} \\ \Delta = 25 - 1000°C \\ N_2 = 40 mL/\text{min}}]{\textit{Decomposition}} \text{Volatiles + Char}$$

The rate of conversion of all the raw materials was as follows:

$$\frac{d\alpha}{dt} = k(T)f(\alpha) \tag{1}$$

Where *k(T)* = reaction rate constant as a function of temperature, and *f*(α) = differential form of the reaction model as a function of conversion.

The extent of conversion (α) in pyrolytic decomposition was expressed in general as:

$$\alpha = \frac{m_i - m_t}{m_i - m_f} \tag{2}$$

Where m_i, m_f, and m_t = mass of all raw materials at initial (t=0), final (t=final), and any time (t>0), respectively.

The Arrhenius equation governed the rate of reaction *k(T)* of all raw materials:

$$k(T) = k_0 \, exp\left(-\frac{E_\alpha}{RT}\right) \tag{3}$$

Where k_o = pre-exponential factor (min^{-1}), E_α = apparent activation energy (kJ/mol), *R* = universal gas constant (J mol^{-1} K^{-1}), and *T* = absolute temperature (K).

From equations (1) and (3)**:**

$$\frac{d\alpha}{dt} = k_o \, exp\left(-\frac{E_\alpha}{RT}\right) f(\alpha) \tag{5}$$

Now, introduce the heating rate (β) as:

$$\beta = \frac{dT}{dt} = \frac{dT}{d\alpha} \times \frac{d\alpha}{dt} \tag{6}$$

From equations (5) and (6)**:**

$$g(\alpha) = \int_0^{\alpha} \frac{d\alpha}{f(\alpha)} = \frac{k_o}{\beta} \int_{T_0}^{T} exp\left(-\frac{E_\alpha}{RT}\right) dT = \frac{k_o E_\alpha}{\beta R} \int_x^{\infty} u^{-2} exp^{-u} du = \frac{k_o E_\alpha}{\beta R} p(x) \tag{7}$$

Where, $x = \frac{E_\alpha}{RT}$. The above equation (7) was an integral form of reaction rate and had no analytical solution; it was solved by employing several approximation techniques.

3.4.1 The apparent activation energy (E_α) and pre-exponential factor (k_o) by the iso-conversional methods

The apparent activation energy (E_α) and pre-exponential factor (k_o) of all raw materials were investigated by using different iso-conversional methods such as DFM, KAS, OFW, STK, and DAE [59]–[64].

3.4.1.1 Differential Friedman method

Both kinetic factors (E_α and k_o) were estimated in this method [59] without using any approximation, which reduces the possibility of inaccuracy.

The generalized DFM equation was denoted by the following:

$$ln\left(\frac{d\alpha}{dt}\right) = ln\left[\beta\left(\frac{d\alpha}{dT}\right)\right] = ln[k_o f(\alpha)^n] - \frac{E_\alpha}{RT_\alpha} \tag{8}$$

The slope and intercept obtained by graphing $ln\left[\beta\left(\frac{d\alpha}{dT}\right)\right]$ Vs. $\frac{1}{T_\alpha}$ were used to calculate the kinetic factors.

3.4.1.2 Kissinger-Akahira-Sunose method

Both kinetic factors (E_α and k_o) were calculated in this method [60] using a Murray and white approximation (Perez-Maqueda et al., 2005) of $p(x)$ in equation (7);

$$p(x) = x^{-2}exp^{-x} \tag{9}$$

By substituting equation (9) in equation (7)**:**

$$ln\left(\frac{\beta}{T_\alpha^2}\right) = ln\left[\frac{k_oR}{E_\alpha g(\alpha)}\right] - \frac{E_\alpha}{RT_\alpha} \tag{10}$$

The slope and intercept obtained by graphing $ln\left(\frac{\beta}{T_\alpha^2}\right)$ Vs. $\frac{1}{T_\alpha}$ were used further to estimate the kinetic factors.

3.4.1.3 Ozawa-Flynn-Wall method

Both kinetic factors (E_α and k_o) were investigated in this method [61], [62] using Doyle's approximation [66] of $p(x)$ in equation (7);

$$p(x) = \exp(-1.0516x - 5.331) \tag{11}$$

Make use of equation (11) in equation (7)**:**

$$ln(\beta) = ln\left[\frac{k_oE_\alpha}{Rg(\alpha)}\right] - 5.331 - 1.0516\frac{E_\alpha}{RT_\alpha} \tag{12}$$

The slope and intercept obtained by graphing $ln(\beta)$ Vs. $\frac{1}{T_\alpha}$ were used further to determine the kinetic factors.

3.4.1.4 Starink method

Both kinetic factors (E_α and k_o) were found in this method [63] using a Starink approximation [63] of $p(x)$ in equation (7);

$$p(x) = \exp(-1.0008x - 0.312)x^{1.92} \tag{13}$$

Using equation (13) in equation (7):

$$ln\left(\frac{\beta}{T_\alpha^{1.92}}\right) = ln\left[\frac{k_o R^{0.92}}{E_\alpha^{0.92} g(\alpha)}\right] - 0.312 - 1.0008\frac{E_\alpha}{RT_\alpha} \tag{14}$$

The slope and intercept obtained by graphing $ln\left(\frac{\beta}{T_\alpha^{1.92}}\right)$ Vs. $\frac{1}{T_\alpha}$ were used further to determine the kinetic factors.

3.4.1.5 Distributed Activation Energy method

Both kinetic factors (E_α and k_o) were examined in this method [64] using an approximation [64] of $p(x)$ in equation (7);

$$p(x) = 0.6075 - x \tag{15}$$

Applying equation (15) in equation (7):

$$ln\left(\frac{\beta}{T_\alpha^2}\right) = ln\left[\frac{k_o R}{E_\alpha}\right] + 0.6075 - \left[\frac{E_\alpha}{RT_\alpha}\right] \tag{16}$$

The slope and intercept obtained by graphing $ln\left(\frac{\beta}{T_\alpha^2}\right)$ Vs. $\frac{1}{T_\alpha}$ were used further to estimate the kinetic factors.

3.4.2 The reaction mechanism

3.4.2.1 Criado's master plot

The reaction mechanism (Z_α) was studied using Criado's master plot (CMP) for all the heating rates during the pyrolysis of all raw materials. The CMP technique [67] was one of the most extensively used methods for finding the different reaction model behavior during biomass pyrolysis. **Table 4.1** contains the various models in both differential and integral form ($f(\alpha)_{Theo}$ and $g(\alpha)_{Theo}$), respectively.

$$Z(\alpha)_{Theo} = f(\alpha)_{Theo} \times g(\alpha)_{Theo} \tag{17}$$

$$Z(\alpha)_{Exp} = \left(\frac{d\alpha}{dt}\right) \times exp\left(\frac{E_\alpha}{RT}\right) \times \int_{T_0}^{T} exp\left(-\frac{E_\alpha}{RT}\right) dT \tag{18}$$

$$Z(\alpha)_{Exp} = \left(\frac{d\alpha}{dt}\right) \times \frac{E_\alpha}{R} \times exp\left(\frac{E_\alpha}{RT}\right) \times p(x) \tag{19}$$

$$Z(0.5)_{Exp} = \left(\frac{d\alpha}{dt}\right) \times \frac{E_{0.5}}{R} \times exp\left(\frac{E_{0.5}}{RT}\right) \times p(x) \tag{20}$$

Where, $p(x) = 0.00484\, exp\ (-1.0516x)$ [66], and the equations (17) and (20) provided the theoretical and experimental master plots, respectively [46], [51], [58], [68], [69].

3.5 Thermodynamic analysis

The thermodynamic analysis (TD), including a change in Gibbs free energy (*ΔG*), change in enthalpy (*ΔH*), and change in entropy (*ΔS*), were estimated for all raw materials (DR, BRT, co-feed (1:1 wt. %), catalytic DR, catalytic co-feed of DR and BRT) using the following equations [46], [51], [58], [68], [69]:

$$k_o = \frac{\beta \times E_\alpha \times e^{\left(\frac{E_\alpha}{RT_m}\right)}}{RT_m^2} \tag{21}$$

$$\Delta G = E_\alpha + RT_m \times ln\left(\frac{K_B T_m}{hk_o}\right) \tag{22}$$

$$\Delta H = E_\alpha - RT_m \tag{23}$$

$$\Delta S = \frac{\Delta H - \Delta G}{T_m} \tag{24}$$

Where T_m = peak decomposition temperature, h = Planck's constant (6.626 × 10^{-34} Js), and K_B = Boltzmann constant (1.381 × 10^{-23} J/K).

3.6 Pyrolysis performance indices

The values of pyrolysis performance indices (PPI) such as flammability index (C, K^{-2} min^{-1}), ignition index (D_i, min^{-3}), burnout index (D_b, min^{-4}), combustion index (S, K^{-3} min^{-2}), and devolatilization index (D_v, K^{-3} min^{-1}) were ascertained for all raw materials (DR, BRT, co-feed (1:1 wt. %), catalytic DR, catalytic co-feed of DR and BRT) at various heating rates (5, 10, 20, 35, and 55 °C min^{-1}) applying the following equations [46], [51], [58], [68], [69]:

$$C = \left(\frac{-R_p}{T_i^2}\right) \tag{25}$$

$$D_i = \left(\frac{-R_p}{t_i \times t_p}\right) \tag{26}$$

$$D_b = \left(\frac{-R_p}{\Delta t_{0.5} \times t_b \times t_p}\right) \tag{27}$$

$$S = \left(\frac{-R_p \times -R_v}{T_i^2 \times T_b}\right) \tag{28}$$

$$D_v = \left(\frac{-R_p \times -R_v}{\Delta T_{0.5} \times T_i \times T_p}\right) \tag{29}$$

Where, R_p = maximum decomposition rate (wt.% min^{-1}), R_v = mean decomposition rate (wt.% min^{-1}), t_i = ignition time (min), t_p = maximum decomposition time (min), t_b = burnout time (min), T_i = ignition temperature (K), T_b = burnout temperature (K), T_p = maximum decomposition temperature (K), $\Delta t_{0.5}$ = time (min) interval for half of the R_p, and $\Delta T_{0.5}$ = temperature (K) interval for half of the R_p.

3.7 Summary of the chapter III.

In this chapter III, the detailed experimental methodology and estimation of modeling equations for kinetic and thermodynamic analysis were provided.

CHAPTER – IV

MODELS- ISO-CONVERSIONAL EQUATIONS EVALUATION

4. Models-Iso-conversional Equations Evaluation

4.1 Solid-state reaction kinetics: Homogenous to heterogeneous processes

All the chemical kinetic concepts were developed first in the gas phase homogenous reactions based on generalizations from empirical studies. Later on, these concepts were applied to the solution phase heterogeneous reactions and eventually to the solid-state processes. Concepts were not developed separately from the solid-state kinetics due to similarities to some homogenous reactions. For instance, historically, the empirical Arrhenius equation was developed first, and then, later on, the theoretical justification and applications of this equation were established. The Arrhenius equation was developed first for the gases and solutions over the collision and transition-state theories, and then, later on, similar justification and applications of this equation were established for solid-state kinetics as well [70]. Therefore, from the homogenous kinetics, many of the solid-state kinetics principles evolved. However, applications of these principles were different because of the difference between the phase of the solutions, like gases, liquids, and solids.

Rate laws:

Solid-state reactions are many types; for a simple understanding of the reaction kinetics, let us consider the example of a single reactant decomposition reaction illustrated as follows:

$$A_{(S)} \rightarrow B_{(S)} + C_{(g)} - - - - - (1)$$

Here,

$A_{(s)}$ is the reactant in the solid phase

$B_{(s)}$ is the desired product in the solid phase

$C_{(s)}$ is the undesired product in the gas phase

According to a power law, the reaction rate is proportional to the reactant or product concentration change per unit of time.

$$A_{(S)} \rightarrow B_{(S)} + C_{(g)} ------ (1)$$

Rate of the reaction ∞ $[A]^n \; or \; ([A_0] - [B])^n \; ([A_0] - [C])^n$

A_0 is the initial concentration of the reaction

n is the order of the reaction (in this case, n=1)

The reaction rate usually studies either reactant or product with decreased and decreasing concentrations. Therefore, the overall reaction rate law expression for the above equation is as follows:

$$A_{(S)} \rightarrow B_{(S)} + C_{(g)} ------ (1)$$

Rate of the reaction ∞ $[A]^n \; or \; ([A_0] - [B])^n \; ([A_0] - [C])^n$

$$\infty - \frac{d[A]}{dt} \infty + \frac{d[B]}{dt} \infty + \frac{d[C]}{dt}$$

$$= -k[A]^n = -k([A_0] - [B])^n = -k\,([A_0] - [C])^n$$

Here,

k is the proportionality of the reaction

n is the order of the reaction (in this case, n=1)

if the reaction is an elementary unimolecular (in this case, n=1) reaction, the rate expression would be

$$Rate = -\frac{d[A]}{dt} = k[A] - - - - - - (2)$$

Integrating the above equation from A_0 to A and 0 to t, the rate expression becomes

$$\frac{ln[A]}{[A_0]} = kt - - - - - - (3)$$

The above expression was usually used for solution kinetics. For the solid-state kinetics, the concentration of the samples was not in the solution phase, so the reactivity was not the same throughout the samples, and the concentration did not reflect the reactivity. By the use of thermal analytical methods, solid-state kinetics can be studied. The thermal analytical methods were conducted in powder XRD, NMR, TGA, DTG, and DSC [71]–[73]. These methods measure the sample weights at various atmospheres, such as nitrogen, argon, helium, oxygen, carbon dioxide, and carbon monoxide, keeping isothermal and non-isothermal conditions. The obtained sample weights data from the thermal analytical instruments were converted to a normalized form called fractional conversion (α). The fractional conversion has a range of 0 to 1, and it measures the progress of the reaction as a function of temperature and time. The fractional conversion of TGA studies can be calculated as follows for both isothermal and non-isothermal processes:

$$\alpha = \frac{m_0 - m_t}{m_0 - m_\infty} - - - - - - (4)$$

Here,

m_0 is the mass of the sample at an initial time,

m_i is the mass of the sample at time t,

m_∞ is the mass of the sample at the final time.

By the use of fractional conversion (α), the solution kinetics reaction rate expression can be defined as follows:

$$Rate = -\frac{d[\alpha]}{dt} = k(1-\alpha) - - - - - - (5)$$

Integrating the above equation from *0* to *α* and *0* to *t*, the rate expression becomes

$$-ln(1-\alpha) = kt - - - - - - (6)$$

For the solid-state reactions, the kinetic modeling and mechanism could depend on several factors, such as the solid sample particles' geometry (size and shape), nuclei formation rate, diffusional properties, and interface advance. All these factors lead to several decomposition models that do not happen in homogenous kinetics. All these models are listed in following **Table 4.1.**

Table 4.1 Expressions for different solid reaction models

Model	**Model code**	**Differential form** $f(\alpha) = \frac{1}{k}\frac{d\alpha}{dt}$	**Integral form** $g(\alpha) = kt$	$Z(\alpha) = f(\alpha) \times g(\alpha)$
Nucleation model				
Power law	P2	$2(\alpha)^{1/2}$	$(\alpha)^{1/2}$	$2(\alpha)^{1/2} \times (\alpha)^{1/2}$
Power law	P3	$3(\alpha)^{2/3}$	$(\alpha)^{1/3}$	$3(\alpha)^{2/3} \times (\alpha)^{1/3}$
Power law	P4	$4(\alpha)^{3/7}$	$(\alpha)^{1/4}$	$4(\alpha)^{3/7} \times (\alpha)^{1/4}$
Avrami-Erofeyev	A2	$2(1-\alpha)[-ln(1-\alpha)]^{1/2}$	$[-ln(1-\alpha)]^{1/2}$	$2(1-\alpha)[-ln(1-\alpha)]^{1/2} \times [-ln(1-\alpha)]^{1/2}$
Avrami-Erofeyev	A3	$3(1-\alpha)[-ln(1-\alpha)]^{2/3}$	$[-ln(1-\alpha)]^{1/3}$	$3(1-\alpha)[-ln(1-\alpha)]^{2/3} \times [-ln(1-\alpha)]^{1/3}$
Avrami-Erofeyev	A4	$4(1-\alpha)[-ln(1-\alpha)]^{3/4}$	$[-ln(1-\alpha)]^{1/4}$	$4(1-\alpha)[-ln(1-\alpha)]^{3/4} \times [-ln(1-\alpha)]^{1/4}$
Geometrical contraction models				
Contracting area	R2	$2(1-\alpha)^{1/2}$	$1-(1-\alpha)^{1/2}$	$2(1-\alpha)^{1/2} \times 1-(1-\alpha)^{1/2}$

Contracting volume	R3	$3(1-\alpha)^{2/3}$	$1-(1-\alpha)^{1/3}$	$3(1-\alpha)^{2/3} \times 1-(1-\alpha)^{1/3}$
Diffusion models				
1-dimensional	D1	$\frac{1}{2}(\alpha)$	$(\alpha)^2$	$\frac{1}{2}(\alpha) \times (\alpha)^2$
2-dimensional	D2	$-ln(1-\alpha)^{-1}$	$(1-\alpha)ln(1-\alpha)+\alpha$	$-ln(1-\alpha)^{-1} \times (1-\alpha)ln(1-\alpha)+\alpha$
3-dimensional	D3	$\frac{3(1-\alpha)^{2/3}}{2(1-(1-\alpha)^{1/3})}$	$\left[1-(1-\alpha)^{1/3}\right]^2$	$\frac{3(1-\alpha)^{1/2}}{2(1-(1-\alpha))^{1/3}} \times \left[1-(1-\alpha)^{1/3}\right]^2$
Reaction order models				
Zero order	F0	1	α	$1 \times \alpha$
First order	F1	$(1-\alpha)$	$-ln(1-\alpha)$	$(1-\alpha) \times -ln(1-\alpha)$
Second order	F2	$(1-\alpha)^2$	$[1-(1-\alpha)^{-1}]/-1$	$(1-\alpha)^2 \times [1-(1-\alpha)^{-1}]/-1$
Third order	F3	$(1-\alpha)^3$	$[1-(1-\alpha)^{-2}]/-2$	$(1-\alpha)^3 \times [1-(1-\alpha)^{-2}]/-2$
Fourth order	F4	$(1-\alpha)^4$	$[1-(1-\alpha)^{-3}]/-3$	$(1-\alpha)^4 \times [1-(1-\alpha)^{-3}]/-3$
Fifth order	F5	$(1-\alpha)^5$	$[1-(1-\alpha)^{-4}]/-4$	$(1-\alpha)^5 \times [1-(1-\alpha)^{-4}]/-4$

Solid-state reaction: kinetic modeling

From the above equations (5) and (6), the following general expressions can be written:

$$Rate = -\frac{d\alpha}{dt} = kf(\alpha) - - - - - (7)$$

$$g(\alpha) = kt - - - - - (8)$$

Here,

f(α) is the differential form of the kinetic reaction model

g(α) is the integral form of the kinetic reaction model

from theArrhenius equation [74], the temperature dependence of the rate constant (*k*) of the reaction was calculated as follows:

$$k = k_0 e^{\left(\frac{-E_\alpha}{RT}\right)} - - - - - (9)$$

Here, k_0 is the frequency factor

-E_α is the activation energy at conversion *α*

R is the universal gas constant

T is the absolute temperature

Substitute the above equation (9) in equations (7) and (8), then the resulting equation as follows:

$$Rate = -\frac{d\alpha}{dt} = k_0 e^{\left(\frac{-E_\alpha}{RT}\right)} f(\alpha) - - - - - (10)$$

$$g(\alpha) = k_0 e^{\left(\frac{-E_\alpha}{RT}\right)} t - - - - - (11)$$

Solid-state reaction: methods

There are many methods available to study solid-state kinetics. These methods were generalized into two categories. Those are

1. Experimental methods
2. Computational methods

Experimental methods: Experimental methods were further categorized into two methods. Those are

1. Isothermal methods
2. Non-isothermal methods.

Isothermal methods

In these methods, the process occurs at a constant temperature (i.e., isothermal). The kinetics were determined by analyzing the conversion (α) vs. time (t) data plot.

Non-isothermal methods

In these methods, the process occurs at varying temperatures (i.e., dynamic mode) at one or more heating rates (β). In solid-state kinetics, these methods are prevalent and have been used in homogenous kinetics [75]. The kinetics were determined by analyzing the conversion (α) vs. temperature (T) data plot. The heating rate (β) (K/min) is usually linear, and it is used to raise the temperature (T) at time t from the initial temperature (T_0).

The mathematical relation between the heating rate and temperature, and time is as follows:

$$T = T_0 + \beta t - - - - - (12)$$

The mathematical relation between the conversion and temperature and time is as follows:

$$\frac{d\alpha}{dT} = \frac{d\alpha}{dT} * \frac{dt}{dT} - - - - - - (13)$$

Here,

$\frac{d\alpha}{dT}$ is the non -isothermal reaction rate

$\frac{d\alpha}{dT}$ is the isothermal reaction rate

$\frac{dt}{dT}$ is the reaction rate

$\beta = \frac{dT}{dt}$; substitute equation (10) in equation (13) as follows:

$$Rate = -\frac{d\alpha}{dt} = k_0 e^{\left(\frac{-E_\alpha}{RT}\right)} f(\alpha) - - - - - - (10)$$

$$\frac{d\alpha}{dT} = \frac{d\alpha}{dT} * \frac{dt}{dT} - - - - - - (13)$$

$$\frac{d\alpha}{dT} = \frac{k_0 e^{\left(\frac{-E_\alpha}{RT}\right)}}{\beta} f(\alpha) - - - - - - (14)$$

The above equation (14) represented the differential form of non-isothermal solid-state kinetic rate law.

An integral form of rate law expression is required to get more accurate solid-state kinetic results. Therefore, integrate the above equation (14)

$$g(\alpha) = \int_0^\alpha \frac{d\alpha}{f(\alpha)} = \frac{k_o}{\beta} \int_{T_0}^{T} exp\left(\frac{-E_\alpha}{RT}\right) dT - - - - - - (15)$$

The above equation (15) represented the integral form of non-isothermal solid-state kinetic rate law.

The above integral is known as "temperature integral" and has no analytic solution. Some methods using non-linear heating programs, such as non-Arrhenius temperature functions of the rate constant or parabolic and hyperbolic functions, have been reported to get the exact solution. However, these methods are not widely implemented. To transfer the temperature integral in equation (15) into general form, let us assume $x = \left(\frac{-E_\alpha}{RT}\right)$ then the equation (15) becomes as follows:

$$g(\alpha) = \frac{k_o E_\alpha}{\beta R} \int_x^\infty \frac{e^{-x} E_\alpha}{x^2} dx - - - - - (16)\, ; if\ p(x) = \int_x^\infty \frac{e^{-x} E_\alpha}{x^2} dx$$

Then the equation (16) becomes as follows:

$$g(\alpha) = \frac{k_o E_\alpha}{\beta R} p(x) - - - - - (17)$$

Here, the exponential integral *p(x)* can be found in the following expressions.

To estimate the exponential/temperature integrals, the following approaches were used:

1. Numerically calculate the value of *p(x)*
2. Convert the value of *p(x)* to an approximate form that can be integrated
3. By the use of a series of expansions approximating the value of *p(x)*

The third approach was widely used, and two series expansions were mainly used for approximating the temperature integral; those are as follows:

I. An asymptotic series expansion:

$$p(x) = \frac{e^{-x}}{x^2}\left[1 - \left(\frac{2!}{x}\right) + \left(\frac{3!}{x^2}\right) - \left(\frac{4!}{x^3}\right) + .. + (-1)^n \left(\frac{(n+1)!}{x^n}\right) + ..\right]$$

II. The Schlömilch series expansion:

$$p(x) = \frac{e^{-x}}{x(x+1)}\left[1 - \left(\frac{1}{(x+2)}\right) + \left(\frac{2}{(x+2)(x+3)}\right) - \left(\frac{4}{(x+2)(x+3)(x+4)}\right) + ..\right]$$

Many authors have developed approximations for the temperature integral [76] and have been reported. Doyle [77] and Senum-Yang [78] of the approximations had great attention and were frequently used for the exponential/temperature integrals.

Doyle approximation

Doyle [77] proposed the approximation using the 1st three terms of the Schlömilch series expansion. The proposed approximation is as follows:

$$\log p(x) = -A - Bx$$

Doyle calculated the parameters in the above equation 2.315 and 0.4567 for the *A* and *B*

$$\log p(x) = -2.3150.467x - - - - - - (18)$$

Senum-Yang approximation

Senum and Yang [78] proposed a more accurate non-linear approximation for the temperature integral.

If variables in Eq. (21) are transformed so that *x* = *zy*, the integralbecomes

If the variables in Eq. (16) were transformed to *x* = *yz*, then the equation (8) becomes as follows:

$$g(\alpha) = \frac{k_o E_\alpha}{\beta R} \int_x^\infty \frac{e^{-x} E_\alpha}{x^2} dx - - - - - - (16)\,; x = yz$$

$$g(\alpha) = \frac{k_o E_\alpha}{\beta Rz} \int_1^\infty \frac{e^{-zy} E_\alpha}{y^2} dy - - - - - - (19)$$

Then equation (19) becomes as follows:

$$g(\alpha) = \frac{k_o E_\alpha}{\beta Rz} E_2(z) - - - - - - (20)$$

E_2 (z) or E_v (z) (“v” is an integer), is a well-known integral for z > 0, the E_v (z)/z as following continued fraction:

$$\frac{E_v(z)}{z}=\frac{e^{-z}}{z}\left[\cfrac{1}{z+\cfrac{v+0}{1+\cfrac{1}{z+\cfrac{v+1}{1+\cfrac{2}{z+\cfrac{v+2}{1+\cfrac{3}{z+\cfrac{v+3}{1+\cfrac{4}{z+\cdots}}}}}}}}}\right] ------(21)$$

In the above-continued fraction, the truncating number of terms such as 1st, 2nd, 3rd, and 4th terms were 1st, 2nd, 3rd, and 4th order degree rational approximations, respectively, known as Senum-Yang approximation and illustrated in the following expressions: for 1st, 2nd, 3rd, and 4th degree

$$\begin{aligned}
p(x) &= \frac{e^{-x}}{x}*\frac{1}{(x+2)}\\
&= \frac{e^{-x}}{x}*\frac{(x+4)}{(x^2+6x+6)}\\
&= \frac{e^{-x}}{x}*\frac{(x^2+10x+18)}{(x^2+12x^2+36x+24)}\\
&= \frac{e^{-x}}{x}*\frac{(x^3+18x^2+86x+96)}{(x^4+20x^3+120x^2+240x+120)}
\end{aligned}$$

4.2 Solid-state reaction: Iso-conversional methods

Two groups of methods are available to evaluate the solid-state kinetics data for isothermal and non-isothermal processes. These methods were generalized into two categories. Those are:

4.2.1 Model-fitting methods

4.2.2 Model-free methods

All these two groups of methods are given in **Figure 4.1**

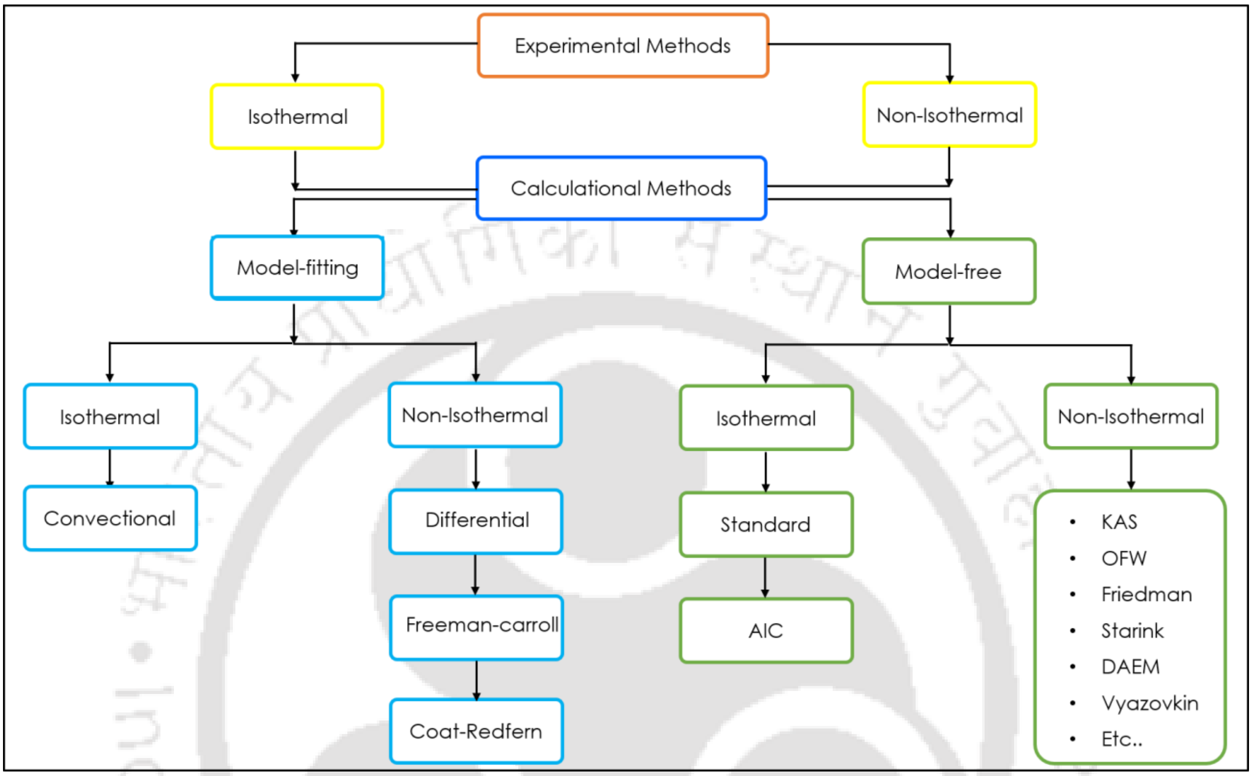

Figure 4.1 Classification of Solid-state reaction methods: model-fitting and model-free methods.

Table 4.2 Comparison of merits and demerits of model-fitting and model-free methods.

Method	Merits	Demerits
Model-fitting	• They are applied for both isothermal and non-isothermal processes. • They are generally used to predict the mechanism of a reaction based on the single heating rate, for instance, the Coats and Redfern method. • Estimates kinetic parameters using all available information.	• These methods lead to questionable interpretations when using forcible fitting of the kinetic parameters (E_α and k_o). • Because of the single heating rate, it is not always possible to predict the proper reaction

		mechanism, and there is also variation in activation energies due to heat/mass transfer effects. - Without prior knowledge of reaction models, it is impossible to obtain kinetic results with lower fluctuations and higher correlation coefficients. Mainly, non-isothermal process TGA data get highly ambiguous kinetic parameters
Model-free	- These methods are used extensively in heterogeneous solid-state kinetics reactions for both isothermal and non-isothermal processes. - Used for multiple heating rates to estimate the proper kinetic parameters - Applied to the reaction models without any moralistic assumptions, and it does not require any prior knowledge of reaction models. - All the iso-conversional methods were model-free methods and used to calculate the kinetic parameters such as activation energy (E_α) and frequency factor (k_o) at the progressive conversion (α). - Temperature integral approximations are used for analyzing the non-isothermal data	- Limitations/Errors/Accuracy of the approximation are debatable, and a more significant number of approximations continue to appear. - Differential methods are less stable and produce deviations in activation energies. - Only accurate for single-step reactions; the points are not on a straight line for multiple reactions.

	• These methods produce less fluctuating kinetic results with high correlation coefficients. • Integral model-free methods are more stable and produce highly accurate activation energies. Furthermore, advanced models are proposed, for example, the VYZ method.	

4.2.1 Model-fitting methods:

These methods used different models to analyze the solid-state kinetics data for isothermal and non-isothermal processes. Based on the observations, the best statistical fit is the best valid model to calculate the good values of activation energy (E_α) and frequency factor (k_0). These methods were further classified for the two processes. Those are:

1. Isothermal model-fitting methods
2. Non-isothermal model-fitting methods

Isothermal model-fitting methods: these methods were also called conventional methods. These methods were simple to use and involved two steps. 1st step, rate constant (k) determination of the model according to the experimental data that fit for best one by the use of equation (8). 2nd step, activation energy (E_α), and frequency factor (k_0) determination of the model according to the experimental data that fits best by the use of the Arrhenius equation (9). However, this method was not used for heterogeneous solid-state kinetics and was mainly applied to homogenous kinetics.

Non-isothermal model-fitting methods: in these methods, there are many model fittings methods available to calculate the (activation energy (E_α) and frequency factor (k_0)) of the non-isothermal processes data. It involves three kinetic parameters as E_α, k_0, and model. These methods were used and extensively used in heterogeneous solid-state kinetics reactions [79]–[82], and they continue to appear. However, these methods were not accurate and not recommended due to the following reasons:

1. They assume the constant value of a constant kinetic triplet (E_{α}, k_0, and model).
2. They determined the kinetic triplet (E_{α}, k_0, and model) at the single heating rate.
3. Due to the single heating rate, the reaction mechanism study was not always sufficient.

There are several non-isothermal model-fitting methods are available, and some of them are discussed below:

Direct differential method (DDM):

This method [83] will give the best linear fit, and it takes the differential form of the non-isothermal kinetic rate law (equation 14) expression as follows:

$$\text{Non} - \text{isothermal rate law} = \frac{d\alpha}{dT} = \frac{k_0 e^{\left(\frac{-E_{\alpha}}{RT}\right)}}{\beta} f(\alpha) - - - - - (14)$$

Rearrange the above equation and apply the logarithm on both sides

$$ln \frac{d\alpha/_{dT}}{f(\alpha)} = ln \frac{k_0}{\beta} - \frac{-E_{\alpha}}{RT} - - - - - - (22)$$

Plot a graph between the $f(\alpha)$ *vs* $1/T$ from the above equation (22); slope = $\frac{-E_{\alpha}}{RT}$ and intercept = $ln \frac{k_0}{\beta}$.

Freeman-Carroll difference-differential method (FCDM):

This method [84] was developed by assuming the order of the reaction model, i.e., $f(\alpha) = (1 - \alpha)^n$. This method was used for single heating rate input. The differential form of the non-isothermal kinetic rate law (equation 14) expression is as follows:

$$\text{Non} - \text{isothermal rate law} = \frac{d\alpha}{dT} = \frac{k_0 e^{\left(\frac{-E_{\alpha}}{RT}\right)}}{\beta} f(\alpha) - - - - - (14)$$

Apply the logarithm on both sides.

$$ln\frac{d\alpha}{dT} = ln\frac{k_0}{\beta} - \frac{-E_\alpha}{RT} + lnf(\alpha) - - - - - (23)$$

If we take the incremental difference (Δ) in the variables of the above equation, then:

$$\Delta ln\frac{d\alpha}{dT} = -\frac{E_\alpha}{R}\Delta\frac{1}{T} + lnf(\alpha) - - - - - (24)$$

Rearrange the above equation (24) as follows:

$$\frac{\Delta ln\frac{d\alpha}{dT}}{\Delta\frac{1}{T}} = \frac{\Delta lnf(\alpha)}{\Delta\frac{1}{T}} - \frac{E_\alpha}{R}\ or\ \frac{\Delta ln\frac{d\alpha}{dT}}{\Delta lnf(\alpha)} = \frac{E_\alpha}{R}\frac{\Delta\frac{1}{T}}{\Delta lnf(\alpha)} - - - - - (25)$$

Plot the graph between the $\frac{\Delta ln\frac{d\alpha}{dT}}{\Delta\frac{1}{T}}$ or $\frac{\Delta ln\frac{d\alpha}{dT}}{\Delta lnf(\alpha)}$ vs $\frac{\Delta lnf(\alpha)}{\Delta\frac{1}{T}}$ from the above equation (25).

From the above slope or intercept, activation energy can be calculated.

Coats-Redfern method (CR): This method [85] was developed by Coats and Redfern and used the asymptotic series expansion for the integral temperature approximation (p(x)). This method was used for single heating rate input. They assumed the 1st order of the reaction model, i.e., but it has been generalized to other reaction models. The integral form of the non-isothermal kinetic rate law CR method expression is as follows:

$$ln\frac{g(\alpha)}{T^2} = ln\left(\frac{k_0 R}{\beta E_\alpha}\left[1 - \left(\frac{2RT_{exp}}{E_\alpha}\right)\right]\right) - \frac{E_\alpha}{RT} - - - - - - -(26)$$

Here,

T_{exp} is the experimental mean temperature

Plot a graph between $ln\frac{g(\alpha)}{T^2}$ vs $\frac{1}{T}$ from the above equation (26) for slope = activation energy, and intercept = frequency factor.

Kissinger method: This method [86], [87] was developed by Kissinger by assuming the order of the reaction model, i.e., $f(\alpha) = (1-\alpha)^n$ from the Kissinger observation at the 2nd derivative of the equation 14, i.e., $\left(\frac{d^2\alpha}{dT^2}\right)$ was zero, and the resultant expression as follows:

$$\frac{E_\alpha \beta}{RT_m^2} = k_0(n(1-\alpha_m)^{n-1})e^{\frac{-E_\alpha}{RT_\alpha}} ------(27)$$

Here,

T_m is the maximum rate of temperature

α_m is the maximum rate of conversion

n is the order of the reaction

Apply the logarithm and rearrange the above equation (27) as follows:

$$ln\frac{\beta}{T_m^2} = ln\left(\frac{k_0R(n(1-\alpha_m)^{n-1})}{E_\alpha}\right) - \frac{E_\alpha}{RT_m} ------(28)$$

Plot a graph between $ln\frac{\beta}{T_m^2}$ vs $\frac{1}{T_m}$ from the above equation (28) for slope = activation energy, and intercept = frequency factor.

The above equation (28) was the generalized form, and it can be applied to any reaction order [88]. This method is not an iso-conversional method because, at the progressive conversion, it does not calculate the activation energy (E_α) valuesbut rather assumes a constant E_α, the same as other methods. Therefore, this method cannot detect the reaction complexities upon the reaction [89].

4.2.2 Model-free methods:

In this method, different models were used to analyze the solid-state kinetics data for isothermal and non-isothermal processes without any moralistic assumptions. All the iso-conversional methods were model-free methods and used to calculate the kinetic parameters such as activation energy (*E*$_\alpha$) and frequency factor (k_0) at the progressive conversion (α) [90]. The frequency factor (k_0) can be determined from the intercept of the linear equation but requires a moralistic assumption. Therefore, for more accuracy, only activation energies were reported by this method. These methods were also called multi-curve methods [91], [92] because several kinetic curves were required to analyze data. These methods were called iso-conversional methods due to multi calculations, from various kinetic curves, at different heating rates on the same conversion value. These methods are further classified for the two processes. Those are:

3. Isothermal model-free methods
4. Non-isothermal model-free methods

The Isothermal model-free methods were further classified into:

Standard iso-conversional method

Friedman's iso-conversional method

Standard iso-conversional method: this method [93],[80] can be used derived from the isothermal homogenous kinetic rate law equation (11) as follows:

$$g(\alpha) = k_0 e^{\left(\frac{-E_\alpha}{RT}\right)} t - - - - - - (11)$$

Apply the logarithm on both sides.

$$lng(\alpha) = lnk_0 \frac{-E_\alpha}{RT} + lnt - - - - - - (29)$$

Rearrange the above equation (29) as follows:

$$-lnt = ln\left(\frac{k_0}{g(\alpha)}\right) - \frac{E_\alpha}{RT} - - - - - - (30)$$

Plot a graph between the $-lnt$ vs $\frac{1}{T}$ from the above equation (30) for each α:

$$-lnt_\alpha = ln\left(\frac{k_0}{g(\alpha)}\right)_\alpha - \frac{E_\alpha}{RT_\alpha} - - - - - - (31)$$

Friedman's iso-conversional method: this method [59] can be used derived from the differential form of the isothermal homogenous kinetic rate law equation (10) as follows:

$$Rate = -\frac{d\alpha}{dt} = k_0 e^{\left(\frac{-E_\alpha}{RT}\right)} f(\alpha) ------ (10)$$

Apply the logarithm on both sides.

$$-ln\frac{d\alpha}{dt} = ln\big(k_0 f(\alpha)\big) - \frac{E_\alpha}{RT} ------ (32)$$

Plot a graph between the $-ln\frac{d\alpha}{dt}$ vs $\frac{1}{T}$ from the above equation (32) for each α.

$$-ln\left(\frac{d\alpha}{dt}\right)_\alpha = ln\big(k_0 f(\alpha)\big)_\alpha - \frac{E_\alpha}{RT_\alpha} ------ (33)$$

Non-isothermal model-free/iso-conversional methods:

In these methods, there are many model-free/iso-conversional methods available to calculate the (activation energy (E_α) and frequency factor (k_0)) of the non-isothermal processes data. It involves three kinetic parameters as E_α, k_0, and model. These methods were used and extensively used in heterogeneous solid-state kinetics reactions [84]–[86], [94], and they continue to appear. However, these methods required the integral temperature approximation (as discussed above) for analyzing the non-isothermal data:

1. Doyle approximation has been used for the linear approximation (which was less accurate) in the Ozawa and Flynn-Wall (OFW) methods
2. Senum-Yang approximation has been used for the non-linear approximation (which was more accurate) in the Vyazovkin methods.

There are several non-isothermal model-free/iso-conversional methods are available, and some of them are discussed below:

Ozawa and Flynn-Wall (OFW) method: This method was developed by Ozawa and Flynn-

Wall [84] independently. This method was used for variable heating rate input. This method can be used derived from the differential form of the non-isothermal kinetic rate law equation (17) as follows:

$$Rate = g(\alpha) = \frac{k_o E_\alpha}{\beta R} p(x) - - - - - (17)$$

Apply the logarithm on both sides.

$$lng(\alpha) = ln\frac{k_o E_\alpha}{\beta R} + lnp(x) - - - - - (34)$$

Substitute Doyle's approximation $lnp(x) = -2.315 + 0.457x$ in the above equation (34)

$$lng(\alpha) = ln\frac{k_o E_\alpha}{\beta R} - 2.315 + 0.457x - - - - - (35)$$

Substitute the $x = \frac{E_\alpha}{RT}$ and rearrange the above equation (35)

$$ln\beta = ln\frac{k_o E_\alpha}{g(\alpha)R} - 2.315 - 0.457\frac{E_\alpha}{RT} - - - - - (36)$$

Plot a graph between the $ln\beta$ vs $\frac{1}{T}$ from the above equation (36) for each α.

$$ln\beta = ln\frac{k_{o\alpha} E_\alpha}{g(\alpha)R} - 2.315 - 0.457\frac{E_\alpha}{RT_\alpha} - - - - - (37)$$

Modified Coats-Redfern (CR) method: this method was developed by Burnham and Braun [95] have transformed the model-fitting CR method equation (26). The integral form of the non-isothermal kinetic rate law Modified Coats-Redfern method expression is as follows:

$$ln\frac{g(\alpha)}{T^2} = ln\left(\frac{k_0 R}{\beta E_\alpha}\left[1 - \left(\frac{2RT_{exp}}{E_\alpha}\right)\right]\right) - \frac{E_\alpha}{RT} - - - - - - -(26)$$

Rearrange the above equation

$$ln\frac{\beta}{T^2} = ln\left(\frac{k_0 R}{E_\alpha g(\alpha)}\left[1 - \left(\frac{2RT_{exp}}{E_\alpha}\right)\right]\right) - \frac{E_\alpha}{RT} - - - - - - -(38)$$

Plot a graph between the $ln\frac{\beta}{T^2}$ vs $\frac{1}{T}$ from the above equation (38) for each α.

$$ln\left(\frac{\beta}{T^2}\right)_{\alpha} = ln\left(\frac{k_{0\alpha}R}{E_{\alpha}g(\alpha)}\left[1-\left(\frac{2RT_{exp}}{E_{\alpha}}\right)\right]\right)-\frac{E_{\alpha}}{RT_{\alpha}} - - - - - - - (39)$$

Kissinger-Akahira-Sunose method (KAS): this method was developed by Kissinger and Akahira-Sunose independently [87]. This method can be used to derive the modification of the Kissinger equation from the non-isothermal kinetic rate law equation (17) as follows:

$$Rate = g(\alpha) = \frac{k_o E_{\alpha}}{\beta R}p(x) - - - - - (17)$$

Apply the logarithm on both sides.

$$lng(\alpha) = ln\frac{k_o E_{\alpha}}{\beta R} + lnp(x) - - - - - (34)$$

Substitute Doyle's approximation $lnp(x) = -2.315 + 0.457x$ in the above equation (34)

$$lng(\alpha) = ln\frac{k_o E_{\alpha}}{\beta R} - 2.315 + 0.457x - - - - - (35)$$

Substitute the $x = \frac{E_{\alpha}}{RT}$ and rearrange the above equation (35)

$$ln\beta = ln\frac{k_o E_{\alpha}}{g(\alpha)R} - 2.315 - 0.457\frac{E_{\alpha}}{RT} - - - - - (36)$$

Plot a graph between the $ln\beta$ vs $\frac{1}{T}$ from the above equation (36) for each α.

$$ln\beta = ln\frac{k_{o\alpha} E_{\alpha}}{g(\alpha)R} - 2.315 - 0.457\frac{E_{\alpha}}{RT_{\alpha}} - - - - - (37)$$

Starink method (STK): this method was developed by M.J Starink [63]. This method used the integral temperature approximations of senum and yang (4th order), starink approximations of Coats and Redfern's in their studies, and finally derived the STK model. This model is derived from the non-isothermal kinetic rate law equation (17) as follows:

$$Rate = g(\alpha) = \frac{k_o E_\alpha}{\beta R} p(x) ------ (17)$$

Apply the logarithm on both sides.

$$lng(\alpha) = ln\frac{k_o E_\alpha}{\beta R} + lnp(x) ------ (35)$$

Substitute the $x = \frac{E_\alpha}{RT}$ and rearrange the above equation (34)

$$ln\frac{\beta}{T^{1.92}} = C_s - 1.0008\frac{E_\alpha}{RT} ------ (38)$$

Here,

C_s is the constant

Plot a graph between the $ln\frac{\beta}{T^{1.92}}$ vs $\frac{1}{T}$ from the above equation (38), slope = $1.0008\frac{E_\alpha}{RT}$ for each α.

4.3 Summary of the chapter IV.

The following statements were obtained from the chapter IV:

- The classification of solid-state reactions as well as the merits and demerits of model-fitting and model-free methods, were discussed.
- The mathematical expression of differential and integral forms for different solid-state reaction models was presented.

CHAPTER – V

RESULTS AND DISCUSSIONS

5. Results and Discussions

5.1 Insights on kinetic triplets and thermodynamic analysis of *Delonix Regia* biomass

5.1.1 Physicochemical characterization

The Physicochemical characteristics such as proximate, ultimate, and HHV of the DR biomass were studied **(Table 5.1.1)**. According to this Table, the DR biomass has low (< 9 %) moisture content and was thus more amenable to pyrolysis. DR biomass contains high volatile matter (about 73 %), and low ash (about 1 %), which indicates the possibility of enhanced pyrolytic properties. The elemental analysis demonstrated high carbon (about 45 %), low hydrogen and nitrogen (about 6 and 1.2 %), and negligible sulphur contents, which was similar to other reports [2], [5]. High carbon content indicates a high heating value (HHV) of the fuel due to a linear relationship between them [96]. The HHV of the DR biomass (about 17.5 MJ kg^{-1}) was consistent with other feedstock such as moringa husk, cascabel thevetia, manikara zapote, DR seeds, pods, and biomass respectively [2], [5], [39] and then found to be a potential feedstock for the pyrolysis.

Table 5.1.1: Physicochemical characterization of *Delonix Regia* biomass

Sample	Proximate analysis (wt. %, dry basis)				Ultimate analysis (wt. %, dry basis-ash free)					H/C	O/C	HHV (M.J./kg)
	VM	FC	Ash	Moisture (%)	C	H	N	S	O			
DR	72.66	16.92	1.22	9.20	45.02	5.96	1.21	NA	47.80	0.13	1.07	17.53

VM: Volatile matter, FC: Fixed carbon, C: Carbon, H: Hydrogen, N: Nitrogen, S: sulphur, O: Oxygen, NA: Not available, HHV: High heating value.

5.1.2 Thermal degradation behavior

The thermal degradation profile of *Delonix Regia* biomass was studied in a thermogravimetric analyzer (TGA) via non-isothermal mode during the pyrolysis process. The TGA was operated at a temperature between 25 to 1000 °C under an inert atmosphere of (nitrogen) 40mL/min at various heating rates. 5, 10, 20, 35, 55 °C min^{-1}. TG thermogram (**Figure 5.1.2 A**) shows that degradation of DR biomass can be described into three stages (I, II, and III). Stage-I (25 °C - 157 °C) indicates dehydration, in which the removal of very light hot volatile matter, bound and unbound moisture takes place. [97] discussed the devolatilization stage of biomass stimulated by tarry vapors at 170 °C and remained till 400 °C temperature. A similar kind of trend was ascertained in the current work, with minor differences attributed to the intrinsic structural properties of biomass. Furthermore, it was affirmed that maximum degradation occurred in stage-II (133 °C - 722 °C) due to the disintegration of hemicellulose (HC) and cellulose (CEL) in the biomass.

The lower and intermediate temperature zones distinguish the second stage once again. In the first zone (250 °C - 340 °C), hemicellulose (HC) decomposed; in the second zone (323 °C - 383 °C), cellulose decomposed **(Table 5.1.2)**. In this stage-II, more significant molecular weight components were fragmented into smaller molecular weight components due to a continuous supply of heat energy. Finally, in stage-III (>550 °C), lignin (LIG) starts decomposition at a slower rate due to its higher thermal stability. The Lignin degradation started at about 200 °C during pyrolysis, which is primarily responsible for pyrolytic degradation [98].

Table 5.1.2: Thermal decomposition parameters of *Delonix Regia* at three stages

Heating Rate (°C min^{-1})	Stages											
	Stage-I				Stage-II				Stage-III			
	TG		DTG		TG		DTG		TG		DTG	
	T_{Range} (°C)	Mass Loss (wt.%)	$DT_{max.}$ (°C)	$DR_{max.}$ (wt.% min^{-1}).	T_{Range} (°C)	Mass Loss (wt.%)	$DT_{max.}$ (°C)	$DR_{max.}$ (wt.% min^{-1}).	T_{Range} (°C)	Mass Loss (wt.%)	$DT_{max.}$ (°C)	$DR_{max.}$ (wt.% min^{-1}).
5	25-133	5.3	42	0.6	133-666	58.4	333	3.2	666-999	6	-	-
10	25-154	7.6	52	1.4	154-718	63.8	345	6.5	718-997	3	-	-
20	25-157	7.4	63	2.5	157-709	63.1	357	12.5	709-997	2	715	0.2
35	25-155	5.6	81	3.4	155-714	64.4	367	21.8	714-992	1.6	809	0.3
55	25-148	6.8	82	6.3	148-722	63.3	377	30.3	722-996	1.7	815	0.4

$DT_{max.}$ - Maximum decomposition temperature

$DR_{max.}$ - Maximum decomposition rate

From DTG findings **(Figure 5.1.2 B)** and a Table presented in ESI, the first peak was observed at 80 °C temperature due to the removal of moisture content from DR biomass. Additionally, the peaks were noticed at 250-340 °C and 323-383°C indicating hemicellulose and cellulose decayed within the temperature ranges of 250-290 °C, and 323-346 °C at 5 °C min^{-1}; 258-300 °C, and 335-356 °C at 10 °C min^{-1}; 266-310 °C, and 347-367 °C at 20 °C min^{-1}; 276-326 °C, and 360-375 °C at 35 °C min^{-1}; 286-340 °C, and 365-383 °C at 55 °C min^{-1} respectively [99]. Finally, no sharp peaks were observed at (>550 °C) temperature for the lignin.

5.1.2.1 Effect of heating rate

The effect of heating rate was studied at five dynamic heating rates (5, 10, 20, 35, and 55 °C min^{-1}). Thermograms (**Figure 5.1.2 (A and B))** demonstrated that, with the increasing heating rate (5, to 55 °C min^{-1}), the thermal decomposition rate of DR biomass increased. A similar trend was also observed for banana leaves [100], DR pods [39], and DR seeds [2]. These reports suggest that lower heating lead to improved heat transfer rates in biomass. In the current study, from the DTG thermogram **(Figure 5.1.2 B), the** maximum decomposition temperature was found to increase from 333 to 377 °C with an increased heating rate from 5 to 55 °C min^{-1}. The maximum weight losses of 58.4 %, 63.8 %, 63.1 %, 64.4 %, and 63.3 % were recorded for 5, 10, 20, 35, and 55 °C min^{-1} heating rates, respectively. Additionally, as the heating rate increased beyond 35 °C min^{-1}, no significant change was observed in the mass loss (≤5 wt. %), which indicates that a heating rate of 35 °C min^{-1} can be utilised as an optimal value for the pyrolysis of DR. Thus, significant variations in weight losses were noticed with increasing heating rates were evidenced by other reports [2], [39], [101], [102].

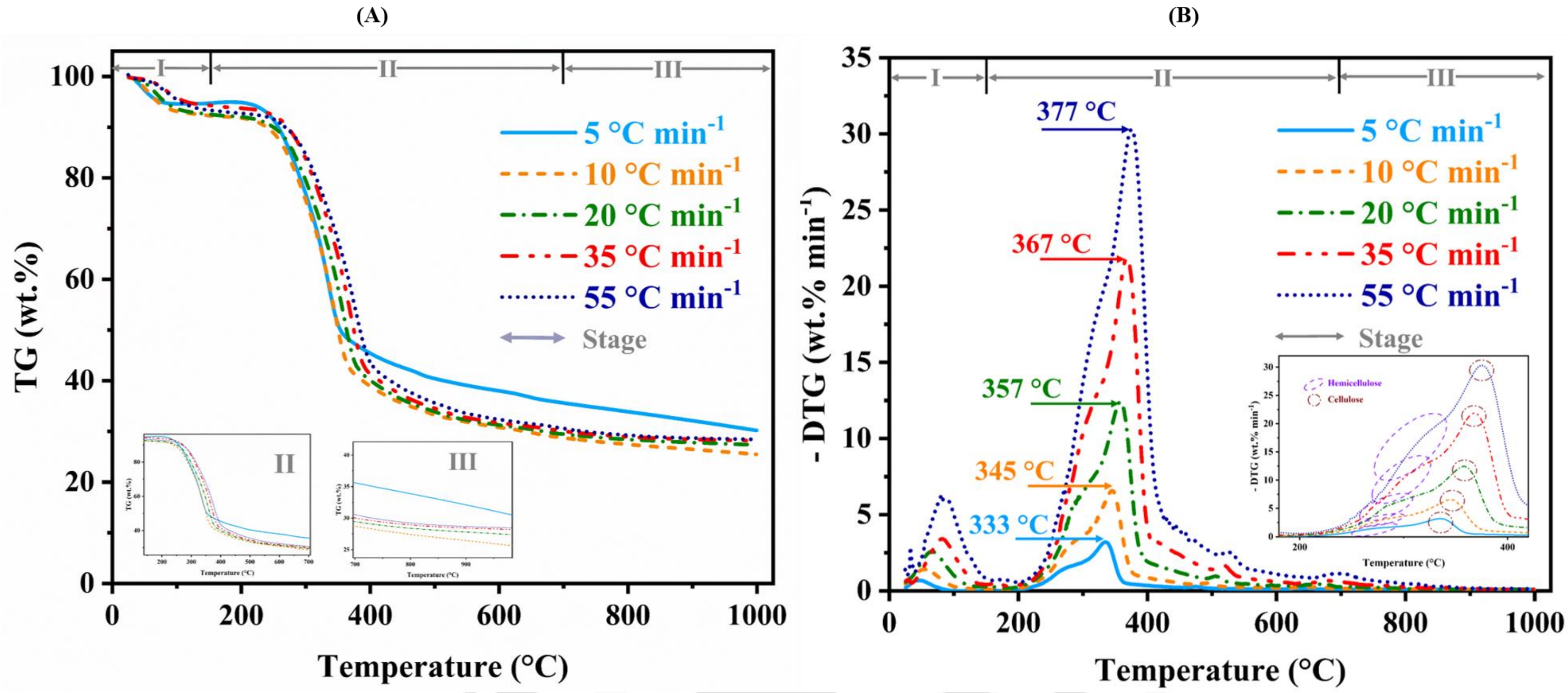

Figure 5.1.2: Thermal degradation behavior of *Delonix Regia* biomass **A)** TG and **B)** DTG. Operating conditions: Raw material: *Delonix Regia* (DR) biomass ~6mg; Nitrogen: 40mL/min, Heating rate: 5, 10, 20, 35 and 55 °C/min, Temperature: 25-1000°C.

5.1.3 Assessment of kinetic triplets

Kinetic triplets (KT) such as apparent activation energy (E_α), pre-exponential factor (k_o), and reaction mechanism (Z_α) were investigated for the pyrolysis of DR biomass by iso-conversional methods, namely Differential Friedman (DFM), Kissinger-Akahira-Sunose (KAS), Ozawa-Flynn-Wall (OFW), Starink (STK), and Distributed Activation Energy (DAE). E_α, and k_o were obtained at multiple heating rates (5, 10, 20, 35, and 55 °C min^{-1}). DFM plot was generated from Eq. (8) by plotting $ln\left[\beta\left(\frac{d\alpha}{dT}\right)\right]$ vs. 1/T, as presented in **Figure 5.1.3.1 (A).** The apparent activation energy and pre-exponential factor were ascertained by equating the slope $\left(\frac{-E_\propto}{R}\right)$ and intercept values at specific conversions have been reported in **Table 5.1.3.2**. A similar kind of approach was followed for KAS, OFW, STK, and DAE methods (as per Eqs. 10, 12, 14, and 16), respectively, and the plots and data are shown in **Figure 5.1.3.1 (B and E)** and **Table 5.1.3.1**. It was observed that the experimental kinetic data was fitted well from conversion 0.1 to 0.7 with high correlation coefficients ($R^2 > 0.98$); however, at conversion above 0.8, the experimental kinetic data was not fitted well due to the formation of secondary reactions that generate substantial quantities of solid residues (char and ash) during the pyrolysis [2], [39].

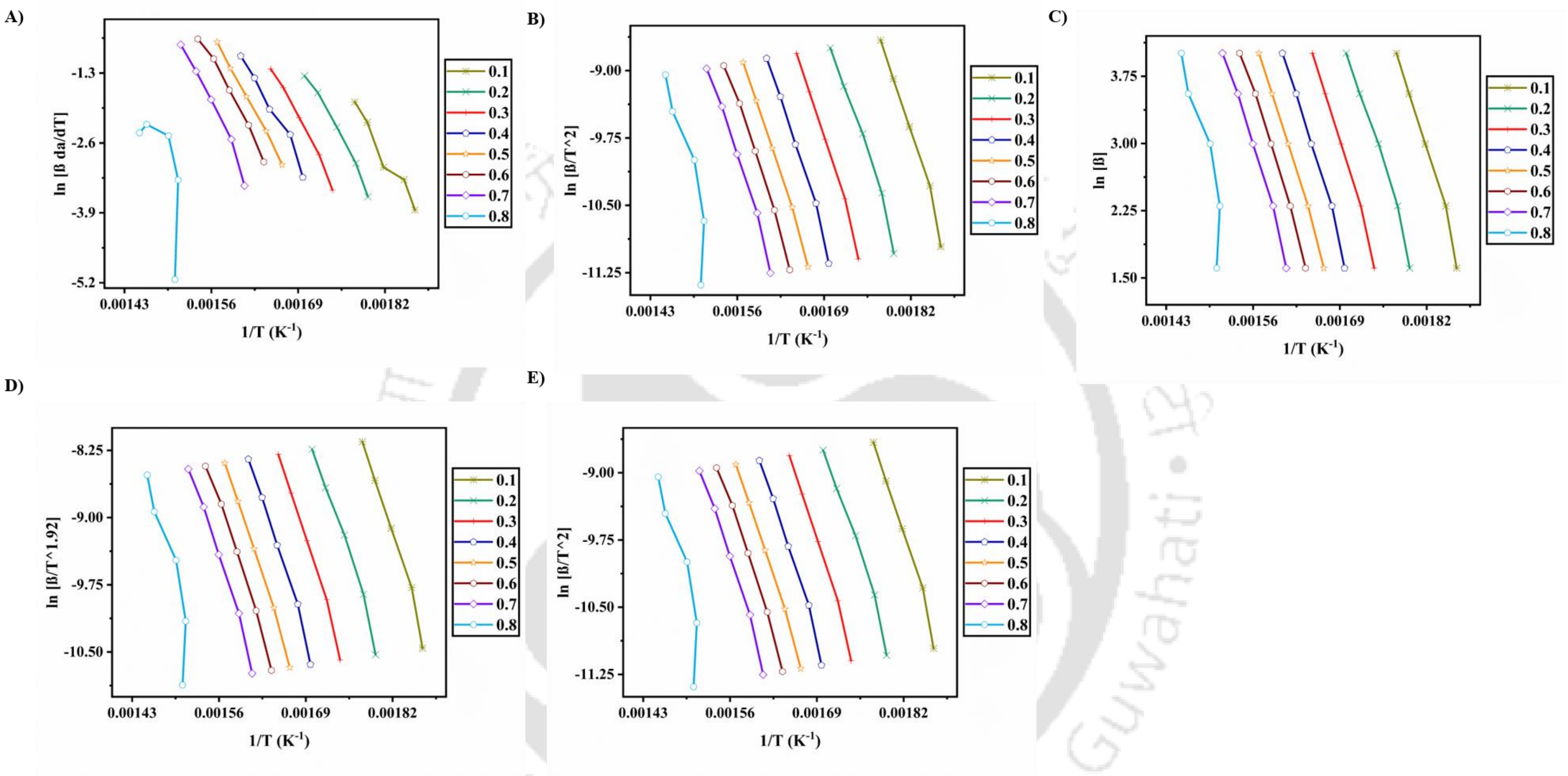

Figure 5.1.3.1: Iso-conversional plots of *Delonix Regia* biomass by **A)** DFM, **B)** KAS, **C)** OFW, **D)** STK, **E)** DAE.

Table 5.1.3.1: Data of iso-conversional lines by five different methods

Heating rate (°C min^{-1})	Conversion (α)	1/T (K^{-1})	Iso-conversional Methods				
			DFM $\ln[\beta\, d\alpha/dT]$	KAS $\ln[\beta/T^2]$	OFW $\ln[\beta]$	STK $\ln[\beta/T^{1.92}]$	DAE $\ln[\beta/T^2]$
5	0.1	0.00186	-3.8	-11.0	1.6	-10.5	-11.0
10	0.1	0.00185	-3.3	-10.3	2.3	-9.8	-10.3
20	0.1	0.00182	-3.1	-9.6	3.0	-9.1	-9.6
35	0.1	0.00179	-2.2	-9.1	3.6	-8.6	-9.1
55	0.1	0.00177	-1.8	-8.7	4.0	-8.2	-8.7
5	0.2	0.00179	-3.6	-11.0	1.6	-10.5	-11.0
10	0.2	0.00178	-3.0	-10.4	2.3	-9.9	-10.4
20	0.2	0.00175	-2.3	-9.7	3.0	-9.2	-9.7
35	0.2	0.00172	-1.7	-9.2	3.6	-8.7	-9.2
55	0.2	0.00170	-1.4	-8.7	4.0	-8.2	-8.7
5	0.3	0.00174	-3.5	-11.1	1.6	-10.6	-11.1
10	0.3	0.00172	-2.8	-10.4	2.3	-9.9	-10.4
20	0.3	0.00169	-2.1	-9.8	3.0	-9.3	-9.8
35	0.3	0.00167	-1.6	-9.2	3.6	-8.7	-9.2
55	0.3	0.00165	-1.2	-8.8	4.0	-8.3	-8.8
5	0.4	0.00170	-3.2	-11.1	1.6	-10.6	-11.1
10	0.4	0.00168	-2.4	-10.5	2.3	-10.0	-10.5
20	0.4	0.00165	-2.0	-9.8	3.0	-9.3	-9.8
35	0.4	0.00162	-1.4	-9.3	3.6	-8.8	-9.3
55	0.4	0.00160	-1.0	-8.9	4.0	-8.3	-8.9
5	0.5	0.00167	-3.0	-11.2	1.6	-10.7	-11.2
10	0.5	0.00164	-2.4	-10.5	2.3	-10.0	-10.5
20	0.5	0.00161	-1.7	-9.9	3.0	-9.3	-9.9
35	0.5	0.00159	-1.2	-9.3	3.6	-8.8	-9.3
55	0.5	0.00157	-0.7	-8.9	4.0	-8.4	-8.9
5	0.6	0.00164	-3.0	-11.2	1.6	-10.7	-11.2
10	0.6	0.00162	-2.3	-10.6	2.3	-10.0	-10.6
20	0.6	0.00159	-1.6	-9.9	3.0	-9.4	-9.9
35	0.6	0.00156	-1.0	-9.4	3.6	-8.8	-9.4
55	0.6	0.00154	-0.7	-8.9	4.0	-8.4	-8.9
5	0.7	0.00161	-3.4	-11.3	1.6	-10.7	-11.3
10	0.7	0.00159	-2.5	-10.6	2.3	-10.1	-10.6
20	0.7	0.00156	-1.8	-9.9	3.0	-9.4	-9.9
35	0.7	0.00154	-1.3	-9.4	3.6	-8.9	-9.4
55	0.7	0.00151	-0.8	-9.0	4.0	-8.5	-9.0
5	0.8	0.00151	-5.1	-11.4	1.6	-10.9	-11.4
10	0.8	0.00151	-3.3	-10.7	2.3	-10.2	-10.7
20	0.8	0.00150	-2.5	-10.0	3.0	-9.5	-10.0
35	0.8	0.00146	-2.3	-9.5	3.6	-8.9	-9.5
55	0.8	0.00145	-2.4	-9.0	4.0	-8.5	-9.0
10	0.6	0.00162	-2.3	-10.6	2.3	-10.0	-10.6

From the results (**Figure 5.1.3.2 and Table 5.1.3.2**), apparent average activation energy, E_α (kJ mol^{-1}) and pre-exponential, k_o (min^{-1}) were 202.34 and 4.98 × 10^{17}; 205.67 and 2.62 × 10^{20}; 204.87 and 4.98 × 10^{17}; 205.89 and 2.04 × 10^{20}; 205.67 and 1.67 × 10^{20}; respectively by all five methods. It was evident that the lowest values of kinetic parameters 202.34 and 204.87 (kJ mol^{-1}) were obtained by the DFM and OFW methods, respectively, for the pyrolysis of DR biomass from 0.1 to 0.8 conversions. The E_α values reported for pyrolysis of DR pods [39] using DFM and OFW methods were 236.5 and 241 kJ mol^{-1}, respectively. For DR seeds [2] using DFM and OFW methods were 152.47 and 191.63 kJ mol^{-1}; for almond shells [42] using KAS and OFW methods, 153 and 152 kJ mol^{-1}; for castor residue [103] using KAS and OFW methods, 165.86 and 167.10 kJ mol^{-1}, respectively. According to the kinetic investigations, the average apparent activation energy values were lower than those of DR pods and more significant than those of DR seeds. Thus, based on the activation energies revealed, pyrolysis of the DR biomass mixture may be more energy-efficient than that of DR pods. However, for all iso-conversional methods, a similar trend of E_α was observed from 0.1 to 0.8 conversion [2], [39], [42], [101], [103].

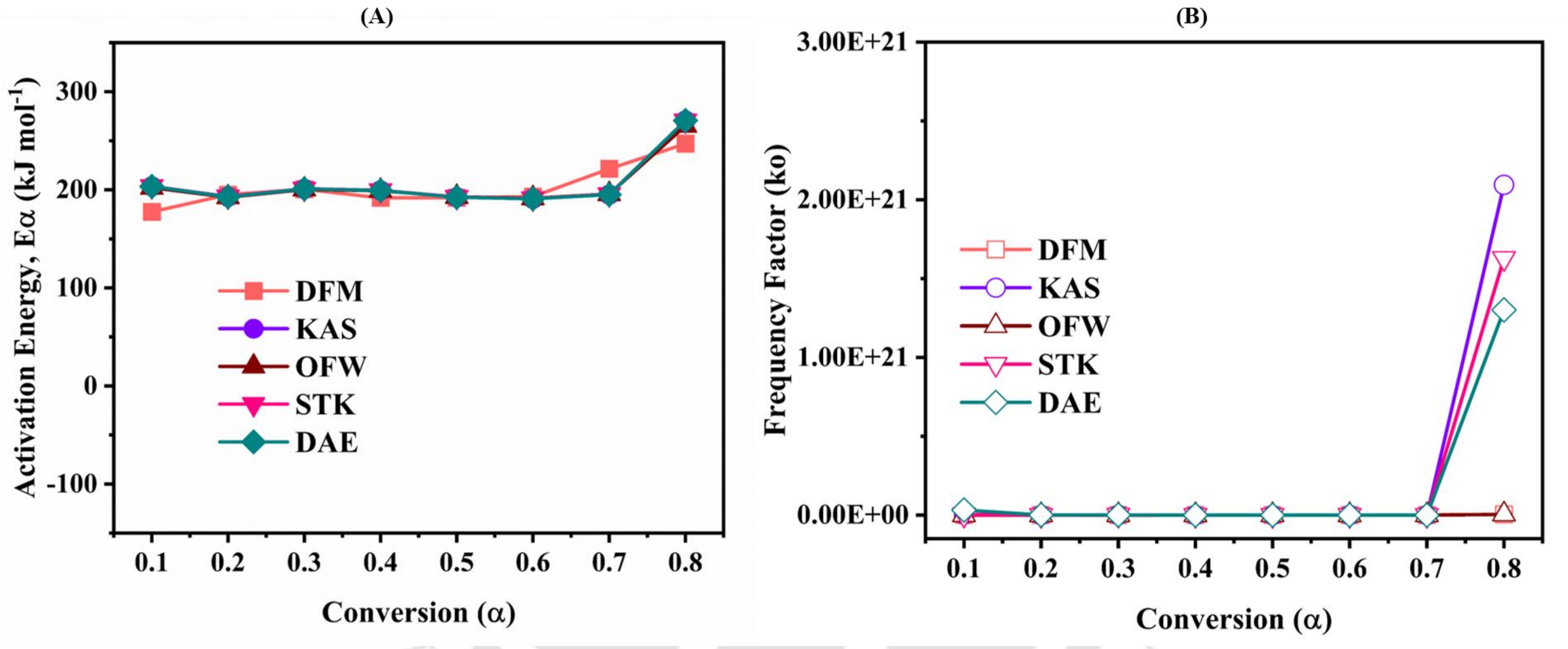

Figure 5.1.3.2: Determination of kinetic factors for *Delonix Regia* biomass by different iso-conversional methods **A)** Activation energy and **B)** Frequency factor.

Table 5.1.3.2: Activation energy and pre-exponential factor from various iso-conversional methods of *Delonix Regia* biomass.

α	Iso-conversional Methods														
	DFM			KAS			OFW			STK			DAE		
	E (kJ mol^{-1})	k_o (min^{-1})	R^2	E (kJ mol^{-1})	k_o (min^{-1})	R^2	E (kJ mol^{-1})	k_o (min^{-1})	R^2	E (kJ mol^{-1})	k_o (min^{-1})	R^2	E (kJ mol^{-1})	k_o (min^{-1})	R^2
0.1	177.57	4.90E+15	0.961	203.38	3.33E+18	0.987	202.09	1.25E+16	0.988	203.58	2.67E+18	0.987	203.38	3.16E+19	0.987
0.2	195.14	7.55E+16	0.988	192.81	1.16E+17	0.985	192.40	5.22E+14	0.987	193.03	9.32E+16	0.985	192.81	5.09E+17	0.985
0.3	200.66	8.70E+16	0.993	200.87	2.70E+17	0.994	200.34	1.19E+15	0.995	201.10	2.17E+17	0.994	200.87	7.50E+17	0.994
0.4	191.82	7.74E+15	0.978	199.26	9.18E+16	0.992	199.06	4.34E+14	0.993	199.50	7.42E+16	0.992	199.26	1.76E+17	0.992
0.5	192.03	5.27E+15	0.999	192.46	1.33E+16	0.997	192.79	6.98E+13	0.998	192.71	1.08E+16	0.997	192.46	1.90E+16	0.997
0.6	193.12	4.91E+15	0.991	190.87	6.76E+15	0.994	191.45	3.74E+13	0.994	191.13	5.50E+15	0.994	190.87	7.27E+15	0.994
0.7	221.40	5.61E+17	0.982	195.13	1.06E+16	0.991	195.68	5.80E+13	0.992	195.40	8.60E+15	0.991	195.13	8.65E+15	0.991
0.8	246.95	3.23E+18	0.413	270.56	2.09E+21	0.813	265.19	3.97E+18	0.825	270.67	1.63E+21	0.813	270.56	1.30E+21	0.813
Avg.	**202.34**	**4.98E+17**	**0.913**	**205.67**	**2.62E+20**	**0.969**	**204.87**	**4.98E+17**	**0.971**	**205.89**	**2.04E+20**	**0.969**	**205.67**	**1.67E+20**	**0.969**

For all iso-conversional methods, it was observed that the variations of E_α and k_o (10^{15} to 10^{16}) increase from 0.1 to 0.3 conversion due to a reaction taking place at the surface of DR biomass, which implies hemicellulose decomposition, and then E_α and k_o ($<10^{15}$) decreases slightly until conversion of 0.6, in which the cellulose was decomposed, and then E_α and k_o ($>10^{17}$) gradually increases until conversion of 0.8 due to high collisions occurring between the molecules, thus a high amount of energy required for biomass pyrolysis [42], [101], [104], [105]. The findings of E_α and k_o suggest that as the heating rate increases, the collision rate of molecules increases, increasing the rate of reaction for pyrolysis of DR biomass. Due to the heterogeneity of DR biomass, the chemical components (hemicellulose, cellulose, and lignin) decompose at different temperatures [100], as evidenced by the variation in E_α and k_o. Thus, the pyrolysis of DR biomass undergoes a complex process with a multi-step reaction mechanism.

Criado's master plot predicted the possible mechanism of pyrolysis of DR biomass. All of Criado's plots were generated from Eqs. (19-20) by plotting z(α)/z(0.5) vs. conversion (α), and presented in **Figure 5.1.3.3 (A and E) and a Table 5.1.3.3**. For instance, at 20 °C min^{-1}, it was demonstrated that the experimental data have shown the trend of second-order reaction (F2) from 0.1 to 0.2 conversion, first-order (F1) and 2-dimensional diffusion (D2) from 0.3 to 0.4 conversion, and then close to volume contraction (R3) and second-order reaction (F2) from 0.6 to 0.7 conversion, and higher-order reaction (>F5) up to 0.8 conversions. Thus, it was evident that the pyrolysis of DR biomass clearly showed a multistep reaction mechanism behavior based on master plot analysis.

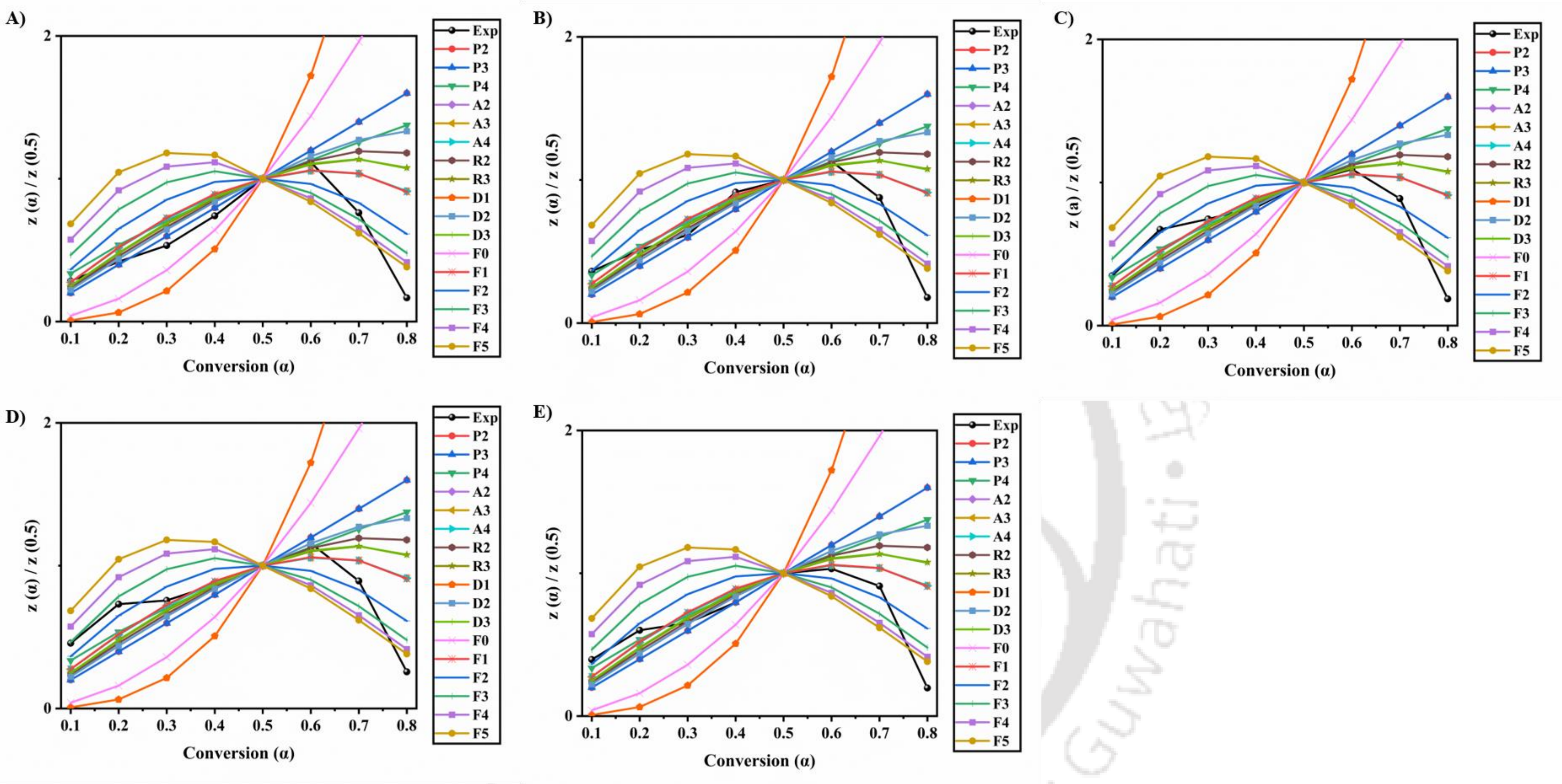

Figure 5.1.3.3: Master plots of *Delonix Regia* biomass at **A)** 5°C min^{-1}, **B)** 10°C min^{-1}**, C)** 20°C min^{-1}**, D)** 35°C min^{-1}**, E)** 55°C min^{-1}.

Table 5.1.3.3: Reaction mechanism of *Delonix Regia* at various heating rates by Criado's method

Conversion (α)	Heating rate (°C min^{-1})				
	5	10	20	35	55
0.1	F1	F2	F2	F3	F2
0.2	P2	A4	F2	F3	F2
0.3	P3	P2	F1	F1	D2
0.4	P3	F1	D2	R3	P2
0.5	-	-	-	-	-
0.6	R2	P4	R3	D2	A4
0.7	D3	F2	F2	F2	F2
0.8	>F5	>F5	>F5	>F5	>F5
Models: P2, P3 – Second and Third Power law models A4 – Fourth Avrami-Erofeyev model R2, R3 – Area and Volume Contracting models D2, D3 – 1 and 3-dimensional Diffusion models F1, F2, F3, F5 – First, Second, Third, Five Reaction order models					

5.1.4 Thermodynamic parameters

Thermodynamic (TD) parameters such as pre-exponential factor (k_o), enthalpy change (ΔH), Gibbs free energy change(ΔG), and entropy change (ΔS) of DR biomass were investigated and presented in **Figure 5.1.4 and Table 5.1.4**. TD calculations were computed using Eqs. 8, 10, 12, 14, and 16 from DFM, KAS, OFW, STK, and DAE methods. TD parameters of DR biomass through DFM, KAS, OFW, STK, and DAE methods were included. **Figure 5.1.4 (A1 and B1)** illustrates the variations in enthalpy change (ΔH) Vs. (α) for both DFM and DAE methods. **Figure 5.1.4 (A1 and B1)** demonstrates that the heating rate has a negligible effect on ΔH.

Also, the variation in enthalpy was affected by changes in activation energy, which depended on conversion value. When conversion (α) was 0.8, the highest enthalpy value was 197.14 kJ mol^{-1} for DFM and 200.47 kJ mol^{-1} for DAE. The positive value of ΔH from 0.1 to 0.8 conversion had been noticed, indicating that the pyrolytic decomposition of DR biomass was endotherm in nature. Furthermore, as the enthalpy of pyrolysis increases from conversion of 0.1 to 0.8, the endothermicity of DR biomass increases. Similar findings of enthalpy values were reported in the literature [2], [39], [42], [100], [101], [103], [106].

Further, the variations in Gibbs free energy change (ΔG) Vs. (α) was depicted in **Figure 5.1.4 (A2 and B2)**. ΔG was a fundamental TD state function that evaluates the degree of spontaneity in reactions. Additionally, ΔG also explained that the amount of energy in the system increases as the reactant approaches activated complex state formation [100], [103], [104]. Slight variations in ΔG values were observed from 0.1 to 0.8 conversion, and the highest value was 181.52 kJ mol^{-1} for DFM and 181.01 kJ mol^{-1} for DAE methods. The positive findings of ΔG demonstrated that DR biomass showed a high degree of reactivity and spontaneity. Finally, the minor variations in Entropy change (ΔS) Vs. (α) was demonstrated in **Figure 5.1.4 (A3 and B3)**. ΔS is a vital TD state function that quantifies the degree of disorder, randomness, or randomness in reactions [107]. For all iso-conversional methods, it was observed that the value of ΔS was increased for 0.1 to 0.3 conversion, decreased slightly until conversion of 0.6, and then gradually increased until 0.8 conversions for all heating rates. These small variations of ΔS values suggested that the pyrolysis of DR biomass experiences minimal physiochemical transformations, and it was very close to thermodynamic equilibrium, which was consistent with the findings of [2], [100], [105], [106], [108] for various biomasses.

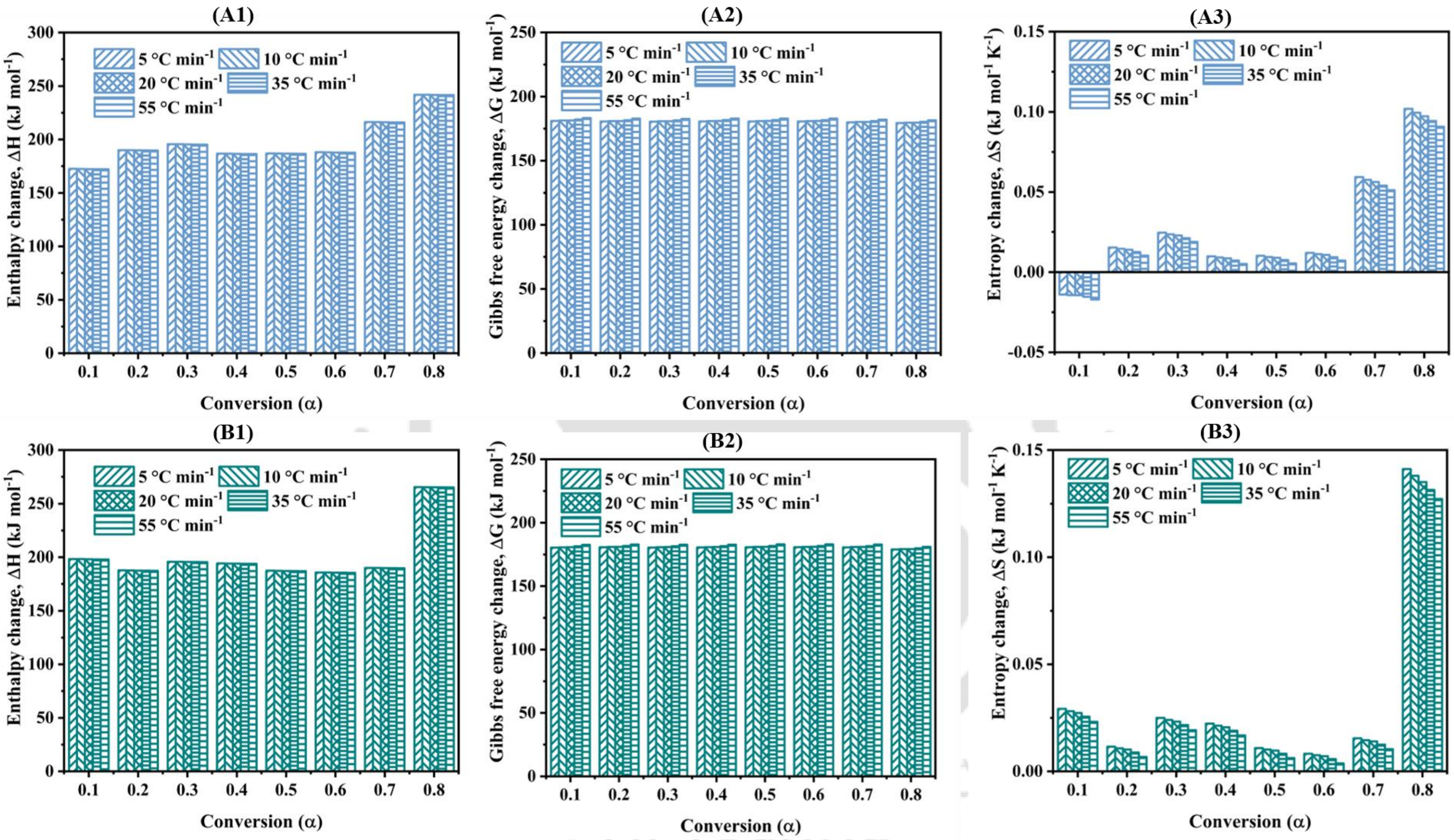

Figure 5.1.4: Thermodynamic plots of *Delonix Regia* biomass **A1 and B1)** change in enthalpy, **A2 and B2)** change in Gibbs energy**, A3 and B3)** change in entropy from DFM and DAE methods.

Table 5.1.4: Thermodynamic properties of *Delonix Regia* biomass pyrolysis at different heating rates.

Table 5.1.4.1: Thermodynamic properties of *Delonix Regia* biomass pyrolysis at a heating rate of 5 °C min^{-1}

α	DFM				KAS				OFW				STK				DAE			
	k_o	ΔH	ΔG	ΔS	k_o	ΔH	ΔG	ΔS	k_o	ΔH	ΔG	ΔS	k_o	ΔH	ΔG	ΔS	k_o	ΔH	ΔG	ΔS
0.1	6.41E+12	172.48	181.08	-0.01	1.16E+15	198.28	180.39	0.03	8.96E+14	196.99	180.42	0.03	1.21E+15	198.48	180.39	0.03	1.16E+15	198.28	180.39	0.03
0.2.	2.22E+14	190.05	180.60	0.02	1.38E+14	187.71	180.66	0.01	1.27E+14	187.30	180.67	0.01	1.45E+14	187.94	180.66	0.01	1.38E+14	187.71	180.66	0.01
0.3	6.72E+14	195.56	180.46	0.02	7.02E+14	195.78	180.46	0.02	6.31E+14	195.25	180.47	0.02	7.35E+14	196.01	180.45	0.03	7.02E+14	195.78	180.46	0.02
0.4	1.13E+14	186.72	180.69	0.01	5.07E+14	194.16	180.50	0.02	4.87E+14	193.96	180.50	0.02	5.32E+14	194.40	180.49	0.02	5.07E+14	194.16	180.50	0.02
0.5	1.18E+14	186.93	180.68	0.01	1.29E+14	187.36	180.67	0.01	1.38E+14	187.70	180.66	0.01	1.36E+14	187.62	180.67	0.01	1.29E+14	187.36	180.67	0.01
0.6	1.47E+14	188.02	180.66	0.01	5.09E-03	185.77	371.58	-0.30	1.05E+14	186.35	180.70	0.01	9.88E+13	186.04	180.71	0.01	9.36E+13	185.77	180.72	0.01

0.7	4.34E+16	216.30	179.96	0.06	2.21E+14	190.03	180.60	0.02	2.47E+14	190.58	180.59	0.02	2.33E+14	190.30	180.60	0.02	2.21E+14	190.03	180.60	0.02
0.8	7.29E+18	241.86	179.40	0.10	8.20E+20	265.46	178.94	0.14	2.80E+20	260.09	179.04	0.13	8.39E+20	265.58	178.94	0.14	8.20E+20	265.46	178.94	0.14
Avg.	**9.17E+17**	**197.24**	**180.44**	**0.03**	**1.03E+20**	**200.57**	**204.23**	**-0.01**	**3.50E+19**	**199.78**	**180.38**	**0.03**	**1.05E+20**	**200.80**	**180.36**	**0.03**	**1.03E+20**	**200.57**	**180.37**	**0.03**

Table 5.1.4.2: Thermodynamic properties of *Delonix Regia* biomass pyrolysis at a heating rate of 10 °C min^{-1}

0.1	6.32E+12	172.38	181.33	-0.01	1.04E+15	198.18	180.62	0.03	8.05E+14	196.89	180.66	0.03	1.08E+15	198.38	180.62	0.03	1.04E+15	198.18	180.62	0.03
0.2.	2.04E+14	189.95	180.84	0.01	1.29E+14	187.61	180.90	0.01	1.19E+14	187.20	180.91	0.01	1.35E+14	187.84	180.89	0.01	1.29E+14	187.61	180.90	0.01
0.3	6.07E+14	195.46	180.69	0.02	6.33E+14	195.68	180.69	0.02	5.71E+14	195.15	180.70	0.02	6.63E+14	195.91	180.68	0.02	6.33E+14	195.68	180.69	0.02
0.4	1.06E+14	186.62	180.93	0.01	4.61E+14	194.06	180.73	0.02	4.43E+14	193.86	180.74	0.02	4.83E+14	194.30	180.72	0.02	4.61E+14	194.06	180.73	0.02
0.5	1.10E+14	186.83	180.92	0.01	1.20E+14	187.26	180.91	0.01	1.28E+14	187.60	180.90	0.01	1.26E+14	187.52	180.90	0.01	1.20E+14	187.26	180.91	0.01
0.6	1.37E+14	187.92	180.89	0.01	9.80E-03	185.67	371.82	-0.30	9.85E+13	186.26	180.94	0.01	9.25E+13	185.94	180.95	0.01	8.78E+13	185.67	180.95	0.01
0.7	3.63E+16	216.20	180.18	0.06	2.04E+14	189.93	180.84	0.01	2.27E+14	190.48	180.82	0.02	2.15E+14	190.20	180.83	0.01	2.04E+14	189.93	180.84	0.01

0.8	5.53E+18	241.76	179.61	0.10	5.69E+20	265.36	179.14	0.14	1.99E+20	259.99	179.24	0.13	5.82E+20	265.48	179.14	0.14	5.69E+20	265.36	179.14	0.14
Avg.	**6.96E+17**	**197.14**	**180.68**	**0.03**	**7.12E+19**	**200.47**	**204.46**	**-0.01**	**2.48E+19**	**199.68**	**180.61**	**0.03**	**7.28E+19**	**200.70**	**180.59**	**0.03**	**7.12E+19**	**200.47**	**180.60**	**0.03**

Table 5.1.4.3: Thermodynamic properties of *Delonix Regia* biomass pyrolysis at a heating rate of 20 °C min^{-1}

0.1	6.39E+12	172.28	181.44	-0.01	9.57E+14	198.08	180.72	0.03	7.45E+14	196.79	180.76	0.03	9.95E+14	198.28	180.72	0.03	9.57E+14	198.08	180.72	0.03
0.2.	1.94E+14	189.85	180.94	0.01	1.23E+14	187.51	181.01	0.01	1.14E+14	187.10	181.02	0.01	1.29E+14	187.74	181.00	0.01	1.23E+14	187.51	181.01	0.01
0.3	5.65E+14	195.36	180.79	0.02	5.89E+14	195.58	180.79	0.02	5.32E+14	195.05	180.80	0.02	6.16E+14	195.81	180.78	0.02	5.89E+14	195.58	180.79	0.02
0.4	1.02E+14	186.52	181.03	0.01	4.31E+14	193.96	180.83	0.02	4.14E+14	193.76	180.84	0.02	4.51E+14	194.20	180.82	0.02	4.31E+14	193.96	180.83	0.02
0.5	1.06E+14	186.73	181.03	0.01	1.15E+14	187.16	181.02	0.01	1.23E+14	187.50	181.01	0.01	1.21E+14	187.42	181.01	0.01	1.15E+14	187.16	181.02	0.01
0.6	1.31E+14	187.82	181.00	0.01	1.89E-02	185.57	371.92	-0.29	9.48E+13	186.16	181.04	0.01	8.91E+13	185.84	181.05	0.01	8.46E+13	185.57	181.06	0.01
0.7	3.13E+16	216.10	180.27	0.06	1.93E+14	189.83	180.94	0.01	2.15E+14	190.38	180.93	0.01	2.04E+14	190.10	180.93	0.01	1.93E+14	189.83	180.94	0.01
0.8	4.35E+18	241.66	179.69	0.10	4.11E+20	265.26	179.21	0.14	1.46E+20	259.89	179.32	0.13	4.20E+20	265.38	179.21	0.14	4.11E+20	265.26	179.21	0.14

Avg.	**5.48E+17**	**197.04**	**180.78**	**0.03**	**5.14E+19**	**200.37**	**204.56**	**-0.01**	**1.83E+19**	**199.58**	**180.71**	**0.03**	**5.25E+19**	**200.60**	**180.69**	**0.03**	**5.14E+19**	**200.37**	**180.70**	**0.03**

Table 5.1.4.4: Thermodynamic properties of *Delonix Regia* biomass pyrolysis at a heating rate of 35 °C min^{-1}

0.1	5.80E+12	172.18	182.14	-0.02	7.93E+14	197.98	181.41	0.03	6.20E+14	196.69	181.44	0.02	8.24E+14	198.18	181.40	0.03	7.93E+14	197.98	181.41	0.03
0.2.	1.65E+14	189.75	181.63	0.01	1.06E+14	187.41	181.70	0.01	9.81E+13	187.00	181.71	0.01	1.11E+14	187.64	181.69	0.01	1.06E+14	187.41	181.70	0.01
0.3	4.73E+14	195.26	181.48	0.02	4.92E+14	195.48	181.48	0.02	4.45E+14	194.95	181.49	0.02	5.14E+14	195.71	181.47	0.02	4.92E+14	195.48	181.48	0.02
0.4	8.78E+13	186.42	181.73	0.01	3.62E+14	193.86	181.52	0.02	3.49E+14	193.66	181.53	0.02	3.79E+14	194.10	181.51	0.02	3.62E+14	193.86	181.52	0.02
0.5	9.14E+13	186.63	181.72	0.01	9.92E+13	187.06	181.71	0.01	1.06E+14	187.40	181.70	0.01	1.04E+14	187.32	181.70	0.01	9.92E+13	187.06	181.71	0.01
0.6	1.13E+14	187.72	181.69	0.01	3.18E-02	185.47	372.62	-0.29	8.19E+13	186.06	181.74	0.01	7.70E+13	185.74	181.74	0.01	7.32E+13	185.47	181.75	0.01
0.7	2.43E+16	216.00	180.95	0.05	1.65E+14	189.73	181.63	0.01	1.83E+14	190.28	181.62	0.01	1.74E+14	190.00	181.63	0.01	1.65E+14	189.73	181.63	0.01
0.8	3.10E+18	241.56	180.36	0.09	2.69E+20	265.16	179.87	0.13	9.77E+19	259.79	179.98	0.12	2.75E+20	265.28	179.87	0.13	2.69E+20	265.16	179.87	0.13
Avg.	**3.90E+17**	**196.94**	**181.46**	**0.02**	**3.37E+19**	**200.27**	**205.24**	**-0.01**	**1.22E+19**	**199.48**	**181.40**	**0.03**	**3.44E+19**	**200.50**	**181.38**	**0.03**	**3.37E+19**	**200.27**	**181.38**	**0.03**

Table 5.1.4.5: Thermodynamic properties of *Delonix Regia* biomass pyrolysis at a heating rate of 55 °C min^{-1}

0.1	4.83E+12	172.08	183.33	-0.02	6.06E+14	197.88	182.58	0.02	4.76E+14	196.59	182.62	0.02	6.29E+14	198.08	182.58	0.02	6.06E+14	197.88	182.58	0.02
0.2.	1.30E+14	189.65	182.81	0.01	8.39E+13	187.31	182.88	0.01	7.78E+13	186.90	182.89	0.01	8.76E+13	187.54	182.87	0.01	8.39E+13	187.31	182.88	0.01
0.3	3.64E+14	195.16	182.66	0.02	3.79E+14	195.38	182.65	0.02	3.44E+14	194.85	182.66	0.02	3.96E+14	195.61	182.64	0.02	3.79E+14	195.38	182.65	0.02
0.4	6.98E+13	186.32	182.90	0.01	2.81E+14	193.76	182.69	0.02	2.70E+14	193.56	182.70	0.02	2.94E+14	194.00	182.69	0.02	2.81E+14	193.76	182.69	0.02
0.5	7.25E+13	186.53	182.90	0.01	7.86E+13	186.96	182.89	0.01	8.37E+13	187.30	182.88	0.01	8.25E+13	187.22	182.88	0.01	7.86E+13	186.96	182.89	0.01
0.6	8.90E+13	187.62	182.87	0.01	4.82E-02	185.37	373.80	-0.29	6.51E+13	185.96	182.91	0.00	6.13E+13	185.64	182.92	0.00	5.84E+13	185.37	182.93	0.00
0.7	1.75E+16	215.90	182.12	0.05	1.30E+14	189.63	182.81	0.01	1.44E+14	190.18	182.79	0.01	1.36E+14	189.90	182.80	0.01	1.30E+14	189.63	182.81	0.01
0.8	2.04E+18	241.46	181.52	0.09	1.64E+20	265.06	181.01	0.13	6.06E+19	259.69	181.12	0.12	1.68E+20	265.18	181.01	0.13	1.64E+20	265.06	181.01	0.13
Avg.	**2.58E+17**	**196.84**	**182.64**	**0.02**	**2.05E+19**	**200.17**	**206.41**	**-0.01**	**7.58E+18**	**199.38**	**182.57**	**0.03**	**2.10E+19**	**200.40**	**182.55**	**0.03**	**2.05E+19**	**200.17**	**182.56**	**0.03**

α – Conversion, k_o – Pre-exponential factor, *ΔH, ΔG and ΔS* - Change in enthalpy, Change in Gibbs free energy, and Chane in entropy

5.1.5 Pyrolysis performance indices

The pyrolysis performance indices (PPI) of the DR biomass throughout the pyrolysis process are depicted in **Table 5.1.5**. In summary, it was observed that as heating rates increased from 5-55°C $\min^{-1}$, all PPI indices (C, D_i, D_b, S, and D_v) increased. It was also noticed that while increasing heating rates, temperatures for igniting/degrading/burning out ($T_i/T_p/T_b$) were increased, whereas respective times ($t_i/t_p/t_b$) were reduced. The highest (1.02×10^{-4}) flammability index C, was obtained due to lower moisture content and higher heating values of DR biomass. The higher (1.08×10^{1} and 5.91×10^{-2}) indices of ignition D_i and burnout D_b, indicated the better combustion ability of DR biomass. The best (3.62×10^{-7}) combustion index (S) revealed that the DR biomass had a good combustion performance characteristic. The higher (6.07×10^{-7}) devolatilization index D_v, means more volatiles were released during the DR biomass pyrolysis. The results followed previous findings by other researchers [39], [109].

Table 5.1.5: Pyrolysis performance indices of *Delonix Regia* biomass pyrolysis.

β	T_i	T_p	T_b	$\Delta T_{0.5}$	t_i	t_p	t_b	$\Delta t_{0.5}$	$-R_p$	$-R_v$	C	D_i	D_b	S	D_v
5	516	606	1256	553	43.6	61.8	192	51	3.2	0.4	1.20E-05	1.19E-03	5.29E-06	3.83E-09	7.40E-09
10	519	618	1246	559	22.1	32.1	94.8	26.2	6.5	0.8	2.41E-05	9.16E-03	8.15E-05	1.55E-08	2.90E-08
20	531	630	1216	569	11.6	16.6	45.9	13.5	12.5	1.5	4.43E-05	6.49E-02	1.22E-03	5.47E-08	9.85E-08
35	539	640	1165	577	6.9	9.8	24.8	7.9	21.8	2.6	7.50E-05	3.22E-01	1.14E-02	1.67E-07	2.85E-07
55	544	650	1161	579	4.4	6.4	15.7	5.1	30.3	4.1	1.02E-04	1.08E+00	5.91E-02	3.62E-07	6.07E-07

β - Heating Rate (°C/min), T_i - ignition temperature (K), T_p - maximum decomposition temperature (K), T_b - burnout temperature (K), $\Delta T_{0.5}$ - temperature interval of half of the $-R_p$ (K), t_i - ignition time (min), t_b - burnout time (min), t_p - maximum decomposition time (min), $\Delta t_{0.5}$ - time interval of half of the $-R_p$ (min), R_p - maximum decomposition rate (wt.%/min), $-R_v$ - mean decomposition rate (wt.%/min), C - flammability index (K^{-2}/min), D_i - ignition index (min^{-3}), D_b - burnout index (min^{-4}), S - combustion index (K^{-3}/min^2), D_v - devolatilization index (K^{-3}/min).

5.1.6 Summary and Comparative analysis with existing work

The summary of objective 1 and the comparative analysis with the **existing** work (**Table 5.1.6**) are discussed below.

Summary of objective 1.

The following statements were obtained from objective 1:

- The thermal degradation behavior of *Delonix regia* (DR) biomass was investigated.
- The effect of the heating rate on the pyrolytic degradation of DR biomass was studied.
- The pyrolytic zone temperature ranging from 133-722 °C was observed with a maximum mass loss of 58-63 wt. %.
- From the kinetic analysis, it was ascertained that the Differential Friedman method yielded the lowest activation energy (202.34 kJ/mol).
- Criado's technique demonstrated the multistep reaction mechanism during the pyrolysis of DR biomass.
- From the thermodynamic analysis, $\Delta H \approx 197$ kJ/mol and $\Delta G \approx 181$ kJ/mol showed the endothermic and non-spontaneity of DR pyrolysis.
- Additionally, the pyrolysis performance indices of DR biomass were reported during the pyrolysis.

Table 5.1.6: Comparative analysis of pyrolysis of *Delonix Regia* biomass.

S.No.	Raw materials	Catalyst	TGA model	Operating conditions			Results		References
	Feed and co-feed	(wt. %)		°C	*Q*	*β*	*Kinetics	*Thermodynamics	
1	*Delonix Regia* pods	-	Perkin Elmer STA-7	29 – 9000	N_2 – 30	5, 10, 20, 50	$E_{\alpha=0.1\text{-}0.65 \text{ and } 0.65\text{-}0.80}$: 196 and 277, 194 and 234, and 194 and 236 by DFM, OFW, STK	$E_{\alpha=0.1\text{-}0.80}$: ΔH: 214, ΔG: 143, and ΔS: 0.116	[39]
2	*Delonix Regia* seeds (8 mg)	-	Perkin Elmer STA-7200	30 – 900	N_2 – 40	10, 20, 30, 40, 50	$E_{\alpha=0.1\text{-}0.80}$ and k_o: 142 and 4.29×10^{09}, 192 and 2.07×10^{19}, 152 and 1.52×10^{14}, and 148 and 4.90×10^{10} *by* KAS, OFW, DFM, DAE	$E_{\alpha=0.1\text{-}0.80}$: ΔH: 147, ΔG: 219, and ΔS: -0.114	[2]
3	*Delonix Regia* biomass: trunks/branches (6 mg)	-	Netsch TG209F1	25 – 1000	N_2 – 40	5, 10, 20, 35, 55	$E_{\alpha=0.1\text{-}0.80}$ and k_o: 202 and 4.98×10^{17}, 206 and 2.62×10^{20}, 205 and 4.98×10^{17}, 206 and 2.04×10^{20}, 206 and	$E_{\alpha=0.1\text{-}0.80}$: ΔH: 197, ΔG: 181 and ΔS: 0.031	Objective 1 [57]

							1.67×10^{20} by DFM, KAS, OFW, STK, DAE		

β – Heating rates (°C min^{-1})

α – Conversion

°*C* – Temperature

Q – Flowrate of carrier gas (mL min^{-1})

Iso – conversional models – Differential Friedman (DFM), Kissinger-Akahira-Sunose (KAS), Ozawa-Flynn-Wall (OFW), Starink (STK), and Distributed Activation Energy (DAE)

*Kinetics – Average values

*Thermodynamics – Average values based on the DFM model at 10 °C min^{-1}

E_α – Activation energy (kJ mol^{-1})

k_o – Frequency factor (s^{-1})

ΔH – Change in enthalpy (kJ mol^{-1})

ΔG – Change in Gibbs free energy (kJ mol^{-1})

ΔS – Change in entropy (kJ mol^{-1} K^{-1})

5.2 Kinetics and thermodynamics investigation of pyrolysis of butyl rubber tube waste

5.2.1 Physicochemical characterization

The Physicochemical characteristics such as proximate, ultimate, and HHV of the Butyl rubber tube (BRT) waste were analyzed and shown in **Table 5.2.1.** The Proximate analysis revealed that BRT waste with no moisture content was more susceptible to pyrolysis [41], [44], [110]. BRT waste contains high volatile matter (about 57 %), and low ash (about 10 %) signifies improved pyrolytic characteristics [111]. The elemental analysis showed high carbon (about 58 %), low hydrogen and sulfur (about 6 % and 1 %, respectively), and no nitrogen contents, which was consistent with earlier results [44], [111]. Due to a linear relationship between carbon content and heating value (HHV), a high carbon content implies a substantial heating value (HHV) of the fuel [112]. The HHV of the BRT waste (about 22 MJ kg^{-1}) was consistent with natural rubber, synthetic rubber, butadiene rubber, and styrene-butadiene rubber [111]–[116] and identified to be a possible feedstock for the pyrolysis process.

Table 5.2.1: Physicochemical characterization of butyl rubber tube waste.

Sample	Proximate analysis (wt. %, dry basis)				Ultimate analysis (wt. %, dry basis-ash free)					H/C	O/C	HHV (M.J./kg)
	VM	FC	Ash	Moisture (%)	C	H	N	S	O			
BRT	56.66	33.76	10.26	57.99	6.22	-	1.1	35.73	0.12	0.63	-	22.06
VM: Volatile matter, FC: Fixed carbon, C: Carbon, H: Hydrogen, N: Nitrogen, S: sulphur, O: Oxygen, NA: Not available, HHV: High heating value.												

5.2.2 Behavior of thermal degradation

During the pyrolysis process, the thermal degradation behavior of Butyl rubber tube (BRT) waste was studied using a non-isothermal mode thermogravimetric analyzer (TGA). At various heating rates (5°C, 10°C, 20°C, 35°C, and 55°C min^{-1}), the TGA was operated at temperatures ranging from 25 to 1000 °C in an inert atmosphere (nitrogen) of 40mL/min. According to the TG pyrograms (Figure 1), the degradation of Butyl rubber tube (BRT) waste can be classified into three zones (I, II, and III). Two significant zones of weight loss described the devolatilization of BRT waste during pyrolysis described as follows:

$$1)\ Polymeric\ compponents\ \rightarrow Volatile\ 1 + Radical\ 1 \qquad (Main\ split\ of\ the\ chain)$$

$$2) \begin{cases} 2a)\ Radical\ 1\ \rightarrow Volatile\ 2 \\ 2b)\ Radical\ 1\ \rightarrow Radical\ 2 \\ 2c)\ Radical\ 2\ \rightarrow Volatile\ 3 \end{cases} \qquad (Depolymerization\ Reactions)$$

$$3)\ Radical\ 2\ \rightarrow Radical\ 3 \qquad (Cyclization\ Reactions)$$

$$4)\ Radical\ 3\ \rightarrow Volatile\ 4 + Radical\ 4 \qquad (Cyclic\ products\ Degradation\ )$$

For the above reaction steps, initially, the polymeric components (isobutylene and isoprene) in BRT (IIR) were fragmented into volatile 1 compounds (monomers) and radical 1 (H_2, CH_4, and CO) [113], [114], [116] at lower temperatures. Then, the radicals were further transformed into volatile compounds (dimers/trimers) by depolymerization reaction at intermediate temperatures. Following that, intermediate radical products were further cracked to yield stable radical 3 products such as aliphatic, aromatic, and H_2S via cyclization reactions [14], [44], [112]–[114]. Finally, the stable radical 3 products were further degraded to volatile 4 and radical 4 products, such as alkenes, alkanes, and solid char, at higher temperatures [112]. A free radical mechanism reaction contributes significantly to the decomposition of BRT waste. The chain scission primarily occurred at the β-position of the BRT [116], [117].

Through the scission and dehydrogenation reactions, the 2-butenyl radical obtained from scission was converted to 1,3-butadiene. Furthermore, chain scission can give rise to other free radicals, which can rearrange into C_5- and C_7-radical species. The C_5- and C_7- radical species can be cyclized to form 1,3- and 1,4-Cyclooctadiene. Because the C-C single bond in -C-C=C- is much stronger than the one in -C-C-C-, the rearrangement of -C-C=C- in C_5 and C_7 radical species can occur only at higher temperatures ($T > 800$ °C) during the pyrolysis of BRT [116], [117]. The pyrolysis pathways of major pyrolytic components such as isoprene, isobutylene, 1,3-butadiene, 1,3-and 1,4-cyclopentadiene significantly affected the pyrolysis of BRT [116], [117].

From the TG and DTG results **(Figure 5.2.2 A to B and Table 5.2.2)**, it was observed that the minor fractions such as plasticizers, oils, and additives were removed at the temperature range from 25-180°C in zone I [111], [112], [118]. At this zone, negligible mass losses from 0.4 to 0.9 wt.% were observed at 5-55°C min^{-1}. The major devolatilization of BRT waste was elucidated at the temperature range from 180 °C and 768 °C in zone II. It was noticed that in this zone II, the formation of radicals and high conversion of BRT occurred rapidly. Several reactions, such as depolymerization and cyclization, occurred with maximum mass loss. The maximum mass losses were from 59.4 to 60.5 wt.% and were ascertained for increased heating rates of 5-50 °C min^{-1}. The pyrograms revealed that higher heating rates resulted in increased decomposition of BRT material.

Table 5.2.2 Thermal degradation of BRT waste at different zones (I, II, and III).

Heating Rate (°C min^{-1})	Zones											
	I (Dehydration Zone)				II (Pyrolytic Zone)				III (Passive Zone)			
	TG		DTG		TG		DTG		TG		DTG	
	T_{Range} (°C)	Mass Loss (wt.%)	$DT_{max.}$ (°C)	$DR_{max.}$ (wt.% min^{-1}).	T_{Range} (°C)	Mass Loss (wt.%)	$DT_{max.}$ (°C)	$DR_{max.}$ (wt.% min^{-1}).	T_{Range} (°C)	Mass Loss (wt.%)	$DT_{max.}$ (°C)	$DR_{max.}$ (wt.% min^{-1}).
5	25-150	0.4	-	-	150-698	60	359	4	698-984	3.5	-	-
10	25-165	0.5	-	-	165-716	59.4	370	7	716-982	1.5	-	-
20	25-153	0.5	68	0.1	153-739	59.7	381	15	739-983	0.7	908	0.1
35	25-179	0.4	31	0.5	179-751	59.9	392	27	751-982	0.7	933	0.3
55	25-181	0.9	34	2.5	181-768	60.5	401	41	768-983	1	961	0.4

$DT_{max.}$ - Maximum degradation temperature

$DR_{max.}$ - Maximum degradation rate

The maximum decomposition of BRT occurred at 359, 370, 381, 392, and 401 °C. The temperature shift was due to increased heating rate delay [119]. Moreover, at a higher heating rate of 50 °C min^{-1}, the maximum DTG (rate of mass loss) was increased. Three peaks of DTG pyrograms for every heating rate signify the major devolatilization of BRT, isobutylene, and isoprene, respectively. Similar kinds of pyrograms trends were reported elsewhere [51], [111], [118]. Furthermore, from **(Figure 5.2.2 B)**, the peaks at 390-459 °C and 620-783 °C indicated isobutylene, and isoprene decayed within the temperature ranges of 390-435 °C and 620-687 °C at 5 °C min^{-1}; 402-450 °C, and 632-709 °C at 10 °C min^{-1}; 421-456 °C, and 635-737 °C at 20 °C min^{-1}; 435-458 °C, and 641-754 °C at 35 °C min^{-1}; 447-459 °C, and 636-783 °C at 55 °C min^{-1} respectively [5], [111]. Additionally, no sharp peaks were observed for the undecomposed solid char at temperatures above 800 °C [110], [117], [119]. Finally, because of more secondary reactions (cyclization products degradation) between IIR co-polymers, approximately 45-55 mass% (5-55 °C min^{-1}) of the tube waste remains undecomposed and may lead to solid char upon pyrolysis [5], [14], [111], [119].

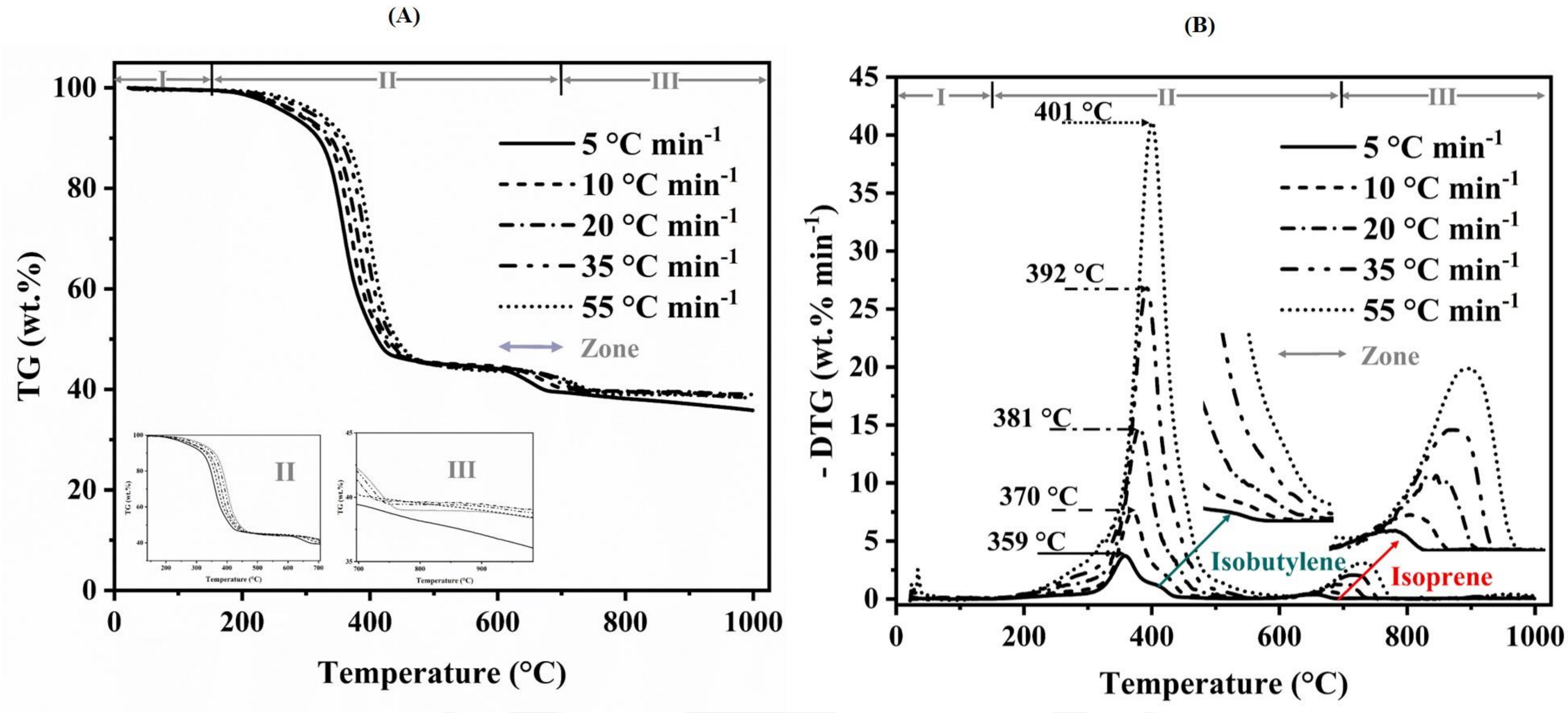

Figure 5.2.2: Thermal degradation of BRT waste **A)** TG and **B)** DTG. Operating conditions: Raw material: BRT waste ~6mg; Nitrogen: 40mL/min, Heating rate: 5, 10, 20, 35 and 55 °C/min, Temperature: 25-1000°C.

5.2.3 Estimation of kinetics

Kinetic triplets (KT) such as apparent activation energy (E_α), pre-exponential factor (k_o), and reaction mechanism (Z_α) were investigated for the pyrolysis of Butyl rubber tube (BRT) waste by model-fitting and model-free iso-conversional approaches. Five iso-conversional approaches (Differential Friedman (DFM), Kissinger-Akahira-Sunose (KAS), Ozawa-Flynn-Wall (OFW), Starink (STK), and Distributed Activation Energy (DAE)) and five multiple heating rates (5, 10, 20, 35, and 55 °C min^{-1}) were employed for the investigation of E_α, and k_o. DFM graph was generated from Eq. (8) by drawing $ln\left[\beta\left(\frac{d\alpha}{dT}\right)\right]$ vs. 1/T, as presented in **Figure 5.2.3.1. (A)** and apparent activation energy and pre-exponential factor were ascertained by equating the slope $\left(\frac{-E_\propto}{R}\right)$ and intercept values at specific conversions were reported in **Table 5.2.3.2**. A similar kind of approach was followed for KAS, OFW, STK, and DAE approaches (as per Eqs. 9, 10, 11, and 12), respectively, and the plots and data are shown in **Figure 5.2.3.1. (B to E) and Table (Table 5.2.3.1).**

It was observed that the experimental kinetic data was fitted well from conversion 0.1 to 0.8 with high correlation coefficients (R^2>0.98). For conversion above 0.8, the experimental kinetic data was not fitted well due to the formation of secondary reactions (cyclization products degradation) that generate substantial quantities of solid residues (char/ash) during the pyrolysis of BRT [117], [119]. From the results **(Figure 5.2.31. (F) and Table 5.2.3.2)**, apparent average activation energy, E_α (kJ mol^{-1}), and pre-exponential, k_o (min^{-1}) were 244.73 and 2.73×10^{24}; 223.37 and 3×10^{24}; 222.67 and 6.52×10^{21}; 223.63 and 2.35×10^{24}; 223.37 and 1.84×10^{24}; obtained respectively for all five approaches. It was evident that the lowest values of kinetic parameters 222.67 and 223.37 (kJ mol^{-1}) are obtained by the OFW and KAS approach, respectively, for the pyrolysis of Butyl rubber tube (BRT) waste from 0.1 to 0.8 conversion. The E_α values reported for pyrolysis of butadiene rubber [44], [116] using DFM and KAS approaches were 200 and 409 kJ mol^{-1}, respectively, and for styrene-butadiene-rubber (SBR) [44], [116] using DFM and KAS approaches were 240 and 305 kJ mol^{-1}, respectively. According to the kinetic investigations, the apparent average activation energy values were lower than those of butadiene rubber and more significant than SBR. Thus, based on the activation energies revealed, pyrolysis of the Butyl rubber tube (BRT) waste mixture may be more energy-efficient than SBR. However, for all iso-conversional approaches, a similar trend of E_α was observed from 0.1 to 0.8 conversion [44], [117], [119].

For all iso-conversional approaches, it was observed that the variations of E_α and k_o (10^{15} to 10^{16}) increased between 0.1 to 0.3 conversion due to a reaction taking place at the surface of BRT waste; which implies decomposition of isobutylene polymer (volatile 1 compounds (monomers) and radical 1 by depolymerization) [113], [114], and then E_α and k_o ($<10^{15}$) decreases slightly to till 0.6, in which the isoprene polymer was decomposed (to radicals and volatile compounds (dimers/trimers) by cyclization reaction), and then E_α and k_o ($>10^{17}$) gradually increases to 0.8 conversion due to high collisions occurring between the molecules (volatile 4 and radical 4 by cyclic degradation), thus a high amount of energy required for rubber waste pyrolysis [14], [112]–[114].

The findings of E_α and k_o suggest that as the heating rate increases, the collision rate of molecules increases, resulting in an increase in the reaction rate for Butyl rubber tube (BRT) waste pyrolysis. Due to the heterogeneity of Butyl rubber tube (BRT) waste, the major polymeric components, such as isobutylene and isoprene, were decomposed at different temperatures [14], [44], as evidenced by the variation in E_α and k_o. Thus, the pyrolysis of Butyl rubber tube (BRT) waste undergoes a complex process with a multi-step reaction mechanism.

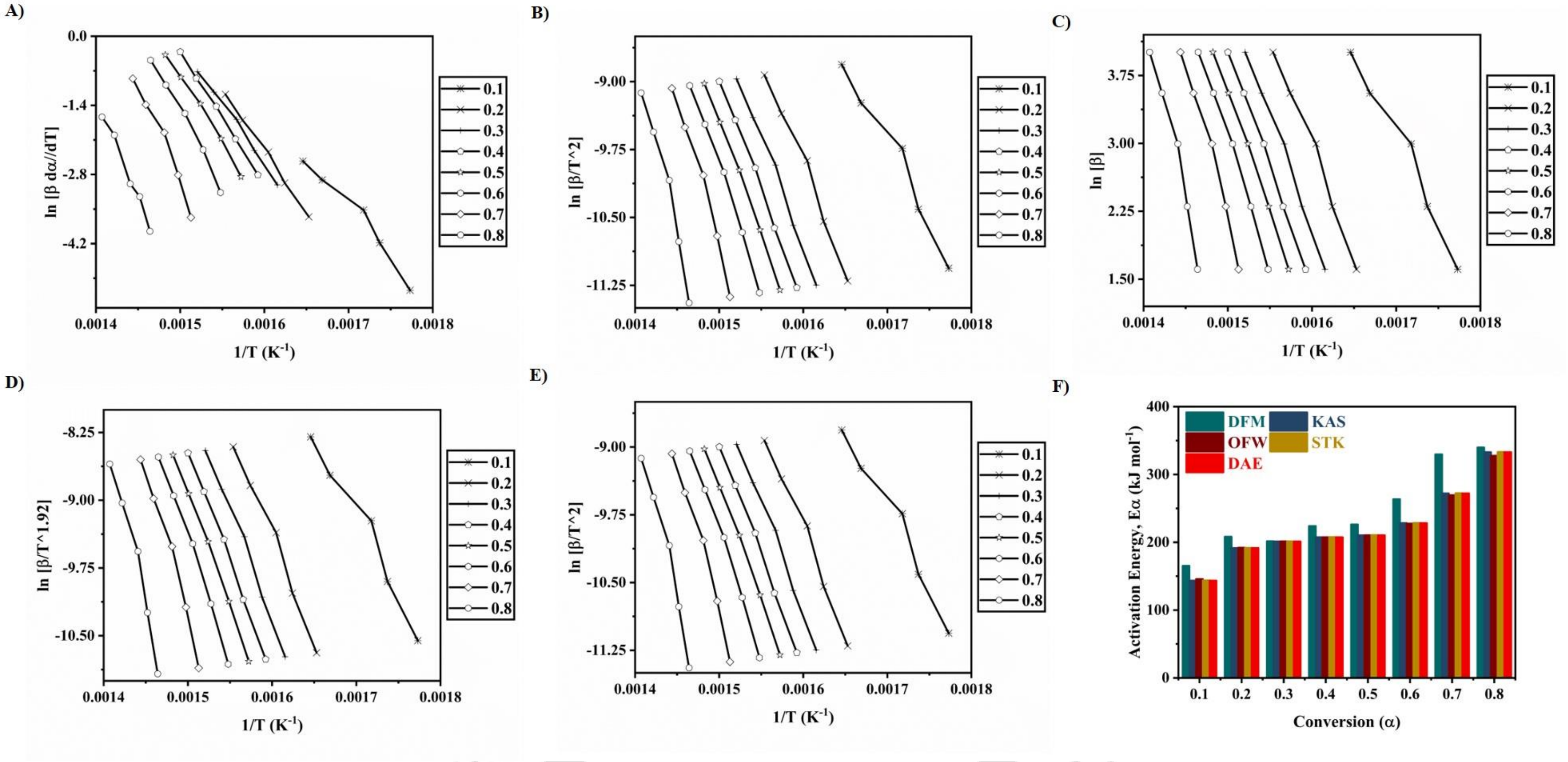

Figure 5.2.3.1: Estimation of kinetics of BRT waste for all models **A)** DFM, **B)** KAS, **C)** OFW, **D)** STK, **E)** DAE: Iso-conversional plots, and **F)** Activation energy plot.

Table 5.2.3.1 Iso-conversional data of BRT waste for five approaches

Heating rate (°C min^{-1})	Conversion (α)	1/T (K^{-1})	Iso-conversional Methods				
			DFM $\ln[\beta\, d\alpha/dT]$	KAS $\ln[\beta/T^2]$	OFW $\ln[\beta]$	STK $\ln[\beta/T^{1.92}]$	DAEM $\ln[\beta/T^2]$
5	0.1	0.00177	-5.1	-11.1	1.6	-10.6	-11.1
10	0.1	0.00174	-4.2	-10.4	2.3	-9.9	-10.4
20	0.1	0.00172	-3.5	-9.7	3.0	-9.2	-9.7
35	0.1	0.00167	-2.9	-9.2	3.6	-8.7	-9.2
55	0.1	0.00165	-2.5	-8.8	4.0	-8.3	-8.8
5	0.2	0.00165	-3.7	-11.2	1.6	-10.7	-11.2
10	0.2	0.00162	-3.0	-10.5	2.3	-10.0	-10.5
20	0.2	0.00160	-2.3	-9.9	3.0	-9.4	-9.9
35	0.2	0.00157	-1.7	-9.4	3.6	-8.8	-9.4
55	0.2	0.00155	-1.2	-8.9	4.0	-8.4	-8.9
5	0.3	0.00162	-3.0	-11.2	1.6	-10.7	-11.2
10	0.3	0.00159	-2.3	-10.6	2.3	-10.1	-10.6
20	0.3	0.00157	-1.7	-9.9	3.0	-9.4	-9.9
35	0.3	0.00154	-1.1	-9.4	3.6	-8.9	-9.4
55	0.3	0.00152	-0.7	-9.0	4.0	-8.5	-9.0
5	0.4	0.00159	-2.8	-11.3	1.6	-10.8	-11.3
10	0.4	0.00157	-2.1	-10.6	2.3	-10.1	-10.6
20	0.4	0.00154	-1.4	-10.0	3.0	-9.4	-10.0
35	0.4	0.00152	-0.9	-9.4	3.6	-8.9	-9.4
55	0.4	0.00150	-0.3	-9.0	4.0	-8.5	-9.0
5	0.5	0.00157	-2.8	-11.3	1.6	-10.8	-11.3
10	0.5	0.00155	-2.1	-10.6	2.3	-10.1	-10.6
20	0.5	0.00152	-1.4	-10.0	3.0	-9.5	-10.0
35	0.5	0.00150	-0.8	-9.4	3.6	-8.9	-9.4
55	0.5	0.00148	-0.4	-9.0	4.0	-8.5	-9.0
5	0.6	0.00155	-3.2	-11.3	1.6	-10.8	-11.3
10	0.6	0.00153	-2.3	-10.7	2.3	-10.1	-10.7
20	0.6	0.00151	-1.6	-10.0	3.0	-9.5	-10.0
35	0.6	0.00148	-1.0	-9.5	3.6	-9.0	-9.5
55	0.6	0.00146	-0.5	-9.0	4.0	-8.5	-9.0
5	0.7	0.00151	-3.7	-11.4	1.6	-10.9	-11.4
10	0.7	0.00150	-2.8	-10.7	2.3	-10.2	-10.7
20	0.7	0.00148	-1.9	-10.0	3.0	-9.5	-10.0
35	0.7	0.00146	-1.4	-9.5	3.6	-9.0	-9.5
55	0.7	0.00144	-0.9	-9.1	4.0	-8.6	-9.1
5	0.8	0.00146	-3.9	-11.4	1.6	-10.9	-11.4
10	0.8	0.00145	-3.2	-10.8	2.3	-10.2	-10.8
20	0.8	0.00144	-3.0	-10.1	3.0	-9.6	-10.1
35	0.8	0.00142	-2.0	-9.6	3.6	-9.0	-9.6
55	0.8	0.00141	-1.6	-9.1	4.0	-8.6	-9.1

Table 5.2.3.2: Activation energy and pre-exponential factor from various iso-conversional approaches for BRT waste pyrolysis

α	Iso-conversional approaches														
	DFM (Differential Friedman)			KAS (Kissinger-Akahira-Sunose)			OFW (Ozawa-Flynn-Wall)			STK (Starink)			DAE (Distributed Activation Energy)		
	E (kJ mol^{-1})	k_o (min^{-1})	R^2	*E* (kJ mol^{-1})	k_o (min^{-1})	R^2	*E* (kJ mol^{-1})	k_o (min^{-1})	R^2	*E* (kJ mol^{-1})	k_o (min^{-1})	R^2	*E* (kJ mol^{-1})	k_o (min^{-1})	R^2
0.1	165.12	1.56E+13	0.962	143.47	6.16E+11	0.970	145.70	5.17E+09	0.974	143.75	5.1E+11	0.971	143.47	5.79E+12	0.970
0.2	208.12	3.06E+16	0.997	191.49	2.58E+15	0.989	191.96	1.40E+13	0.990	191.75	2.1E+15	0.989	191.49	1.13E+16	0.989
0.3	201.54	7.56E+15	0.995	201.10	1.12E+16	0.994	201.33	5.73E+13	0.995	201.37	9.0E+15	0.994	201.10	3.05E+16	0.994
0.4	223.90	4.32E+17	0.999	207.31	2.94E+16	0.998	207.37	1.46E+14	0.998	207.58	2.4E+16	0.998	207.31	5.64E+16	0.998
0.5	226.26	4.83E+17	0.995	210.32	4.29E+16	0.998	210.36	2.13E+14	0.998	210.59	3.5E+16	0.998	210.32	6.14E+16	0.998
0.6	263.59	2.51E+20	0.989	228.25	9.41E+17	0.994	227.55	4.08E+15	0.995	228.51	7.6E+17	0.994	228.25	1.01E+18	0.994
0.7	329.59	1.16E+25	0.974	272.10	1.66E+21	0.983	269.44	5.28E+18	0.984	272.33	1.3E+21	0.983	272.10	1.36E+21	0.983
0.8	339.72	1.02E+25	0.984	332.94	2.40E+25	0.969	327.62	5.45E+22	0.971	333.13	1.9E+25	0.969	332.94	1.48E+25	0.969
Avg.	**244.73**	**2.73E+24**	**0.987**	**223.37**	**3.00E+24**	**0.987**	**222.67**	**6.82E+21**	**0.988**	**223.63**	**2.35E+24**	**0.987**	**223.37**	**1.84E+24**	**0.987**
α – Conversion, *E* – Activation energy, k_o – Frequency factor															

The possible mechanism of pyrolysis of Butyl rubber tube (BRT) waste was predicted by Criado's. All of Criado's plots were generated from Eqs. (13-16) by drawing a graph z(α)/z(0.5) vs. α, and presented in **Figure 5.2.3.2 (A to E)** and **Table 5.2.3.3**. For instance, at 20 °C min^{-1}, it was demonstrated that the experimental data had shown the trend of 3-dimensional diffusion (D3) and first-order (F1) from 0.1 to 0.2 conversion, second (F2) and third-order (F3) from 0.3 to 0.4 conversion, and then higher-order reaction (>F5) from 0.6 to 0.8 conversions. Pyrolysis of BRT waste clearly showed a multistep reaction mechanism behavior based on master plot analysis.

Table 5.2.3.3: Reaction mechanism by Criado's method of BRT waste at multiple heating rates

Conversion *(α)*	Heating rate (°C min^{-1})				
	5	10	5	35	5
0.1	D2	0.1	D2	0.1	D2
0.2	F2	0.2	F2	0.2	F2
0.3	D3	0.3	D3	0.3	D3
0.4	F4	0.4	F4	0.4	F4
0.5	-	0.5	-	0.5	-
0.6	>F5	0.6	>F5	0.6	>F5
0.7	>F5	0.7	>F5	0.7	>F5
0.8	>F5	0.8	>F5	0.8	>F5

Reaction mechanism models:
P2, P3 – Second and Third Power law models
A4 – Fourth Avrami-Erofeyev model
R2, R3 – Area and Volume Contracting models
D2, D3 – 1 and 3-dimensional Diffusion models
F1, F2, F3, F5 – First, Second, Third, Five Reaction order models

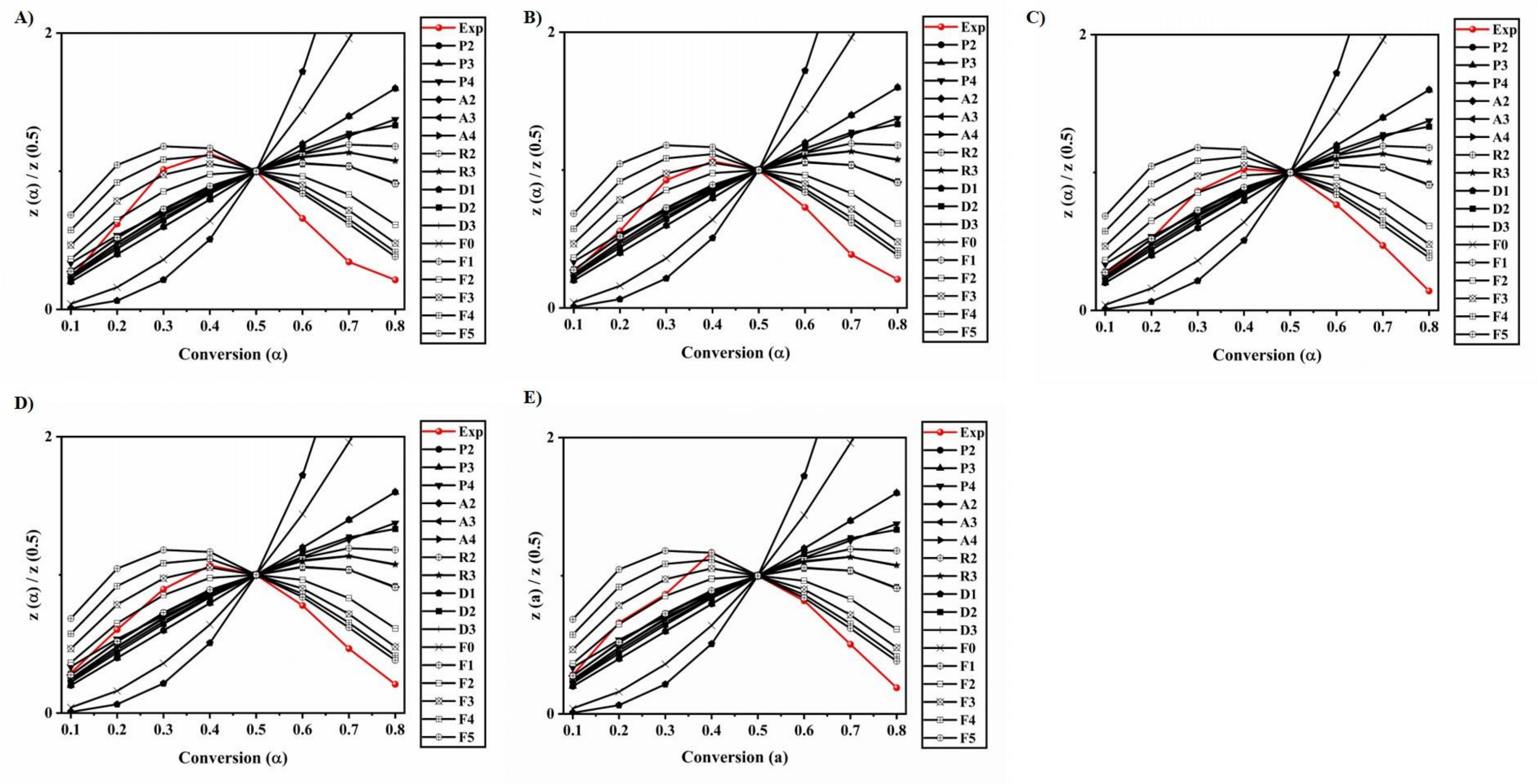

Figure 5.2.3.2: Master plots of BRT waste **A)** 5°C min^{-1}, **B)** 10°C min^{-1}**, C)** 20°C min^{-1}**, D)** 35°C min^{-1}**, E)** 55°C min^{-1}.

5.2.4 Estimation of thermodynamics

Thermodynamic (TD) parameters, including pre-exponential factor (k_o), Enthalpy change (ΔH), and Gibbs free energy change(ΔG) of BRT waste, were investigated and presented in **Figure 5.2.4.** TD calculations were computed using Eqs. 17, 18, and 19 from DFM, KAS, OFW, STK, and DAE approaches. TD parameters of BRT waste through DFM and DAE were included in **Figure 5.2.4**, while KAS, OFW, and STK approaches were included in **(Table 5.2.4)**. **Figure 5.2.4 (A1 and B1)** illustrates the variations in enthalpy change (ΔH) Vs. (α) for both DFM and DAE approach. **Figure 5.2.4 (A1 and B1)** demonstrates that the heating rate has a negligible effect on ΔH. Also, the variation in enthalpy was affected by changes in activation energy, which depended on conversion value. When conversion (α) was 0.8, the highest enthalpy value was 183.77 kJ mol^{-1} for DFM and 183.87 kJ mol^{-1} for DAE. The positive value of ΔH from 0.1 to 0.8 conversion had been noticed, indicating that the pyrolytic decomposition of Butyl rubber tube (BRT) waste was endotherm.

Furthermore, as the enthalpy change was increased from 0.1 to 0.8 conversion, the endothermicity of Butyl rubber tube (BRT) waste increased. Further, the variations in Gibbs free energy change (ΔG) Vs. (α) was depicted in **Figure 5.2.4 (A2 and B2)**. ΔG was a fundamental TD state function that evaluates the degree of spontaneity in reactions. Additionally, ΔG also explained that the energy in the system increases as the reactant approaches activated complex state formation [41], [51]. The slight variations in ΔG values were observed between 0.1 to 0.8 conversion, and the maximum value was 185.63 kJ mol^{-1} for DFM and 183.87 kJ mol^{-1} for DAE approaches was ascertained. The variation of ΔG results revealed that Butyl rubber tube (BRT) waste exhibited high reactivity and spontaneity.

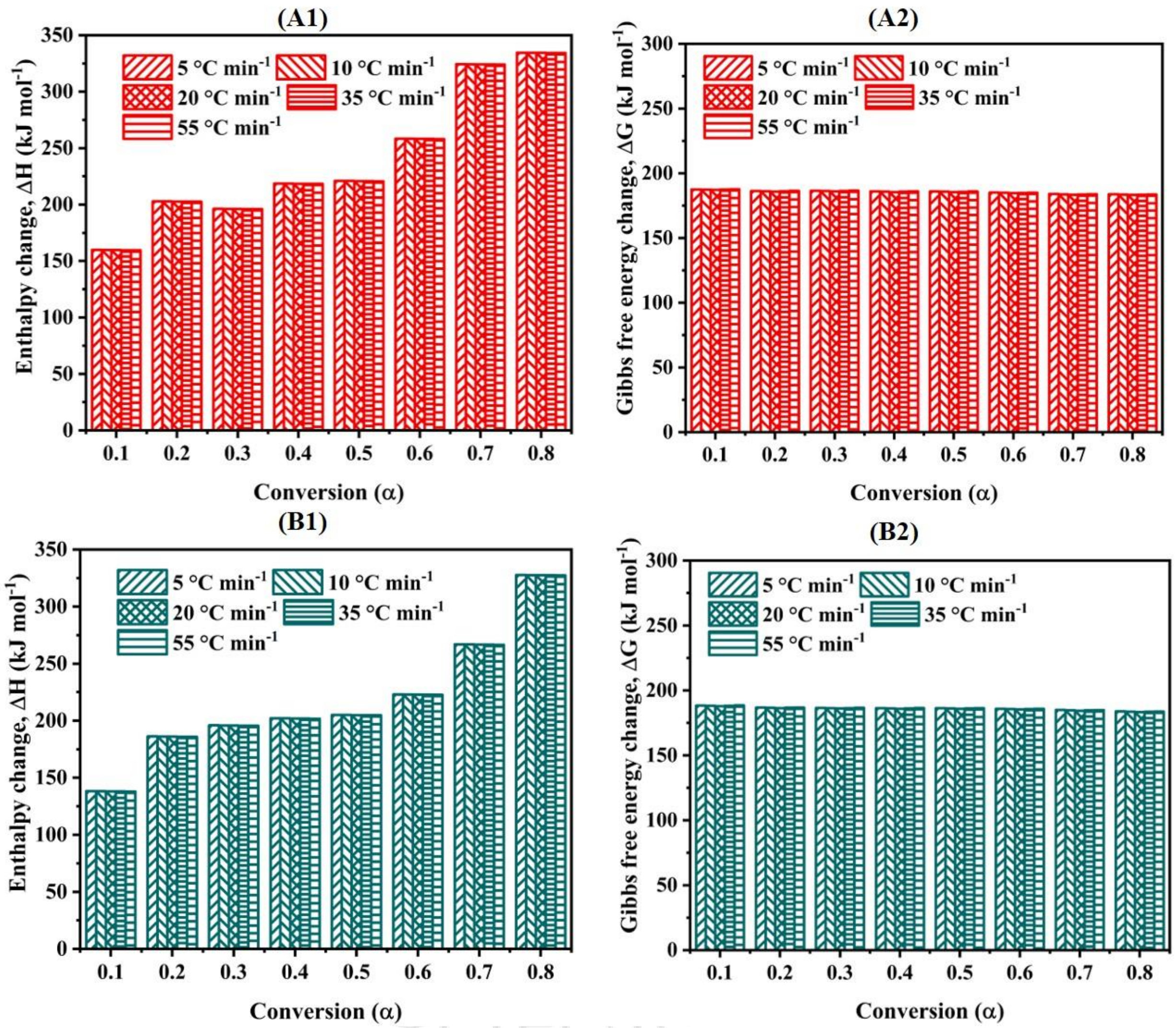

Figure 5.2.4: Thermodynamic plots of BRT waste **A1 and B1)** change in enthalpy, **A2 and B2)** change in Gibbs energy**, A3 and B3)** change in entropy from DFM and DAE approaches.

Table 5.2.4: Thermodynamic properties of butyl rubber tube pyrolysis at different heating rates.

Table 5.2.4.1 Thermodynamic properties of BRT waste at a heating rate of 5 °C min^{-1}

α	DFM			KAS			OFW			STK			DAE		
	k_o	ΔH	ΔG	k_o	ΔH	ΔG	k_o	ΔH	ΔG	k_o	ΔH	ΔG	k_o	ΔH	ΔG
0.1	1.84E+11	159.86	187.56	2.60E+09	138.22	188.30	4.03E+09	140.44	188.22	2.74E+09	138.49	188.29	2.60E+09	138.22	188.30
0.2	8.32E+14	202.87	186.34	3.23E+13	186.23	186.78	3.54E+13	186.71	186.77	3.40E+13	186.50	186.77	3.23E+13	186.23	186.78
0.3	2.30E+14	196.29	186.51	2.11E+14	195.85	186.52	2.21E+14	196.07	186.52	2.22E+14	196.11	186.52	2.11E+14	195.85	186.52
0.4	1.80E+16	218.64	185.96	7.10E+14	202.06	186.36	7.18E+14	202.11	186.36	7.47E+14	202.32	186.36	7.10E+14	202.06	186.36
0.5	2.85E+16	221.00	185.90	1.28E+15	205.07	186.29	1.29E+15	205.10	186.29	1.35E+15	205.33	186.28	1.28E+15	205.07	186.29
0.6	4.04E+19	258.33	185.10	5.73E-03	223.00	414.11	3.67E+16	222.30	185.87	4.42E+16	223.25	185.85	4.20E+16	223.00	185.86
0.7	1.44E+25	324.33	183.93	2.11E+20	266.84	184.93	1.26E+20	264.19	184.99	2.20E+20	267.07	184.93	2.11E+20	266.84	184.93

0.8	1.02E+26	334.47	183.77	2.76E+25	327.68	183.87	9.85E+24	322.36	183.96	2.86E+25	327.88	183.87	2.76E+25	327.68	183.87
Avg	**1.46E+25**	**239.48**	**185.63**	**3.44E+24**	**218.12**	**214.65**	**1.23E+24**	**217.41**	**186.12**	**3.58E+24**	**218.37**	**186.11**	**3.44E+24**	**218.12**	**186.12**

Table 5.2.4.2 Thermodynamic properties of BRT waste at a heating rate of 10 °C min^{-1}

0.1	2.08E+11	159.77	187.40	3.15E+09	138.13	188.15	4.84E+09	140.35	188.06	3.32E+09	138.40	188.14	3.15E+09	138.13	188.15
0.2	8.16E+14	202.78	186.16	3.34E+13	186.14	186.60	3.66E+13	186.62	186.59	3.51E+13	186.40	186.60	3.34E+13	186.14	186.60
0.3	2.31E+14	196.19	186.33	2.12E+14	195.76	186.34	2.21E+14	195.98	186.34	2.23E+14	196.02	186.33	2.12E+14	195.76	186.34
0.4	1.68E+16	218.55	185.77	6.98E+14	201.97	186.18	7.06E+14	202.02	186.18	7.35E+14	202.23	186.17	6.98E+14	201.97	186.18
0.5	2.64E+16	220.91	185.71	1.24E+15	204.98	186.10	1.25E+15	205.01	186.10	1.31E+15	205.24	186.09	1.24E+15	204.98	186.10
0.6	3.31E+19	258.24	184.89	1.11E-02	222.90	413.91	3.38E+16	222.20	185.68	4.06E+16	223.16	185.66	3.86E+16	222.90	185.66
0.7	9.53E+24	324.24	183.70	1.68E+20	266.75	184.72	1.01E+20	264.10	184.78	1.76E+20	266.98	184.72	1.68E+20	266.75	184.72
0.8	6.54E+25	334.38	183.54	1.80E+25	327.59	183.65	6.55E+24	322.27	183.73	1.87E+25	327.79	183.64	1.80E+25	327.59	183.65

Avg	**9.36E+24**	**239.38**	**185.44**	**2.25E+24**	**218.03**	**214.46**	**8.19E+23**	**217.32**	**185.93**	**2.34E+24**	**218.28**	**185.92**	**2.25E+24**	**218.03**	**185.93**

Table 5.2.4.3 Thermodynamic properties of BRT waste at a heating rate of 20 °C min^{-1}

0.1	2.39E+11	159.68	187.11	3.87E+09	138.04	187.87	5.92E+09	140.26	187.79	4.08E+09	138.31	187.86	3.87E+09	138.04	187.87
0.2	8.20E+14	202.69	185.85	3.54E+13	186.05	186.30	3.87E+13	186.52	186.29	3.72E+13	186.31	186.30	3.54E+13	186.05	186.30
0.3	2.36E+14	196.10	186.02	2.18E+14	195.67	186.04	2.27E+14	195.89	186.03	2.29E+14	195.93	186.03	2.18E+14	195.67	186.04
0.4	1.60E+16	218.46	185.45	7.03E+14	201.87	185.87	7.11E+14	201.93	185.87	7.39E+14	202.14	185.86	7.03E+14	201.87	185.87
0.5	2.50E+16	220.82	185.40	1.24E+15	204.88	185.79	1.25E+15	204.92	185.79	1.30E+15	205.15	185.79	1.24E+15	204.88	185.79
0.6	2.79E+19	258.15	184.57	2.14E-02	222.81	413.60	3.19E+16	222.11	185.36	3.82E+16	223.07	185.34	3.64E+16	222.81	185.35
0.7	6.53E+24	324.15	183.35	1.38E+20	266.66	184.39	8.39E+19	264.01	184.45	1.44E+20	266.89	184.39	1.38E+20	266.66	184.39
0.8	4.34E+25	334.29	183.19	1.22E+25	327.50	183.30	4.52E+24	322.18	183.38	1.27E+25	327.70	183.29	1.22E+25	327.50	183.30
Avg	**6.24E+24**	**239.29**	**185.12**	**1.53E+24**	**217.94**	**214.15**	**5.65E+23**	**217.23**	**185.62**	**1.58E+24**	**218.19**	**185.61**	**1.53E+24**	**217.94**	**185.61**

Table 5.2.4.4 Thermodynamic properties of BRT waste at a heating rate of 35 °C min^{-1}

0.1	2.45E+11	159.59	187.44	4.24E+09	137.94	188.22	6.43E+09	140.17	188.13	4.46E+09	138.22	188.20	4.24E+09	137.94	188.22
0.2	7.37E+14	202.60	186.16	3.34E+13	185.96	186.62	3.65E+13	186.43	186.61	3.51E+13	186.22	186.61	3.34E+13	185.96	186.62
0.3	2.17E+14	196.01	186.34	2.00E+14	195.58	186.35	2.08E+14	195.80	186.34	2.10E+14	195.84	186.34	2.00E+14	195.58	186.35
0.4	1.37E+16	218.37	185.75	6.33E+14	201.78	186.18	6.40E+14	201.84	186.18	6.65E+14	202.05	186.17	6.33E+14	201.78	186.18
0.5	2.13E+16	220.73	185.70	1.11E+15	204.79	186.10	1.11E+15	204.83	186.10	1.16E+15	205.06	186.09	1.11E+15	204.79	186.10
0.6	2.12E+19	258.06	184.85	3.62E-02	222.72	413.90	2.70E+16	222.02	185.67	3.23E+16	222.98	185.64	3.08E+16	222.72	185.65
0.7	4.05E+24	324.06	183.62	1.02E+20	266.57	184.68	6.25E+19	263.92	184.73	1.06E+20	266.80	184.67	1.02E+20	266.57	184.68
0.8	2.61E+25	334.19	183.45	7.51E+24	327.41	183.56	2.82E+24	322.09	183.65	7.78E+24	327.61	183.56	7.51E+24	327.41	183.56
Avg	**3.77E+24**	**239.20**	**185.41**	**9.38E+23**	**217.84**	**214.45**	**3.53E+23**	**217.14**	**185.93**	**9.73E+23**	**218.10**	**185.91**	**9.38E+23**	**217.84**	**185.92**

Table 5.2.4.5 Thermodynamic properties of BRT waste at a heating rate of 55 °C min^{-1}

0.1	2.51E+11	159.52	187.67	4.59E+09	137.87	188.46	6.92E+09	140.09	188.37	4.82E+09	138.14	188.45	4.59E+09	137.87	188.46
0.2	6.82E+14	202.52	186.37	3.22E+13	185.88	186.84	3.51E+13	186.36	186.82	3.38E+13	186.15	186.83	3.22E+13	185.88	186.84
0.3	2.04E+14	195.94	186.55	1.88E+14	195.50	186.56	1.96E+14	195.72	186.56	1.97E+14	195.76	186.56	1.88E+14	195.50	186.56
0.4	1.22E+16	218.30	185.96	5.87E+14	201.71	186.39	5.93E+14	201.77	186.39	6.16E+14	201.97	186.39	5.87E+14	201.71	186.39
0.5	1.88E+16	220.65	185.90	1.02E+15	204.72	186.31	1.03E+15	204.75	186.31	1.07E+15	204.99	186.31	1.02E+15	204.72	186.31
0.6	1.72E+19	257.98	185.05	5.54E-02	222.65	414.10	2.39E+16	221.95	185.87	2.84E+16	222.91	185.85	2.71E+16	222.65	185.85
0.7	2.80E+24	323.98	183.80	8.09E+19	266.49	184.87	4.99E+19	263.84	184.92	8.44E+19	266.72	184.86	8.09E+19	266.49	184.87
0.8	1.76E+25	334.12	183.63	5.14E+24	327.33	183.74	1.96E+24	322.01	183.83	5.33E+24	327.53	183.74	5.14E+24	327.33	183.74
Avg	**2.55E+24**	**239.13**	**185.62**	**6.42E+23**	**217.77**	**214.66**	**2.45E+23**	**217.06**	**186.13**	**6.66E+23**	**218.02**	**186.12**	**6.42E+23**	**217.77**	**186.13**

α – Conversion, k_o – Pre-exponential factor, ΔH *and* ΔG - Change in enthalpy and Gibbs free energy (kJ mol^{-1})

5.2.5 Pyrolysis performance characteristics (PPC)

The pyrolysis performance characteristics of the Butyl rubber tube (BRT) waste throughout the pyrolysis process are shown in **Table 5.2.5**. From the tabulated data, it was observed that all the characteristic values, such as flammability (C), ignition (D_i), burnout (D_b), combustion (S), and devolatilization (D_v) of BRT waste, were increased from 5 to 55°C min^{-1} heating rates. Also, at the increased heating rates, the values of temperatures (ignition T_i, degradation T_p, burnout T_b) and times (ignition t_i, degradation t_p, burnout t_b) factors of BRT waste were increased and decreased, respectively. The higher C value of BRT waste was (1.14×10^{-4}) observed at 55°C min^{-1} because of lower moisture content. The higher D_i and D_b values of BRT waste (1.82×10^{-1} and 9.59×10^{-3}) indicated good combustion ability. The higher S value of BRT waste (3.19×10^{-7}) suggested a better combustion performance. The higher D_v value of BRT waste (5.34×10^{-7}) revealed the formation of more volatile matter when it was subjected to pyrolysis. The ascertained PPC findings of the current research work were consistent with the other reports [41], [51].

Table 5.2.5: Pyrolysis performance characteristics of BRT waste.

β	T_i	T_p	T_b	$\Delta T_{0.5}$	t_i	t_p	t_b	$\Delta t_{0.5}$	$-R_p$	$-R_v$	C	D_i	D_b	S	D_v
5	561	632	1248	608	4.8	4	190	62	3.7	0.3	1.18E-05	1.93E-01	7.85E-05	2.83E-09	5.15E-09
10	573	643	1216	618	27.5	7	91.9	32	7.5	0.6	2.28E-05	3.90E-02	3.64E-04	1.13E-08	1.98E-08
20	580	654	1185	628	14.1	15	39.3	16.5	14.7	1.2	4.37E-05	6.95E-02	1.51E-03	4.43E-08	7.41E-08
35	594	665	1202	640	8.4	27	39.1	9.8	26.8	2.1	7.60E-05	1.18E-01	2.59E-03	1.33E-07	2.23E-07
55	601	674	1212	646	5.5	41	16.6	6.3	41.1	3.4	1.14E-04	1.82E-01	9.59E-03	3.19E-07	5.34E-07

5.2.6 Summary and Comparative analysis with existing work

A summary of objective 2 and the comparative analysis with existing work (**Table 5.2.6**) was discussed below.

Summary of the objective 2.

The following statements were obtained from objective 2:

- The behavior of thermal degradation of butyl rubber tube (BRT) waste was evaluated.
- The heating rate effect on the thermal degradation of BRT waste was studied.
- The pyrolytic zone temperature ranging from 150-768 °C was noticed with a maximum mass loss of about 60.5 wt. %.
- Based on the kinetic study, it was ascertained that the Ozawa-Flynn-Wall model estimated the lowest average activation energy of 222.67 kJ/mol.
- The multistep reaction mechanism was predicted from conversion (0.1 to 0.8) during the BRT pyrolysis by Criado's model.
- Based on the thermodynamic study, $\Delta H \approx 183.77$ kJ/mol and $\Delta G \approx 185.63$ kJ/mol indicated the endothermic and non-spontaneity of BRT pyrolysis.
- Furthermore, the pyrolysis performance characteristics for BRT were discussed.

Table 5.2.6: Comparative analysis of pyrolysis of butyl rubber tube waste.

1	Natural rubber (10 mg)	-	Mettler Toledo TGA/DSC 1	30 – 600	N_2 –100	2, 5, 10, 15, 20	$E_{\alpha=0.1\text{-}1.0}$ and k_o: 434 and 32.2 by DFM	-	[44]
2	Polyisoprene synthetic (10 mg)	-	Mettler Toledo TGA/DSC 1	30 – 600	N_2 –100	2, 5, 10, 15, 20	$E_{\alpha=0.1\text{-}1.0}$ and k_o: 372 and 27.2 by DFM	-	[44]
3	Butadiene rubber (10 mg)	-	Mettler Toledo TGA/DSC 1	30 – 600	N_2 –100	2, 5, 10, 15, 20	$E_{\alpha=0.1\text{-}1.0}$ and k_o: 244 and 15.1 by DFM	-	[44]
4	Styrene Butadiene rubber (10 mg)	-	Mettler Toledo TGA/DSC 1	30 – 600	N_2 –100	2, 5, 10, 15, 20	$E_{\alpha=0.1\text{-}1.0}$ and k_o: 235 and 14.7 by DFM	-	[44]
5	Milk packet waste (10 mg)	-	Exstar-SII 6300	35 – 800	N_2 – 100	5, 10, 20	$E_{\alpha=0.1\text{-}0.95}$ and k_o: 175 and 1.46×10^{13}, 178 and	$E_{\alpha=0.1\text{-}0.80}$: ΔH: 172, ΔG: 160, and ΔS:	[45]

							1.47 × 10^{13} by KAS, OFW	0.018	
6	Polyethylene	-	Perkin Elmer STA-8000	25 – 900	N_2 – 50	10, 20, 30	$E_{\alpha=0.1\text{-}0.90}$: 156, 159, 148, 171, by KAS, OFW, STK, DFM	$E_{\alpha=0.1\text{-}0.80}$: ΔH: 176, ΔG: 222, and ΔS: 0.145	[41]
7	Butyl rubber tube waste (6 mg)	-	Netsch TG209F1	25 – 1000	N_2 – 40	5, 10, 20, 35, 55	$E_{\alpha=0.1\text{-}0.80}$ and k_o: 245 and 2.73 × 10^{24}, 223 and 3.01 × 10^{24}, 223 and 6.82 × 10^{21}, 223 and 2.35 × 10^{24}, 223 and 1.84 × 10^{24} by DFM, KAS, OFW, STK, DAE	$E_{\alpha=0.1\text{-}0.80}$: ΔH: 239, and ΔG: 185	Objective 2

β – Heating rates (°C min^{-1})

α – Conversion

°C – Temperature

Q – Flowrate of carrier gas (mL min^{-1})

Iso – conversional models – Differential Friedman (DFM), Kissinger-Akahira-Sunose (KAS), Ozawa-Flynn-Wall (OFW), Starink (STK), and Distributed Activation Energy (DAE)

*Kinetics – Average values

*Thermodynamics – Average values based on DFM model at 10 °C min^{-1}

E_α – Activation energy (kJ mol^{-1})

k_o – Frequency factor (s^{-1})

ΔH – Change in enthalpy (kJ mol^{-1})

ΔG – Change in Gibbs free energy (kJ mol^{-1})

ΔS – Change in entropy (kJ mol^{-1} K^{-1})

5.3 Reaction kinetics and thermodynamic analysis of non-isothermal co-pyrolysis of *Delonix Regia* and tube waste

5.3.1 Physio-chemical characterization

The characterization results, including proximate (ASTM E1756-08 for moisture content, ASTME872-82 for volatile matter, ASTM E1755-01 for ash content) and ultimate analysis of DR and TW were carried out and discussed in our earlier works [5], [6]; hence are not repeated; however, a summary was provided in a tabular form **(Table 5.3.1)**. The HHV of DR biomass was 17.53 MJ/kg, and that of TW was 22.07 MJ/kg. Their co-feed of 1:1 ratio yielded higher yield and HHV bio-oil [5], [6]; thus, to investigate their kinetics and thermodynamics, the same ratio was maintained in this work.

Table 5.3.1 Proximate and ultimate analysis of DR and TW

Sample	Proximate analysis (wt. %, dry basis)				Ultimate analysis (wt. %, dry basis-ash free)					H/C	O/C	HHV (M.J./kg)
	VM	FC	Ash	Moisture (%)	C	H	N	S	O			
DR*	72.66	16.92	1.22	45.02	5.96	1.21	NA	47.80	0.13	1.07	9.20	17.53
TW*	56.65	33.75	10.25	57.98	6.21	NA	1.09	35.72	0.11	0.62	NA	22.07

VM: Volatile matter, FC: Fixed carbon, C: Carbon, H: Hydrogen, N: Nitrogen, S: sulphur, O: Oxygen, NA: Not available, HHV: High heating value.

5.3.2 Thermogravimetric analysis (TGA)

The TGA analysis of co-pyrolysis of DR and TW (1:1 on a dry weight basis) feedstock was carried out at different heating rates (5, 10, 20, 35, 55°C min^{-1}) at a temperature ranging from 25 to 1000°C and at a nitrogen flow rate of 40mL/min. The TGA and DTG of co-feed at different heating rates have been shown in **Figure 5.3.2 (A) and (B),** respectively. All the thermograms show that the entire pyrolysis of DR and TW co-feed was divided into three zones: I-Dehydration zone (25-150°C); II-Pyrolytic zone (150-780°C); III-Passive zone (780-1000°C). However, these zones' temperature conditions varied with heating rates and feedstock type. It was observed that the heating rate alters the position of different zones and kinetic parameters T_{Range}, DT_{max}, and DR_{max} in TG and DTG thermograms of dehydration, pyrolytic and passive zones, respectively, and a summary of changes in these kinetic parameters have been displayed **(Table 5.3.2)**. In summary, for pyrolysis and passive zones, T_{Range}, DT_{max}, and DR_{max} shifted towards the higher temperature side when the heating rate increased from 5 to 55 °C min^{-1}; however, for the dehydration zone, except T_{Range}, other parameters displayed a reverse trend as compared to different two zones while increasing the heat rates.

Table 5.3.2 Different zones and degradation parameters of co-pyrolysis of *Delonix Regia* and tube waste at different heating rates.

Heating Rate (°C min^{-1})	Zones											
	I (Dehydration Zone)				II (Pyrolytic Zone)				III (Passive Zone)			
	TG		DTG		TG		DTG		TG		DTG	
	T_{Range} (°C)	Mass Loss (wt.%)	$DT_{max.}$ (°C)	$DR_{max.}$ (wt.% min^{-1}).	T_{Range} (°C)	Mass Loss (wt.%)	$DT_{max.}$ (°C)	$DR_{max.}$ (wt.% min^{-1}).	T_{Range} (°C)	Mass Loss (wt.%)	$DT_{max.}$ (°C)	$DR_{max.}$ (wt.% min^{-1}).
5	25-152	3.5	86	2.5	152-696	63.4	340	2.8	696-998	4.2	-	-
10	25-148	2.3	74	2.2	148-719	62.8	352	5.5	719-995	1.9	-	-
20	25-155	3.5	61	1.2	155-737	63.5	364	11	737-993	1	791	0.1
35	25-169	3.7	51	0.4	169-766	63	376	19.8	766-991	0.7	782	0.2
55	25-152	3.2	37	0.4	152-782	63.8	388	31	782-993	0.5	801	0.2
$DT_{max.}$ - Maximum degradation temperature and $DR_{max.}$ - Maximum degradation rate												

In Zone-I (25-150°C), the significant water removal and low molecular weight components occurred with a 2-4% weight loss. For the co-pyrolysis of DR and TW, the weight losses were 3.5, 2.3, 3.5, 3.7, and 3.2% at 5, 10, 20, 30, and 55 °C $\text{min}^{-1,}$ respectively (see Figure 1A). Zone-II (150-780°C) was the essential pyrolysis zone, and the maximum degradation and decomposition of the feed occurred with 62-65% weight loss. The main components, hemicellulose (HC), cellulose (CEL), lignin (LIG), isobutylene (IB), and isoprene (IP), in the co-feed mixture of DR and TW, undergo pyrolysis with the temperature to evolve various volatile species. In this Zone-II, higher molecular weight components break down into smaller molecular weight components in the presence of a constant supply of heat energy.

It has been found that HC contains more moisture content than lignin, resulting in a lower softening point for hemicellulose. Also, it reduced the thermal decomposition range of pyrolysis temperature [98]. Xylan was a primary constituent of hemicellulose; due to its lower thermal stability, it could be hydrolyzed and dehydrated quickly [98]. The degradation of xylan produces primarily water, formic acid, acetic acid, methanol, propionic acid, 2-furfuraldehyde, butanone, hydroxy-1-butanone, hydroxy-1- propanone that could be identified in the bio-oil [98]. In comparison to HC, CEL degrades primarily via three routes. The first route involves the depolymerization of cellulose; via the scission of chemical bonds - dehydration, formation of free radicals, and oxygenated substituents (for example, carboxyl groups, carbonyls, peroxides). All these reactions occur at lower temperatures at less than 280°C [98]. The second route encompasses the depolymerization of cellulose glycosidic bonds, producing a tar-rich pyrolysate containing oligosaccharides, anhydrosugars, levoglucose, and some glucose compounds that were formed between 280-500°C [98].

The third route was a direct conversion of cellulose into low molecular weight compounds like volatile products and gases; via dehydration, decarboxylation, disproportionation, and fission at temperatures greater than 500°C [98].

From **Figure 5.3.2 (A and B)**, TG and DTG thermograms demonstrated that as the heating rate increased, the TG thermograms shifted to a higher temperature region without affecting the degradation spectrum. This behavior manifested as increased heating rates and decreased mass transfer efficiency. As the heating rate increases, peaks shift to higher temperatures, indicating that the feedstock has attained the required degradation temperature in a shorter period. From **Figure 5.3.2 (A),** when the heating rate was increased in the order of 5, 10, 25, 35, and 50°C/min^{-1}, the TG thermograms of DR and TW mixtures shifted from 696°C, 720°C, 741°C, 784°C, and 787°C respectively. The temperature shift occurred due to variations in the degradation temperature of the DR and TW mixture with changes in heating rates (5-55°C min^{-1}). Compared to the lower heating rate (5°C min^{-1}), degradation occurred moderately (31 wt.% min^{-1}) at the higher heating rate (55°C min^{-1}) due to heat transfer limitations between the feed particles.

Additionally, the maximum amount of heat exchange between particles occurred. According to a report, the degradation rate increased as the heating rate increased. From **Figure 5.3.2 (B)**, it was clear that a similar kind of trend was also observed in the present study. Furthermore, the volatile matter was insignificantly affected at higher heating rates. From (**Table 5.3.2)**, it was recorded that the significant weight losses in this zone – II (in the range of about 152-782°C) were 63.4%, 62.8%, 63.5%, 63%, and 63.8% at 5, 10, 20, 30, and 55 °C min^{-1} respectively**.** Less significant alteration of mass losses trend was observed with increasing heating rates. It was also demonstrated that by increasing the heating rate, the total volume of volatile compounds increases, whereas decreasing the heating rate results in volatile compounds remaining in the reactor for longer. Therefore, the longer residence time favored the generation of secondary reactions like re-condensation, re-polymerization, and cracking reactions, all of which contribute to bio-char growth [120]. The slight reduction in volatilization was attributed to mass and heat exchange constraints during the pyrolysis.

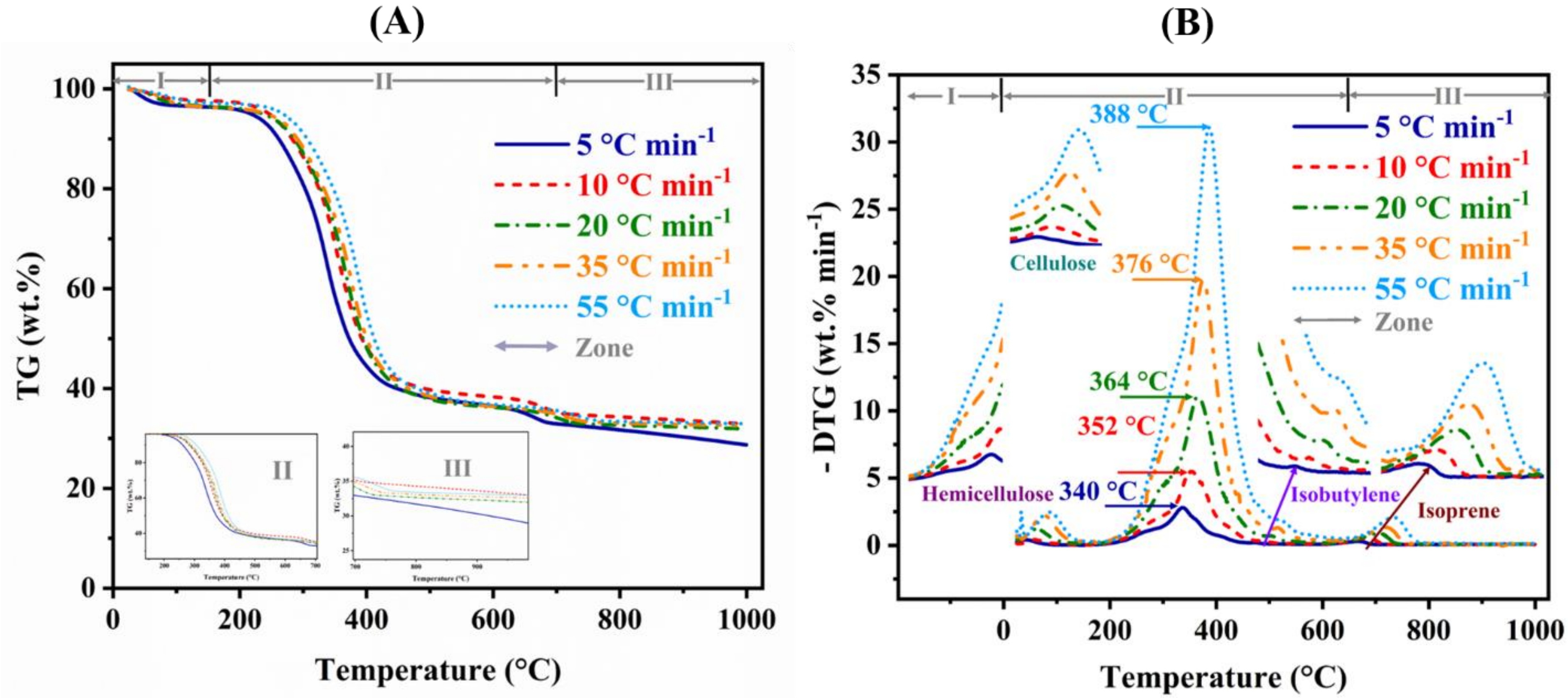

Figure 5.3.2: Thermogravimetry and differential thermal gravimetry of *Delonix Regia* and tube waste co-feed **A)** TG and **B)** DTG

Based on the DTG results **(Figure 5.3.2 B)**, the peaks observed at 226-348°C indicated hemicelluloses decayed within the temperature range of 226-284, 243-315, 260-333, 268-343, and 272-348 °C at 5, 10, 20, 35, and 55 °C min^{-1} heating rates, respectively. Also, peaks observed at 310-412°C confirmed the breakdown of cellulose with the temperature range of 310-385, 312-395, 326-396, 338-404, and 355-412 °C at 5, 10, 20, 35, and 55 °C min^{-1} heating rates, respectively. At the same time, lignin decay occurred at a slower rate (but at >500°C) with no sharper peaks**.** Blasi et al. [99] stated that HC, CEL, and LIG decayed at 225-325°C, 325-375°C, and 417-607°C, respectively. Furthermore, peaks observed at 460-546°C represent the detection of isobutylene with the temperature range of 460-492, 465-511, 484-533, 495-542, and 501-546 °C at 5, 10, 20, 35, and 55 °C min^{-1} heating rates, respectively [5].

Finally, peaks observed at 629-789°C correspond to the isoprene with the temperature range of 629-707, 641-738, 649-762, 652-775, and 661-789 °C at 5, 10, 20, 35, and 55 °C min^{-1} heating rates, respectively [5]. Kawale and Kishore [5] investigated DR and TW putrefaction for bio-oil production and reported degradation temperatures for isobutylene and isoprene components of 380°C and 740°C, respectively. The obtained TGA results from the present study were consistent with similar studies reported in the literature [2], [6], [39], [121], [122].

In zone III (695-1000°C), the lignin was decomposed (>500°C) very slowly due to the higher thermal stability. Dehydration of lignin began at approximately 200 °C during pyrolysis, which is primarily responsible for its thermal degradation [98]. The degradation of lignin cleavage attributed to C–O bonds leads to a single oxygen atom product. Whereas methoxy cleavage C–O bonds form products containing two oxygen atoms between the temperatures 327 and 377 °C, cleavage of the sideways chain C–C bonds occurred between the aromatic ring and carbon [98]. Furthermore, biochar was formed due to the decay of weaker bonds (alkyl-aryl ether) under mild reaction conditions [98]. From Table **(Table 5.3.2)**, significantly less decay in mass losses was observed in zone - III, decreasing from 4.5% to 0.5%, observed at 696-993 °C with increasing heating rates (5-55°C/min). Thus, it was confirmed that no further devolatilization took place; however, the unburnt materials like carbon and ash were still present in the solid phase of biochar.

5.3.3 Determination of apparent activation energy (E_α)

The kinetic parameters, activation energy (E_α), and frequency factor (k_o) were calculated using different iso-conversional methods for the co-pyrolysis of DR biomass and TW co-feed of 1:1 ratio on a dry weight basis. Both model-free and model fittings methods, including DFM, KAS, OFW, STK, and DAEM, were used with the first-order reaction model to evaluate the kinetic analysis. The temperature range between 150 and 800 °C was selected for the kinetic studies over the conversion ranging from 0.1 to 0.8 at different heating rates (5, 10, 20, 35, and 55 °C min^{-1}). The results show that for the conversion values from 0.1 to 0.8, data fitted satisfactorily by all iso-conversional models. However, the correlation coefficient dropped significantly at higher conversions between 0.9 and 1.0; thus, the higher conversion cases had not been included in the results.

The activation energy (E_α), frequency factor (k_o), and correlation coefficient (R^2) were calculated using the best regression fit equations and reported in Table 1. The activation energies for DFM, KAS, OFW, STK, and DAEM methods (as per Eqs. 9, 10, 11, 12, and 13, respectively) were calculated from linear plots of ln $[\beta\, d\alpha/dT]$ vs. 1/T, ln $[\beta/T^2]$ vs. 1/T, ln$[\beta]$ vs. 1/T, ln$[\beta/T^{1.92}]$ vs. 1/T, and ln$[\beta/T^2]$ vs. 1/T respectively for different conversion (α) values. The plots of five iso-conversional methods for calculating E_α for co-pyrolysis of DR and TW show similar trends. The linear plots for calculating kinetic parameters using all iso-conversional methods for DR and TW co-feed in the conversion range of $\alpha = 0.2–0.8$ have been shown in **Figure 5.3.3.1 (A-E)**. The data of iso-conversional lines versus the reciprocal of temperature for the DR and TW co-feed mixture obtained using the five iso-conversional methods at different heating rates (5-55°C min^{-1}) have been summarized in **Table 5.3.3.1**.

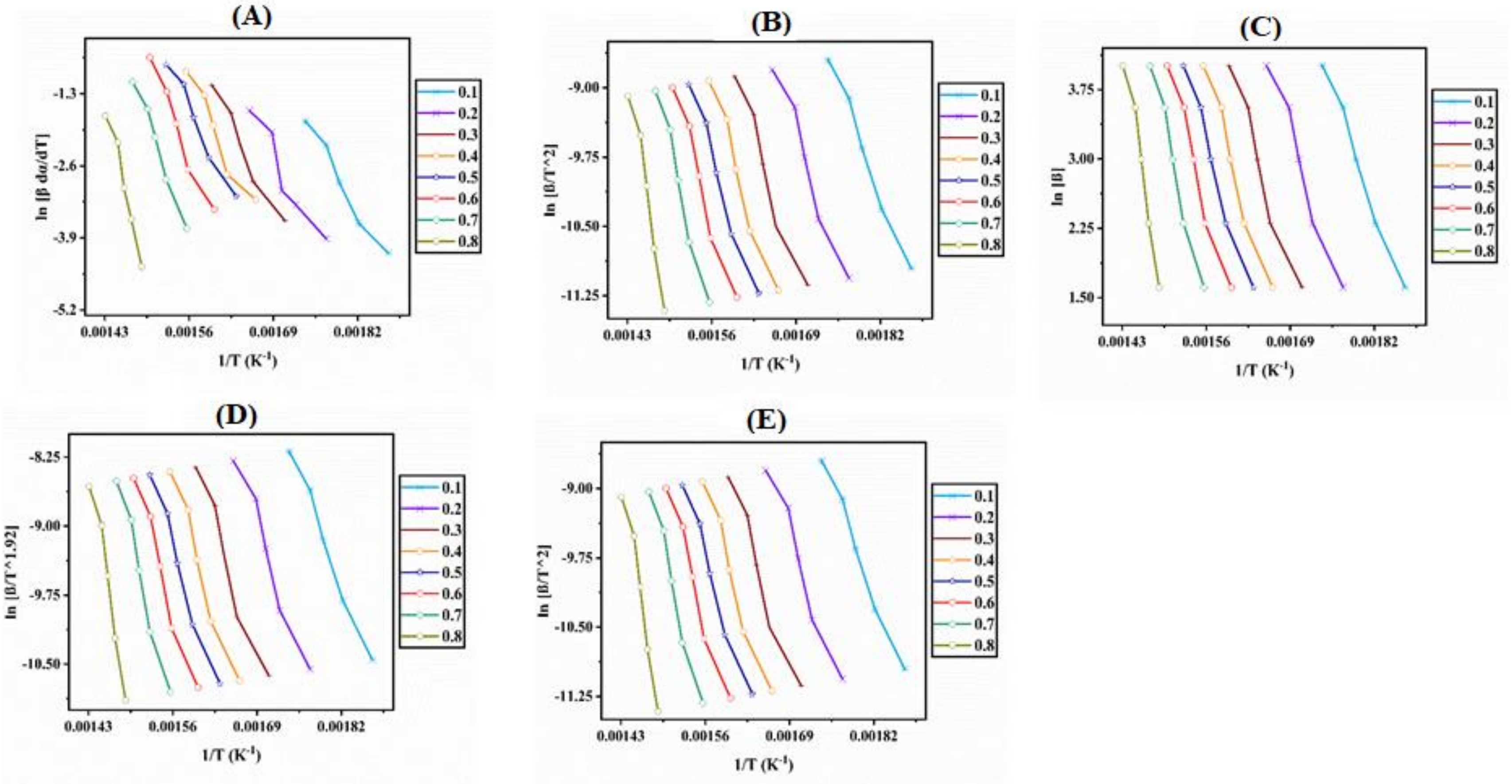

Figure 5.3.3.1: Iso-conversional lines versus 1/T plots of *Delonix Regia* and tube waste at different conversion and heating rates using different models:

A) DFM, **B)** KAS, **C)** OFW, **D)** STK, **E)** DAEM.

Table 5.3.3.1 Iso-conversional lines versus 1/T data of *Delonix Regia* and tube waste co-pyrolysis at different conversion and heating rates.

Heating rate (°C min^{-1})	Conversion (α)	1/T (K^{-1})	Iso-conversional Methods				
			DFM $\ln\,[\beta\, d\alpha/dT]$	KAS $\ln\,[\beta/T^2]$	OFW $\ln[\beta]$	STK $\ln[\beta/T^{1.92}]$	DAEM $\ln[\beta/T^2]$
5	0.1	0.00187	-4.2	-11.0	1.6	-10.5	-11.0
10	0.1	0.00182	-3.6	-10.3	2.3	-9.8	-10.3
20	0.1	0.00179	-2.9	-9.7	3.0	-9.1	-9.7
35	0.1	0.00177	-2.2	-9.1	3.6	-8.6	-9.1
55	0.1	0.00174	-1.8	-8.7	4.0	-8.2	-8.7
5	0.2	0.00177	-3.9	-11.1	1.6	-10.6	-11.1
10	0.2	0.00172	-3.3	-10.4	2.3	-9.9	-10.4
20	0.2	0.00170	-3.0	-9.8	3.0	-9.2	-9.8
35	0.2	0.00169	-2.0	-9.2	3.6	-8.7	-9.2
55	0.2	0.00165	-1.6	-8.8	4.0	-8.3	-8.8
5	0.3	0.00171	-3.6	-11.1	1.6	-10.6	-11.1
10	0.3	0.00166	-2.9	-10.5	2.3	-10.0	-10.5
20	0.3	0.00164	-2.2	-9.8	3.0	-9.3	-9.8
35	0.3	0.00162	-1.6	-9.3	3.6	-8.8	-9.3
55	0.3	0.00160	-1.1	-8.9	4.0	-8.4	-8.9
5	0.4	0.00166	-3.2	-11.2	1.6	-10.7	-11.2
10	0.4	0.00162	-2.8	-10.5	2.3	-10.0	-10.5
20	0.4	0.00160	-1.9	-9.9	3.0	-9.4	-9.9
35	0.4	0.00158	-1.3	-9.3	3.6	-8.8	-9.3
55	0.4	0.00156	-0.9	-8.9	4.0	-8.4	-8.9
5	0.5	0.00163	-3.1	-11.2	1.6	-10.7	-11.2
10	0.5	0.00159	-2.5	-10.6	2.3	-10.1	-10.6
20	0.5	0.00157	-1.7	-9.9	3.0	-9.4	-9.9
35	0.5	0.00155	-1.1	-9.4	3.6	-8.9	-9.4
55	0.5	0.00152	-0.8	-9.0	4.0	-8.4	-9.0
5	0.6	0.00160	-3.4	-11.3	1.6	-10.8	-11.3
10	0.6	0.00156	-2.7	-10.6	2.3	-10.1	-10.6
20	0.6	0.00154	-1.8	-10.0	3.0	-9.4	-10.0
35	0.6	0.00153	-1.3	-9.4	3.6	-8.9	-9.4
55	0.6	0.00150	-0.6	-9.0	4.0	-8.5	-9.0
5	0.7	0.00156	-3.7	-11.3	1.6	-10.8	-11.3
10	0.7	0.00152	-2.8	-10.7	2.3	-10.2	-10.7
20	0.7	0.00151	-2.1	-10.0	3.0	-9.5	-10.0
35	0.7	0.00150	-1.6	-9.5	3.6	-8.9	-9.5
55	0.7	0.00147	-1.1	-9.0	4.0	-8.5	-9.0
5	0.8	0.00149	-4.4	-11.4	1.6	-10.9	-11.4
10	0.8	0.00147	-3.6	-10.7	2.3	-10.2	-10.7
20	0.8	0.00146	-3.0	-10.1	3.0	-9.5	-10.1
35	0.8	0.00145	-2.2	-9.5	3.6	-9.0	-9.5
55	0.8	0.00143	-1.7	-9.1	4.0	-8.6	-9.1

Based on kinetic results obtained from **Figure 5.3.3.1 (A-E)** and **Table 5.3.3.2**, the average activation energy, E_α (kJ mol^{-1}), and frequency factor, k_o (min^{-1}) values of co-pyrolysis of DR and TW calculated by the five models were 230.47 and 2.55×10^{30}; 208.13 and 8.31×10^{26}; 207.78 and 1.58×10^{24}; 208.38 and 6.47×10^{26}; 208.13 and 5.15×10^{26}; respectively. From **Figure 5.3.3.1 (A-E)**, a strong correlation ($R^2 > 0.97$) was observed for the conversion (α) ranging from 0.1 to 0.8 for all the iso-conversional models. The average activation energy and frequency factors against the values of conversion have been shown in **Figure 5.3.3.2 (A-B)**. It was observed that the values of activation energy were increased with conversion value. And thus, it demonstrated the dependence of the activation energy (E_α) on conversion (α), especially when the conversion was 0.5 – 0.8.

To be specific, it was noticed that by all the methods, the activation energy increases marginally with the conversion value up to 0.5 because of the hemicellulose and cellulose degradation of DR and then increases rapidly with a massive change in E_α values for the conversion values from 0.5 to 0.8 range due to degradation of isobutylene and isoprene of TW. This kind of alteration of activation energies appeared due to biomass and tube waste mixture degradation. Further, the variations of E_α conformed to that mixture following the multi-step reaction pathway instead of a single path of reaction during the pyrolysis process. DR biomass and TW mixtures were heterogeneous; thus, the chemical structural constituents (hemicellulose, cellulose, lignin, isobutylene, isoprene, and plasticizer) had an individual degradation temperature range as was reflected in the variation of E_α and heating rates.

Furthermore, it was found that the reaction surface was influenced by mass diffusion in biomass [123]. Further, it was well known that the pyrolysis method, operation, heating rates, mathematical analysis, etc., affect the activation energy. Finally, because the thermal degradation process involves various changes (chemical and physical) linked to transport phenomena, adsorption, desorption, and other factors, it wasn't easy to present a single set of kinetic parameters in mathematical expressions [124]. Also, it was recorded that the high correlation coefficient (R^2 >0.96) was achieved, which specified that all the iso-conversional methods (DFM, KAS, OFW, STK, and DAEM) display the best regression fit with minor errors/deviation. In addition, all the iso-conversional methods produced accurate results with the least error. However, the average value of E_α obtained using DFM was generally slightly more significant than the other four methods. DFM was a different method that relied on the derivative data conversion, making it vulnerable to experimental noise and numerical instability. The DFM method exhibits a similar effect in this study, with higher activation energy (230.47 kJ mol^{-1}, R^2 =0.96).

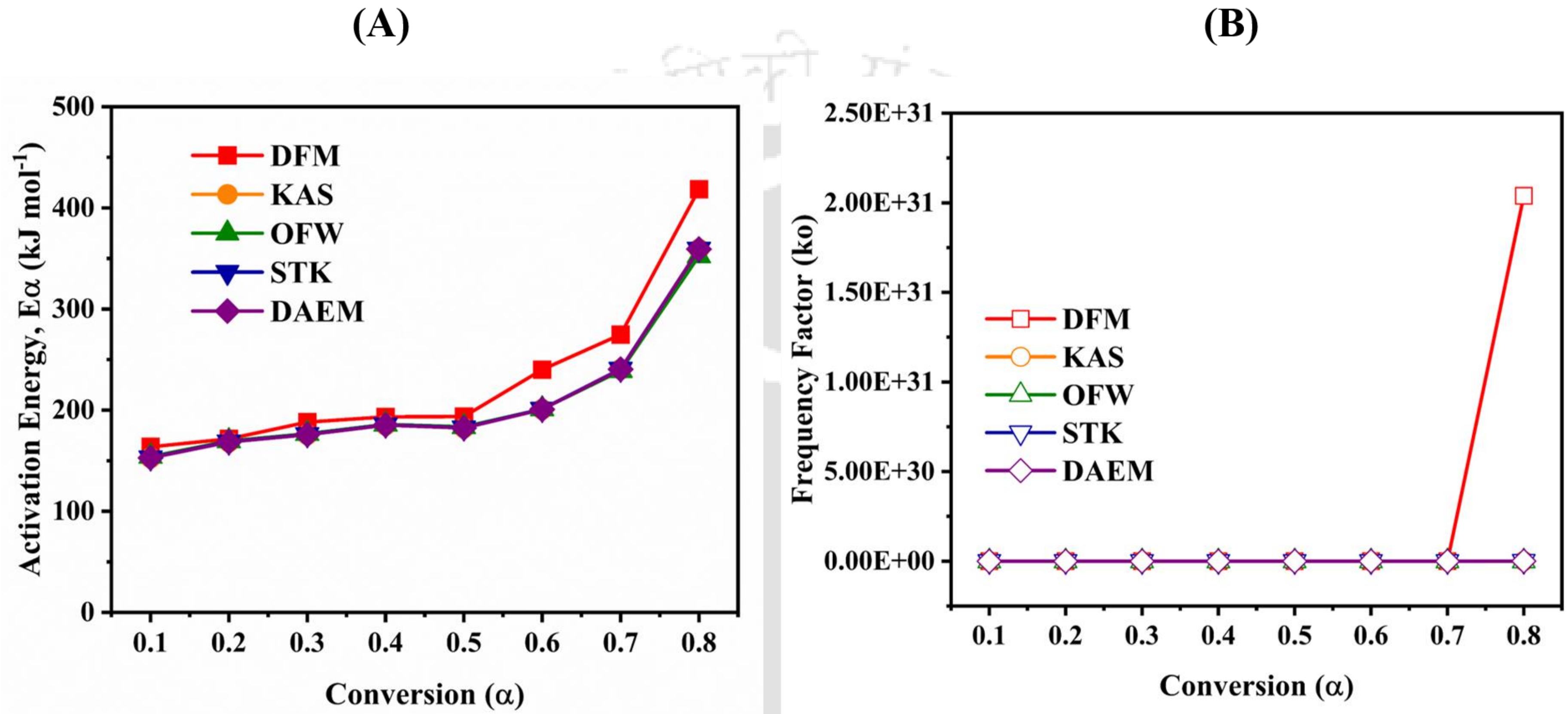

Figure 5.3.3.2: Activation energy and frequency factor of co-pyrolysis of *Delonix Regia* and tube waste by various iso-conversional methods **A)** Activation energy Vs. Conversion **B)** Frequency factor Vs. Conversion.

Table 5.3.3.2: Activation energy and frequency factor of co-pyrolysis of *Delonix Regia* and tube waste by various iso-conversional methods.

α	Iso-conversional Methods														
	DFM (Differential Friedman)			KAS (Kissinger-Akahira-Sunose)			OFW (Ozawa-Flynn-Wall)			STK (Starink)			DAEM (Distributed Activation Energy Method)		
	E (kJ mol^{-1})	k_o (min^{-1})	R^2	E (kJ mol^{-1})	k_o (min^{-1})	R^2	E (kJ mol^{-1})	k_o (min^{-1})	R^2	E (kJ mol^{-1})	k_o (min^{-1})	R^2	E (kJ mol^{-1})	k_o (min^{-1})	R^2
0.1	163.64	1.38E+14	0.970	152.86	2.65E+13	0.987	154.12	1.77E+11	0.988	153.10	2.17E+13	0.987	152.86	2.47E+14	0.987
0.2	171.56	1.60E+14	0.908	168.54	2.66E+14	0.964	169.50	1.62E+12	0.968	168.79	2.17E+14	0.964	168.54	1.17E+15	0.964
0.3	188.19	2.14E+15	0.964	175.71	4.65E+14	0.958	176.66	2.80E+12	0.962	175.97	3.80E+14	0.958	175.71	1.30E+15	0.958
0.4	193.48	3.63E+15	0.937	185.18	1.75E+15	0.967	185.91	1.00E+13	0.971	185.44	1.43E+15	0.968	185.18	3.36E+15	0.967
0.5	193.74	2.64E+15	0.972	182.43	6.70E+14	0.977	183.49	4.10E+12	0.979	182.71	5.47E+14	0.977	182.43	9.66E+14	0.977
0.6	240.03	8.23E+18	0.970	200.74	1.50E+16	0.969	201.09	7.92E+13	0.971	201.01	1.22E+16	0.969	200.74	1.63E+16	0.969
0.7	274.83	1.76E+21	0.985	240.39	1.39E+19	0.976	239.03	5.39E+16	0.978	240.64	1.11E+19	0.976	240.39	1.15E+19	0.976
0.8	418.31	2.04E+31	0.969	359.23	6.65E+27	0.967	352.45	1.26E+25	0.969	359.40	5.17E+27	0.967	359.23	4.12E+27	0.967
Avg.	**230.47**	**2.55E+30**	**0.96**	**208.13**	**8.31E+26**	**0.97**	**207.78**	**1.58E+24**	**0.97**	**208.38**	**6.47E+26**	**0.97**	**208.13**	**5.15E+26**	**0.97**

α – Conversion, E – Activation energy, k_o – Frequency factor

From **Figure 5.3.3.2 (A),** it was found that the activation energy fluctuated significantly, which confirmed the presence of multipart, multi-step reactions, as well as parallel, sequential, and competitive reactions [26], [28]. The alteration of E_α was due to the breakage of chemical bonds between the biomass and plastic, which had different thermal degradation temperature ranges [28]. Furthermore, the particle size and chemical structure of DR biomass (hemicellulose, cellulose, lignin) and tube waste (TW) (isobutylene, isoprene) feedstock influence the variations of activation energy. The weaker fractions, like hemicellulose, decomposed very quickly at low temperatures (<300 °C) and conversions (<0.5), whereas the stronger fractions, other than hemicellulose, were hard to break and it required additional energy [100], [106]. As a result, most of the co-pyrolysis of DR biomass and TW cracking occurs at higher temperatures (from 250 to 650 °C) and conversion ranges (from 0.5 to 0.8).

Based on the outcomes of the DFM model, Criado's method due to applied to predict the possible reaction mechanism of co-pyrolysis of DR and TW mixture at all five heating rates (5-55°C min^{-1}) throughout the conversion range (0.1-0.8) [67]. Over the conversion range, z(α)/z(0.5) experimental master curves were plotted using Eq. (21), and the theoretical master curves were plotted using Eq. (22). **Figure 5.3.3.3 (A to E)** shows the master plots of co-pyrolysis of DR and TW mixture in the conversion (α) range of 0.1 to 0.8 for all heating rates from 5 to 55 °C min^{-1}. The co-pyrolysis of the DR and TW mixture did not follow a single-step reaction mechanism; instead, it followed multi-step reaction mechanisms because of the complex composition of the mixture.

Different theoretical models were proposed for solid-state heterogeneous reactions like nucleation models; power law (P) and Avrami-erofeyev (A), geometrical contraction models (R), diffusional models (D), and reaction order models (F) [46], [58], [68], [69], [125], [126]. Nucleation models were related to the phase transformation that depends upon time, temperature, and materials heterogeneity (impurities, surfaces, defects, and edge dislocation)

[125]. The geometrical contraction model (R) governs the degradation of the reaction rate on the surface of the crystal lattice, which is dependent on its shape and size [125]. The diffusion (D) model governs the reaction between the reactants from different crystal lattices [125]. The reaction order model (F) dictates that the rate of reaction was proportional to the fraction or quantity of reactants and their concentration (wt. %) [125]. Different combinations of the model's schemes were observed during the degradation of the DR and TW mixture over the heating rates and conversions. For each conversion value, the possible reaction mechanism against different heating rates has been identified by Criado's master plot and summarized in **Table 5.3.3.3**.

In summary, the co-pyrolysis of the DR: TW (1:1wt. %) mixture at 5 °C min^{-1} of heat rate has initially followed second-order reaction (F2) then by R3, D2, and again F2 as the conversion changes from 0.1 to 0.4 respectively, whereas for conversions (0.6-0.8) the reaction followed mechanism of reaction order greater than fifth-order reaction (F5). At 10 °C min^{-1}, it was observed that F2 was followed by A4, A4, and P3 as the conversion increased from 0.1 to 0.4, respectively, and >F5 for the rest of the conversion values. At 20 °C min^{-1}, it was found that F3 followed by P3, D3, and F1 for conversion values from 0.1 to 0.4, respectively, whereas F4 at the conversion of 0.6 and >F5 for further higher conversions of 0.7-0.8. At 35 °C min^{-1}, it was displayed that F3 followed by A2, R2, and P3 for conversions from 0.1 to 0.4, respectively, and ≥ F5 for the conversion values of 0.6-0.8. At 55 °C min^{-1}, it was reported that F4 followed by P4, F2, and F2 for conversion values varying from 0.1 to 0.4, respectively, and R3, F4, and F5 for conversions of 0.6, 0.7, and 0.8 respectively. Finally, in summary, from the master plot analysis, higher reaction order (≥ F5) was observed from conversion (0.6-0.8) at various heating rates (5-55°C min^{-1}).

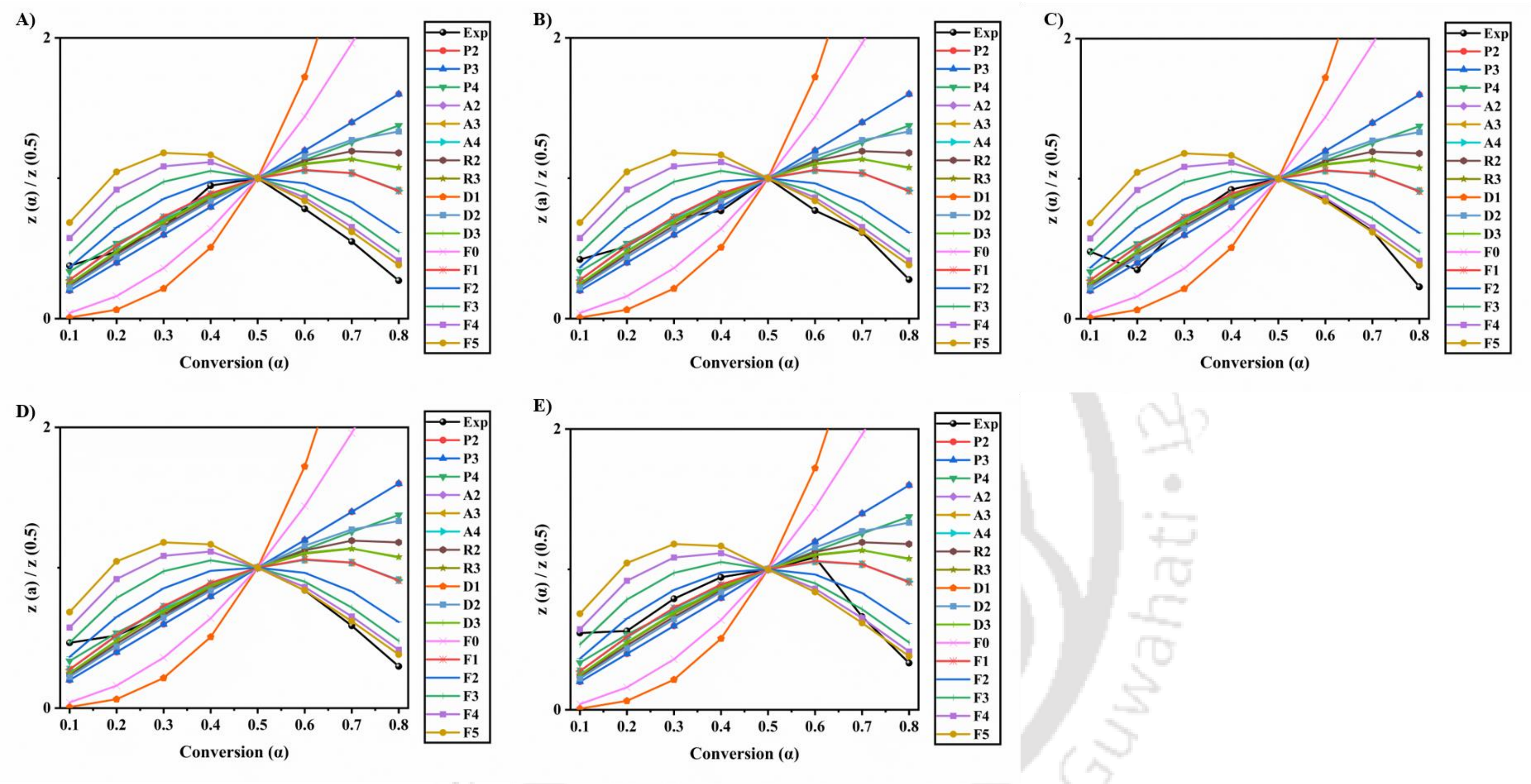

Figure 5.3.3.3: Prediction of the reaction mechanism of *Delonix Regia* and tube waste co-pyrolysis by Criado's method based on the DFM model at different heating rates: **A)** 5°C min^{-1}, **B)** 10°C min^{-1}, **C)** 20°C min^{-1}, **D)** 35°C min^{-1}, **E)** 55 °C min^{-1}.

Table 5.3.3.3: Prediction of the reaction mechanism of *Delonix Regia* and tube waste co-pyrolysis by Criado's method based on the DFM model at different heating rates.

Conversion *(α)*	Heating rate (°C min^{-1})				
	5	10	20	35	55
0.1	F2	F2	F3	F3	F4
0.2	R3	A4	P3	A2	P4
0.3	D2	A4	D3	R2	F2
0.4	F2	P3	F1	R3	F2
0.5	-	-	-	-	-
0.6	>F5	>F5	F4	F5	R3
0.7	>F5	F5	F5	F5	F4
0.8	>F5	>F5	>F5	>F5	F5

Reaction mechanism models:
P3, P4 – Third, and Fourth Power-law models
A4 – Fourth Avrami-Erofeyev model
R2, R3 – Area and Volume Contracting models
D2, D3 – 1, and 3-dimensional Diffusion models
F1, F2, F3, F4, F5 – First, Second, Third, Fourth, Five Reaction order models

5.3.4 Thermodynamic properties

The thermodynamic properties, change in enthalpy (*ΔH*), and change in Gibbs free energy (*ΔG*) of DR and TW mixture during pyrolytic degradation were calculated for different heating rates and shown in **Figure 5.3.4.** All thermodynamic properties calculations were based on DFM iso-conversional method for heating rates ranging from 5 to 55 °C min^{-1}. For each heating rate, the variations in thermodynamic properties against conversion values, along with the average properties, have been presented in **(Table 5.3.4)**; and discussed herein. The change in enthalpy

(ΔH) is a thermodynamic state function. It measures the exchange of heat energy between the reactant and activated complex constituents (transition state) [104]. The average ΔH values were found to be 225.38, 225.28, 225.18, 225.08, and 224.98 kJ mol^{-1} at 5, 10, 20, 35, and 55 °C min-^{1} respectively, as shown in **Figure 5.3.4 (A)** and **Table 5.3.4**. The positive enthalpy values in the range of 225.38-224.98 for 5-55 °C min^{-1}, respectively, indicated the endothermic nature of the pyrolysis reaction of co-feed. It may thus be inferred that endothermic reactions occur with increasing heating rates throughout the conversion [127]. However, the heating rate has less influence on the magnitude of the average enthalpy. Further, the difference between the average values of E_α and ΔH was also approximately 5 kJ mol^{-1}, indicating the ease of formation of products from the DR and TW mixture during the pyrolysis process, and these results were consistent with other published reports [109] [39], [128].

The change in Gibbs free energy (ΔG) is a thermodynamic state function, and it is used to describe whether a reaction is spontaneous or non-spontaneous and its direction. The average ΔG values were 179.99, 180.22, 180.31, 180.99, and 182.15 kJ mol^{-1}, respectively, at 5, 10, 20, 35, and 55 °C min-^{1} as shown in **Figure 5.3.4 (B)** and **Table 5.3.4.** The results indicated that the average values of ΔG increased from approximately 179.99 to 182.15 as heating rates increased from 5-55°C min^{-1}. The ΔG obtained in this study at 10°C min^{-1} for DR and TW co-feed (180.22 kJ mol^{-1}) is smaller than that of Mishra and Mohanty [2] studied for DR seeds only (219 kJ mol^{-1}) and more significant than the Ayokunle et al. [1] studied for DR pods only (143 kJ mol^{-1}), Chen et al. [127] studied for Pinus Silvestri pine needle (160 kJ mol^{-1}). The results of **Figure 5.3.4 (B)** revealed that the positive variations in ΔG demonstrated non-spontaneous reaction behaviour for the co-feed mixture for all values of the conversion.

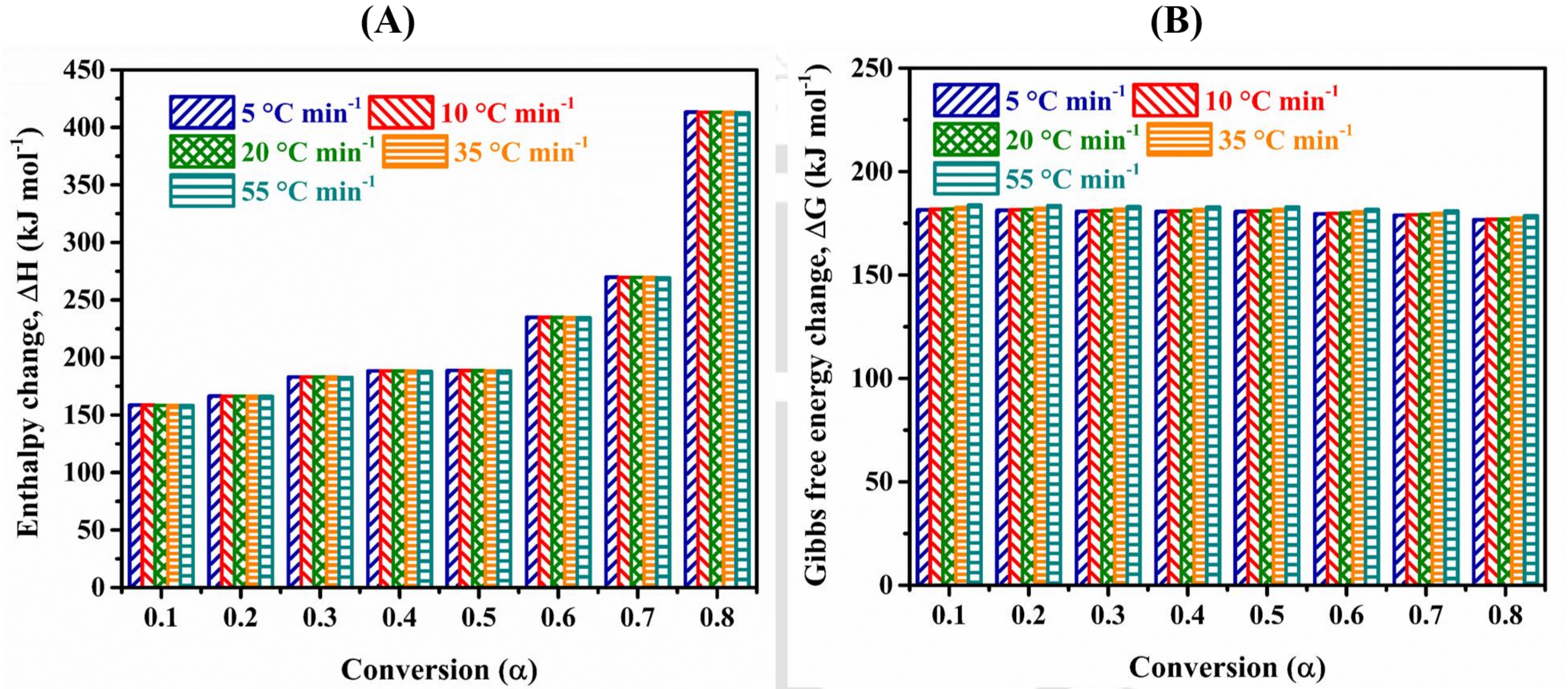

Figure 5.3.4: Thermodynamic properties of *Delonix Regia* and tube waste co-pyrolysis by DFM iso-conversional method: **A)** Enthalpy change, and **B)** Gibbs free energy change.

Table 5.3.4: Thermodynamic properties of non-catalytic co-pyrolysis of Delonix Regia and tube waste at the DFM method for different heating rates.

α	5 °C min-1			10 °C min^{-1}			20 °C min^{-1}			35 °C min^{-1}			55 °C min^{-1}		
	k_o	ΔH	ΔG	k_o	ΔH	ΔG	k_o	ΔH	ΔG	k_o	ΔH	ΔG	k_o	ΔH	ΔG
0.1	3.84E+11	158.54	181.50	3.99E+11	158.44	181.75	4.24E+11	158.34	181.87	4.04E+11	158.24	182.58	3.53E+11	158.14	183.78
0.2	1.91E+12	166.46	181.26	1.92E+12	166.36	181.51	1.99E+12	166.26	181.62	1.84E+12	166.17	182.33	1.56E+12	166.07	183.52
0.3	5.46E+13	183.10	180.79	5.17E+13	183.00	181.03	5.03E+13	182.90	181.13	4.40E+13	182.80	181.83	3.54E+13	182.70	183.01
0.4	1.58E+14	188.38	180.65	1.47E+14	188.28	180.88	1.40E+14	188.18	180.99	1.20E+14	188.08	181.68	9.52E+13	187.98	182.86
0.5	1.67E+14	188.65	180.64	1.55E+14	188.55	180.88	1.48E+14	188.45	180.98	1.27E+14	188.35	181.67	1.00E+14	188.25	182.85
0.6	1.82E+18	234.94	179.55	1.42E+18	234.84	179.76	1.15E+18	234.74	179.85	8.35E+17	234.64	180.52	5.64E+17	234.54	181.67
0.7	1.93E+21	269.73	178.86	1.32E+21	269.63	179.06	9.35E+20	269.53	179.13	6.04E+20	269.43	179.79	3.63E+20	269.33	180.93
0.8	4.94E+33	413.21	176.72	1.97E+33	413.11	176.88	8.31E+32	413.02	176.90	3.25E+32	412.92	177.52	1.21E+32	412.82	178.62
Avg	**6.18E+32**	**225.38**	**179.99**	**2.46E+32**	**225.28**	**180.22**	**1.04E+32**	**225.18**	**180.31**	**4.06E+31**	**225.08**	**180.99**	**1.51E+31**	**224.98**	**182.15**
α – Conversion, k_o – Frequency factor, ΔH- Enthalpy change (kJ mol^{-1}), ΔG- Gibbs free energy change (kJ mol^{-1})															

5.3.5 Thermal performance indices (TPI)

The thermal performance indices of the DR and TW mixture during pyrolytic degradation were summarized in **Table 5.3.5**. In summary, it was noticed that all the TPI indices C, D_i, D_b, S, and D_v were increased with increasing heating rates from 5-55°C min^{-1}. While increasing the heating rates, the ignition, degradation, and burnout temperatures (T_i, T_p, and T_b) were increased, and corresponding time intervals (t_i, t_p, and t_b) were decreased. The higher value (9.78×10^{-5}) of the DR and TW mixture's flammability indices (C) could be attributed to lower moisture and higher heating values. The higher values (9.72×10^{-1} and 5.57×10^{-2}) of both ignition (D_i) and burnout (D_b) indices indicate the better combustion capability for the DR and TW mixture. The high value (3.35×10^{-7}) of the combustion index (S) implies the actual combustion performance of the DR and TW mixtures to burnout. The higher value (5.16×10^{-7}) of devolatilization indices (D_v) signifies that volatiles was released more efficiently during the co-pyrolysis process. The obtained trend was similar and consistent with previous studies reported by other authors [39], [109].

Table 5.3.5: Thermal performance indices of *Delonix Regia* and tube waste co-pyrolysis at different heating rates.

β	T_i	T_p	T_b	$\Delta T_{0.5}$	t_i	t_p	t_b	$\Delta t_{0.5}$	$-R_p$	$-R_v$	C	D_i	D_b	S	D_v
5	520	613	1254	572	44.5	63.1	191	54.9	2.8	0.3	1.04E-05	9.97E-04	4.23E-06	2.48E-09	4.61E-09
10	540	625	1228	591	24.3	32.7	93.1	29.3	5.5	0.6	1.89E-05	6.92E-03	6.17E-05	9.22E-09	1.65E-08
20	545	637	1191	595	12.3	16.9	44.7	17.8	11	1.4	3.70E-05	5.29E-02	8.18E-04	4.35E-08	7.46E-08
35	552	649	1130	603	7.2	10	23.8	8.7	19.8	2.4	6.50E-05	2.75E-01	9.56E-03	1.38E-07	2.20E-07
55	563	661	1111	614	4.83	6.6	14.8	5.7	31	3.8	9.78E-05	9.72E-01	5.57E-02	3.35E-07	5.16E-07

β - Heating Rate (K min^{-1}), T_i - ignition temperature (K), T_p - maximum degradation temperature (K), T_b - burnout temperature (K), $\Delta T_{0.5}$ - temperature interval of half of the $-R_p$ (K), t_i - ignition time (min), t_b - burnout time (min), t_p - maximum degradation time (min), $\Delta t_{0.5}$ - time interval of half of the $-R_p$ (min), $-R_p$ - maximum degradation rate (wt.% min^{-1}), $-R_v$ - mean degradation rate (wt.% min^{-1}), C - flammability index (K^{-2} min^{-1}), D_i - ignition index (min^{-3}), D_b - burnout index (min^{-4}), S - combustion index (K^{-3} min^{-2}), D_v - devolatilization index (K^{-3} min^{-1}).

5.3.6 Summary and Comparative analysis with existing work

A summary of objective 3 and the comparative analysis with existing work (**Table 5.3.6**) was discussed below.

Summary of the objective 3.

The following statements were obtained from objective 3:

- The thermal decomposition of co-pyrolysis of *Delonix regia* (DR) biomass and butyl rubber tube (BRT) waste was analyzed.
- The heating rate effect on the thermal decomposition of co-pyrolysis of DR and BRT waste was studied.
- The pyrolytic zone temperature between 150 to 780 °C was estimated with a maximum mass loss of about 63.5 wt. %.
- It was evident that the Ozawa-Flynn-Wall model determined the lowest average activation energy of 207.78 kJ/mol according to the kinetic report.
- Prediction of the reaction mechanism by Criado's master plot method indicated the multistep reaction mechanism.
- According to the kinetic report, $\Delta H \approx 225.18$ kJ/mol and $\Delta G \approx 180.31$ kJ/mol suggested the endothermic and non-spontaneity of co-pyrolysis of DR and BRT waste.
- In addition, the thermal performance indices of co-pyrolysis of DR and BRT waste were elucidated.

Table 5.3.6: Comparative analysis of Non – catalytic co – pyrolysis of DR and BRT (1:1 wt. %) wastes.

S.No.	Raw materials	Catalyst	TGA model	Operating conditions			Results		References
	Feed and co-feed	(wt. %)		°C	*Q*	*β*	*Kinetics	*Thermodynamics	
1	Corncob: Polyethylene (3:1)	-	Perkin Elmer STA-8000	25 – 900	N_2 – 50	10, 20, 30	$E_{\alpha=0.1\text{-}0.90}$: 216, 216, 216, 221, by KAS, OFW, STK, DFM	$E_{\alpha=0.1\text{-}0.80}$: ΔH: 227, ΔG: 226, and ΔS: 0.015	[41]
2	Wettorrified bamboo: LLDPE (1:1)	-	Netsch TG209F1	30 – 800	N_2 – 20	5, 10, 20, 40	$E_{\alpha=0.1\text{-}0.80}$: 264, 261, 256, by KAS, OFW, DFM	-	[46]
3	Pinewood: HDPE (1:1)	-	TA-SDT650	25 – 850	N_2 – 100	5, 10, 20	$E_{\alpha=0.1\text{-}0.90}$ and k_o: 177 and 3.57×10^{17} for KAS,	$E_{\alpha=0.1\text{-}0.90}$: ΔH: 182, and ΔG: 196	[47]
4	*Delonix Regia*: Butyl rubber tube waste (1:1)	-	Netsch TG209F1	25 – 1000	N_2 – 40	5, 10, 20, 35, 55	$E_{\alpha=0.1\text{-}0.80}$ and k_o: 230 and 2.55×10^{30}, 208 and 8.31×10^{26}, 208 and 1.58×10^{24}, 208 and 6.47×10^{26}, 208 and	$E_{\alpha=0.1\text{-}0.80}$: ΔH: 225, and ΔG: 180	Objective 3 [51]

							5.15×10^{26} by DFM, KAS, OFW, STK, DAE		

β – Heating rates (°C min^{-1})

α – Conversion

°C – Temperature

Q – Flowrate of carrier gas (mL min^{-1})

Iso – conversional models – Differential Friedman (DFM), Kissinger-Akahira-Sunose (KAS), Ozawa-Flynn-Wall (OFW), Starink (STK), and Distributed Activation Energy (DAE)

*Kinetics – Average values

*Thermodynamics – Average values based on the DFM model at 10 °C min^{-1}

E_{α} – Activation energy (kJ mol^{-1})

k_{o} – Frequency factor (s^{-1})

ΔH – Change in enthalpy (kJ mol^{-1})

ΔG – Change in Gibbs free energy (kJ mol^{-1})

ΔS – Change in entropy (kJ mol^{-1} K^{-1})

5.4 In–situ pyro–catalytic decomposition of *Delonix Regia* biomass: Kinetic triplets and thermodynamic Investigation

5.4.1 Thermal stability characteristics of pyro-catalytic decomposition of DR biomass

Figure 5.4.1.2 (A1 to A3, B1 to B3, and C1 to C3) represents the TG and DTG pyrograms of pyro-catalytic decomposition (PCD) of DR biomass in the presence of different catalysts, namely zeolite (Na–Y), 10 wt. % of noble metal on activated carbon (Pt/C), and 1–1 wt. % of two metallic oxide (TiO_2–ZnO) respectively. From **Figure 5.4.1.2**, it can be observed that the PCD of DR biomass took place in three zones. The primary zone formed was in the temperature range of (25 – 150 °C), mainly consisting of moisture and light molecular weight compounds. The secondary zone was generally considered an active pyrolytic zone with the decomposition of major compounds such as hemicellulose and cellulose [34], [53], [129]. Additionally, it should be noted that the lignin decomposition also starts in this zone. At the same time, a significant part of lignin decomposition was noted in the third zone at temperatures of >500 °C [100], [130]. In the third stage, the decomposition of the biomass was slow, and such a trend was contributed by the lignin compound. Furthermore, from the pyrograms **(Figure 5.4.1.1)**, it was observed that when the heating rate was maintained at 10 °C min^{-1}, the catalysts were quite stable with 76.4 wt. %, 56.2 wt. %, and 98.8 wt. % mass remaining for Na–Y, Pt/C and TiO_2–ZnO respectively.

From A1 to A3, Figure 5.4.1.2 represents the TG and DTG pyrograms of PCD of DR biomass at 30, 20, and 10 wt. % of Na–Y. The TG pyrograms at 5 – 55 °C min^{-1} showed a mass loss of 53 – 51 wt. %, 58 – 56 wt. %, and 62 – 60 wt. % for 30, 20, and 10 wt. % of Na–Y, respectively. The DTG pyrograms at 5 – 55 °C min^{-1} showed the different maximum decomposition temperatures were 323 – 362 °C, 326 – 366 °C, and 326 – 368 °C for 30, 20, and 10 wt. % of Na–Y, respectively. It was observed that as the catalyst (Na–Y) loading increased, the mass loss decreased significantly and was consistent with other studies [34],

[131]. At higher temperatures, around 500 – 1000 °C, the DTG curves reach zero, implying the completion of the PCD of DR biomass which was positive from the yield and conversion viewpoint. Moreover, the increase in heating rate resulted in a shift in TG and DTG curves in a non-catalytic pyrolysis process, indicating an improper heat transfer to the particles [130], [132]. Likewise, a shift in the TG-DTG pyrograms was observed in the presence of a catalyst. This shift of pyrograms for a catalytic pyrolysis process also depends on the pore size, surface area, and availability of acid sites (combination of Lewis and Bronsted sites) in a zeolite catalyst [34], [58], [133].

From B1 to B3, Figure 5.4.1.2 represents the TG and DTG pyrograms of PCD of DR biomass at 30, 20, and 10 wt. % of Pt/C. The TG pyrograms at 5 – 55 °C min^{-1} showed a mass loss of 55 – 53 wt. %, 63 – 60 wt. %, and 64 – 59 wt. % for 30, 20, and 10 wt. % of Pt/C, respectively. It was observed that as the catalyst (Pt/C) ratio increased, the mass loss decreased significantly. The DTG pyrograms at 5 – 55 °C min^{-1} showed the different maximum decomposition temperatures were 334 – 372 °C, 334 – 372 °C, and 334 – 373 °C for 30, 20, and 10 wt. % of Pt/C, respectively. The significant reactions contributing to the weight loss were decarbonylation, decarboxylation, and dehydrogenation. The lower catalytic activity of the Pt/C catalyst compared to the zeolite catalyst was due to lower surface area (55 $\text{m}^2\ \text{g}^{-1}$) and lower pore volume [129], [134].

From C1 to C3, Figure 5.4.1.2 represents the TG and DTG pyrograms of PCD of DR biomass at 30, 20, and 10 wt. % of TiO_2–ZnO. The TG pyrograms at 5–55 °C min^{-1} showed a mass loss of 54 – 50 wt. %, 56 – 55 wt. %, and 63 – 62 wt. % for 30, 20, and 10 wt. % of TiO_2–ZnO, respectively. It was observed that as the catalyst (TiO_2–ZnO) ratio increased, the mass loss decreased significantly [34], [135]. The DTG pyrograms at 5 – 55 °C min^{-1} showed the different maximum decomposition temperatures were 332 – 371 °C, 332 – 371 °C, and 332 – 370 °C for 30, 20, and 10 wt. % of TiO_2–ZnO respectively. In comparison to the above catalysts, the catalyst stability of TiO_2–ZnO was superior **(Figure 5.4.1.1)**. This indicates that the contribution of the catalyst for PCD of DR biomass during the pyrolysis was low (leftover mass was high for all loadings).

Catalysts with lower loading (10, 20 wt. %) provided better thermal decomposition of the biomass when compared to higher loading at 30 wt. %. This trend can be attributed to the coke deposition on the catalyst surface at higher loadings for all the catalysts [35], [55]. The corresponding non-catalytic thermal decomposition of DR biomass was found to be varying from 30.2 – 25.5 wt. % as the heating rate increased from 5-55 °C min^{-1} [130].

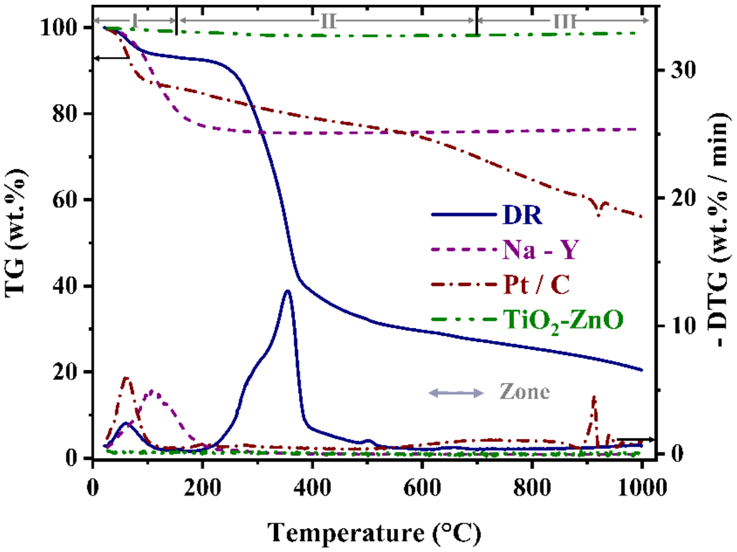

Figure 5.4.1.1 Thermal stability variations in TG and DTG pyrograms of *Delonix Regia* (DR) biomass and three different catalysts: zeolite (Na–Y), 10 wt. % of noble metal on activated carbon (Pt/C), and 1–1 wt. % of bi-metallic oxide (TiO_2–ZnO) at 10 °C min^{-1}.

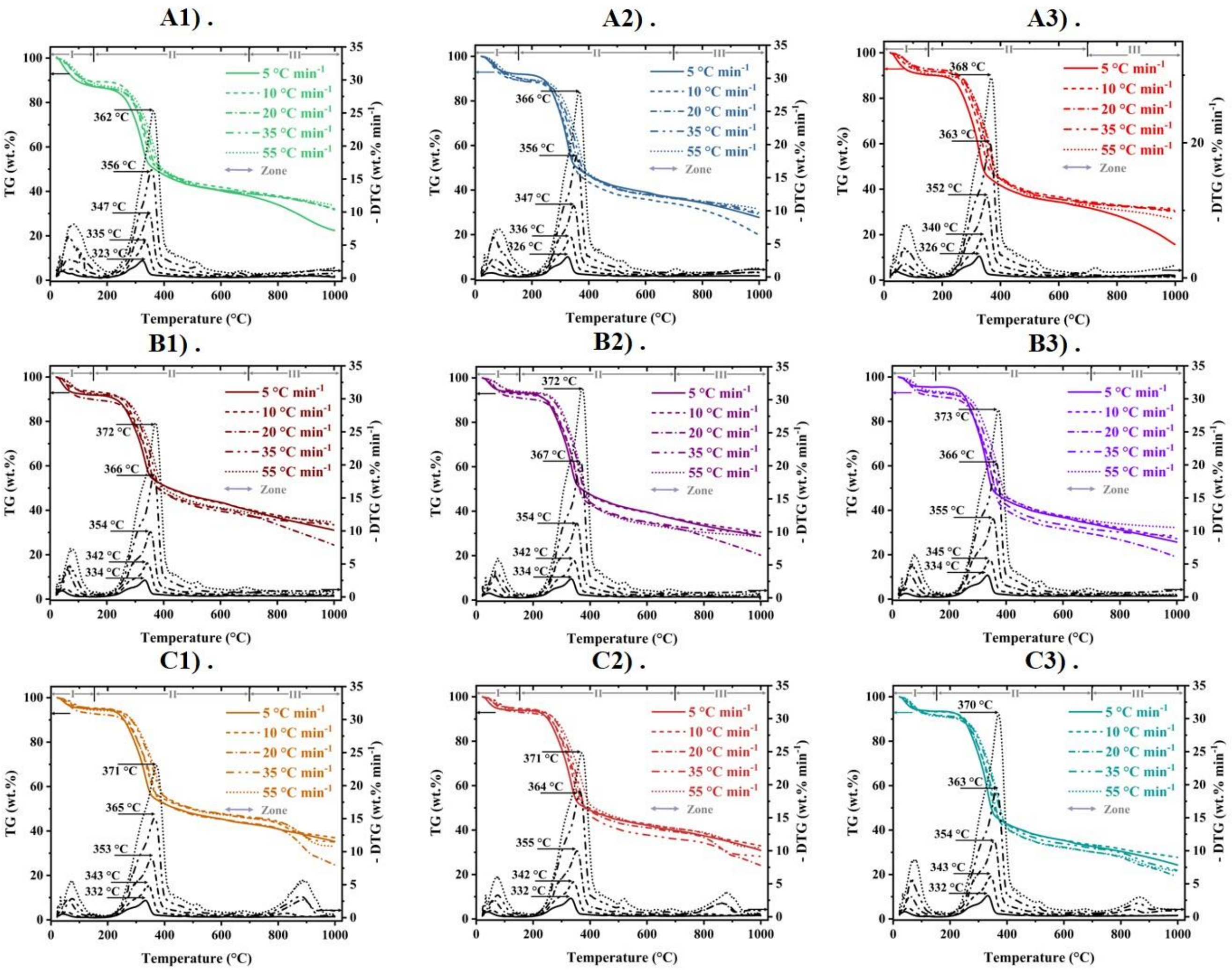

Figure 5.4.1.2 Variations of TG and DTG pyrograms as a function of temperature: A1), A2), and A3) for DR:Na–Y (1:30, 1:20, and 1:10 wt.%), B1), B2), and B3) for DR:Pt/C (1:30, 1:20, and 1:10 wt.%), and C1), C2), and C3) for DR:TiO_2–ZnO (1:30, 1:20, and 1:10 wt.%).

5.4.2 Kinetic triplets for pyro-catalytic decomposition of DR biomass

From the surface area analysis of a catalyst, it was known that as the surface area of the catalyst decreases, the active sites available for the reaction decreases, which states that the activity of the catalyst was less [34], [136]. Additionally, the thermal decomposition of a catalyst demonstrates that the rigid pore walls provide enough strength to the active sites, which enhances the thermal stability of the catalyst. This facilitates the usage of the catalyst at higher temperatures (>1000 °C) without losing its properties [34], [136]. Moreover, during the prolonged catalytic reactions, more gaseous products adsorb on the active sites by blocking the pores, which enhances the coke formation on the catalyst, thereby reducing the number of active sites available for the reaction [34], [135]. This also increases the activation energy required to initiate the reaction.

Figure 5.4.2.1 (A1) and Table 5.4.2.1.1 shows the variation of activation energy in the presence of zeolite Na–Y catalyst at 30, 20, and 10 wt. %. From the kinetic triplet analysis (**Figure 5.4.2.1 (A1)**), it was observed that using zeolite Na–Y catalyst, the average E_{α} (kJ mol^{-1}) and k_o (min^{-1}) values decreased from 203 and 7.59 E+17 to 182 and 1.33 E+16 as the catalyst loading was varied from 30 to 10 wt. % using the model–fitting (DFM) technique. When compared to the corresponding non–catalytic pyrolysis of DR biomass with an average E_{α} of 195 kJ mol^{-1} [130], the Na-Y catalyst process provided lower average activation energy of 181 kJ mol^{-1}. While the remaining model–free (four) techniques yielded average E_{α} (kJ mol^{-1}) and k_o (min^{-1}) values of 205 and 9.70 E+19, 191 and 1.96 E+19, and 181 and 1.83 E+17 at 30, 20, and 10 wt. % of Na–Y, respectively.

It was observed that the average E_{α} value decreased (181 kJ mol^{-1}) with decreasing Na–Y ratio (10 wt.%). Hence, Na–Y with lower loading (10 wt.%) was found to be a suitable catalyst for the catalytic pyrolysis of DR biomass. In addition to the zeolite Na–Y, the other catalysts used in the kinetic triplet estimation of pyro-catalytic decomposition (PCD) of DR biomass were Pt/C and TiO_2–ZnO. In the case of the Pt/C catalyst, the findings showed that the average E_α (kJ mol^{-1}) and k_o (min^{-1}) values decreased from 218 and 1.28 E+21 to 200 and 9.62 E+17 when the catalyst (Pt/C) loading was decreased from 30 to 10 wt. % using the model–fitting (DFM) technique. While the remaining model–free (four) techniques yielded average E_α (kJ mol^{-1}) and k_o (min^{-1}) values of 211 and 4.73 E+18, 204 and 1.06 E+18, and 204 and 2.03 E+19 at 30, 20, and 10 wt. % of Pt/C, respectively. It was observed that the average E_α value decreased with decreasing Pt/C ratio [129], [134].

Figure 5.4.2.1 (A2) and Table (Table 5.4.2.1.2) show the activation energy variation in the presence of 10 wt. % of Pt/C catalyst at 30, 20, and 10 wt. %. Further, **Figure 5.4.2.1 (A3) and Table (Table 5.4.2.1.3)** demonstrate the variation of activation energy in the presence of 1–1 wt. % of TiO_2–ZnO catalyst at 30, 20, and 10 wt. %. The findings showed that the average E_α (kJ mol^{-1}) and k_o (min^{-1}) values decreased from 196 and 1.03 E+17 to 191 and 7.34 E+16 and increased to 201 and 3.41 E+17 when the catalyst (TiO_2–ZnO) loading was decreased from 30 to 20 and 10 wt. % using the model–fitting (DFM) technique. While the remaining model–free (four) techniques yielded average E_α (kJ mol^{-1}) and k_o (min^{-1}) values of 192 and 3.72 E+17, 194 and 2.30 E+18, and 204 and 6.17 E+19 at 30, 20, and 10 wt. % of TiO_2–ZnO, respectively. It was observed that the average E_α value increased with decreasing TiO_2–ZnO ratio. The probable reasons for such alteration of average E_α values can be attributed to the reasons stated earlier.

The above findings clearly define the effect of the catalyst in determining the kinetic triplets. Though the activation energy during pyrolysis increased from conversion 0.1 to 0.4, there was a slight decrease at a conversion of 0.5–0.6 and then increased up to 0.7. This was due to the decomposition of the hemicellulose compounds in the conversion range of 0.1 – 0.4, while cellulose was from 0.5 – 0.6 and lignin for conversion >0.7 [39], [130]. At higher temperatures (>500 °C), lignin decomposition was prominent, which increases the activation energy due to the denser molecules. As the catalyst loading in the feedstock ratio increases, more coke deposition occurs on the catalyst's surface, leading to the increased activation energy. The results of the present study follow a similar trend observed in recent works by [34], [35], [55], [137].

For all the catalysts used in the present study, each catalyst contributes differently to the pyrolysis reactions. Different reactions include dehydration, hydrogenation, decarboxylation, decarbonylation, and deoxygenation. The Pt/C catalyst was known for hydrogenation and higher deoxygenation reactions [129], [134]. In comparison, the TiO_2–ZnO bimetallic catalyst enhances the dehydration of alcohols to olefins and the production of lower hydrocarbon compounds. Furthermore, the TiO_2 catalyst helps convert xylene, an intermediate of hemicellulose decomposition [138]. Additionally, the zeolite catalyst provides a higher acid site, promoting the decarbonylation and deoxygenation reactions [35]. Hence, it can be seen that all these catalysts play a significant role differently in the decomposition of biomass.

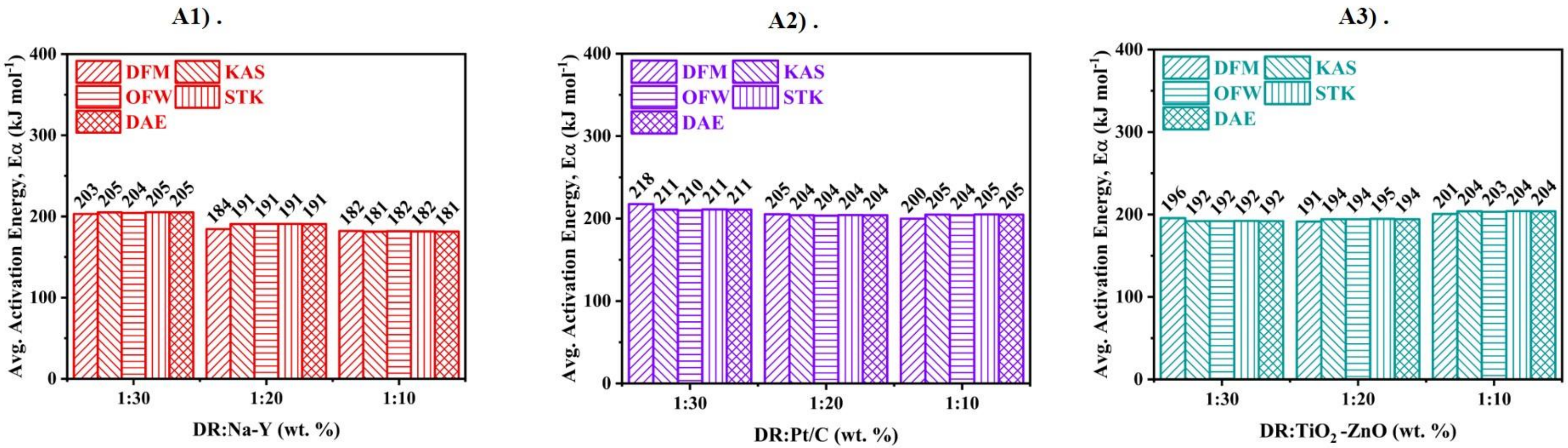

Figure 5.4.2.1 Variations of average activation energy over the catalyst: A1) (DR:Na–Y), A2) (DR:Pt/C), and A3) (DR:TiO_2–ZnO).

Table 5.4.2.1.1 Kinetic parameters including activation energy, E_α (kJ mol^{-1}) and frequency factor, k_o (s^{-1}) of catalytic (Na–Y) pyrolysis of *Delonix Regia* (DR) biomass by various iso-conversional techniques.

α	Iso-conversional techniques														
	DFM			KAS			OFW			STK			DAE		
	E_α	k_o	R^2	E_α	k_o	R^2	E_α	k_o	R^2	E_α	k_o	R^2	E_α	k_o	R^2
	DR:Na–Y (1:30 wt.%)														
0.1	195.61	2.81E+17	0.911	215.50	6.82E+19	0.740	213.48	2.22E+17	0.755	215.69	5.43E+19	0.741	215.50	6.47E+20	0.740
0.2	195.73	9.71E+16	0.954	210.60	5.88E+18	0.958	209.25	2.20E+16	0.961	210.81	4.70E+18	0.958	210.60	2.63E+19	0.958
0.3	201.56	1.61E+17	0.995	207.07	1.29E+18	0.982	206.15	5.27E+15	0.984	207.30	1.03E+18	0.982	207.07	3.61E+18	0.982
0.4	212.40	7.88E+17	0.982	207.90	8.10E+17	0.993	207.15	3.44E+15	0.994	208.13	6.51E+17	0.993	207.90	1.59E+18	0.993
0.5	188.48	4.79E+15	0.999	199.20	8.79E+16	0.999	199.06	4.20E+14	0.999	199.45	7.11E+16	0.999	199.20	1.27E+17	0.999
0.6	199.15	2.85E+16	0.997	195.10	2.72E+16	1.000	195.32	1.40E+14	1.000	195.36	2.21E+16	1.000	195.10	2.97E+16	1.000
0.7	228.03	3.95E+18	0.996	199.41	4.47E+16	1.000	199.57	2.27E+14	1.000	199.67	3.62E+16	1.000	199.41	3.71E+16	1.000
Avg.	203.00	7.59E+17	0.976	204.97	1.09E+19	0.953	204.28	3.62E+16	0.956	205.20	8.68E+18	0.953	204.97	9.70E+19	0.953
	DR:Na–Y (1:20 wt.%)														

0.1	178.34	6.63E+15	0.995	209.45	1.44E+19	0.983	207.83	5.08E+16	0.984	209.65	1.15E+19	0.983	209.45	1.37E+20	0.983
0.2	180.25	4.21E+15	0.992	190.10	7.61E+16	0.991	189.77	3.49E+14	0.992	190.33	6.14E+16	0.991	190.10	3.41E+17	0.991
0.3	184.84	5.18E+15	0.995	187.41	2.15E+16	0.997	187.46	1.07E+14	0.998	187.64	1.74E+16	0.997	187.41	6.04E+16	0.997
0.4	177.97	7.98E+14	0.995	185.82	8.78E+15	0.999	186.17	4.65E+13	0.999	186.07	7.13E+15	0.999	185.82	1.72E+16	0.999
0.5	185.60	2.70E+15	0.999	188.94	1.09E+16	0.997	189.32	5.79E+13	0.997	189.19	8.85E+15	0.997	188.94	1.57E+16	0.997
0.6	179.74	6.59E+14	0.999	184.23	3.12E+15	0.999	184.98	1.79E+13	0.999	184.50	2.54E+15	0.999	184.23	3.40E+15	0.999
0.7	204.07	4.58E+16	0.989	188.58	5.34E+15	0.999	189.27	3.03E+13	1.000	188.85	4.35E+15	0.999	188.58	4.44E+15	0.999
Avg.	184.40	9.43E+15	0.995	190.65	2.08E+18	0.995	190.68	7.34E+15	0.995	190.89	1.66E+18	0.995	190.65	1.96E+19	0.995
	DR:Na–Y (1:10 wt.%)														
0.1	173.24	2.30E+15	0.992	188.65	1.30E+17	0.982	188.03	5.57E+14	0.984	188.86	1.04E+17	0.982	188.65	1.23E+18	0.982
0.2	180.52	4.26E+15	0.989	179.34	7.11E+15	0.992	179.53	3.65E+13	0.993	179.57	5.77E+15	0.992	179.34	3.19E+16	0.992
0.3	184.87	4.91E+15	0.987	178.17	2.92E+15	0.990	178.66	1.60E+13	0.991	178.41	2.37E+15	0.990	178.17	8.19E+15	0.990
0.4	184.52	2.35E+15	0.970	181.01	2.95E+15	0.991	181.60	1.64E+13	0.992	181.27	2.40E+15	0.991	181.01	5.77E+15	0.991
0.5	173.59	2.14E+14	0.997	181.93	2.34E+15	0.991	182.66	1.34E+13	0.992	182.19	1.90E+15	0.991	181.93	3.37E+15	0.991
0.6	170.01	8.63E+13	0.999	178.99	9.52E+14	0.994	180.01	5.81E+12	0.995	179.26	7.78E+14	0.994	178.99	1.04E+15	0.994
0.7	207.88	7.91E+16	0.973	180.92	1.05E+15	0.994	182.00	6.45E+12	0.994	181.19	8.57E+14	0.994	180.92	8.71E+14	0.994
Avg.	182.09	1.33E+16	0.987	181.29	2.10E+16	0.991	181.78	9.31E+13	0.992	181.54	1.69E+16	0.991	181.29	1.83E+17	0.991

Table 5.4.2.1.2 Kinetic parameters including activation energy and frequency factor of catalytic (Pt/C) pyrolysis of *Delonix Regia* (DR) biomass by various iso-conversional techniques.

α	Iso-conversional technique														
	DFM			KAS			OFW			STK			DAE		
	E_α	k_o	R^2	E_α	k_o	R^2	E_α	k_o	R^2	E_α	k_o	R^2	E_α	k_o	R^2
	DR:Pt/C (1:30 wt.%)														
0.1	186.10	4.45E+16	0.995	195.16	7.51E+17	0.991	194.21	3.01E+15	0.991	195.37	6.03E+17	0.991	195.16	7.13E+18	0.991
0.2	199.76	2.62E+17	0.971	192.38	1.34E+17	0.982	191.94	6.02E+14	0.984	192.60	1.08E+17	0.982	192.38	6.02E+17	0.982
0.3	206.02	3.42E+17	0.986	205.65	9.53E+17	0.987	204.83	3.98E+15	0.988	205.87	7.66E+17	0.987	205.65	2.67E+18	0.987
0.4	215.71	1.04E+18	0.988	217.29	4.55E+18	0.987	216.15	1.80E+16	0.988	217.52	3.65E+18	0.987	217.29	8.91E+18	0.987
0.5	232.46	1.66E+19	0.965	218.65	3.20E+18	0.991	217.65	1.30E+16	0.992	218.89	2.57E+18	0.992	218.65	4.62E+18	0.991
0.6	211.63	2.03E+17	0.986	218.45	1.91E+18	0.994	217.62	8.02E+15	0.995	218.69	1.53E+18	0.994	218.45	2.08E+18	0.994
0.7	270.97	8.93E+21	0.972	228.55	8.51E+18	0.989	227.40	3.39E+16	0.990	228.79	6.83E+18	0.989	228.55	7.07E+18	0.989
Avg.	217.52	1.28E+21	0.980	210.88	2.86E+18	0.989	209.97	1.15E+16	0.990	211.10	2.29E+18	0.989	210.88	4.73E+18	0.989
		DR:Pt/C (1:20 wt.%)													

0.1	183.32	2.18E+16	0.990	184.57	5.70E+16	0.986	184.17	2.56E+14	0.988	184.79	4.60E+16	0.986	184.57	5.41E+17	0.986
0.2	194.48	8.17E+16	0.980	191.86	1.15E+17	0.978	191.46	5.18E+14	0.980	192.09	9.25E+16	0.978	191.86	5.14E+17	0.978
0.3	203.82	2.12E+17	0.983	204.13	6.72E+17	0.983	203.39	2.85E+15	0.985	204.35	5.40E+17	0.983	204.13	1.88E+18	0.983
0.4	209.88	3.48E+17	0.985	209.79	1.01E+18	0.981	209.02	4.28E+15	0.983	210.03	8.16E+17	0.981	209.79	1.99E+18	0.981
0.5	203.44	6.37E+16	0.990	212.53	9.55E+17	0.993	211.82	4.09E+15	0.994	212.77	7.68E+17	0.993	212.53	1.38E+18	0.993
0.6	208.06	1.12E+17	0.989	209.47	3.40E+17	0.991	209.08	1.55E+15	0.992	209.72	2.74E+17	0.991	209.47	3.71E+17	0.991
0.7	234.36	1.05E+19	0.969	216.39	8.78E+17	0.991	215.82	3.87E+15	0.992	216.64	7.08E+17	0.991	216.39	7.29E+17	0.991
Avg.	205.34	1.62E+18	0.984	204.11	5.76E+17	0.986	203.53	2.49E+15	0.988	204.34	4.63E+17	0.987	204.11	1.06E+18	0.986
	DR:Pt/C (1:10 wt.%)														
0.1	182.32	2.11E+16	0.771	208.89	1.39E+19	0.972	207.31	4.92E+16	0.974	209.09	1.11E+19	0.972	208.89	1.32E+20	0.972
0.2	206.09	1.07E+18	0.986	195.99	2.97E+17	0.976	195.37	1.29E+15	0.978	196.21	2.39E+17	0.976	195.99	1.33E+18	0.976
0.3	218.55	5.12E+18	0.992	209.69	2.36E+18	0.985	208.67	9.46E+15	0.987	209.91	1.89E+18	0.985	209.69	6.61E+18	0.985
0.4	210.99	4.86E+17	0.991	209.51	1.06E+18	0.985	208.74	4.47E+15	0.986	209.75	8.52E+17	0.985	209.51	2.07E+18	0.985
0.5	182.78	1.19E+15	0.971	208.52	4.71E+17	0.990	207.99	2.09E+15	0.991	208.76	3.80E+17	0.990	208.52	6.79E+17	0.990
0.6	197.56	1.56E+16	0.995	199.35	4.92E+16	0.993	199.43	2.46E+14	0.994	199.60	3.98E+16	0.993	199.35	5.37E+16	0.993
0.7	200.90	1.96E+16	0.984	201.11	4.88E+16	0.994	201.26	2.47E+14	0.995	201.37	3.95E+16	0.994	201.11	4.05E+16	0.994
Avg.	199.88	9.62E+17	0.956	204.72	2.59E+18	0.985	204.11	9.56E+15	0.986	204.96	2.07E+18	0.985	204.72	2.03E+19	0.985

Table 5.4.2.1.3 Kinetic parameters including activation energy and frequency factor of catalytic (TiO_2-ZnO) pyrolysis of *Delonix Regia* (DR) biomass by various iso-conversional techniques.

α	Iso-conversional technique														
	DFM			KAS			OFW			STK			DAE		
	E_α	k_o	R^2	E_α	k_o	R^2	E_α	k_o	R^2	E_α	k_o	R^2	E_α	k_o	R^2
	DR:TiO_2-ZnO (1:30 wt.%)														
0.1	182.29	2.03E+16	0.994	190.07	2.24E+17	0.988	189.37	9.46E+14	0.989	190.28	1.80E+17	0.988	190.07	2.12E+18	0.988
0.2	180.15	4.22E+15	0.998	185.34	3.15E+16	0.992	185.22	1.51E+14	0.993	185.57	2.55E+16	0.992	185.34	1.41E+17	0.992
0.3	203.05	2.32E+17	0.997	192.18	6.42E+16	0.993	191.99	3.04E+14	0.994	192.41	5.19E+16	0.993	192.18	1.80E+17	0.993
0.4	193.96	1.66E+16	0.997	193.36	4.10E+16	0.998	193.35	2.01E+14	0.998	193.61	3.32E+16	0.998	193.36	8.02E+16	0.998
0.5	192.98	8.20E+15	0.982	194.86	3.25E+16	0.999	194.97	1.64E+14	0.999	195.11	2.64E+16	0.999	194.86	4.69E+16	0.999
0.6	199.51	2.20E+16	0.981	192.56	1.36E+16	0.999	192.95	7.23E+13	0.999	192.82	1.10E+16	0.999	192.56	1.48E+16	0.999
0.7	216.89	4.20E+17	0.997	195.29	1.62E+16	0.999	195.71	8.65E+13	0.999	195.55	1.31E+16	0.999	195.29	1.34E+16	0.999
Avg.	195.55	1.03E+17	0.992	191.95	6.04E+16	0.995	191.94	2.75E+14	0.996	192.19	4.87E+16	0.995	191.95	3.72E+17	0.995
		DR:TiO_2-ZnO (1:20 wt.%)													

0.1	194.55	3.01E+17	0.993	198.62	1.56E+18	0.990	197.50	6.05E+15	0.991	198.82	1.25E+18	0.990	198.62	1.48E+19	0.990
0.2	187.06	1.97E+16	0.998	191.04	1.07E+17	0.994	190.64	4.83E+14	0.994	191.26	8.61E+16	0.994	191.04	4.78E+17	0.994
0.3	199.61	1.10E+17	0.995	197.73	2.07E+17	0.996	197.27	9.24E+14	0.997	197.96	1.67E+17	0.996	197.73	5.79E+17	0.996
0.4	201.32	7.73E+16	0.999	195.79	6.93E+16	0.996	195.66	3.32E+14	0.996	196.04	5.60E+16	0.996	195.79	1.36E+17	0.996
0.5	186.94	2.92E+15	0.984	197.24	5.25E+16	0.998	197.24	2.58E+14	0.998	197.49	4.25E+16	0.998	197.24	7.57E+16	0.998
0.6	181.56	7.27E+14	0.994	188.97	6.74E+15	0.999	189.53	3.72E+13	0.999	189.23	5.48E+15	0.999	188.97	7.36E+15	0.999
0.7	188.61	1.95E+15	0.995	191.33	7.47E+15	0.999	191.94	4.16E+13	0.999	191.60	6.07E+15	0.999	191.33	6.20E+15	0.999
Avg.	191.38	7.34E+16	0.994	194.39	2.87E+17	0.996	194.26	1.16E+15	0.996	194.63	2.30E+17	0.996	194.39	2.30E+18	0.996
	DR:TiO_2-ZnO (1:10 wt.%)														
0.1	198.77	8.28E+17	0.985	212.94	4.44E+19	0.970	211.10	1.49E+17	0.973	213.13	3.53E+19	0.970	212.94	4.21E+20	0.970
0.2	196.23	1.44E+17	0.981	203.42	1.72E+18	0.975	202.40	6.85E+15	0.977	203.64	1.38E+18	0.975	203.42	7.70E+18	0.975
0.3	210.90	1.19E+18	0.992	203.15	6.76E+17	0.984	202.42	2.86E+15	0.986	203.38	5.44E+17	0.984	203.15	1.90E+18	0.984
0.4	201.09	7.85E+16	0.992	204.16	3.98E+17	0.994	203.61	1.75E+15	0.995	204.40	3.21E+17	0.994	204.16	7.79E+17	0.994
0.5	194.26	1.21E+16	0.999	201.40	1.24E+17	0.999	201.18	5.85E+14	0.999	201.64	1.00E+17	0.999	201.40	1.79E+17	0.999
0.6	193.52	7.64E+15	1.000	201.35	8.02E+16	1.000	201.29	3.91E+14	1.000	201.60	6.49E+16	1.000	201.35	8.75E+16	1.000
0.7	210.02	1.32E+17	0.999	200.62	4.92E+16	1.000	200.76	2.49E+14	1.000	200.88	3.99E+16	1.000	200.62	4.09E+16	1.000
Avg.	200.69	3.41E+17	0.993	203.86	6.77E+18	0.989	203.25	2.32E+16	0.990	204.10	5.40E+18	0.989	203.86	6.17E+19	0.989

Variations of reaction pathways of pyro–catalytic decomposition (PCD) of DR biomass were analyzed by Criado's master plot technique. All the plots were obtained from Equations (19 – 20) by graphing with conversion ($\alpha = 0.1 - 0.7$) at 10 °C min^{-1} and were depicted in **Figure 5.4.2.2 (A1 – A3)** and **Table 5.4.2.2**. **Figure 5.4.2.2 (A1)** indicated the reaction pathways of F2, P4, A3, F0, A4, F3 for 1:30 wt. % of DR:Na – Y; F2, P4, R2, F2, F1, A4 for 1:20 wt. % of DR:Na–Y; and F2, P4, R2, F0, R3, F4 for 1:10 wt.% of DR:Na–Y. **Figure 5.4.2.2 (A2)** showed the reaction pathways of F4, F3, F3, F4, D1, P2 for 1:30 wt. % of DR:Pt/C; P4, D3, P3, F0, F2, A4 for 1:20 wt. % of DR:Pt/C; and P4, D2, P3, F0, F5, F3 for 1:10 wt.% of DR:Pt/C. **Figure 5.4.2.2 (A3)** exhibited the reaction pathways of F4, F1, F3, F4, D3, R2 for 1:30 wt. % of DR:TiO_2–ZnO; A4, P4, P3, D3, F4, F2 for 1:20 wt. % of DR:TiO_2–ZnO; and F2, R2, P3, F3, D3, F1 for 1:30 wt.% of DR:TiO_2–ZnO. As a result, the PCD of DR biomass was revealed to follow a multistep reaction pathway rather than a single reaction pathway for all three catalysts at each composition [34], [130], [139].

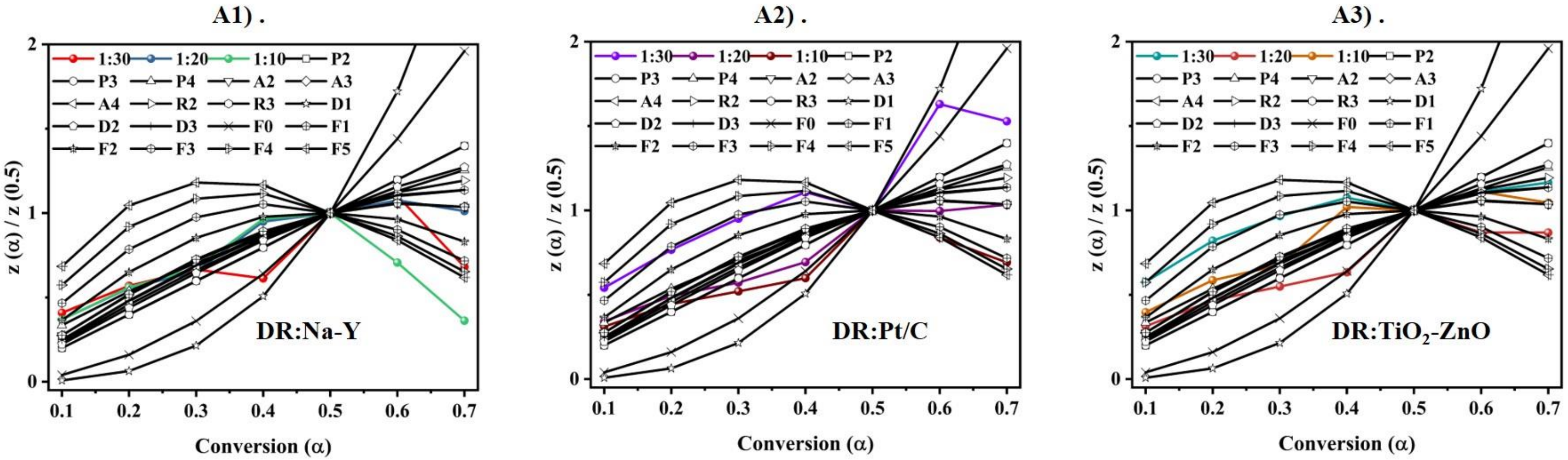

Figure 5.4.2.2 Variations of reaction pathways with conversion by Criado's master plot technique: **A1)** (DR:Na–Y), **A2)** (DR:Pt/C), and **A3)** (DR: TiO_2–ZnO) at 10°C min^{-1}.

Table 5.4.2.2 Variations of reaction pathways with conversion by Criado's master plot technique for all three catalysts at 10 °C min^{-1}

(α)	DR:Na-Y			DR:Pt/C			DR:TiO_2-ZnO		
	(1:30 wt. %)	(1:20 wt. %)	(1:10 wt. %)	(1:30 wt. %)	(1:20 wt. %)	(1:10 wt. %)	(1:30 wt. %)	(1:20 wt. %)	(1:10 wt. %)
0.1	F2	F2	F2	F4	P4	P4	F4	A4	F2
0.2	P4	P4	P4	F3	D3	D2	F1	P4	R2
0.3	A3	R2	R2	F3	P3	P3	F3	P3	P3
0.4	F0	F2	F0	F4	F0	F0	F4	D3	F3
0.5	-	-	-	-	-	-	-	-	-
0.6	A4	F1	R3	D1	F2	F5	D3	F4	D3
0.7	F3	A4	F4	P2	A4	F3	R2	F2	F1
Models: A4 – Fourth Avrami-Erofeyev P2, P3, and P4 – Second, Third, and Fourth order Power law R2, R3 – Area and Volume Contracting D1, D2, and D3 – 1, 2 and 3-dimensional Diffusion F2, F3, and F4 – First, Second, Third, and Fourth order Reaction									

5.4.3 Thermodynamic investigation for pyro-catalytic decomposition of DR biomass

Figure 5.4.3 (A1, A2, and A3) shows the variation of thermodynamic properties, including enthalpy change (*ΔH*) of pyro-catalytic decomposition (PCD) of DR biomass in the presence of zeolite Na–Y, 10 wt. % of Pt/C, and 1–1 wt. % of TiO_2–ZnO catalysts with feedstock ratios of 30, 20, and 10 wt. % respectively for the DFM technique. The change in enthalpy (*ΔH*) was defined as the energy required for a molecule to move from the ground state to a higher energy state [34], [39], [136]. Hence, the change in enthalpy was similar to the activation energy. The thermodynamic parameter analysis found that the *ΔH* varied from 177, 195, 196 kJ mol^{-1} at 10 wt. % catalyst loading of zeolite Na–Y, 10 wt. % of Pt/C, and 1–1 wt. % of TiO_2–ZnO catalysts, respectively. It varied from 179, 200, and 186 kJ mol^{-1} at 20 wt. % catalyst loading of zeolite Na–Y, 10 wt. % of Pt/C, and 1–1 wt. % of TiO_2–ZnO catalysts, respectively. Whereas, it can be seen that the variation in enthalpy change can be noted as 198, 212, and 190 kJ mol^{-1} at 30 wt. % catalyst loading of zeolite Na–Y, 10 wt. % of Pt/C, and 1–1 wt. % of TiO_2–ZnO catalysts, respectively. The change in enthalpy during the non-catalytic pyrolysis of DR biomass was found to be 190 kJ mol^{-1} [130]. The results indicate that the ΔH values of catalytic pyrolysis at 10 wt. % loading of zeolite Na–Y, and 20 wt. % of 1–1 wt. % of TiO_2–ZnO catalyst exhibited a lower value when compared to non-catalytic pyrolysis of DR biomass. Furthermore, it can also be seen that the ΔH was positive, indicating that the reaction was indigenously endothermic in nature. Though initially, during the beginning of the reaction, the ΔH values were noted to be lower, there was a slight increase at higher conversions (>0.6), indicating that more energy was required for the reaction to proceed at higher conversion [34].

Figure 5.4.3 (B1, B2, and B3) shows the variation of thermodynamic properties, including change in Gibbs free energy (ΔG) of pyro-catalytic decomposition (PCD) of DR biomass in the presence of zeolite Na–Y, 10 wt. % of Pt/C, and 1–1 wt. % of TiO_2–ZnO catalysts with feedstock ratios of 30, 20, and 10 wt. % respectively for the DFM technique. The change in Gibbs free energy was defined as an increase in the overall energy of the process to form an activated complex [34], [39], [136]. The calculations of change in Gibbs free energy of the current study show that it has varied from 178,178,176 kJ mol^{-1} for all the three catalysts at catalyst loading from 30, 20, and 10 wt. % respectively. The ΔG value obtained during non-catalytic pyrolysis of DR biomass was 180 kJ mol^{-1} [130]. The results show the feedstock potential to determine the energy content of the biomass. Also, ΔH and ΔG were found to be positive, indicating that additional energy was required to perform the PCD of DR biomass resulting in non-spontaneity of the reaction.

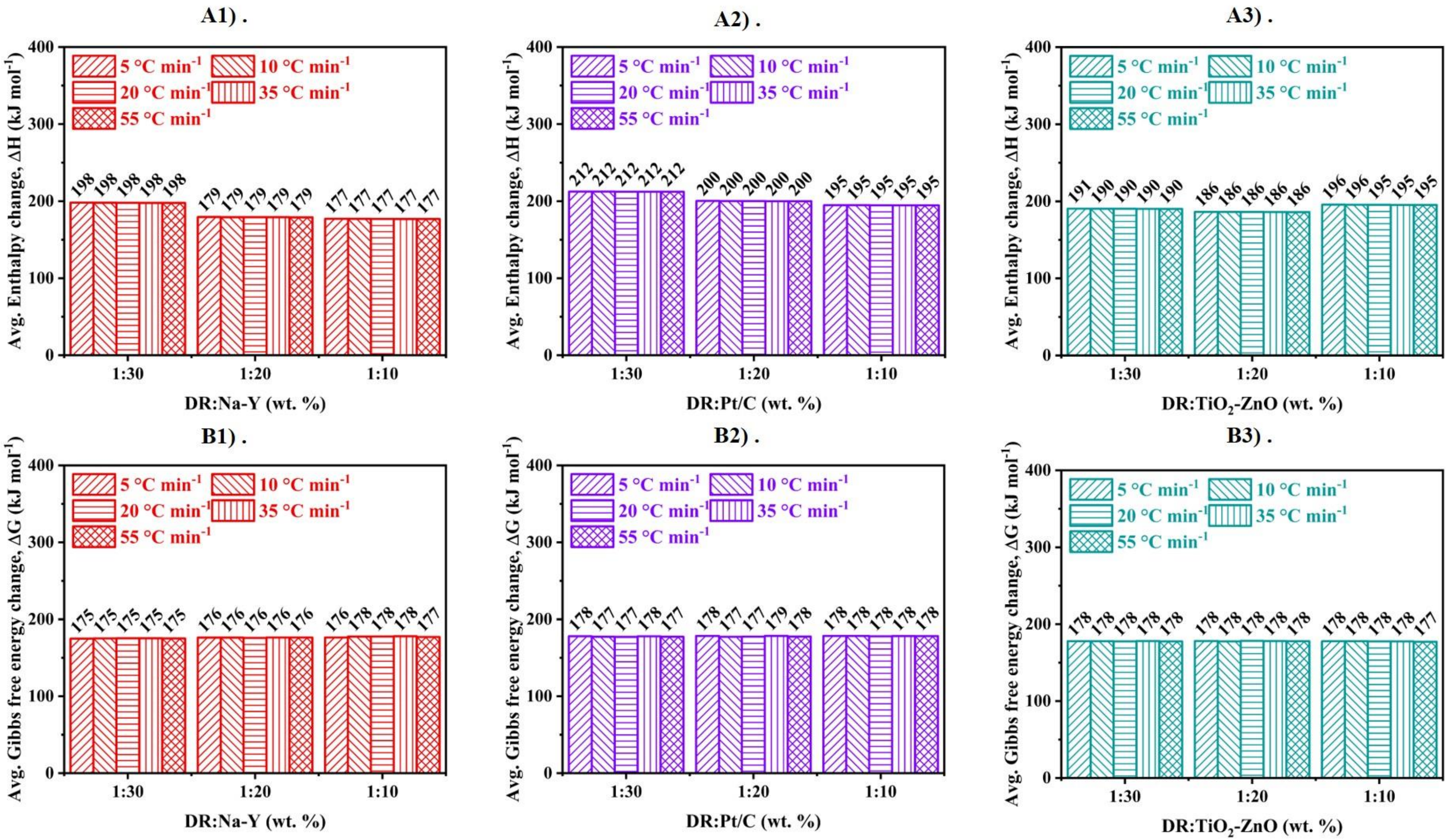

Figure 5.4.3 Variations in average thermodynamic properties over the catalyst: **A1)**, **A2)**, and **A3)** for enthalpy change (kJ mol^{-1}), **B1)**, **B2)**, and **B3)** for change in Gibbs free energy (kJ mol^{-1}) at the DFM technique.

5.4.4 Indices of pyrolysis performance for pyro-catalytic decomposition of DR biomass

The indices of pyrolysis performance (IPP) of the PCD of DR biomass at three catalysts, including zeolite (Na–Y), 10 wt. % of noble metal on activated carbon (Pt/C), and 1–1 wt. % of two metallic oxides (TiO_2–ZnO) from 30 to 10 wt.% loading was shown in **Table 5.4.4**. According to the IPP findings, all parameters (C, D_i, D_b, S, and D_v) were increased with increasing heating rates (5 – 55 °C min^{-1}) at three catalysts. Furthermore, in comparison to the other catalyst loadings, the 10 wt. % of zeolite Na–Y exhibited the lowest IPP parameters. This might occur because the zeolite Na–Y has a larger surface area and is stable at higher temperatures [140]. The higher flammability index ($C = 8.78\times 10^{-5}$), suggesting a lower moisture content and larger heating value. The higher ignition and burnout indices (D_i and D_b $= 944 \times 10^{-3}$ and 4540×10^{-5}), indicated the higher combustibility. The higher combustion index ($S = 26.5 \times 10^{-8}$), exhibited stronger combustion characteristics. The higher devolatilization index ($D_v = 48.3 \times 10^{-8}$), demonstrated the generation of a significant quantity of volatile content during the pyro-catalytic decomposition (PCD) of DR biomass [39], [109], [130].

Table 5.4.4 Characteristics of indices of pyrolysis performance for various catalytic pyrolysis of *Delonix Regia* biomass

β	DR:Na–Y (1:30 wt.%)					DR:Na–Y (1:20 wt.%)					DR:Na–Y (1:10 wt.%)				
	$C \times 10^{-5}$	$D_i \times 10^{-3}$	$D_b \times 10^{-5}$	$S \times 10^{-8}$	$D_v \times 10^{-8}$	$C \times 10^{-5}$	$D_i \times 10^{-3}$	$D_b \times 10^{-5}$	$S \times 10^{-8}$	$D_v \times 10^{-8}$	$C \times 10^{-5}$	$D_i \times 10^{-3}$	$D_b \times 10^{-5}$	$S \times 10^{-8}$	$D_v \times 10^{-8}$
5	1.02	1.06	0.451	0.322	0.630	1.16	1.18	0.523	0.338	0.669	1.25	1.28	0.546	0.427	0.834
10	2.16	8.53	7.08	1.19	2.23	2.21	8.64	7.60	1.43	2.78	2.34	9.07	7.74	1.34	2.49
20	3.54	53.4	93.0	3.91	7.37	3.92	59.1	104.1	4.51	8.57	4.41	65.4	115	5.05	9.22
35	5.71	254	785	11.2	20.9	6.47	2870	878.1	13.0	24.1	7.01	306	973	14.1	25.1
55	8.78	944	4540	26.5	48.3	9.82	10500	5010	30.6	55.3	10.2	10900	5280	33.8	61.9
	DR:Pt/C (1:30 wt.%)					DR:Pt/C (1:20 wt.%)					DR:Pt/C (1:10 wt.%)				
5	1.03	1.04	0.422	0.290	0.543	1.16	1.17	0.478	0.338	0.633	1.34	1.34	0.549	0.402	0.757
10	2.01	7.79	6.39	1.09	2.01	2.18	8.45	7.10	1.24	2.30	2.17	8.32	7.13	1.28	2.40
20	3.66	54.3	93.6	4.50	8.40	4.18	61.8	107.1	5.40	10.1	4.27	62.8	113	5.61	10.6
35	6.75	294	878	13.0	23.1	7.57	329	998.1	15.4	27.1	7.23	314	988	15.1	27.1
55	9.10	954	4720	27.2	49.1	11.1	11700	5710	36.3	64.8	9.94	10400	6550	140	55.0
	DR:TiO_2–ZnO (1:30 wt.%)					DR:TiO_2–ZnO (1:20 wt.%)					DR:TiO_2–ZnO (1:10 wt.%)				
5	1.03	1.04	0.446	0.272	0.523	1.10	1.10	0.472	0.308	0.549	1.27	1.27	0.537	0.389	0.747
10	1.85	7.11	6.19	0.950	1.78	2.04	7.89	6.79	1.11	2.10	2.39	9.23	7.73	1.41	2.61
20	3.28	48.5	85.5	4	7.53	3.64	53.6	95.7	4.48	8.46	4.20	61.9	110	5.51	10.4
35	5.50	240	749	10.4	18.5	6.76	295	927	14.0	25.5	7.11	312	935	15.9	28.9
55	7.96	836	4210	24.5	43.9	8.67	912	4590	27.2	48.5	10.9	11500	5470	38.7	69.7

5.4.5 Summary and Comparative analysis with existing work

The summary of objective 4 and the comparative analysis with existing work (**Table 5.4.5**) was discussed below.

Summary of the objective 4.

The following statements were obtained from objective 4:

- The thermal stability characteristics of pyro-catalytic decomposition (PCD) of *Delonix regia* (DR) biomass were elucidated in the presence of three different catalysts, namely zeolite (Na-Y), 10 wt. % of noble metal on activated carbon (Pt/C), and 1-1 wt. % of TiO_2-ZnO respectively.
- From thermal analysis, the mass loss of 53 – 51 wt. %, 58 – 56 wt. %, and 62 – 60 wt. % for 30, 20, and 10 wt. % of Na–Y; 63 – 60 wt. %, and 64 – 59 wt. % for 30, 20, and 10 wt. % of Pt/C; and 54 – 50 wt. %, 56 – 55 wt. %, and 63 – 62 wt. % for 30, 20, and 10 wt. % of TiO_2–ZnO, respectively, were ascertained at 5-55 °C/min.
- At 10 wt. % of zeolite (Na-Y) loading, the lowest average activation energy of 181 kJ/mol was estimated from the KAS technique.
- Variations of reaction pathways were shown for the PCD of DR biomass at three different catalysts from Criado's technique.
- $\Delta H \approx 177$ kJ/mol and $\Delta G \approx 178$ kJ/mol from the Differential Friedman technique suggested the exothermicity and non-spontaneity of PCD of DR biomass at 10 wt. % of zeolite (Na-Y) loading.
- Finally, the indices of pyrolysis performance for PCD of DR biomass were discussed.

Table 5.4.5: Comparative analysis of in – situ catalytic pyrolysis of DR biomass.

S.No.	Raw materials	Catalyst	TGA model	Operating conditions			Results		References
	Feed and co-feed	(wt. %)		°C	Q	β	*Kinetics	*Thermodynamics	
1	Sunan candlenut oilcake (1 wt.%)	Zeolite (5 wt.%)	Leco-701	30 – 950	N_2 – 10	10, 20, 30, 40	$E_{\alpha=0.15\text{-}0.80}$: 331, 325, 418 for OFW, KAS, DFM	-	[55]
2	Pinewood (10 mg)	HZSM – 5	TA-SDT650	25 – 850	N_2 – 100	5, 10, 20	$E_{\alpha=0.1\text{-}0.90}$: 167 for KAS	-	[47]
3	Poplar sawdust (10 mg)	Fe-Ni/ZSM-5 (1:1)	Perkin Elmer STA-8000	25 – 900	N_2 – 100	5, 10, 20, 40	$E_{\alpha=0.15\text{-}0.90}$: 156, 152, 154, 152 for DFM, STK, OFW, KAS	$E_{\alpha=0.1\text{-}0.80}$: ΔH: 163, and ΔG: 158	[34]
4	*Delonix Regia* (6 mg)	Na-Y zeolite (30, 20, 10 wt.%)	Netsch TG209F1	25 – 1000	N_2 – 40	5, 10, 20, 35, 55	$E_{\alpha=0.1\text{-}0.7}$ and k_o: 182 and 1.33× 10^{16}, 181 and 2.10 × 10^{16}, 181 and 9.31 × 10^{13}, 181 and 1.69× 10^{16}, 181 and 1.83× 10^{17} by DFM,	$E_{\alpha=0.1\text{-}0.80}$: ΔH: 177, and ΔG: 178	Objective 4

							KAS, OFW, STK, DAE at 10 wt. % Na-Y		
5	*Delonix Regia* (6 mg)	Pt/C (30, 20, 10 wt.%)	Netsch TG209F1	25 – 1000	N_2 – 40	5, 10, 20, 35, 55	$E_{\alpha=0.1-0.7}$ and k_o: 200 and 9.62×10^{17}, 208 and 2.59×10^{18}, 204 and 9.56×10^{15}, 205 and 2.07×10^{18}, 205 and 2.03×10^{19} by DFM, KAS, OFW, STK, DAE at 10 wt.% Pt/C	$E_{\alpha=0.1-0.80}$: ΔH: 195, and ΔG: 178	Objective 4
6	*Delonix Regia* (6 mg)	TiO_2-ZnO (1:1) (30, 20, 10 wt.%)	Netsch TG209F1	25 – 1000	N_2 – 40	5, 10, 20, 35, 55	$E_{\alpha=0.1-0.7}$ and k_o: 191 and 7.34×10^{16}, 194 and 2.87×10^{17}, 194 and 1.16×10^{15}, 195 and 2.30×10^{17}, 194 and 2.30×10^{18} by DFM, KAS, OFW, STK, DAE at 20 wt.% TiO_2-ZnO	$E_{\alpha=0.1-0.80}$: ΔH: 186, and ΔG: 178	Objective 4

β – Heating rates (°C min^{-1})

α – Conversion

°C – Temperature

Q – Flowrate of carrier gas (mL min^{-1})

Iso – conversional models – Differential Friedman (DFM), Kissinger-Akahira-Sunose (KAS), Ozawa-Flynn-Wall (OFW), Starink (STK), and Distributed Activation Energy (DAE)

*Kinetics – Average values

*Thermodynamics – Average values based on the DFM model at 10 °C min^{-1}

E_α – Activation energy (kJ mol^{-1})

k_o – Frequency factor (s^{-1})

ΔH – Change in enthalpy (kJ mol^{-1})

ΔG – Change in Gibbs free energy (kJ mol^{-1})

ΔS – Change in entropy (kJ mol^{-1} K^{-1})

5.5 Pyro–catalytic co–pyrolysis of *Delonix Regia* and butyl rubber tube: kinetic modeling and thermodynamic insights

5.5.1 Evaluation of thermal degradation behavior of pyro–catalytic co–pyrolysis of DR and BRT

TG and DTG thermograms of the pyro-catalytic co-pyrolysis (PCCP) of DR and BRT co-feed (1:1) in the presence of catalysts (Na–Y (zeolite), Pt/C (10 wt. % of noble metal on activated carbon), and TiO_2–ZnO (1–1 wt. % of bimetallic oxide), correspondingly) were illustrated in **Figure 5.5.1.2 (A1 to A3, B1 to B3, and C1 to C3)**. Three distinct zones of PCCP of DR and BRT co–feed degradation were depicted in **Figure 5.5.1**. The initial zone, consisting release of water and low–molecular–weight molecules, formed at temperatures between 25 and 150 °C. Degradation of critical components like hemicellulose and cellulose interact with isobutylene and isoprene during the co–pyrolysis in the active pyrolytic secondary zone [51], [117], [141], [142]. It should also be mentioned that lignin degradation begins at this stage. At temperatures above 550 °C, the third zone showed significant lignin breakdown [100], [130]. The lignin component contributes to the slow disintegration of the biomass in the third stage.

Additionally, the thermograms **(Figure 5.5.1.1)** indicated that the catalysts exhibited better stability, with 76.4 wt.%, for Na-Y, 56.2 wt.% for Pt/C, and 98.8 wt.% for TiO_2-ZnO correspondingly, when the heating rate was kept constant at 20 °C / min. The TG and DTG thermograms of PCCP of DR and BRT co–feed at 30, 20, and 10% wt. % Na – Y were depicted from **A1 to A3 in Figure 5.5.1.2**. The TG thermograms at 5 – 55 °C / min revealed weight losses of 53 – 51 wt. %, 58 – 56 wt. %, and 62 – 60 wt. % for Na – Y doses of 30, 20, and 10 wt. %, correspondingly. The maximal degradation temperatures for 30, 20, and 10 wt. % of Na – Y, correspondingly, was 354 – 391 °C, 327 – 372 °C, and 334 – 389 °C, according to the DTG thermograms at 5 – 55 °C / min. The weight loss dropped dramatically as the catalyst (Na

– Y) dosage was raised [40], [143]. As the temperature was increased between 500 and 1000 °C, the DTG curves flattened out, indicating that the PCCP of DR and BRT co–feed was complete. In addition, the rise in heating rate led to a shift in the TG and DTG curves in the absence of a catalyst during the co–pyrolysis process, suggesting an inefficient heat transmission to the particles [51], [132], [140]. A change in the TG – DTG thermograms was also seen in the presence of a catalyst. The pore size, surface area, and accessibility of acidic sites (Lewis and Brønsted sites coalescence) in a zeolite each play a role in this thermogram shift for a catalytic co–pyrolysis process [30], [34], [58], [132].

The TG and DTG thermograms of PCCP of DR and BRT co–feed at 30, 20, and 10 wt. % of Pt/C were shown in **Figure 5.5.1.2 from B1 to B3**. Thermogravimetric (TG) thermograms obtained at 5 – 55 °C / min revealed weight loss of 55 – 53 wt. %, 63 – 60 wt. %, and 64 – 59 wt. % for 30, 20, and 10 wt. % Pt/C, correspondingly. It was found that the weight loss markedly reduced as the catalyst (Pt/C) ratio increased. The maximal degradation temperatures were 335 – 383 °C, 338 – 380 °C, and 336 – 383 °C for 30, 20, and 10 wt. % Pt/C, correspondingly, according to the DTG thermograms at 5 – 55 °C / min. Decarbonylation, decarboxylation, and dehydrogenation were key processes contributing to weight reduction. Due to its smaller surface area and pore capacity, the Pt/C catalyst reported less catalytic activity than the zeolite catalyst [34], [134].

The TG and DTG thermograms of the PCCP of DR and BRT co–feed at 30, 20, and 10 wt. % of TiO_2 – ZnO were exhibited in **Figure 5.5.1.2 from C1 to C3**. The TG thermograms at 5–55 °C / min indicated a weight loss of 54 – 50 wt. %, 56 – 55 wt. %, and 63 – 62 wt. % for 30, 20, and 10 wt. % TiO_2 – ZnO, correspondingly. It was shown that the weight loss dramatically decreased when the catalyst (TiO_2 – ZnO) ratio continued to increase. The maximal degradation temperatures were 349 – 389 °C, 337 – 387 °C, and 343 – 3 84 °C for 30, 20, and 10 wt. % of TiO_2 – ZnO, correspondingly, according to the DTG thermograms at 5

– 55 °C / min. TiO_2 – ZnO has better catalytic stability than the aforementioned catalysts **(Figure 5.5.1.1)**. This suggests that the catalyst had a minimal impact on the degradation of the DR and BRT co – feed during the co – pyrolysis (unconverted co – feed was high for all dosages) [34], [136].

In comparison to a more significant dose at 30 wt. %, a catalyst with a lower dosage (10, 20 wt. %) enabled improved thermal degradation of the biomass. This pattern can be explained by coke deposition at higher doses on the catalytic surface for all catalysts [34], [143]. In agreement with this, it was discovered that the non–catalytic thermal breakdown of the DR and BRT co–feed varied between 30.2 – 25.5 wt. % as the heating rate progressed from 5 to 55 °C / min [51].

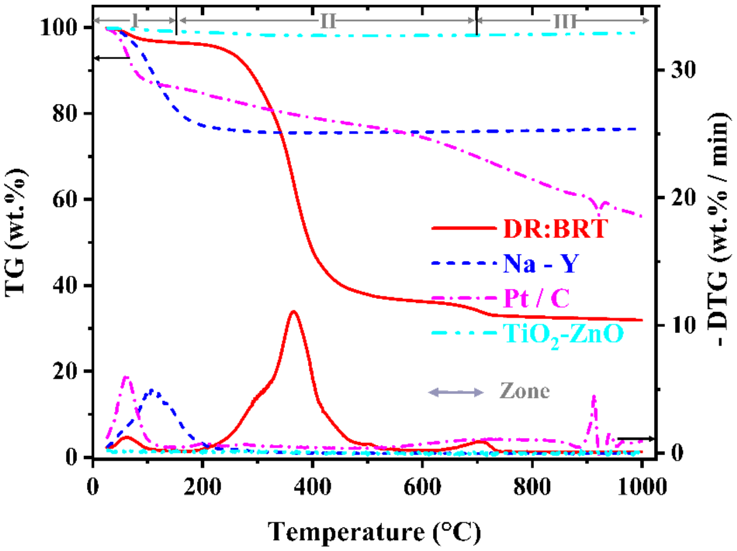

Figure 5.5.1.1 Temperature-dependent variations in TG and DTG thermograms of co-pyrolysis of Delonix Regia (DR) biomass and Butyl Rubber Tube (BRT) waste and three different types of catalysts were utilized: zeolite (Na–Y), noble metal on activated carbon (10 wt. % Pt/C), and bi–metal oxide (1:1 wt. % of TiO_2–ZnO) at 20 °C / min.

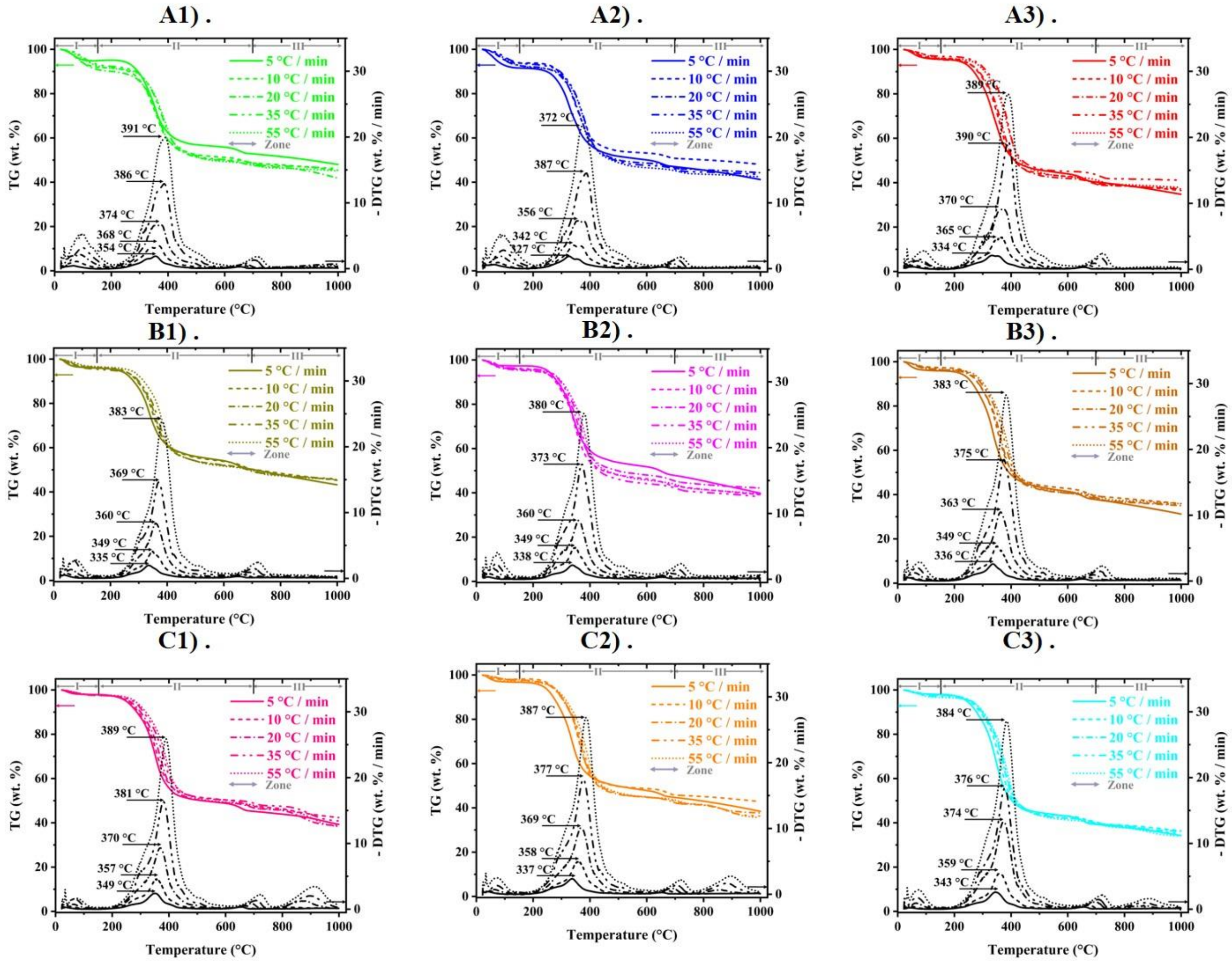

Figure 5.5.1.2 Temperature-dependent variations in TG and DTG thermograms of co-pyrolysis of *Delonix Regia* (DR) biomass and butyl rubber tube (BRT) waste for various catalysts: **A1), A2),** and **A3)** for DR:BRT:Na-Y (1:1:30, 1:1:20, and 1:1:10 wt.%), **B1), B2),** and **B3)** for DR:BRT:Pt/C (1:1:30, 1:1:20, and 1:1:10 wt.%), and **C1), C2),** and **C3)** for DR:BRT:TiO_2-ZnO (1:1:30, 1:1:20, and 1:1:10 wt.%).

5.5.2 Kinetic modeling for pyro–catalytic co–pyrolysis of DR and BRT

Catalyst activity can be predicted from its surface area since fewer active sites mean less of the catalyst was exposed to the reactants, and hence less of the catalyst was used. Consequently, the thermal disintegration of a catalyst reveals that the rigid pore walls provide sufficient strength to the active sites, which promotes the thermal stability of the catalyst [34], [136]. This was demonstrated by the fact that thermal degradation occurs. This makes it feasible to use the catalyst at temperatures above 1000 °C without losing its characteristics [34], [136]. Additionally, the adsorption of more gaseous products takes place on the active sites over time by clogging the porous structure, which promotes the development of coke on the catalyst and decreases the active surface area present for the reactions. Because of this, more energy was needed to start the reaction [34], [58], [136].

Figure 5.5.2.1 (A1) and Table 5.5.2.1.1 illustrate the change of activation energy in the presence of Na – Y catalyst at dosages of 30, 20, and 10 wt. %, correspondingly. Using the model–fitting (OFW) model, the kinetic analysis (**Figure 5.5.2.1 (A1)**) showed that when zeolite Na – Y was used, the average E_α (kJ / mol) and k_o (min^{-1}) values dropped from 275 and 5.36 E+24 to 180 and 5.95 E+16 as the amount of catalyst changed from 30 to 10 wt. %. Pyro–catalytic co–pyrolysis (PCCP) of DR and BRT yielded an activation energy of 180 kJ / mol, which was lower than the average E_α of 186 kJ / mol produced by the non–catalytic pyrolysis of the same feedstock [51]. The remaining (four) model–free models produced average E_α (kJ / mol) and k_o (s^{-1}) values of 275 and 5.36 E+24, 224 and 2.46 E+21, and 180 and 5.95 E+16 at 30, 20, and 10% wt. % Na – Y, correspondingly. With a lower Na – Y ratio (10 wt. %), the average E_α value was found to be lower (180 kJ / mol). A lower dosage of Na – Y (10 wt. %) was shown to be effective in catalyzing the co- pyrolysis of DR and BRT co- feed.

The other catalysts used in the development of the kinetic modeling for PCCP of DR and BRT co–feed, in addition to the zeolite Na – Y, were Pt/C and TiO_2 – ZnO. When the catalyst (Pt/C) dose was reduced from 30 to 20 and then to 10 wt. %, correspondingly, using the model–fitting (OFW) model, the results showed that the average E_α (kJ / mol) and k_o (s^{-1}) values increased from 246 and 3.60 E+29 to 251 and 4.27 E+22 and then sharply dropped to 203 and 1.31 E+18. It was discovered that the average E_α value followed the trend described above for the Pt/C ratio. The change of activation energy in the presence of Pt/C at 30, 20, and 10 wt. % was depicted in **Figure 5.5.2.1 (A2) and Table 5.5.2.1.2** correspondingly.

Additionally, **Figure 5.5.2.1 (A3) and Table 5.5.2.1.3** show the activation energy changes when TiO_2 – ZnO catalyst was present at 30, 20, and 10% dosages. The results revealed that when the catalyst dosage (TiO_2 – ZnO) was reduced from 30 to 20 and subsequently 10 wt. % using the model–fitting (OFW) model, the average E_α (kJ / mol) and k_o (s^{-1}) values declined from 228 and 1.43 E+19 to 182 and 8.11 E+14 and quickly increased to 239 and 3.19 E+21. The average E_α value was found to be reduced by 4 folds, while the TiO_2 – ZnO ratio was found to increase by 5 folds. The earlier mentioned factors are most likely to be responsible for this alteration of average E_α values [34], [40], [58], [136], [140].

The Na–Y zeolite catalyst has the lowest kinetic parameters of all the catalysts employed in the PCCP of DR and BRT processes. For a 10 wt. % Na–Y zeolite catalyst, the activation energy determined by the OFW rate equation increased uniformly as the reaction progressed. Because the polymers such as BRT contain weak bonds, thermal degradation may begin at approximately 150 °C [140], [142]. So, the activation energy was lowest when the reaction initially started. At the later stages of thermal deterioration, the activation energy rose due to the breakdown of complex organic matter. The decreased activation energy for conversion stages 0.1 – 0.2, which was the initial stage in the progression of the reaction, may have been due to the devolatilization of the processing oil and other volatile additives [141], [142], [144]. Activation energies in the range of 214.59 – 255.94 kJ / mol for stages 0.2 – 0.6 of conversion, related to the maximum conversion rate at approximately 334–389 °C, suggest the degradation of complex organic materials such hemicellulose, cellulose, and iso – butylene. This stage consisted primarily of the deterioration of DR and BRT co – feed [51], [117], [141], [142]. At the same time, the third conversion stage (0.6–0.7) was dominated by the breakdown of isoprene and lignin [51], [142].

Each catalyst used in the current study offers different contributions to the co–pyrolysis process. Dehydration, hydrogenation, decarboxylation, decarbonylation, deoxygenation, repolymerization, and re-condensation are among the several reactions. For more significant deoxygenation reactions and hydrogenation, the Pt/C catalyst was well–known [134]. On the other hand, the TiO2 – ZnO catalyst improves the removal of water molecules of alcohols to alkenes and the generation of lower molecular weight hydrocarbon compounds. In addition, xylene, an intermediary in the breakdown of hemicellulose, can be converted with the aid of the TiO_2 catalyst [138]. Additionally, the increased acid site offered by the zeolite catalyst facilitates the decarbonylation and deoxygenation processes [35]. Thus, it was clear that each of these catalysts was important for biomass degradation.

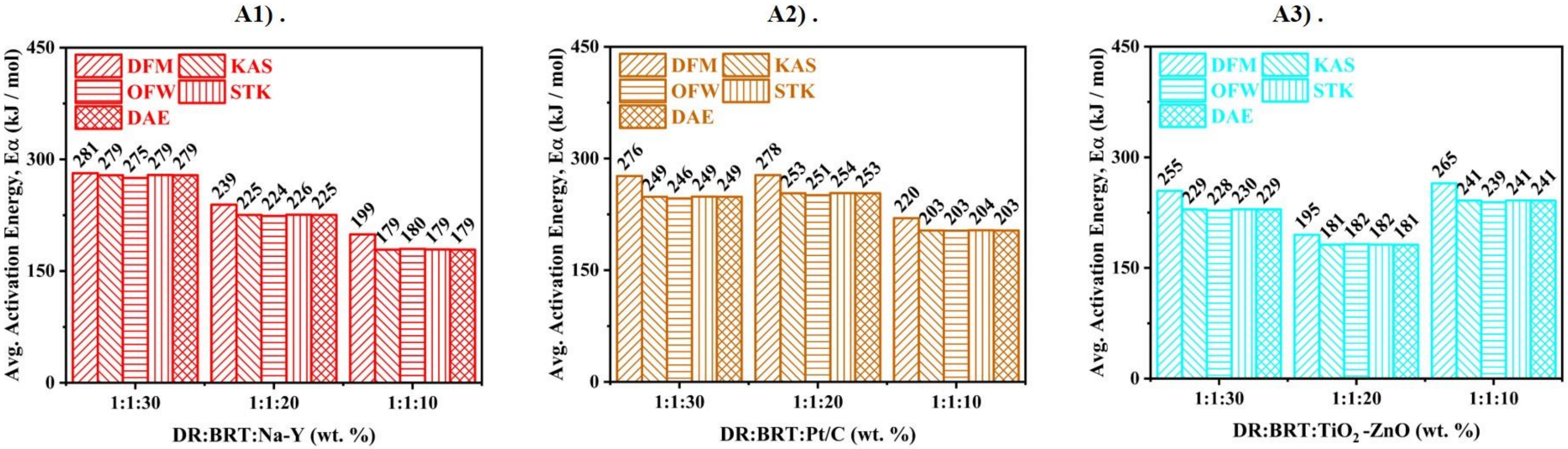

Figure 5.5.2.1 Variations in average activation energy of co-pyrolysis of *Delonix Regia* (DR) biomass and butyl rubber tube (BRT) waste for various catalysts: **A1)** (DR:BRT:Na-Y), **A2)** (DR:BRT:Pt/C), and **A3)** (DR:BRT:TiO_2-ZnO).

Table 5.5.2.1.1 Kinetic factors of catalytic (Na-Y) co-pyrolysis of *Delonix Regia* (DR) biomass and butyl rubber tube (BRT) waste using various iso-conversional methodologies, including activation energy and frequency factor.

α	Iso-conversional methodologies														
	DFM			KAS			OFW			STK			DAE		
	E_α	k_o	R^2	E_α	k_o	R^2	E_α	k_o	R^2	E_α	k_o	R^2	E_α	k_o	R^2
	DR:BRT:Na-Y (1:1:30 wt.%)														
0.1	279.05	2.19E+24	0.855	315.84	2.19E+28	0.823	309.36	3.72E+25	0.831	315.97	1.70E+28	0.823	315.84	2.08E+29	0.823
0.2	242.14	1.54E+20	0.948	275.58	4.66E+23	0.947	271.52	1.14E+21	0.951	275.76	3.67E+23	0.947	275.58	2.09E+24	0.947
0.3	243.52	8.67E+19	0.949	240.04	1.23E+20	0.952	238.00	4.16E+17	0.956	240.26	9.76E+19	0.952	240.04	3.44E+20	0.952
0.4	266.15	2.86E+21	0.954	255.67	1.23E+21	0.938	253.10	3.85E+18	0.942	255.89	9.75E+20	0.938	255.67	2.40E+21	0.938
0.5	256.55	2.14E+20	0.971	257.21	7.97E+20	0.965	254.75	2.57E+18	0.968	257.43	6.34E+20	0.965	257.21	1.15E+21	0.965
0.6	294.96	1.14E+23	0.975	274.81	1.05E+22	0.978	271.69	3.10E+19	0.980	275.03	8.34E+21	0.978	274.81	1.15E+22	0.978
0.7	387.94	4.33E+29	0.960	331.99	1.40E+26	0.968	326.31	2.97E+23	0.970	332.17	1.09E+26	0.968	331.99	1.16E+26	0.968
Avg.	281.47	6.18E+28	0.945	278.73	3.15E+27	0.939	274.96	5.36E+24	0.942	278.93	2.44E+27	0.939	278.73	2.97E+28	0.939
		DR:BRT:Na-Y (1:1:20 wt.%)													

0.1	183.15	3.60E+15	0.838	230.88	2.75E+20	0.896	228.48	8.48E+17	0.903	231.07	2.18E+20	0.897	230.88	2.61E+21	0.896
0.2	188.63	4.22E+15	0.931	197.88	6.42E+16	0.949	197.52	2.93E+14	0.954	198.12	5.18E+16	0.950	197.88	2.88E+17	0.949
0.3	190.02	2.98E+15	0.961	190.87	7.58E+15	0.963	191.13	3.94E+13	0.966	191.12	6.15E+15	0.963	190.87	2.13E+16	0.963
0.4	200.80	1.41E+16	0.974	192.14	5.99E+15	0.971	192.55	3.20E+13	0.974	192.40	4.86E+15	0.971	192.14	1.17E+16	0.971
0.5	244.98	2.92E+19	0.968	208.84	9.27E+16	0.967	208.65	4.39E+14	0.970	209.10	7.49E+16	0.967	208.84	1.34E+17	0.967
0.6	283.22	1.65E+22	0.991	242.50	3.01E+19	0.982	240.88	1.11E+17	0.983	242.74	2.41E+19	0.982	242.50	3.29E+19	0.982
0.7	382.95	2.74E+29	0.942	314.53	7.38E+24	0.981	309.65	1.72E+22	0.982	314.72	5.79E+24	0.981	314.53	6.13E+24	0.981
Avg.	239.11	3.91E+28	0.944	225.38	1.05E+24	0.958	224.12	2.46E+21	0.962	225.61	8.27E+23	0.959	225.38	8.76E+23	0.958
	DR:BRT:Na-Y (1:1:10 wt.%)														
0.1	123.67	1.46E+10	0.815	145.83	3.54E+12	0.950	147.56	2.66E+10	0.956	146.09	2.92E+12	0.950	145.83	3.36E+13	0.950
0.2	143.81	4.03E+11	0.911	145.93	1.42E+12	0.922	148.13	1.18E+10	0.931	146.21	1.17E+12	0.923	145.93	6.36E+12	0.922
0.3	166.33	2.32E+13	0.946	154.38	4.34E+12	0.935	156.48	3.45E+10	0.942	154.66	3.59E+12	0.935	154.38	1.22E+13	0.935
0.4	178.89	1.85E+14	0.968	166.13	3.03E+13	0.941	167.89	2.18E+11	0.947	166.41	2.49E+13	0.941	166.13	5.93E+13	0.941
0.5	217.09	1.35E+17	0.953	179.07	2.61E+14	0.951	180.39	1.69E+12	0.956	179.35	2.13E+14	0.952	179.07	3.76E+14	0.951
0.6	236.64	3.35E+18	0.988	205.96	2.91E+16	0.968	206.16	1.49E+14	0.971	206.23	2.36E+16	0.968	205.96	3.18E+16	0.968
0.7	328.98	2.12E+25	0.962	253.91	1.17E+20	0.969	252.00	4.16E+17	0.972	254.15	9.37E+19	0.969	253.91	9.75E+19	0.969
Avg.	199.34	3.03E+24	0.935	178.74	1.68E+19	0.948	179.80	5.95E+16	0.954	179.01	1.34E+19	0.948	178.74	1.39E+19	0.948

Table 5.5.2.1.2 Kinetic factors of catalytic (Pt/C) co-pyrolysis of *Delonix Regia* (DR) biomass and Butyl rubber tube (BRT) waste using various iso-conversional methodologies, including activation energy and frequency factor.

α	Iso-conversional methodologies														
	DFM			KAS			OFW			STK			DAE		
	E_α	k_o	R^2	E_α	k_o	R^2	E_α	k_o	R^2	E_α	k_o	R^2	E_α	k_o	R^2
	DR:BRT:Na-Y (1:1:30 wt.%)														
0.1	192.84	3.94E+16	0.970	197.83	3.25E+17	0.971	197.03	1.35E+15	0.973	198.04	2.61E+17	0.971	197.83	3.09E+18	0.971
0.2	203.04	7.51E+16	0.961	208.25	6.78E+17	0.960	207.40	2.82E+15	0.963	208.48	5.45E+17	0.960	208.25	3.04E+18	0.960
0.3	194.78	6.58E+15	0.970	207.53	2.24E+17	0.964	207.03	9.98E+14	0.967	207.77	1.80E+17	0.964	207.53	6.27E+17	0.964
0.4	211.28	1.18E+17	0.969	211.23	2.58E+17	0.977	210.76	1.16E+15	0.979	211.48	2.08E+17	0.977	211.23	5.06E+17	0.977
0.5	251.64	1.19E+20	0.960	224.28	1.96E+18	0.969	223.37	8.13E+15	0.971	224.53	1.57E+18	0.969	224.28	2.82E+18	0.969
0.6	320.41	1.60E+25	0.930	269.28	5.21E+21	0.947	266.38	1.58E+19	0.951	269.49	4.14E+21	0.947	269.28	5.69E+21	0.947
0.7	561.44	1.38E+43	0.805	421.85	1.89E+33	0.751	411.79	2.52E+30	0.761	421.96	1.45E+33	0.752	421.85	1.57E+33	0.751
Avg.	276.49	1.97E+42	0.938	248.61	2.70E+32	0.934	246.25	3.60E+29	0.938	248.82	2.07E+32	0.934	248.61	2.24E+32	0.934
		DR:BRT:Pt/C (1:1:20 wt.%)													

0.1	218.59	1.55E+19	0.971	223.95	1.35E+20	0.972	221.81	4.36E+17	0.974	224.14	1.07E+20	0.972	223.95	1.28E+21	0.972
0.2	237.18	1.12E+20	0.963	232.42	1.57E+20	0.949	230.32	5.17E+17	0.953	232.63	1.25E+20	0.950	232.42	7.02E+20	0.949
0.3	233.43	1.67E+19	0.970	244.92	5.71E+20	0.963	242.53	1.82E+18	0.966	245.12	4.54E+20	0.963	244.92	1.60E+21	0.963
0.4	228.71	3.86E+18	0.947	231.74	1.84E+19	0.973	230.23	6.83E+16	0.975	231.97	1.47E+19	0.973	231.74	3.60E+19	0.973
0.5	279.72	3.04E+22	0.958	240.09	5.18E+19	0.953	238.36	1.87E+17	0.957	240.32	4.14E+19	0.953	240.09	7.47E+19	0.953
0.6	339.93	8.22E+26	0.941	271.25	1.00E+22	0.916	268.20	2.96E+19	0.921	271.46	7.93E+21	0.916	271.25	1.09E+22	0.916
0.7	405.87	2.44E+31	0.629	328.76	1.40E+26	0.711	323.15	2.99E+23	0.724	328.94	1.10E+26	0.711	328.76	1.17E+26	0.711
Avg.	277.63	3.48E+30	0.911	253.30	2.01E+25	0.919	250.66	4.27E+22	0.924	253.51	1.57E+25	0.920	253.30	1.67E+25	0.919
	DR:BRT:Pt/C (1:1:10 wt.%)														
0.1	168.76	3.81E+14	0.991	172.34	1.81E+15	0.991	172.67	9.60E+12	0.992	172.57	1.47E+15	0.991	172.34	1.72E+16	0.991
0.2	191.00	8.85E+15	0.982	184.18	6.67E+15	0.979	184.38	3.43E+13	0.981	184.42	5.41E+15	0.979	184.18	2.99E+16	0.979
0.3	187.38	1.78E+15	0.987	189.86	8.11E+15	0.984	190.12	4.22E+13	0.985	190.11	6.58E+15	0.984	189.86	2.27E+16	0.984
0.4	192.33	2.93E+15	0.961	189.84	4.48E+15	0.991	190.35	2.44E+13	0.992	190.11	3.64E+15	0.992	189.84	8.77E+15	0.991
0.5	212.77	1.01E+17	0.991	197.34	1.27E+16	0.989	197.67	6.69E+13	0.990	197.61	1.03E+16	0.989	197.34	1.84E+16	0.989
0.6	254.19	1.19E+20	0.994	220.60	6.74E+17	0.992	219.99	2.96E+15	0.993	220.86	5.43E+17	0.992	220.60	7.35E+17	0.992
0.7	333.27	6.86E+25	0.980	269.38	2.95E+21	0.990	266.62	9.19E+18	0.991	269.61	2.34E+21	0.990	269.38	2.45E+21	0.990
Avg.	219.96	9.80E+24	0.984	203.36	4.22E+20	0.988	203.12	1.31E+18	0.989	203.61	3.35E+20	0.988	203.36	3.50E+20	0.988

Table 5.5.2.1.3 Kinetic factors of catalytic (TiO_2-ZnO) co-pyrolysis of *Delonix Regia* (DR) biomass and Butyl rubber tube (BRT) waste using various iso-conversional methodologies, including activation energy and frequency factor.

α	Iso-conversional methodologies														
	DFM			KAS			OFW			STK			DAE		
	E_α	k_o	R^2	E_α	k_o	R^2	E_α	k_o	R^2	E_α	k_o	R^2	E_α	k_o	R^2
	DR:BRT:TiO_2-ZnO (1:1:30 wt.%)														
0.1	218.60	1.56E+19	0.946	185.79	3.20E+16	0.979	185.52	1.48E+14	0.981	186.02	2.58E+16	0.979	185.79	3.03E+17	0.979
0.2	221.10	3.31E+18	0.939	211.69	1.66E+18	0.947	210.65	6.65E+15	0.952	211.91	1.33E+18	0.948	211.69	7.44E+18	0.947
0.3	220.54	9.26E+17	0.952	226.10	9.20E+18	0.949	224.71	3.49E+16	0.953	226.33	7.36E+18	0.949	226.10	2.58E+19	0.949
0.4	237.38	1.38E+19	0.980	225.50	3.75E+18	0.965	224.38	1.50E+16	0.968	225.74	3.01E+18	0.965	225.50	7.34E+18	0.965
0.5	242.32	2.09E+19	0.972	229.93	5.18E+18	0.974	228.77	2.06E+16	0.976	230.17	4.15E+18	0.974	229.93	7.47E+18	0.974
0.6	283.96	2.28E+22	0.959	242.67	3.50E+19	0.965	241.07	1.30E+17	0.968	242.91	2.80E+19	0.965	242.67	3.81E+19	0.965
0.7	357.86	5.26E+27	0.945	283.71	3.52E+22	0.956	280.32	1.00E+20	0.960	283.93	2.78E+22	0.956	283.71	2.92E+22	0.956
Avg.	254.54	7.51E+26	0.956	229.34	5.03E+21	0.962	227.92	1.43E+19	0.965	229.57	3.98E+21	0.962	229.34	4.19E+21	0.962
		DR:BRT:TiO_2-ZnO (1:1:20 wt.%)													

0.1	161.40	7.61E+13	0.879	171.04	1.37E+15	0.884	171.40	7.29E+12	0.894	171.27	1.11E+15	0.885	171.04	1.30E+16	0.884
0.2	156.19	6.59E+12	0.817	161.87	5.94E+13	0.860	163.12	3.89E+11	0.873	162.13	4.87E+13	0.861	161.87	2.66E+14	0.860
0.3	174.89	1.51E+14	0.913	167.02	7.51E+13	0.885	168.36	4.96E+11	0.896	167.29	6.15E+13	0.885	167.02	2.10E+14	0.885
0.4	178.31	1.91E+14	0.916	174.44	2.02E+14	0.928	175.67	1.29E+12	0.935	174.71	1.66E+14	0.928	174.44	3.96E+14	0.928
0.5	192.78	2.28E+15	0.967	178.21	2.89E+14	0.949	179.46	1.84E+12	0.954	178.49	2.37E+14	0.949	178.21	4.17E+14	0.949
0.6	214.90	8.06E+16	0.982	190.15	2.02E+15	0.955	191.00	1.18E+13	0.959	190.43	1.65E+15	0.955	190.15	2.20E+15	0.955
0.7	286.04	1.55E+22	0.993	227.52	1.32E+18	0.975	226.76	5.66E+15	0.977	227.77	1.06E+18	0.975	227.52	1.09E+18	0.975
Avg.	194.93	2.21E+21	0.924	181.46	1.89E+17	0.919	182.25	8.11E+14	0.927	181.73	1.52E+17	0.920	181.46	1.59E+17	0.919
	DR:BRT:TiO_2-ZnO (1:1:10 wt.%)														
0.1	199.70	2.61E+17	0.956	187.27	4.68E+16	0.959	186.86	2.11E+14	0.962	187.49	3.77E+16	0.959	187.27	4.44E+17	0.959
0.2	229.60	1.94E+19	0.919	215.93	4.25E+18	0.936	214.59	1.61E+16	0.941	216.14	3.40E+18	0.937	215.93	1.90E+19	0.936
0.3	243.73	9.80E+19	0.946	240.53	1.76E+20	0.939	238.35	5.81E+17	0.944	240.75	1.40E+20	0.939	240.53	4.95E+20	0.939
0.4	239.79	2.24E+19	0.953	232.39	1.53E+19	0.956	230.84	5.65E+16	0.960	232.62	1.22E+19	0.957	232.39	2.99E+19	0.956
0.5	263.41	1.17E+21	0.971	240.68	4.32E+19	0.966	238.92	1.55E+17	0.968	240.91	3.45E+19	0.966	240.68	6.23E+19	0.966
0.6	297.63	3.09E+23	0.955	258.38	7.17E+20	0.972	255.94	2.32E+18	0.974	258.61	5.70E+20	0.972	258.38	7.82E+20	0.972
0.7	380.32	3.57E+29	0.995	313.64	9.69E+24	0.987	308.71	2.24E+22	0.988	313.83	7.60E+24	0.987	313.64	8.05E+24	0.987
Avg.	264.88	5.11E+28	0.956	241.26	1.39E+24	0.959	239.17	3.19E+21	0.962	241.48	1.09E+24	0.959	241.26	1.15E+24	0.959

Criado's master plot model was used to analyse various pyro–catalytic co-pyrolysis (PCCP) of DR and BRT co–feed reaction mechanisms. **Figure 5.5.2.2 (A1–A3)** and **Table 5.5.2.2** illustrate all the plots that were obtained from Equations (12–15) using graphing with conversion ($\alpha = 0.1–0.7$) at 20 °C / min. Figure 5.5.2.2 (A1) showed the reaction mechanisms P4, F2, F2, F2, F2, >F5, from 1:1:30 wt. %; P4, F3, F2, F3, R2, F3 from 1:1:20 wt. % and P4, R2, F1, F2, A4, F2 from 1:1:10 wt. % of DR:BRT:Na – Y, correspondingly. **Figure 5.5.2.2 (A2)** showed the reaction mechanisms P4, A2, R3, F2, F5, >F5, from 1:1:30 wt. %; P4, P3, D2, A4, F5, F5 from 1:1:20 wt. % and P4, P3, P2, A4, F3, F3 from 1:1:10 wt. % of DR:BRT:Pt/C, correspondingly. **Figure 5.5.2.2 (A3)** showed the reaction mechanisms A4, D2, P3, P2, F3, F4, from 1:1:30 wt. %; P4, F0, P2, P4, F2, F3 from 1:1:20 wt. % and F1, R3, P3, R3, F2, F3 from 1:1:10 wt. % of DR:BRT:TiO_2 – ZnO, correspondingly. As a result, it was observed that for all three catalysts at each composition, the pyro–catalytic co-pyrolysis of DR and BRT co–feed follows a multistep reaction mechanism rather than a single reaction step [34], [51].

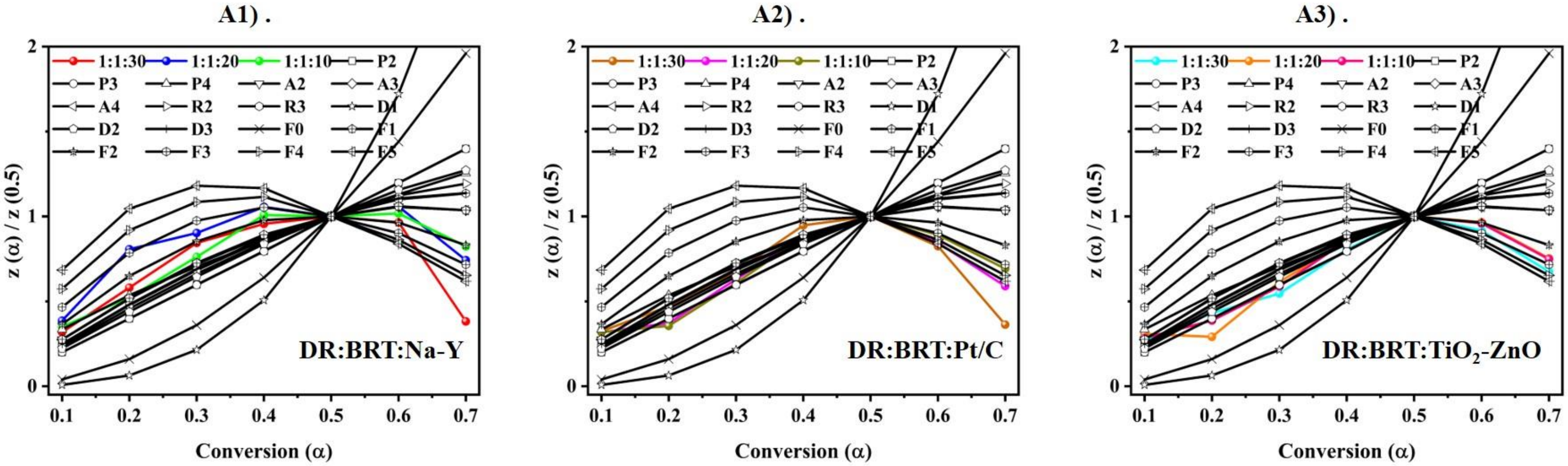

Figure 5.5.2.2 Variations of reaction mechanisms with the conversion of co-pyrolysis of *Delonix Regia* (DR) biomass and butyl rubber tube (BRT) waste by using Criado's master plot for various catalysts: **A1)** (DR:BRT:Na-Y), **A2)** (DR:BRT:Pt/C), and **A3)** (DR:BRT:TiO_2-ZnO) at 20 °C / min.

Table 5.5.2.2 Variations of reaction mechanism with conversion by Criado's master plot model for all three catalysts at 20 °C / min.

(α)	DR:BRT:Na-Y			DR:BRT:Pt/C			DR:BRT:TiO_2-ZnO		
	(1:1:30 wt. %)	(1:1:20 wt. %)	(1:1:10 wt. %)	(1:1:30 wt. %)	(1:1:20 wt. %)	(1:1:10 wt. %)	(1:1:30 wt. %)	(1:1:20 wt. %)	(1:1:10 wt. %)
0.1	P4	P4	P4	P4	P4	P4	A4	P4	F1
0.2	F2	F3	R2	A2	P3	P3	D2	F0	R3
0.3	F2	F2	F1	R3	D2	P2	P3	P2	P3
0.4	F2	F3	F2	F2	A4	A4	P2	P4	R3
0.5	-	-	-	-	-	-	-	-	-
0.6	F2	R2	A4	F5	F5	F3	F3	F2	F2
0.7	>F5	F3	F2	>F5	F5	F3	F4	F3	F3

Models:
A4 – Fourth Avrami-Erofeyev
P4 – Fourth order Power law
R2, R3 – Area and Volume Contracting
D2– 2-dimensional Diffusion
F1, F2, F3, F4, and F5 – First, Second, Third, Fourth, Five order Reaction

5.5.3 Thermodynamic insights for pyro–catalytic co–pyrolysis of DR and BRT

Enthalpy change (*ΔH*) of the pyro–catalytic co–pyrolysis of DR and BRT in the presence of Na – Y zeolite catalyst, Pt/C, and TiO_2 – ZnO catalyst with feedstock ratios of 30, 20, and 10%, correspondingly, was shown in **Figure 5.5.3 (A1, A2, and A3)** for the OFW model. The energy necessary for a molecule to transition from its ground state to a higher energy state is known as the change in enthalpy *(ΔH)* [34], [136]. As a result, the enthalpy changes resembled activation energy. The *ΔH* was observed to vary between 175, 195, and 234 kJ / mol at 10 wt. % catalyst dose of Na – Y, zeolite, Pt/C, and TiO_2 – ZnO catalyst, correspondingly, according to the assessment of thermodynamic parameters. Furthermore, it varied from 219, 245, and 177 kJ / mol at catalyst dosages of 20 wt. % for Na – Y, zeolite, Pt/C, and TiO_2 – ZnO, correspondingly. While the difference in enthalpy change at 30 wt. % catalyst dosages of Na – Y, zeolite, Pt/C, and TiO_2 – ZnO catalyst, correspondingly, can be seen to be 270, 241, and 223 kJ / mol. It was determined that the non–catalytic pyrolysis of the co–feed of DR and BRT changed the enthalpy by 225 kJ / mol. The findings clearly show that as compared to non–catalytic pyrolysis of DR and BRT co–feed, the enthalpy values of catalytic co–pyrolysis at 10 wt. % dose of Na – Y zeolite and 20 wt. % of TiO_2 – ZnO catalyst exhibited a lower value. It was also obvious that the ΔH value was positive, implying that the reaction was naturally endothermic. Although the ΔH values were initially reported to be lower at the initial stage, there was a minor increase at greater conversions (>0.6), suggesting that more energy was needed for the reaction to progress.

Enthalpy change (ΔH) of the catalytic co–pyrolysis of DR and BRT co–feed in the presence of Na – Y zeolite catalyst, Pt/C, and TiO_2 – ZnO catalyst with feedstock ratios of 30, 20, and 10%, correspondingly, was shown in **Figure 5.5.3 (B1, B2, and B3)** for the OFW model. The shift in Gibbs free energy was defined as an increase in the total amount of energy required for the formation of an activated complex [34], [51]. According to the results of the present investigation, the Gibbs free energy has changed by 180, 173, and 178 kJ / mol for the three catalysts at catalytic dosages of 30, 20, and 10 wt. %, correspondingly. The pyrolysis in the absence of a catalyst of the DR and BRT co–feed produced a ΔG value of 180 kJ / mol. The results were found to demonstrate the ability of the feedstock to estimate the energy content of the feed. Additionally, the positive values of ΔH and ΔG showed that more energy was needed to conduct the catalytic co–pyrolysis of the DR and BRT co–feed, which prevented the reaction from occurring spontaneously [34], [51], [136].

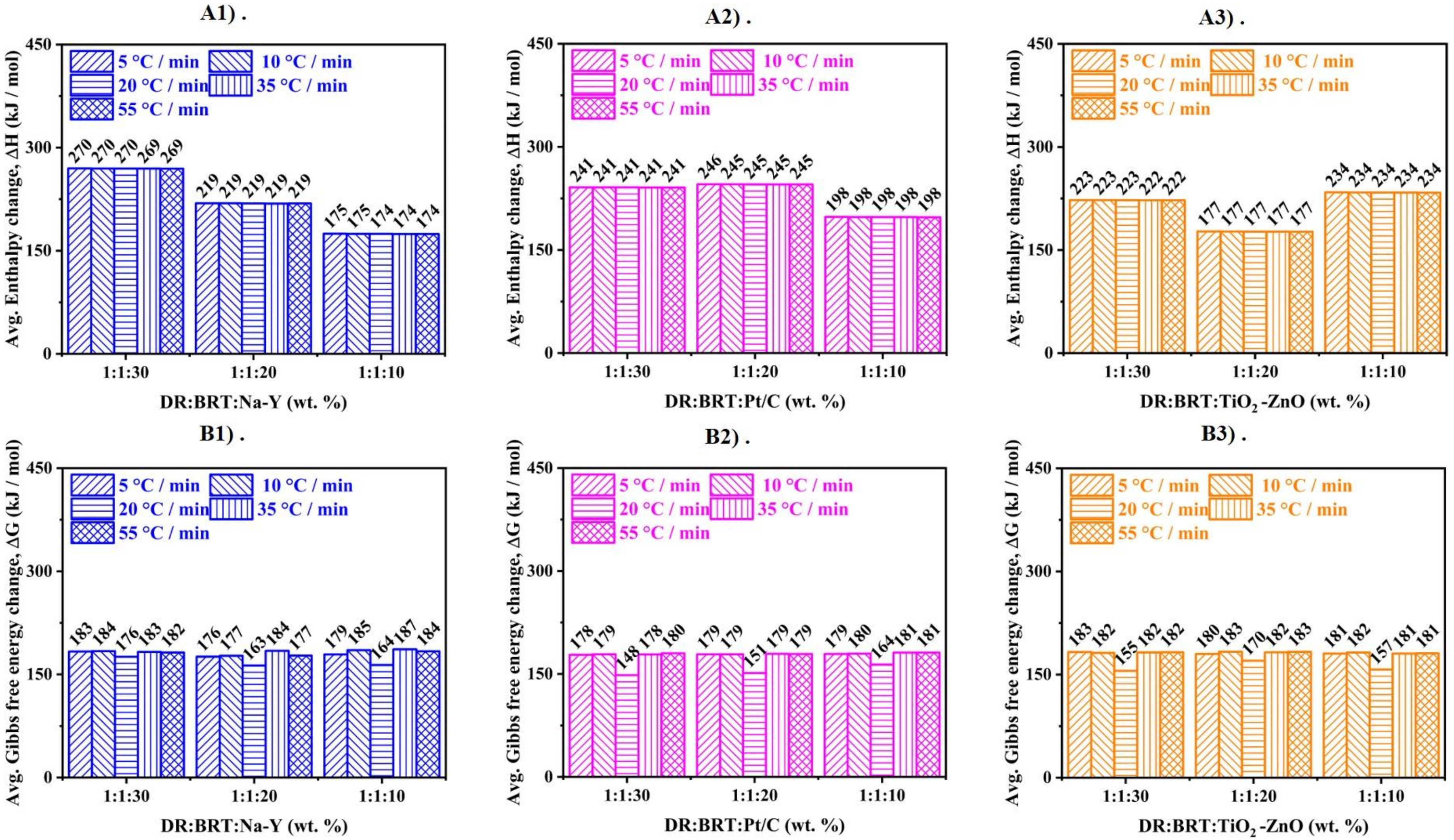

Figure 5.5.3 Variations in average thermodynamic properties of co-pyrolysis of *Delonix Regia* (DR) biomass and butyl rubber tube (BRT) waste for various catalysts: **A1), A2),** and **A3)** for enthalpy change (kJ / mol), **B1), B2),** and **B3)** for change in Gibbs free energy (kJ / mol) at the OFW methodology.

5.5.4 Indices of thermal performance for pyro–catalytic co–pyrolysis of DR and BRT

Table 5.5.4 displays the indices of thermal performance (ITP) of the PCCP of DR and BRT co–feed at all three (zeolite (Na–Y), noble metal on activated carbon (10 wt. % Pt/C), and metal oxide (1:1 wt. % of TiO_2–ZnO)) catalysts between 30 to 10 wt. % dosage. From the results, it was found that the for all three catalysts, the ITP (C, D_i, D_b, S, and D_v) values were increased with an increased heating rate between 5 – 55 °C / min [51]. However, the Na – Y (10 wt. %) shows the lowest ITP values compared to the other two catalysts. This could be due to the Na-Y catalyst's higher surface area and thermal stability [140]. The maximum index of flammability ($C = 8.61\times 10^{-5}$), indicated the higher heating value and lesser moisture level. The maximum indices of ignition ($D_i = 855.54 \times 10^{-3}$), and burnout ($D_b = 4181.50 \times 10^{-5}$), attributed to greater combustion ability. The maximum index of combustion ($S = 25.01 \times 10^{-8}$), shows the high performance of combustion characteristics. The maximum index of devolatilization ($D_v = 41.30 \times 10^{-8}$), implies that a large amount of volatile matter was liberated during the pyro–catalytic co–pyrolysis (PCCP) of DR and BRT.

Table 5.5.4 Indices of pyrolysis performance for various catalytic co-pyrolysis of *Delonix Regia* (DR) biomass and Butyl rubber tube (BRT) waste

β	DR:BRT:Na-Y (1:1:30 wt.%)					DR:BRT:Na-Y (1:1:20 wt.%)					DR:BRT:Na-Y (1:1:10 wt.%)				
	$C \times 10^{-5}$	$D_i \times 10^{-3}$	$D_b \times 10^{-5}$	$S \times 10^{-8}$	$D_v \times 10^{-8}$	$C \times 10^{-5}$	$D_i \times 10^{-3}$	$D_b \times 10^{-5}$	$S \times 10^{-8}$	$D_v \times 10^{-8}$	$C \times 10^{-5}$	$D_i \times 10^{-3}$	$D_b \times 10^{-5}$	$S \times 10^{-8}$	$D_v \times 10^{-8}$
5	0.71	0.66	0.27	0.15	0.27	0.71	0.68	0.31	0.16	0.31	0.84	0.85	0.33	0.41	0.41
10	1.19	4.19	3.82	0.53	0.97	1.19	4.81	4.27	0.54	1.01	1.90	6.89	5.18	0..99	1.66
20	2.21	30.37	54.87	2.09	3.81	2.21	34.82	65.81	2.26	4.08	3.28	46.15	78.95	3.46	5.88
35	4.09	165.58	550.03	6.52	11.19	4.09	192.06	608.23	7.93	13.29	6.58	264.79	828.28	12.25	18.26
55	6.19	609.03	3185.7	15.93	27.26	6.19	728.32	3712.25	18.87	32.82	8.61	855.54	4181.50	25.01	41.30
	DR:BRT:Pt/C (1:1:30 wt.%)					DR:BRT:Pt/C (1:1:20 wt.%)					DR:BRT:Pt/C (1:1:10 wt.%)				
5	0.75	0.74	0.3	0.17	0.32	0.82	0.81	0.32	0.21	0.36	1.06	1.06	0.39	0.29	0.53
10	1.51	5.65	4.66	0.68	1.2	1.82	6.86	5.61	0.92	1.61	2.09	7.95	5.91	1.11	1.87
20	3.01	43.37	74.08	2.75	4.7	3.34	48.63	81.27	3.28	5.52	3.93	56.75	90.28	4.26	71.85
35	5.1	219.13	658.85	8.26	13.72	6.14	260.86	747.53	10.99	18.69	6.82	289.99	782.03	12.91	20.94
55	7.86	795.52	3868.1	20.26	33.02	8.65	885.47	4131.51	24.11	40.67	10.21	1043.21	4512.31	30.31	48.85
	DR:BRT:TiO_2-ZnO (1:1:30 wt.%)					DR:BRT:TiO_2-ZnO (1:1:20 wt.%)					DR:BRT:TiO_2-ZnO (1:1:10 wt.%)				
5	1.01	0.98	0.35	0.25	0.42	0.98	0.98	0.36	0.24	0.44	1.09	1.07	0.37	0.29	0.5
10	1.77	6.57	4.99	0.84	1.43	1.94	7.17	5.38	0.92	1.54	2.14	7.89	5.78	1.12	1.87
20	3.55	50.36	77.39	3.63	5.92	3.79	53.7	84.55	3.97	6.47	4.78	103.62	213.14	6.48	10.51
35	5.98	249.77	661.93	10.25	16.58	6.13	257.12	746.53	11.45	19.01	6.45	271.41	777.42	12.25	20.22
55	8.99	898.44	3829.9	25.11	40.75	9.21	923.03	4120.2	27.1	44.53	9.97	1010.5	4478.9	30.01	49.62

5.5.5 Summary and Comparative analysis with existing work

A summary of objective 5 and the comparative analysis with existing work (**Table 5.5.5**) was discussed below.

Summary of objective 5.

The following statements were obtained from objective 5:

- The thermal degradation behavior of pyro-catalytic co-pyrolysis (PCCP) of *Delonix regia* (DR) biomass and butyl rubber tube (BRT) co-feed (1:1) was evaluated in the presence of three different catalysts such as Na-Y zeolite, Pt/C, and TiO_2-ZnO (1:1 wt.%) correspondingly.
- A thermal degradation study shows a mass loss of 53 – 51 wt. %, 58 – 56 wt. %, and 62 – 60 wt. % for 30, 20, and 10 wt. % of Na–Y; 63 – 60 wt. %, and 64 – 59 wt. % for 30, 20, and 10 wt. % of Pt/C; and 54 – 50 wt. %, 56 – 55 wt. %, and 63 – 62 wt. % for 30, 20, and 10 wt. % of TiO_2–ZnO, correspondingly, were ascertained at 5-55 °C/min.
- Kinetic modeling results computed the lowest average activation energy of 182 kJ/mol by the Ozawa-Flynn-Wall method for Na-Y zeolite of 10 wt.% dosages.
- Variations of the reaction mechanism with conversion (0.1-0.7) were illustrated by Criado's method for the PCCP of DR and BRT.
- Thermodynamic insights reported the $\Delta H \approx 175$ kJ/mol and $\Delta G \approx 178$ kJ/mol by the Ozawa-Flynn-Wall method implied the endothermic and non-spontaneity of PCCP of DR and BRT for Na-Y zeolite of 10 wt.% dosages.
- Finally, the indices of pyrolysis performance for PCCP of DR and BRT were explained.

Table 5.5.5: Comparative analysis of In – situ catalytic co-pyrolysis of DR and BRT (1:1 wt. %) wastes

S.No.	Raw materials	Catalyst	TGA model	Operating conditions			Results		References
	Feed and co-feed	(wt. %)		°C	Q	β	*Kinetics	*Thermodynamics	
42	Rural solid waste* : microalgae (chlorella vulgaris) (1:1)	MgO (1.57%)	Mettler Toledo TGA/DSC 1	50 – 800	N_2 – 80	20, 30, 40	$E_{\alpha=0.1\text{-}0.80}$: 221 and 223 for OFW and KAS	-	[49]
43	Rural solid waste* : microalgae (chlorella vulgaris) (1:1)	HZSM-5 (4.89%)	Mettler Toledo TGA/DSC 1	50 – 800	N_2 – 80	20, 30, 40	$E_{\alpha=0.1\text{-}0.80}$: 225 and 223 for OFW and KAS	-	[49]
45	Wettorrified bamboo: Linear low-density polyethylene (1:1)	HZSM – 5	Netsch TG209F1	30 – 800	N_2 – 20	5, 10, 20, 40	$E_{\alpha=0.1\text{-}0.80}$: 135, 137, 135, by KAS, OFW, DFM	-	[58]
47	*Delonix Regia*: Butyl rubber tube waste (1:1)	Na-Y zeolite	Netsch TG209F1	25 – 1000	N_2 – 40	5, 10, 20, 35, 55	$E_{\alpha=0.1\text{-}0.7}$ and k_o: 199 and 3.03×10^{24}, 179 and 1.68×10^{19}, 180 and 5.95×10^{16}, 179 and	$E_{\alpha=0.1\text{-}0.80}$: ΔH: 175, and ΔG: 179	Objective 5

		(30, 20, 10 wt.%)					1.34×10^{19}, 179 and 1.39×10^{19} by DFM, KAS, OFW, STK, DAE at 10 wt.% Na-Y		
48	*Delonix Regia*: Butyl rubber tube waste (1:1)	Pt/C (30, 20, 10 wt.%)	Netsch TG209F1	25 – 1000	N_2 – 40	5, 10, 20, 35, 55	$E_{\alpha=0.1\text{-}0.7}$ and k_o: 220 and 9.80×10^{24}, 203 and 4.22×10^{20}, 203 and 1.31×10^{18}, 204 and 3.35×10^{20}, 203 and 3.50×10^{20} by DFM, KAS, OFW, STK, DAE	$E_{\alpha=0.1\text{-}0.80}$: ΔH: 198, and ΔG: 179	Objective 5
49	*Delonix Regia*: Butyl rubber tube waste (1:1)	TiO_2-ZnO (1:1) (30, 20, 10 wt.%)	Netsch TG209F1	25 – 1000	N_2 – 40	5, 10, 20, 35, 55	$E_{\alpha=0.1\text{-}0.7}$ and k_o: 195 and 2.21×10^{21}, 181 and 1.89×10^{17}, 182 and 8.11×10^{14}, 182 and 1.52×10^{17}, 181 and 1.59×10^{17} by DFM, KAS, OFW, STK, DAE at 20 wt.% TiO_2-ZnO	$E_{\alpha=0.1\text{-}0.80}$: ΔH: 177, and ΔG: 180	Objective 5
Rural solid waste* – (kitchen waste 61%, plastic and rubber 16%, paper 12%, textiles 4% and leaves 3%)									

β – Heating rates (°C min^{-1})

α – Conversion

°C – Temperature

Q – Flowrate of carrier gas (mL min^{-1})

Iso – conversional models – Differential Friedman (DFM), Kissinger-Akahira-Sunose (KAS), Ozawa-Flynn-Wall (OFW), Starink (STK), and Distributed Activation Energy (DAE)

*Kinetics – Average values

*Thermodynamics – Average values based on the DFM model at 10 °C min^{-1}

E_α – Activation energy (kJ mol^{-1})

k_o – Frequency factor (s^{-1})

ΔH – Change in enthalpy (kJ mol^{-1})

ΔG – Change in Gibbs free energy (kJ mol^{-1})

ΔS – Change in entropy (kJ mol^{-1} K^{-1})

5.6 Summary of the chapter V.

The following statements were obtained from the chapter V:

- The findings of the physicochemical characterization, thermal degradation behavior, assessment of kinetic triplets, thermodynamic parameters, and pyrolysis performance indices of the non-catalytic pyrolysis of DR biomass were described.
- The results of the non-catalytic pyrolysis of BRT waste were given, along with the physicochemical characterization, behavior of thermal degradation, estimation of kinetics and thermodynamics, and pyrolysis performance characteristics.
- The outcomes of the non-catalytic co-pyrolysis of DR and BRT mixture, such as thermogravimetric analysis, kinetic values, reaction mechanism, thermodynamic properties, and thermal performance indices, were reported.
- In-situ catalytic decomposition of DR biomass results including thermal stability characteristics, kinetic triplets, thermodynamic investigation, and indices of pyrolysis performance, was studied.
- Finally, the PCCP of DR and BRT feedstock findings, such as thermal degradation, kinetic modeling, thermodynamic insights, and indices of thermal performance, were evaluated.

CHAPTER VI

CONCLUSIONS AND FUTURE SCOPE

6.1 Conclusions

6.1.1 Insights on kinetic triplets and thermodynamic analysis of *Delonix Regia* biomass

The temperature ranges of 155–714 °C have provided a maximum mass loss (about 64.4%) for *Delonix Regia* biomass. Activation energy recorded from DFM, KAS, OFW, STK, and DAE was 202.34–205.89 kJ mol^{-1}. Among all iso-conversional methods, the DFM (202.34 kJ mol^{-1}) was in proximity to the OFW (204.87 kJ mol^{-1}). The pre-exponential factor varied between 4.98×10^{17}–2.04×10^{20} s^{-1}, indicating that pyrolysis occurred at a higher reaction rate. Furthermore, a 5 kJ mol^{-1} difference was observed between the average values of E_α and ΔH.

6.1.2 Kinetics and thermodynamics investigation of pyrolysis of butyl rubber tube waste

Temperatures between 150 and 768 °C result in the highest mass loss (about 60.5 %) for Butyl rubber tube (BRT) waste. The activation energy of DFM, KAS, OFW, STK, and DAE was estimated to be between 222.67 and 244.73 kJ mol^{-1}. Among all approaches, the OFW (222.67 kJ mol^{-1}) propinquity to the KAS (223.37 kJ mol^{-1}). The pre-exponential factor varied between 6.82×10^{21} and 2.73×10^{24} s^{-}1, demonstrating a higher reaction rate of Butyl rubber tube (BRT) waste during pyrolysis. Additionally, a variation of 5 kJ mol^{-1} was found between the average E_α and ΔH values.

6.1.3 Reaction kinetics and thermodynamic analysis of non-isothermal co-pyrolysis of *Delonix Regia* and tube waste

OFW method indicated the lowest activation energy, E_α (207.78. kJ mol^{-1}), amongst all five methods applied. Average E_α (kJ mol^{-1}) and frequency factor, k_o (min^{-1}) values calculated by DFM, KAS, OFW, STK, and DAEM models were 230.47 and 2.55×10^{30}; 208.13 and 8.31×10^{26}; 207.78 and 1.58×10^{24}; 208.38 and 6.47×10^{26}; 208.13 and 5.15×10^{26}; respectively. Average ΔH (kJ mol^{-1}) and ΔG (kJ mol^{-1}) values were 225.38, 179.9; 225.28, 180.22; 225.18, 180.31; 225.08, 180.99; and 224.98, 182.15 respectively. Furthermore, it was observed that thermal performance indices also increased as heating rates increased.

6.1.4 In–situ pyro–catalytic decomposition of *Delonix Regia* biomass: Kinetic triplets and thermodynamic Investigation

PCD of DR biomass occurred with a major weight loss of 53 – 51 wt. %, 58 – 56 wt. %, and 62 – 60 wt. % for 30, 20, and 10 wt. % of Na–Y; 63 – 60 wt. %, and 64 – 59 wt. % for 30, 20, and 10 wt. % of Pt/C; and 54 – 50 wt. %, 56 – 55 wt. %, and 63 – 62 wt. % for 30, 20, and 10 wt. % of TiO_2–ZnO, respectively, were ascertained at 5-55 °C/min. From kinetic triplets, the KAS technique at DR:Na–Y (1:10 wt. %) yielded the lowest average E_α (kJ mol^{-1}) and k_o (min^{-1}) values of 181.29 and 2.10 E+16. Furthermore, Criado's confirmed the reaction pathway as second order (F2), power-law (P4), contraction area (R2), zero order (F0), contraction volume (R3), and fourth order (F4) at 20 °C min^{-1} for DFM technique at DR:Na–Y (1:10 wt. %). From thermodynamic investigation, 5 kJ mol^{-1} discrepancy between E_α and ΔH was noticed from the DFM technique

6.1.5 Pyro–catalytic co–pyrolysis of *Delonix Regia* and butyl rubber tube: Kinetic modeling and thermodynamic insights

The target of the proposed work was to compute the kinetic modeling (KM) and thermodynamic insights (TI) for the pyro-catalytic co-pyrolysis (PCCP) of *Delonix Regia* (DR) and Butyl rubber tube (BRT). For PCCP of DR and BRT (1:1 co-feed), three different types of catalysts were utilized: zeolite (Na–Y), noble metal on activated carbon (10 wt. % Pt/C), and bi–metal oxide (1:1 wt. % TiO_2–ZnO) of loading between 30 – 10 wt. %. For computing KM and TI, several iso-conversional models were Differential Friedman (DFM), Ozawa–Flynn–Wall (OFW), Kissinger–Akahira–Sunose (KAS), Starink (STK), and Distributed Activation Energy (DAE) were applied. At DR:BRT:Na-Y (1:1:10 wt. %), the OFW model ascertained the lowest average values of activation energy E_α (kJ / mol) and pre-exponential factor k_o (s^{-1}) as 180 and 5.95E+16, respectively whereas ΔH (kJ / mol) and ΔG (kJ / mol) as 175 and 180 for TI correspondingly.

6.2 Future scope

- Numerous heterogeneous catalysts, including zeolites and metal oxides, can be utilized to pyrolyze *Delonix Regia* biomass, butyl rubber tube waste, and its co-feed mixture.
- More Iso-conversional models must be developed, and more effort is needed to standardize the domain of solid-state kinetics analytically, computationally, and theoretically.
- The current investigation could be expanded to include a broader range of solid waste materials (biomass and polymer wastes) in order to ascertain the kinetic and thermodynamic behaviors.
- Additionally, Py-GC/MS and Py-FTIR can be employed to study the product distributions from analytical pyrolysis
- Computational fluid dynamic (CFD) simulation studies would provide new dimensions to the findings of current experimental research work.

6.3 Summary of the chapter VI.

In this chapter VI, the significant findings of each objective were described first, followed by a discussion of the future scope of the thesis.

References

[1] A. O. Balogun, P. P. I. , AdekunleA.Adeleke, S. O.Adegoke, and A. M. A. & A. McDonald, “Kinetics modeling thermodynamic and thermal performance assessments of pyrolytic decomposition of husk and DR pod.” Nature, pp. 1–12, 2021, doi: 10.1038/s41598-021-93407-1.

[2] R. kumar Mishra and K. Mohanty, “Kinetic analysis and pyrolysis behavior of low-value waste lignocellulosic biomass for its bioenergy potential using thermogravimetric analyzer,” *Materials Science for Energy Technologies*, vol. 4, pp. 136–147, 2021, doi: 10.1016/j.mset.2021.03.003.

[3] E. F. Gilman, D. G. Wastson, R. W. Klein, A. K. Koeser, D. R. Hilbert, and D. C. McLean, “Delonix regia : Royal poincian,” 2019. doi: edis.ifas.ufl.edu/pdf/ST/ST22800.pdf.

[4] O. Hook raf, “Delonix regia,” 2009. doi: apps.worldagroforestry.org/treedb2/AFTPDFS/Delonix_regia.PDF.

[5] H. D. Kawale and N. Kishore, “Thermochemical putrefaction of Delonix regia biomass and tube waste to produce high-quality pyrolytic bio-oil,” *Journal of Thermal Analysis and Calorimetry*, no. 0123456789, 2021, doi: 10.1007/s10973-021-10725-2.

[6] H. D. Kawale and N. Kishore, “Comparative study on pyrolysis of Delonix Regia, Pinewood sawdust and their co-feed for plausible bio-fuels production,” *Energy*, vol. 203, p. 117921, 2020, doi: 10.1016/j.energy.2020.117921.

[7] D. Bourguignon, “Biomass for electricity and heating. Opportunities and challenges. European Parliamentary Research Service.,” 2015, no. September, pp. 1–8, doi: www.europarl.europa.eu/RegData/etudes/BRIE/2015/568329/EPRS_BRI(2015)568329_EN.pdf.

[8] N. Tripathi, C. D. Hills, R. S. Singh, and C. J. Atkinson, “Biomass waste utilisation in low-carbon products: harnessing a major potential resource,” *npj Climate and Atmospheric Science*, vol. 2, no. 1, 2019, doi: 10.1038/s41612-019-0093-5.

[9] EPA, “Advancing Sustainable Materials Management: 2018 Fact Sheet,” United Sates, 2020. doi: www.epa.gov/sites/default/files/2021-01/documents/2018_ff_fact_sheet_dec_2020_fnl_508.pdf.

[10] P. T. Williams, “Pyrolysis of waste tyres: A review,” *Waste Management*, vol. 33, no. 8, pp. 1714–1728, 2013, doi: 10.1016/j.wasman.2013.05.003.

[11] K. Shimada, R. Ikeda, H. Kikura, and H. Takahashi, “Enhancement of diversity in production and application utilizing electrolytically polymerized rubber sensors with MCF: 1st report on consummate fabrication combining varied kinds of constituents with porous permeant stocking-like rubber,” *Sensors*, vol. 20, no. 17, pp. 1–26, 2020, doi: 10.3390/s20174658.

[12] D. Armada *et al.*, “Global evaluation of the chemical hazard of recycled tire crumb rubber employed on worldwide synthetic turf football pitches,” *Science of the Total Environment*, vol. 812, p. 152542, 2022, doi: 10.1016/j.scitotenv.2021.152542.

[13] J. Xu *et al.*, “High-value utilization of waste tires: A review with focus on modified carbon black from pyrolysis,” *Science of the Total Environment*, vol. 742, p. 140235, 2020, doi: 10.1016/j.scitotenv.2020.140235.

[14] N. Nkosi, E. Muzenda, J. Gorimbo, and M. Belaid, “Developments in waste tyre thermochemical conversion processes: gasification, pyrolysis and liquefaction,” *RSC Advances*, vol. 11, no. 20, pp. 11844–11871, 2021, doi: 10.1039/d0ra08966d.

[15] A. R. Gamboa, A. M. A. Rocha, L. R. dos Santos, and J. A. de Carvalho, “Tire pyrolysis oil in Brazil: Potential production and quality of fuel,” *Renewable and Sustainable*

Energy Reviews, vol. 120, no. November, 2020, doi: 10.1016/j.rser.2019.109614.

[16] J. Nikiema and Z. Asiedu, “A review of the cost and effectiveness of solutions to address plastic pollution,” *Environmental Science and Pollution Research*, vol. 29, no. 17, pp. 24547–24573, 2022, doi: 10.1007/s11356-021-18038-5.

[17] M. Labaki and M. Jeguirim, “Thermochemical conversion of waste tyres—a review,” *Environmental Science and Pollution Research*, vol. 24, no. 11, pp. 9962–9992, 2017, doi: 10.1007/s11356-016-7780-0.

[18] M. A. Sibeko, A. O. Adeniji, O. O. Okoh, and S. P. Hlangothi, “Trends in the management of waste tyres and recent experimental approaches in the analysis of polycyclic aromatic hydrocarbons (PAHs) from rubber crumbs,” *Environmental Science and Pollution Research*, vol. 27, no. 35, pp. 43553–43568, 2020, doi: 10.1007/s11356-020-09703-2.

[19] M. S. Mettler, D. G. Vlachos, and P. J. Dauenhauer, “Top ten fundamental challenges of biomass pyrolysis for biofuels,” *Energy and Environmental Science*, vol. 5, no. 7, pp. 7797–7809, 2012, doi: 10.1039/c2ee21679e.

[20] B. B. Uzoejinwa, X. He, S. Wang, A. El-Fatah Abomohra, Y. Hu, and Q. Wang, “Co-pyrolysis of biomass and waste plastics as a thermochemical conversion technology for high-grade biofuel production: Recent progress and future directions elsewhere worldwide,” *Energy Conversion and Management*, vol. 163, no. December 2017, pp. 468–492, 2018, doi: 10.1016/j.enconman.2018.02.004.

[21] T. M. H. Dabros *et al.*, “Transportation fuels from biomass fast pyrolysis, catalytic hydrodeoxygenation, and catalytic fast hydropyrolysis,” *Progress in Energy and Combustion Science*, vol. 68, pp. 268–309, 2018, doi: 10.1016/j.pecs.2018.05.002.

[22] R. W. Jenkins, A. D. Sutton, and D. J. Robichaud, *Pyrolysis of Biomass for Aviation*

Fuel. Elsevier Inc., 2016.

[23] Y. W. Huang, M. Q. Chen, and Y. Li, “An innovative evaluation method for kinetic parameters in distributed activation energy model and its application in thermochemical process of solid fuels,” *Thermochimica Acta*, vol. 655. pp. 42–51, 2017, doi: 10.1016/j.tca.2017.06.009.

[24] T. K. Vo *et al.*, “Pyrolysis characteristics and kinetics of microalgal Aurantiochytrium sp. KRS101,” *Energy*, vol. 118, pp. 369–376, 2017, doi: 10.1016/j.energy.2016.12.040.

[25] A. Pandey, B. Thallada, S. Michael, and S. Rajeev Kumar, *Recent Advances in Thermo-Chemical Conversion of Biomass*. Elsevier, 2015.

[26] S. Vyazovkin, A. K. Burnham, J. M. Criado, L. A. Pérez-Maqueda, C. Popescu, and N. Sbirrazzuoli, “ICTAC Kinetics Committee recommendations for performing kinetic computations on thermal analysis data,” *Thermochimica Acta*, vol. 520, no. 1–2, pp. 1–19, 2011, doi: 10.1016/j.tca.2011.03.034.

[27] Q. He, L. Ding, Y. Gong, W. Li, J. Wei, and G. Yu, “Effect of torrefaction on pinewood pyrolysis kinetics and thermal behavior using thermogravimetric analysis,” *Bioresource Technology*, vol. 280, no. January, pp. 104–111, 2019, doi: 10.1016/j.biortech.2019.01.138.

[28] C. N. Arenas, M. V. Navarro, and J. D. Martínez, “Pyrolysis kinetics of biomass wastes using isoconversional methods and the distributed activation energy model,” *Bioresource Technology*, vol. 288, no. May, p. 121485, 2019, doi: 10.1016/j.biortech.2019.121485.

[29] H. D. Kawale and N. Kishore, “Comprehensive study on thermochemical putrefaction of Delonix Regia in non-catalytic, catalytic and hydro-catalytic pyrolysis atmospheres,” *Renewable Energy*, vol. 173. pp. 223–236, 2021, doi: 10.1016/j.renene.2021.03.139.

[30] Y. Xue, A. Kelkar, and X. Bai, "Catalytic co-pyrolysis of biomass and polyethylene in a tandem micropyrolyzer," *Fuel*, vol. 166, pp. 227–236, 2015, doi: 10.1016/j.fuel.2015.10.125.

[31] H. D. Kawale and N. Kishore, "Production of hydrocarbons from a green algae (Oscillatoria)with exploration of its fuel characteristics over different reaction atmospheres," *Energy*, vol. 178, pp. 344–355, 2019, doi: 10.1016/j.energy.2019.04.103.

[32] R. Miandad *et al.*, "Catalytic pyrolysis of plastic waste: Moving toward pyrolysis based biorefineries," *Frontiers in Energy Research*, vol. 7, no. MAR, pp. 1–17, 2019, doi: 10.3389/fenrg.2019.00027.

[33] E. O. Ajala, J. O. Ighalo, M. A. Ajala, A. G. Adeniyi, and A. M. Ayanshola, "Sugarcane bagasse: a biomass sufficiently applied for improving global energy, environment and economic sustainability," *Bioresources and Bioprocessing*, vol. 8, no. 1, 2021, doi: 10.1186/s40643-021-00440-z.

[34] Y. Li, D. Yellezuome, R. Liu, J. Cai, and Y. Gao, "Investigation of product selectivity and kinetics of poplar sawdust catalytic pyrolysis over bi-metallic Iron-Nickel/ZSM-5 catalyst," *Bioresource Technology*, vol. 349, no. January, p. 126838, 2022, doi: 10.1016/j.biortech.2022.126838.

[35] S. Gupta and P. Mondal, "Catalytic pyrolysis of pine needles with nickel doped gamma-alumina: Reaction kinetics, mechanism, thermodynamics and products analysis," *Journal of Cleaner Production*, vol. 286. 2021, doi: 10.1016/j.jclepro.2020.124930.

[36] D. V. Suriapparao, R. Gautam, and L. Rao Jeeru, "Analysis of pyrolysis index and reaction mechanism in microwave-assisted ex-situ catalytic co-pyrolysis of agro-residual and plastic wastes," *Bioresource Technology*, vol. 357, no. April, 2022, doi: 10.1016/j.biortech.2022.127357.

[37] A. A. Adeleke, J. K. Odusote, P. P. Ikubanni, O. A. Lasode, M. Malathi, and D. Paswan, “The ignitability, fuel ratio and ash fusion temperatures of torrefied woody biomass,” *Heliyon*, vol. 6, no. 3, p. e03582, 2020, doi: 10.1016/j.heliyon.2020.e03582.

[38] L. Dai *et al.*, “Microwave-assisted catalytic fast co-pyrolysis of soapstock and waste tire for bio-oil production,” *Journal of Analytical and Applied Pyrolysis*, vol. 125, pp. 304–309, 2017, doi: 10.1016/j.jaap.2017.03.012.

[39] A. O. Balogun, A. A. Adeleke, P. P. Ikubanni, S. O. Adegoke, A. M. Alayat, and A. G. Mcdonald, “Kinetics modeling , thermodynamics and thermal performance assessments of pyrolytic decomposition of Moringa oleifera husk and Delonix regia pod,” Nature, 2021. doi: 10.1038/s41598-021-93407-1.

[40] S. Xu *et al.*, “Synergistic effects of catalytic co-pyrolysis of macroalgae with waste plastics,” *Process Safety and Environmental Protection*, vol. 137, pp. 34–48, 2020, doi: 10.1016/j.psep.2020.02.001.

[41] S. Singh, T. Patil, S. P. Tekade, M. B. Gawande, and A. N. Sawarkar, “Studies on individual pyrolysis and co-pyrolysis of corn cob and polyethylene: Thermal degradation behavior, possible synergism, kinetics, and thermodynamic analysis,” *Science of the Total Environment*, vol. 783, p. 147004, 2021, doi: 10.1016/j.scitotenv.2021.147004.

[42] T. Rasool, I. Najar, V. C. Srivastava, and A. Pandey, “Pyrolysis of almond (Prunus amygdalus) shells: Kinetic analysis, modeling, energy assessment and technical feasibility studies,” *Bioresource Technology*, vol. 337, no. June, p. 125466, 2021, doi: 10.1016/j.biortech.2021.125466.

[43] J. Wang *et al.*, “Understanding pyrolysis mechanisms of pinewood sawdust and sugarcane bagasse from kinetics and thermodynamics,” *Industrial Crops and Products*,

vol. 177, no. August 2021, p. 114378, 2022, doi: 10.1016/j.indcrop.2021.114378.

[44] B. Danon, N. M. Mkhize, P. Van Der Gryp, and J. F. Görgens, "Combined model-free and model-based devolatilisation kinetics of tyre rubbers," *Thermochimica Acta*, vol. 601, pp. 45–53, 2015, doi: 10.1016/j.tca.2014.12.003.

[45] G. Singh, A. K. Varma, S. Almas, A. Jana, P. Mondal, and J. Seay, "Pyrolysis kinetic study of waste milk packets using thermogravimetric analysis and product characterization," *Journal of Material Cycles and Waste Management*, vol. 21, no. 6, pp. 1350–1360, 2019, doi: 10.1007/s10163-019-00891-9.

[46] M. Alam, D. Rammohan, A. Bhavanam, and N. R. Peela, "Wet torrefaction of bamboo saw dust and its co-pyrolysis with plastic," *Fuel*, vol. 285, no. July 2020, p. 119188, 2021, doi: 10.1016/j.fuel.2020.119188.

[47] W. Wang *et al.*, "Kinetic and thermodynamic analyses of co-pyrolysis of pine wood and polyethylene plastic based on Fraser-Suzuki deconvolution procedure," *Fuel*, vol. 322, no. March, p. 124200, 2022, doi: 10.1016/j.fuel.2022.124200.

[48] Q. H. Ng, B. L. F. Chin, S. Yusup, A. C. M. Loy, and K. Y. Y. Chong, "Modeling of the co-pyrolysis of rubber residual and HDPE waste using the distributed activation energy model (DAEM)," *Applied Thermal Engineering*, vol. 138, no. November 2017, pp. 336–345, 2018, doi: 10.1016/j.applthermaleng.2018.04.069.

[49] F. Tang, Z. Yu, Y. Li, L. Chen, and X. Ma, "Catalytic co-pyrolysis behaviors, product characteristics and kinetics of rural solid waste and chlorella vulgaris," *Bioresource Technology*, vol. 299, no. November 2019, p. 122636, 2020, doi: 10.1016/j.biortech.2019.122636.

[50] M. Alam, A. Bhavanam, A. Jana, J. kumar S. Viroja, and N. R. Peela, "Co-pyrolysis of bamboo sawdust and plastic: Synergistic effects and kinetics," *Renewable Energy*, vol.

149. pp. 1133–1145, 2020, doi: 10.1016/j.renene.2019.10.103.

[51] D. Rammohan, N. Kishore, and R. V. S. Uppaluri, “Reaction kinetics and thermodynamic analysis of non-isothermal co-pyrolysis of Delonix regia and tube waste,” *Bioresource Technology Reports*, vol. 18, no. January, p. 101032, 2022, doi: 10.1016/j.biteb.2022.101032.

[52] L. Wang, H. Lei, J. Liu, and Q. Bu, “Thermal decomposition behavior and kinetics for pyrolysis and catalytic pyrolysis of Douglas fir,” *RSC Advances*, vol. 8, no. 4, pp. 2196–2202, 2018, doi: 10.1039/c7ra12187c.

[53] D. K. Ratnasari, W. Yang, and P. G. Jönsson, “Kinetic study of an H-ZSM-5/Al-MCM-41 catalyst mixture and its application in lignocellulose biomass pyrolysis,” *Energy and Fuels*, vol. 33, no. 6. pp. 5360–5367, 2019, doi: 10.1021/acs.energyfuels.9b00866.

[54] A. K. Vuppaladadiyam *et al.*, “Thermal Characteristics and Kinetic Analysis of Woody Biomass Pyrolysis in the Presence of Bifunctional Alkali Metal Ceramics,” *ACS Sustainable Chemistry and Engineering*, vol. 7, no. 1, pp. 238–248, 2019, doi: 10.1021/acssuschemeng.8b02967.

[55] R. Made, A. Nyoman, Suprapta Winaya, Ghurri, and W. Ketut Gede, “Comprehensive kinetic study of pyrolysis of sunan candlenut: The effect of using iron oxide, zeolite and ZSM-5 as bed materials,” *International Journal of Heat and Technology*, vol. 39, no. 2, pp. 493–502, 2021, doi: 10.18280/ijht.390219.

[56] M. Alam, D. Rammohan, and N. R. Peela, “Catalytic co-pyrolysis of wet-torrefied bamboo sawdust and plastic over the zeolite H-ZSM-5: Synergistic effects and kinetics,” *Renewable Energy*, vol. 178, pp. 608–619, 2021, doi: 10.1016/j.renene.2021.06.109.

[57] D. Rammohan, N. Kishore, and R. V. S. Uppaluri, “Insights on Kinetic Triplets and Thermodynamic Analysis of Delonix Regia Biomass Pyrolysis,” *Bioresource*

Technology, vol. 358, no. May, p. 127375, 2022, doi: 10.1016/j.biortech.2022.127375.

[58] M. Alam, D. Rammohan, and N. R. Peela, “Catalytic co-pyrolysis of wet-torrefied bamboo sawdust and plastic over the zeolite H-zsm-5: Synergistic effects and kinetics,” *Renewable Energy*, vol. 178, pp. 608–619, 2021, doi: 10.1016/j.renene.2021.06.109.

[59] H. L. Friedman, “Kinetics of thermal degradation of char-forming plastics from thermogravimetry. Application to a phenolic plastic,” *Journal of Polymer Science Part C: Polymer Symposia*, vol. 6, no. 1, pp. 183–195, 1964, doi: 10.1002/polc.5070060121.

[60] T. Akahira and T. Sunnose, *Tans. Joint convection of four electrical institues*, vol. 16. 1971, pp. 22–31.

[61] T. Ozawa, “A New Method of Analyzing Thermogravimetric Data,” *Bulletin of the Chemical Society of Japan*, vol. 38, no. 11, pp. 1881–1886, 1965, doi: 10.1246/bcsj.38.1881.

[62] J. H. Flynn and L. A. Wall, “General Treatment of the Thermogravimetry of Polymers,” *Journal of Research of the National Bureau of Standards - A. Physics and Chemistry*, vol. 70A, no. 6, pp. 487–523, 1966, doi: 10.1080/00048407212341221.

[63] M. J. Starink, “The determination of activation energy from linear heating rate experiments: A comparison of the accuracy of isoconversion methods,” *Thermochimica Acta*, vol. 404, no. 1–2, pp. 163–176, 2003, doi: 10.1016/S0040-6031(03)00144-8.

[64] K. Miura and T. Maki, “A Simple Method for Estimating f(E) and k0(E) in the Distributed Activation Energy Model,” *Energy and Fuels*, no. 12, pp. 864–869, 1998, doi: pubs.acs.org/doi/pdf/10.1021/ef970212q.

[65] L. A. Perez-Maqueda, P. E. Sanchez-Jimenez, and J. M. Criado, “Kinetic Analysis of Solid-State Reactions: Precision of the Activation Energy Calculated by Integral Methods,” Wiley Inter Science, 2005. doi: 10.1002/kin.20115.

[66] C. D. Doyle, “Series Approximations to the equation of Thermogravimetric Data,” *Nature*, vol. 207, no. 4994, pp. 290–291, 1965, doi: 10.1038/207290a0.

[67] J. M. Criado, J. Málek, and A. Ortega, “Applicability of the master plots in kinetic analysis of non-isothermal data,” *Thermochimica Acta*, vol. 147, no. 2, pp. 377–385, 1989, doi: 10.1016/0040-6031(89)85192-5.

[68] A. Sahoo, R. Gautam, S. Kumar, and K. Mohanty, “Energy optimization from a binary mixture of non-edible oilseeds pyrolysis: Kinetic triplets analysis using Thermogravimetric Analyser and prediction modeling by Artificial Neural Network,” *Journal of Environmental Management*, vol. 297, no. July. Elsevier Ltd, p. 113253, 2021, doi: 10.1016/j.jenvman.2021.113253.

[69] D. Irmak Aslan, P. Parthasarathy, J. L. Goldfarb, and S. Ceylan, “Pyrolysis reaction models of waste tires: Application of Master-Plots method for energy conversion via devolatilization,” *Waste Management*, vol. 68, no. 2017, pp. 405–411, 2017, doi: 10.1016/j.wasman.2017.06.006.

[70] A. K. Galwey and M. E. Brown, “Application of the arrhenius equation to solid state kinetics: Can this be justified?,” *Thermochimica Acta*, vol. 386, no. 1, pp. 91–98, 2002, doi: 10.1016/S0040-6031(01)00769-9.

[71] B. L. Kirsch, E. K. Richman, A. E. Riley, and S. H. Tolbert, “In-situ x-ray diffraction study of the crystallization kinetics of mesoporous titania films,” *Journal of Physical Chemistry B*, vol. 108, no. 34, pp. 12698–12706, 2004, doi: 10.1021/jp036442p.

[72] A. R. Jones, R. Winter, P. Florian, and D. Massiot, “Tracing the reactive melting of glass-forming silicate batches by in situ23Na NMR,” *Journal of Physical Chemistry B*, vol. 109, no. 10, pp. 4324–4332, 2005, doi: 10.1021/jp045705s.

[73] M. Bertmer, R. C. Nieuwendaal, A. B. Barnes, and S. E. Hayes, “Solid-state

photodimerization kinetics of α-trans-cinnamic acid to α-truxillic acid studied via solid-state NMR," *Journal of Physical Chemistry B*, vol. 110, no. 12, pp. 6270–6273, 2006, doi: 10.1021/jp057417h.

[74] K. J. Laidler, "The development of the arrhenius equation," *Journal of Chemical Education*, vol. 61, no. 6, pp. 494–498, 1984, doi: 10.1021/ed061p494.

[75] L. A. Luzzi and H. V. Maulding, "Preparation and evaluation of the prolonged release properties of nylon microcapsules," *Journal of Pharmaceutical Sciences*, vol. 59, no. 3, pp. 338–341, 1970, doi: 10.1002/jps.2600590313.

[76] J. H. Flynn, "The 'temperature integral' - Its use and abuse," *Thermochimica Acta*, vol. 300, no. 1–2, pp. 83–92, 1997, doi: 10.1016/S0040-6031(97)00046-4.

[77] C. D. Doyle, "Estimating isothermal life from thermogravimetric data," *Journal of Applied Polymer Science*, vol. 6, no. 24, pp. 639–642, 1962, doi: 10.1002/app.1962.070062406.

[78] G. I. Senum and R. T. Yang, "Rational approximations of the integral of the Arrhenius function," *Journal of Thermal Analysis*, vol. 11, no. 3, pp. 445–447, 1977, doi: 10.1007/BF01903696.

[79] M. Maciejewski, "Computational aspects of kinetic analysis. Part B: The ICTAC Kinetics Project - The decomposition kinetics of calcium carbonate revisited, or some tips on survival in the kinetic minefield," *Thermochimica Acta*, vol. 355, no. 1–2, pp. 145–154, 2000, doi: 10.1016/S0040-6031(00)00444-5.

[80] S. Vyazovkin, "Computational aspects of kinetic analysis. Part C. The ICTAC Kinetics Project - The light at the end of the tunnel?," *Thermochimica Acta*, vol. 355, no. 1–2, pp. 155–163, 2000, doi: 10.1016/S0040-6031(00)00445-7.

[81] M. E. Brown *et al.*, "Computational aspects of kinetic analysis Part A: The ICTAC

Kinetics Project-data, methods and results," *Thermochimica Acta*, vol. 355, no. 1–2, pp. 125–143, 2000, doi: 10.1016/S0040-6031(00)00443-3.

[82] B. Roduit, "Computational aspects of kinetic analysis. Part E: The ICTAC Kinetics Project - Numerical techniques and kinetics of solid state processes," *Thermochimica Acta*, vol. 355, no. 1–2, pp. 171–180, 2000, doi: 10.1016/S0040-6031(00)00447-0.

[83] A. R. Salvador, E. G. Calvo, and V. M. Andres, "Kinetic analysis of thermogravimetric data. Reaction rate determination," *Thermochimica Acta*, vol. 78, no. 1–3, pp. 93–100, 1984, doi: 10.1016/0040-6031(84)87136-1.

[84] J. R. MacCallum and J. Tanner, "Interpretation of the kinetics of thermogravimetric analysis," *The Journal of Physical Chemistry*, vol. 73, no. 3, pp. 751–751, 1969, doi: 10.1021/j100723a050.

[85] A. W. Coats and J. P. Redfern, "Kinetic parameters from thermogravimetric data," *Polymer Letters*, vol. 3, pp. 917–920, 1965, doi: 10.1038/201068a0.

[86] H. E. Kissinger, "Variation of Peak Temperature With Heating Rate In Differential Thermal Analysis," *Journal 0 f Research of the National Bureau of Standards*, vol. 57, no. 4, p. 2712, 1956, doi: 10.1002/9781119959809.ch9.

[87] H. E. Kissinger, "Reaction Kinetics in Differential Thermal Analysis," *Analytical Chemistry*, vol. 29, no. 11, pp. 1702–1706, 1957, doi: 10.1021/ac60131a045.

[88] J. P. Elder, "The general applicability of the kissinger equation in thermal analysis," *Journal of Thermal Analysis*, vol. 30, pp. 657–669, 1985.

[89] C. A. W. Sergey Vyazovkin*, "Model-free and model-fitting approaches to kinetic analysis of isothermal and nonisothermal data," *Thermochimica Acta*, vol. 340–341, pp. 53–68, 1999.

[90] P. Šimon, “Isoconversional methods: Fundamentals, meaning and application,” *Journal of Thermal Analysis and Calorimetry*, vol. 76, no. 1, pp. 123–132, 2004, doi: 10.1023/B:JTAN.0000027811.80036.6c.

[91] J. Zsakó, “Kinetic analysis of thermogravimetric data, VI - Some problems of deriving kinetic parameters from TG curves,” *Journal of Thermal Analysis*, vol. 5, no. 2–3, pp. 239–251, 1973, doi: 10.1007/BF01950372.

[92] J. Zsakó, “Kinetic analysis of thermogravimetric data: XXIX. Remarks on the ‘many curves’ methods,” *Journal of Thermal Analysis*, vol. 46, no. 6, pp. 1845–1864, 1996, doi: 10.1007/BF01980788.

[93] A. Khawam and D. R. Flanagan, “Role of isoconversional methods in varying activation energies of solid-state kinetics: I. isothermal kinetic studies,” *Thermochimica Acta*, vol. 429, no. 1, pp. 93–102, 2005, doi: 10.1016/j.tca.2004.11.030.

[94] I. T. S. A.W. Coats, J.P .Redfern, “Kinetic Parameters from Thermogravimetric Data,” *Nature*, vol. 201, no. 4914, pp. 68–69, 1964.

[95] A. K. Burnham, “Global kinetic analysis of complex materials,” *Energy and Fuels*, vol. 13, no. 1, pp. 1–22, 1999, doi: 10.1021/ef9800765.

[96] M. S. Ahmad *et al.*, “Kinetic analyses and pyrolytic behavior of Para grass (Urochloa mutica) for its bioenergy potential,” *Bioresource Technology*, vol. 224, pp. 708–713, 2017, doi: 10.1016/j.biortech.2016.10.090.

[97] F. Nturanabo, G. Byamuisha, and G. Colonna Preti, “Performance appraisal of the casamance kiln as replacement to the traditional charcoal kilns in Uganda,” *Second International Conference on Advances in Engineering and Technology*. pp. 530–536, 2010.

[98] L. Li, J. S. Rowbotham, H. Christopher Greenwell, and P. W. Dyer, *An Introduction to*

Pyrolysis and Catalytic Pyrolysis: Versatile techniques for Biomass Conversion. Elsevier B.V., 2013.

[99] C. Di Blasi, “Modeling chemical and physical processes of wood and biomass pyrolysis,” *Progress in Energy and Combustion Science*, vol. 34, no. 1, pp. 47–90, 2008, doi: 10.1016/j.pecs.2006.12.001.

[100] R. K. Singh, D. Pandey, T. Patil, and A. N. Sawarkar, “Pyrolysis of banana leaves biomass: Physico-chemical characterization, thermal decomposition behavior, kinetic and thermodynamic analyses,” *Bioresource Technology*, vol. 310, no. April, p. 123464, 2020, doi: 10.1016/j.biortech.2020.123464.

[101] J. Komandur, R. Vinu, and K. Mohanty, “Pyrolysis kinetics and pyrolysate composition analysis of Mesua ferrea L: A non-edible oilseed towards the production of sustainable renewable fuel,” *Bioresource Technology*, vol. 351, no. March, p. 126987, 2022, doi: 10.1016/j.biortech.2022.126987.

[102] R. K. Gautam *et al.*, “Biochar for remediation of agrochemicals and synthetic organic dyes from environmental samples: A review,” *Chemosphere*, vol. 272, p. 129917, 2021, doi: 10.1016/j.chemosphere.2021.129917.

[103] R. Kaur, P. Gera, M. K. Jha, and T. Bhaskar, “Pyrolysis kinetics and thermodynamic parameters of castor (Ricinus communis) residue using thermogravimetric analysis,” *Bioresource Technology*, vol. 250, no. September 2017, pp. 422–428, 2018, doi: 10.1016/j.biortech.2017.11.077.

[104] Y. Xu and B. Chen, “Investigation of thermodynamic parameters in the pyrolysis conversion of biomass and manure to biochars using thermogravimetric analysis,” *Bioresource Technology*, vol. 146, pp. 485–493, 2013, doi: 10.1016/j.biortech.2013.07.086.

[105] X. Yuan, T. He, H. Cao, and Q. Yuan, “Cattle manure pyrolysis process: Kinetic and thermodynamic analysis with isoconversional methods,” *Renewable Energy*, vol. 107, pp. 489–496, 2017, doi: 10.1016/j.renene.2017.02.026.

[106] P. Singh, R. K. Singh, P. V. Gokul, S. U. Hasan, and A. N. Sawarkar, “Thermal degradation and pyrolysis kinetics of two Indian rice husk varieties using thermogravimetric analysis,” *Energy Sources, Part A: Recovery, Utilization and Environmental Effects*, pp. 1–12, 2020, doi: 10.1080/15567036.2020.1736215.

[107] G. D. Mumbach *et al.*, “Thermal investigation of plastic solid waste pyrolysis via the deconvolution technique using the asymmetric double sigmoidal function: Determination of the kinetic triplet, thermodynamic parameters, thermal lifetime and pyrolytic oil composition for clean,” *Energy Conversion and Management*, vol. 200, no. July, p. 112031, 2019, doi: 10.1016/j.enconman.2019.112031.

[108] V. Dhyani, J. Kumar, and T. Bhaskar, “Thermal decomposition kinetics of sorghum straw via thermogravimetric analysis,” *Bioresource Technology*, vol. 245, no. August, pp. 1122–1129, 2017, doi: 10.1016/j.biortech.2017.08.189.

[109] Z. Xu *et al.*, “Comparison of combustion and pyrolysis behavior of the peanut shells in air and N2: Kinetics, thermodynamics and gas emissions,” *Sustainability*, vol. 12, no. 2, 2020, doi: 10.3390/su12020464.

[110] V. Volli, A. R. K. Gollakota, and C. M. Shu, “Comparative studies on thermochemical behavior and kinetics of lignocellulosic biomass residues using TG-FTIR and Py-GC/MS,” *Science of the Total Environment*, vol. 792, p. 148392, 2021, doi: 10.1016/j.scitotenv.2021.148392.

[111] D. Pradhan and R. K. Singh, “Characterization of the Liquid Product Obtained by the Pyrolysis of a Bicycle Tube,” *Energy Sources, Part A: Recovery, Utilization and*

Environmental Effects, vol. 37, no. 19, pp. 2099–2106, 2015, doi: 10.1080/15567036.2011.608106.

[112] B. Khiari, S. Kordoghli, D. Mihoubi, F. Zagrouba, and M. Tazerout, “Modeling kinetics and transport phenomena during multi-stage tire wastes pyrolysis using Comsol,” *Waste Management*, vol. 78, pp. 337–345, 2018, doi: 10.1016/j.wasman.2018.06.002.

[113] S. Kordoghli, M. Paraschiv, R. Kuncser, M. Tazerout, and F. Zagrouba, “Catalysts’ influence on thermochemical decomposition of waste tires,” *Environmental Progress and Sustainable Energy*, vol. 36, no. 5, pp. 1560–1567, 2017, doi: 10.1002/ep.12605.

[114] S. Kordoghli, B. Khiari, M. Paraschiv, F. Zagrouba, and M. Tazerout, “Impact of different catalysis supported by oyster shells on the pyrolysis of tyre wastes in a single and a double fixed bed reactor,” *Waste Management*, vol. 67, pp. 288–297, 2017, doi: 10.1016/j.wasman.2017.06.001.

[115] B. Lah, D. Klinar, and B. Likozar, “Pyrolysis of natural, butadiene, styrene-butadiene rubber and tyre components: Modelling kinetics and transport phenomena at different heating rates and formulations,” *Chemical Engineering Science*, vol. 87, pp. 1–13, 2013, doi: 10.1016/j.ces.2012.10.003.

[116] M. G. Aboelkheir, L. Y. Visconte, G. E. Oliveira, R. D. Toledo Filho, and F. G. Souza, “The biodegradative effect of Tenebrio molitor Linnaeus larvae on vulcanized SBR and tire crumb,” *Science of the Total Environment*, vol. 649, pp. 1075–1082, 2019, doi: 10.1016/j.scitotenv.2018.08.228.

[117] F. Xu *et al.*, “TG-FTIR and Py-GC/MS study on pyrolysis mechanism and products distribution of waste bicycle tire,” *Energy Conversion and Management*, vol. 175, no. September, pp. 288–297, 2018, doi: 10.1016/j.enconman.2018.09.013.

[118] R. Peñalver *et al.*, “Assessing the level of airborne polystyrene microplastics using

thermogravimetry-mass spectrometry: Results for an agricultural area," *Science of the Total Environment*, vol. 787, p. 147656, 2021, doi: 10.1016/j.scitotenv.2021.147656.

[119] J. Han, W. Li, D. Liu, L. Qin, W. Chen, and F. Xing, "Pyrolysis characteristic and mechanism of waste tyre: A thermogravimetry-mass spectrometry analysis," *Journal of Analytical and Applied Pyrolysis*, vol. 129, no. December 2017, pp. 1–5, 2018, doi: 10.1016/j.jaap.2017.12.016.

[120] S. Maiti, S. Purakayastha, and B. Ghosh, "Thermal characterization of mustard straw and stalk in nitrogen at different heating rates," *Fuel*, vol. 86, no. 10–11, pp. 1513–1518, 2007, doi: 10.1016/j.fuel.2006.11.016.

[121] D. Irmak Aslan, P. Parthasarathy, J. L. Goldfarb, and S. Ceylan, "Pyrolysis reaction models of waste tires: Application of Master-Plots method for energy conversion via devolatilization," *Waste Management*, vol. 68, no. 2017, pp. 405–411, 2017, doi: 10.1016/j.wasman.2017.06.006.

[122] J. D. Martínez *et al.*, "Co-pyrolysis of biomass with waste tyres: Upgrading of liquid bio-fuel," *Fuel Processing Technology*, vol. 119, pp. 263–271, 2014, doi: 10.1016/j.fuproc.2013.11.015.

[123] S. Hu, A. Jess, and M. Xu, "Kinetic study of Chinese biomass slow pyrolysis: Comparison of different kinetic models," *Fuel*, vol. 86, no. 17–18, pp. 2778–2788, 2007, doi: 10.1016/j.fuel.2007.02.031.

[124] C. Buratti, M. Barbanera, P. Bartocci, and F. Fantozzi, "Thermogravimetric analysis of the behavior of sub-bituminous coal and cellulosic ethanol residue during co-combustion," *Bioresource Technology*, vol. 186, pp. 154–162, 2015, doi: 10.1016/j.biortech.2015.03.041.

[125] A. Khawam and D. R. Flanagan, "Solid-state kinetic models: Basics and mathematical

fundamentals," *Journal of Physical Chemistry B*, vol. 110, no. 35, pp. 17315–17328, 2006, doi: 10.1021/jp062746a.

[126] L. A. Pérez-Maqueda, A. Ortega, and J. M. Criado, "The use of master plots for discriminating the kinetic model of solid state reactions from a single constant-rate thermal analysis (CRTA) experiment," *Thermochimica Acta*, vol. 277, no. 1–2. pp. 165–173, 1996, doi: 10.1016/0040-6031(95)02746-7.

[127] R. Chen, Q. Li, X. Xu, D. Zhang, and R. Hao, "Combustion characteristics, kinetics and thermodynamics of Pinus Sylvestris pine needle via non-isothermal thermogravimetry coupled with model-free and model-fitting methods," *Case Studies in Thermal Engineering*, vol. 22. 2020, doi: 10.1016/j.csite.2020.100756.

[128] M. S. Ahmad *et al.*, "Pyrolysis, kinetics analysis, thermodynamics parameters and reaction mechanism of Typha latifolia to evaluate its bioenergy potential," *Bioresource Technology*, vol. 245, no. July, pp. 491–501, 2017, doi: 10.1016/j.biortech.2017.08.162.

[129] K. Lazdovica, L. Liepina, and V. Kampars, "Catalytic pyrolysis of wheat bran for hydrocarbons production in the presence of zeolites and noble-metals by using TGA-FTIR method," *Bioresource Technology*, vol. 207, pp. 126–133, 2016, doi: 10.1016/j.biortech.2016.01.117.

[130] D. Rammohan, N. Kishore, and R. V. S. Uppaluri, "Insights on kinetic triplets and thermodynamic analysis of Delonix regia biomass pyrolysis," *Bioresource Technology*, vol. 358, no. March, p. 127375, 2022, doi: 10.1016/j.biortech.2022.127375.

[131] Z. Sun *et al.*, "Thermogravimetric and kinetics investigation of pine wood pyrolysis catalyzed with alkali-treated CaO/ZSM-5," *Energy Conversion and Management*, vol. 146, pp. 182–194, 2017, doi: 10.1016/j.enconman.2017.04.104.

[132] V. Sridevi *et al.*, "Understanding of synergy in non-isothermal microwave-assisted in-

situ catalytic co-pyrolysis of rice husk and polystyrene waste mixtures," *Bioresource Technology*, vol. 360, no. July, p. 127589, 2022, doi: 10.1016/j.biortech.2022.127589.

[133] V. Balasundram *et al.*, "Thermogravimetric catalytic pyrolysis and kinetic studies of coconut copra and rice husk for possible maximum production of pyrolysis oil," *Journal of Cleaner Production*, vol. 167, pp. 218–228, 2017, doi: 10.1016/j.jclepro.2017.08.173.

[134] R. Shakya, S. Adhikari, R. Mahadevan, E. B. Hassan, and T. A. Dempster, "Catalytic upgrading of bio-oil produced from hydrothermal liquefaction of Nannochloropsis sp.," *Bioresource Technology*, vol. 252, no. November 2017, pp. 28–36, 2018, doi: 10.1016/j.biortech.2017.12.067.

[135] K. Siwińska-Stefańska *et al.*, "TiO2-ZnO binary oxide systems: Comprehensive characterization and tests of photocatalytic activity," *Materials*, vol. 11, no. 5, pp. 1–19, 2018, doi: 10.3390/ma11050841.

[136] R. Muhammad *et al.*, "Conditions optimization and physiochemical analysis of oil obtained by catalytic pyrolysis of scrap tube rubber using mgo as catalyst," *Catalysts*, vol. 11, no. 3, pp. 1–13, 2021, doi: 10.3390/catal11030357.

[137] A. H. Rony *et al.*, "Kinetics, thermodynamics, and physical characterization of corn stover (Zea mays) for solar biomass pyrolysis potential analysis," *Bioresource Technology*, vol. 284, no. January, pp. 466–473, 2019, doi: 10.1016/j.biortech.2019.03.049.

[138] J. C. Védrine, "Recent developments and prospectives of acid-base and redox catalytic processes by metal oxides," *Applied Catalysis A: General*, vol. 575, no. December 2018, pp. 170–179, 2019, doi: 10.1016/j.apcata.2019.02.012.

[139] L. Luo *et al.*, "Insight into master plots method for kinetic analysis of lignocellulosic biomass pyrolysis," *Energy*, vol. 233, p. 121194, 2021, doi:

10.1016/j.energy.2021.121194.

[140] L. Wang, M. Chai, R. Liu, and J. Cai, "Synergetic effects during co-pyrolysis of biomass and waste tire: A study on product distribution and reaction kinetics," *Bioresource Technology*, vol. 268, no. July, pp. 363–370, 2018, doi: 10.1016/j.biortech.2018.07.153.

[141] N. M. Mkhize, P. van der Gryp, B. Danon, and J. F. Görgens, "Effect of temperature and heating rate on limonene production from waste tyre pyrolysis," *Journal of Analytical and Applied Pyrolysis*, vol. 120, pp. 314–320, 2016, doi: 10.1016/j.jaap.2016.04.019.

[142] T. Menares, J. Herrera, R. Romero, P. Osorio, and L. E. Arteaga-Pérez, "Waste tires pyrolysis kinetics and reaction mechanisms explained by TGA and Py-GC/MS under kinetically-controlled regime," *Waste Management*, vol. 102, pp. 21–29, 2020, doi: 10.1016/j.wasman.2019.10.027.

[143] B. Qu *et al.*, "Kinetic analysis of waste tire pyrolysis with metal oxide and zeolitic catalysts," *Journal of Analytical and Applied Pyrolysis*, vol. 152, no. July, 2020, doi: 10.1016/j.jaap.2020.104949.

[144] S. Seidelt, M. Müller-Hagedorn, and H. Bockhorn, "Description of tire pyrolysis by thermal degradation behaviour of main components," *Journal of Analytical and Applied Pyrolysis*, vol. 75, no. 1, pp. 11–18, 2006, doi: 10.1016/j.jaap.2005.03.002.

Research Output

The following items were published/submitted/under review from the proposed dissertation objectives.

List of publications:

1. **D. Rammohan**, N. Kishore, R.V.S. Uppaluri, “Insights on kinetic triplets and thermodynamic analysis of *Delonix Regia* biomass pyrolysis” **Bioresource Technology** – https://doi.org/10.1016/j.biortech.2022.127375 **(Published) [IF 11.889].**
2. **D. Rammohan**, N. Kishore, R.V.S. Uppaluri, “Reaction kinetics and thermodynamic analysis of non-Isothermal co-pyrolysis of *Delonix Regia* and tube waste” **Bioresource Technology Reports** – https://doi.org/10.1016/j.biteb.2022.101032 **(Published) [Cite score 6.7].**
3. **D. Rammohan**, N. Kishore, R.V.S. Uppaluri, “Pyro catalytic co-pyrolysis of *Delonix Regia* and butyl rubber tube: Kinetic modeling and thermodynamic insights” **Renewable Energy** – https://doi.org/10.1016/j.renene.2022.10.099 **(Published) [IF 8.634].**
4. **D. Rammohan**, N. Kishore, R.V.S. Uppaluri, “Kinetics and thermodynamic investigation of pyrolysis of butyl rubber tube waste” **European Journal of Sustainable Development Research** – https://doi.org/10.29333/ejosdr/12878 **(Published) [IF 0.61].**
5. **D. Rammohan**, N. Kishore, R.V.S. Uppaluri, “Thermogravimetric analysis of pyrolysis of Delonix regia biomass in the presence of zeolite, mixed metal oxides and carbon supported noble metal catalysts” **Results in Engineering** – **(Accepted-Proofread) [Cite score 3.9].**

6. **D. Rammohan**, N. Kishore, R.V.S. Uppaluri, "Reaction kinetics of non-isothermal pyrolysis of tube waste in thermogravimetric analyzer" **NERC Conference Proceedings – (Revision Submitted).**

List of conference participated:

1. **D. Rammohan**, N. Kishore and R.V.S. Uppaluri, "Co-pyrolysis of *Delonix Regia* trunks and tube waste: Reaction kinetics and thermodynamic analysis" for paper and poster presentation in Biotechnology for Resource Efficiency Energy, Environment, Chemicals and Health, BRE3CH-2021, during Dec 1-4, 2021 at Council of Scientific and Industrial Research (CSIR-IIP), Dehradun, India**. (International)**
2. **D. Rammohan,** N. Kishore and R.V.S. Uppaluri, "Analytical pyrolysis of tube waste: Reaction kinetics study" for paper and poster presentation submitted in North-Eastern Research Conclave, NERC-2022, during May 20-22, 2022 at Indian Institute of Technology Guwahati (IIT G), Guwahati, India. **(National)**